University of Rome *Tor Vergata*

Department of Electronic Engineering

Sensorial and Learning Systems Engineering

XX Cycle

Electronic Tongue systems for food and environmental applications

Candidate

Giorgio M. Verrelli

Tutor

Prof. A. D'Amico

Coordinator

Prof. C. Di Natale

Universitá di Roma *Tor Vergata*

Dipartimento di Ingegneria Elettronica

Ingegneria dei Sistemi Sensoriali e di Apprendimento

XX Ciclo

Sviluppo di sistemi Lingua Elettronica per applicazioni alimentari e ambientali

Candidato

Giorgio M. Verrelli

Tutor

Prof. A. D'Amico

Coordinatore

Prof. C. Di Natale

There's a road, long and winding;

the lights are blindin′, but it gets there!

(Bryan Adams)

Acknowledgments

First of all, I would like to give my special thanking to the Doctorate Coordinator, Prof. R. Marino, to my Doctorate Supervisor Prof. C. Di Natale, to Prof. A. D'Amico and Prof. R. Paolesse from our University for their important contribution to this thesis.

Thanks to FILAS and European project *GoodFood* for financial support.

I would also like to thank Prof. Lorenzelli, Dr. Siciliano and all the co-workers, for giving me the possibility to establish a continuous and fruitful collaboration with FBK-irst of Trento and CNR of Lecce, in the framework of WP5 of GoodFood project.

I am deeply indebted with all my friends from laboratories of Electronic Engineering and Sciences and Chemical Technologies Departments, and CNR-IMM, where I have been able to perform the most part of my work.

Finally I would like to dedicate this special goal to my family (father Sante, mother Tommasina and my brothers Cristiano and Natalia) and Giorgia, for giving me their love and serenity.

Preface

Last decades have been characterized by an increasing attention in the environmental monitoring, in the analysis of wastes from industrial plants, in the control of quality of agro-alimentary products, in the field of medical analysis, etc. The needing of accuracy and easiness of such analysis, has brought to the development of several sensorial devices for the detection of different kinds of analytes, both in gas and in liquid media, able to give fast and reliable results. Furthermore, in the last century, a great impulse to the research has been given by the improvements gained in the electronics in several fields, also very different each other. The electronics application border lines are getting even larger and, in the last years, more frequently, is possible to see applications in fields traditionally reserved to other scientific disciplines.
A generic sensor can be defined, according to IUPAC definition, as a *system able to respond to an external stimulus (mechanical, chemical, acoustic, etc) by the modification of one or more of its properties*. So, the response given by sensor, is shown by the variation of some physico-chemical parameter, such as temperature, mass, volume, electric charge, resistance, etc. The variation shown by the sensing part of sensor (the so-called *chemically interactive material*, CIM, since it can interact with target species) must be read in a proper way by a device named *transducer*, which transforms it in a readable signal, generally an electrical signal.
The performances of the single sensor in term of stability, reproducibility and selectivity are strictly related to the sensing material characteristics; for this reason, the last years have seen an increasing interest on the analysis of chemical and physical properties of several compounds, with the aim to find the most suitable one for the specific application or the ones which can better integrate in an array, to give all the required information, and to improve the characteristics of the already existing ones.
From this point of view, the exploitation in the field of organic compounds as sensing material, is giving encouraging results: the progresses in the synthesis of synthetic receptors allow the fine tuning of the sensor selectivity towards different target molecules, by varying the weak interactions between sensing material and analytes.
Among the developed receptors, pyrrolic macrocycles, such as porphyrins and corroles, may be one of the most promising CIMs, because of the richness of their properties and of their stability. Besides, their chemistry is well known,

and allows the modulation of their sensing properties by synthetic modifications to the molecule skeleton, by complexing metal ions in the core or by introducing peripheral substituents. Porphyrins also play an important role in nature, since they are involved in many biological functions such as the transport of oxygen in blood or the photosynthesis of vegetables.
The use of array of highly cross-selective chemical sensors seems to be one of the most promising ways to perform analysis on complex matrices; they are commonly named *Electronic Nose* (headspace analysis) and *Electronic Tongue* (liquid matrices, [1] ,[2]), even if the definition of the last one in not perfectly established yet [see Chapter 1]. This approach gives the possibility of real time monitoring of the target matrices, even by remote control, without the needing of complex sample pre-treatment, if compared with classical methods, such as chromatography and spectroscopy ([3]) and many applications have been already reported ([4] - [6]).
The development of sensorial systems for the emulation or the overcoming of natural sensors characteristics, needs a complex work, with the interaction of different study fields: it is in fact necessary the contribution of the chemistry and the physics for the realization of the sensing layer able to interact with the chemical environment, of micro-electronic engineering for the electric circuits to be combined with sensors and the support of geometry and mathematics for data analysis.
In particular, the Electronic Tongue systems try to artificially emulate the biological perception mechanism of the human organ, which performs several complex sensing functions. In the case of taste, receptors spread on the tongue surface, are stimulated by chemical substances and send information to nervous fibers and, therefore, to brain. In its most general meaning, a receptor is a structure which modifies itself when excited by an environmental stimulus, determining the production of a signal: so, all the receptors are transducers too, since they transform the signals from one form to another one. A sensorial receptor is a cell (often a neuron) specialized in responding to an external stimulus by producing an electric signal; in other words it translates sensorial stimulus in the nervous system language. The stimulation of a sensorial receptor generates a reception potential, whose amplitude is proportional to stimulus intensity. These potentials causes the release of a neuro-transmitter on a post-synaptic neuron which produces action potentials which reach the brain. In parallel with the natural sensorial system, the Electronic Tongue system structure can be ideally divided in several stages, everyone with a specific task:

- Sensing part, in contact with the ambient, which performs the same function of biological receptors;
- Transducer, which gets info from the receptors and transform them in an easily readable signal, often electric;
- Data processing, that can be assimilated to the nervous fibers and has the aim to acquire signals given by sensors and send them to the processor for the data analysis by techniques which mimic cerebral elaboration.

Several examples of these arrays have been reported in the literature and, although some of these devices have reached the market becoming commercially available ([6], [7]), some issues remain to be optimized for the development of reliable instruments.
In this thesis, we report the study of different sensing materials and, finally, the development of several arrays based on potentiometric chemical sensors. In particular:

- Chemical properties of metal wires were studied; we also investigated the influence of some parameters affecting the measure stability and reproducibility;

- Chemical and cross-sensitivity properties of several complexes of porphyrin analogs were studied, by depositing them on the platinum sensor surface by two different techniques, according to the application: electropolymerization and PVC-based membranes;

- Different chemical sensor arrays were developed for the detection of prostate tumor from urines (data fusion with electronic nose), for the control of the fermentation process of red wine and for the detection of some analytes in white wines mimicking storage and spoilage defects;

- An innovative miniaturized system for the detection of sophisticating elements in white wines was developed; it was based on a miniaturized potentiometric chemical sensor array on a silicon wafer at the outlet of a silicon-based micro-separation column.

Bibliography

[1] Yu. Vlasov, A. Legin, A.M. Rudnitskaya, A. D′Amico, C. Di Natale. Sensors and Actuators B. 65 (2000) 235-236

[2] K.J. Albert, N. S. Lewis, C. L. Schauer, G. A. Sotzing, S. E. Stitzel, T. P. Vaid, D. R. Walt. Chem. Rev. 100 (2000) 2595-2626

[3] H.B. Glasgow, J.M. Burkholder, R.E. Reed, A.J. Lewitus, J.E. Kleinman. J. Exp. Marine Biol. Ecol. 300 (2004) 409-448

[4] F. Winquist, R. Bjorklund, C. Krantz-Kulcker, I. Lundstrom, K. Ostergren, T. Skoglund. Sensors and Actuators B. 111-112 (2005) 299-304

[5] S. Buratti, S. Benedetti, M. Scampicchio, E.C. Pangerod. Analytica Chimica Acta 525 (2004) 133-139

[6] R. Martinez-Manez, J. Soto, E. Garcia-Breijo, L. Gil, J. Ibanez, E. Llobet. Sensors and Actuators B. 104 (2005) 302-307

[7] P. Ivanov, E. Llobet, X. Vilanova, J. Brezmes, J. Hubalek, X. Correig. Sensors and Actuators B. 99 (2004) 201-206

Introduction

Classification of electrochemical methods of analysis Although there are only three principal sources for the analytical signal (potential, current, and charge), a wide variety of experimental designs are possible.
The simplest division is between bulk methods, which measure properties of the whole solution (e.g. the measurement of a solution conductivity, which is proportional to the total concentration of dissolved ions), and interfacial methods, in which the signal is a function of phenomena occurring at the interface between an electrode and the solution in contact with the electrode (e.g. the determination of pH using a pH electrode).
According to our work, we want to focus our attention just on the interfacial electrochemical methods.

Interfacial Electrochemical Methods The diversity of interfacial electrochemical methods is evident from the partial family tree shown in figure 1. At the first level, interfacial electrochemical methods are divided into static methods and dynamic methods:

- In static methods no current passes between the electrodes, and the concentrations of species in the electrochemical cell remain unchanged or static. Potentiometry, in which the potential of an electrochemical cell is measured under static conditions, is one of the most important quantitative electrochemical methods, and will be better discussed in next paragraph;

- The largest division of interfacial electrochemical methods is the group of dynamic methods, in which current flows and concentrations change as the result of a redox reaction. Dynamic methods are further subdivided by whether we choose to control the current or the potential. In controlled-current coulometry, we completely oxidize or reduce the analyte by passing a fixed current through the analytical solution. Controlled-potential methods are subdivided further into controlled-potential coulometry and amperometry, in which a constant potential is applied during the analysis, and voltammetry, in which the potential is systematically varied.

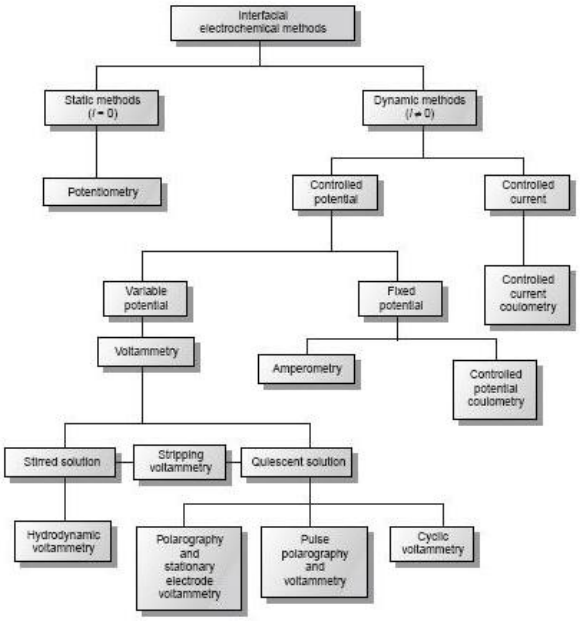

Figure 1: Partial family tree for interfacial electrochemical methods of analysis

Controlling and Measuring Current and Potential Electrochemical measurements are made in an electrochemical cell, consisting of two or more electrodes and associated electronics for controlling and measuring the current and potential.
The simplest electrochemical cell uses two electrodes: the potential of one of the electrodes is sensitive to the analyte concentration and is called the working or indicator electrode. The second electrode, which is called the counter electrode serves to complete the electric circuit and provides a reference potential against which the working electrode potential is measured. Ideally the counter electrode potential remains constant so that any change in the overall cell potential is attributed to the working electrode. In a dynamic method, where the passage of current changes the concentration of species in the electrochemical cell, the potential of the counter electrode may change over time. This problem is eliminated by replacing the counter electrode with two electrodes: a reference electrode, through which no current flows and whose potential remains constant; and an auxiliary electrode that completes the electric circuit and through which current is allowed to flow.
Although many different electrochemical methods of analysis are possible (figure 1) there are only three basic experimental designs:

- measuring the potential under static conditions of no current flow;
- measuring the potential while controlling the current;

- measuring the current while controlling the potential.

Each of these experimental designs, however, is based on Ohm law that a current, i, passing through an electric circuit of resistance, R, generates a potential, E; thus:

$$E = i \cdot R$$

Each of these experimental designs also uses a different type of instrument. To aid in understanding how they control and measure current and potential, these instruments are described as if they were operated manually. To do so the analyst observes a change in current or potential and manually adjusts the instrument settings to maintain the desired experimental conditions. It is important to understand that modern electrochemical instruments provide an automated, electronic means of controlling and measuring current and potential. They do so by using very different electronic circuitry than that shown here.

Potentiometers Measuring the potential of an electrochemical cell under conditions of zero current is accomplished using a potentiometer. A schematic diagram of a manual potentiometer is shown in figure 2.
The current in the upper half of the circuit is

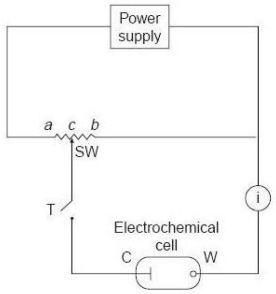

Figure 2: Schematic diagram of a manual potentiostat: C = counter electrode; W = working electrode; SW = slide-wire resistor; T = tap key; i = galvanometer

$$i_{up} = \frac{E_{PS}}{R_{ab}} \tag{1}$$

where E_{PS} is the power supply potential, and R_{ab} is the resistance between points a and b of the slide-wire resistor. In a similar manner, the current in the lower half of the circuit is

$$i_{low} = \frac{E_{cell}}{R_{cb}} \tag{2}$$

where E_{cell} is the potential difference between the working electrode and the counter electrode, and R_{cb} is the resistance between the points c and b of the

slide-wire resistor.
When

$$i_{up} = i_{low} = 0 \tag{3}$$

no current flows through the galvanometer and the cell potential is given by

$$E_{cell} = \frac{R_{cb}}{R_{ab}} \cdot E_{PS} \tag{4}$$

To make a measurement the tap key is pressed momentarily, and the current is noted at the galvanometer. If a nonzero current is registered, then the slide wire is adjusted and the current remeasured. This process is continued until the galvanometer registers a current of zero. Using the tap key minimizes the total amount of current allowed to flow through the cell. Provided that the total current is negligible, the change in the analyte concentration is insignificant.

Galvanostats A galvanostat is used for dynamic methods, such as constant-current coulometry, in which it is necessary to control the current flowing through an electrochemical cell. A schematic diagram of a manual constant-current galvanostat is shown in figure 3.

If the resistance, R, of the galvanostat is significantly larger than the resis-

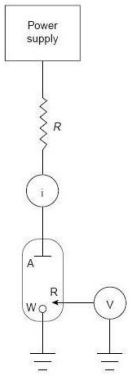

Figure 3: Schematic diagram of a galvanostat: R = resistor; i = galvanometer; A = auxiliary electrode; W = working electrode; R = reference electrode; V = voltmeter or potentiometer (optional)

tance of the electrochemical cell, and the applied voltage from the power supply is much greater than the cell potential, then the current between the auxiliary and working electrodes is equal to

$$i = \frac{E_{PS}}{R} \tag{5}$$

The potential of the working electrode, which changes as the composition of the electrochemical cell changes, is monitored by including a reference electrode and a high-impedance potentiometer.

Potentiostats A potentiostat is used for dynamic methods when it is necessary to control the potential of the working electrode. Figure 4 shows a schematic diagram for a manual potentiostat that can be used to maintain a constant cell potential.

The potential of the working electrode is monitored by a reference electrode

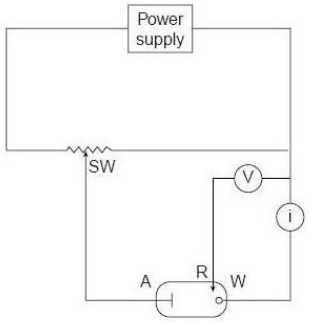

Figure 4: Schematic diagram of a manual potentiostat: SW = slide-wire resistor; A = auxiliary electrode; R = reference electrode; W = working electrode; V = voltmeter or potentiometer; i = galvanometer

connected to the working electrode through a high-impedance potentiometer. The desired potential is achieved by adjusting the slide-wire resistor connected to the auxiliary electrode. If the working electrode potential begins to drift from the desired value, then the slide-wire resistor is manually readjusted, returning the potential to its initial value. The current flowing between the auxiliary and working electrodes is measured with a galvanostat. Modern potentiostats include waveform generators allowing a time-dependent potential profile, such as a series of potential pulses, to be applied to the working electrode.

Electrochemical sensors: an overview

Potentiometric sensors Potentiometric measurements are made using a potentiometer to determine the difference in potential between a working or indicator electrode and a counter electrode (see figure 2). Since no significant current flows in potentiometry, the role of the counter electrode is reduced to that of supplying a reference potential; thus, the counter electrode is usually called the reference electrode. In this section we introduce the conventions used

in describing potentiometric electrochemical cells and the relationship between the measured potential and concentration.

Potentiometric Electrochemical Cells A schematic diagram of a typical potentiometric electrochemical cell is shown in figure 5.

Note that the electrochemical cell is divided into two half-cells, each containing an electrode immersed in a solution containing ions whose concentrations determine the electrode potential. This separation of electrodes is necessary to prevent the redox reaction from occurring spontaneously on the surface of one of the electrodes, short-circuiting the electrochemical cell and making the measurement of cell potential impossible. A salt bridge containing an inert electrolyte, such as KCl, connects the two half-cells. The ends of the salt bridge are fixed with porous frits, allowing ions to move freely between the half-cells and the salt bridge, while preventing the contents of the salt bridge from draining into the half-cells. This movement of ions in the salt bridge completes the electric circuit. By convention, the electrode on the left is considered to be the anode, where oxidation occurs:

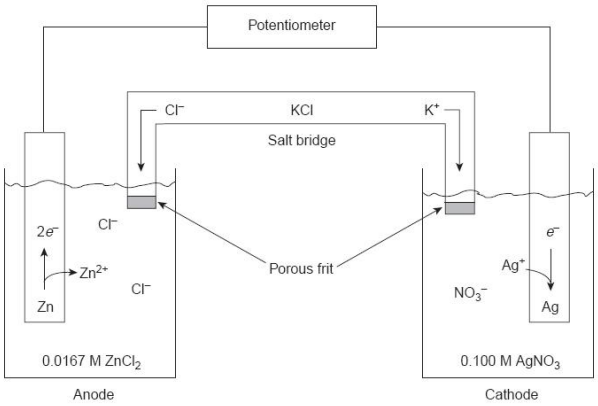

Figure 5: Electrochemical cell for potentiometry

$$Ag^{+}_{(aq)} + e^{-} \rightleftharpoons Ag_{(s)} \tag{6}$$

The electrochemical cell potential, therefore, is for the reaction

$$Zn_{(s)} + 2Ag^{+}_{(aq)} \rightleftharpoons 2Ag_{(s)} + Zn^{2+}_{(aq)} \tag{7}$$

Also, by convention, potentiometric electrochemical cells are defined such that the indicator electrode is the cathode (right half-cell) and the reference electrode is the anode (left half-cell).

Shorthand Notation for Electrochemical Cells Although figure 5 provides a useful picture of an electrochemical cell, it does not provide a convenient representation. A more useful representation is a shorthand or schematic, notation that uses symbols to indicate the different phases present in the electrochemical cell, as well as the composition of each phase. A vertical slash (|) indicates a phase boundary where a potential develops, and a comma (,) separates species in the same phase or two phases where no potential develops. Shorthand cell notations begin with the anode and continue to the cathode. The electrochemical cell in figure 5, for example, is described in shorthand notation as

$$Zn_{(s)}|ZnCl_2(aq, 0,0167M)\|AgNO_3(aq, 0,100M)|Ag_{(s)} \tag{8}$$

The double vertical slash (‖) indicates the salt bridge, the contents of which are normally not indicated. Note that the double vertical slash implies that there is a potential difference between the salt bridge and each half-cell.

Potential and Concentration: the Nernst Equation The potential of a potentiometric electrochemical cell is given as

$$E_{cell} = E_c - E_a \tag{9}$$

where E_c and E_a are reduction potentials for the reactions occurring at the cathode and anode. These reduction potentials are a function of the concentrations of those species responsible for the electrode potentials, as given by the Nernst equation

$$E = E^0 - \frac{R \cdot T}{n \cdot F} \cdot lnQ \tag{10}$$

where E^0 is the standard-state reduction potential, R is the gas constant, T is the temperature in Kelvins, n is the number of electrons involved in the reduction reaction, F is Faraday constant and Q is the reaction quotient.
Under typical laboratory conditions (temperature of 25 ^{0}C or 298 K) the Nernst equation becomes

$$E = E^0 - \frac{0,05916}{n} \cdot lnQ \tag{11}$$

where E is given in volts.
Despite the apparent ease of determining an analyte concentration using the Nernst equation, several problems make this approach impractical. One problem is that standard-state potentials are temperature-dependent, and most values listed in reference tables are for a temperature of 25 ^{0}C. This difficulty can be overcome by maintaining the electrochemical cell at a temperature of 25 ^{0}C or by measuring the standard-state potential at the desired temperature. Another problem is that the Nernst equation is a function of activities, not concentrations. As a result, cell potentials may show significant matrix effects. This

problem is compounded when the analyte participates in additional equilibria. This problem can be minimized by replacing the standard-state potential with a matrix-dependent formal potential. Most tables of standard-state potentials also include a list of selected formal potentials.
A more serious problem is the presence of additional potentials in the electrochemical cell, not accounted in the previous equations. In writing the shorthand notation for the electrochemical cell in figure 5, for example, we use a double slash (||) for the salt bridge, indicating that a potential difference exists at the interface between each end of the salt bridge and the solution in which it is immersed. The origin of this potential, which is called a liquid junction potential, and its significance are discussed in the following section.

Liquid Junction Potentials A liquid junction potential develops at the interface between any two ionic solutions that differ in composition and for which the mobility of the ions differs. We can consider, for example, solutions of 0.1 M HCl and 0.01 M HCl separated by a porous membrane (figure 6).
Since the concentration of HCl on the left side of the membrane is greater

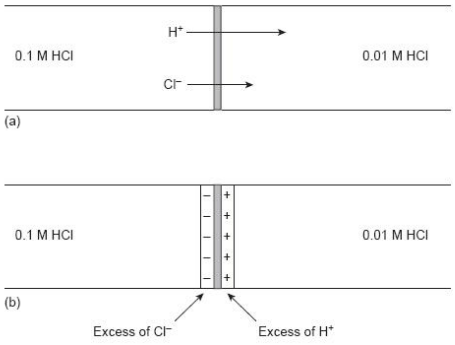

Figure 6: Origin of liquid junction potential between solutions of 0.1 M HCl and 0.01 M HCl

than that on the right side of the membrane, there is a net diffusion of H^+ and Cl^- in the direction of the arrows. The mobility of H^+, however, is greater than that for Cl^-, as shown by the difference in the lengths of their respective arrows. As a result, the solution on the right side of the membrane develops an excess of H^+ and has a positive charge (figure 6). Simultaneously, the solution on the left side of the membrane develops a negative charge due to the greater concentration of Cl^-. The difference in potential across the membrane is called a liquid junction potential, E_{lj}.
The magnitude of the liquid junction potential is determined by the ionic composition of the solutions on the two sides of the interface and may be as large

as 30-40 mV. For example, a liquid junction potential of 33.09 mV has been measured at the interface between solutions of 0.1 M HCl and 0.1 M NaCl ([1]). The magnitude of a salt bridge liquid junction potential is minimized by using a salt, such as KCl, for which the mobilities of the cation and anion are approximately equal. The magnitude of the liquid junction potential also is minimized by incorporating a high concentration of the salt in the salt bridge. For this reason salt bridges are frequently constructed using solutions that are saturated with KCl. Nevertheless, a small liquid junction potential, generally of unknown magnitude, is always present. When the potential of an electrochemical cell is measured, the contribution of the liquid junction potential must be included. Thus, previous equation is rewritten as

$$E_{cell} = E_c - E_a + E_{lj} \tag{12}$$

Metallic Indicator Electrodes The potential of a metallic electrode is determined by the position of a redox reaction at the electrode-solution interface. Three types of metallic electrodes are commonly used in potentiometry, each of which is considered in the following discussion.

Electrodes of the First Kind When a copper electrode is immersed in a solution containing Cu^{2+}, the potential of the electrode due to the reaction

$$Cu^{2+}_{(aq)} + 2e^- \rightleftharpoons Cu_{(s)} \tag{13}$$

is determined by the concentration of copper ion.

$$E = E^0_{Cu^{2+}/Cu} - \frac{0,05916}{2} \cdot log\frac{1}{[Cu^{2+}]} = +0,3419 - \frac{0,05916}{2} \cdot log\frac{1}{[Cu^{2+}]} \tag{14}$$

If the copper electrode is the indicator electrode in a potentiometric electrochemical cell that also includes a saturated calomel reference electrode

$$SCE \| Cu^{2+}_{(unk)} | Cu_{(s)} \tag{15}$$

then the cell potential can be used to determine an unknown concentration of Cu^{2+} in the indicator half-cell

$$E_{cell} = E_{ind} - E_{ref} + E_{lj} = +0,3419 - \frac{0,05916}{2} \cdot log\frac{2}{[Cu^{2+}]} \tag{16}$$

Metallic indicator electrodes in which a metal is in contact with a solution containing its ion are called electrodes of the first kind. In general, for a metal M, in a solution of M^{n+}, the cell potential is given as

$$E_{cell} = K - \frac{0,05916}{n} \cdot log\frac{2}{[M^{n+}]} \tag{17}$$

where K is a constant that includes the standard-state potential for the M^{n+}/M redox couple, the potential of the reference electrode, and the junction potential. For a variety of reasons, including slow kinetics for electron transfer, the existence of surface oxides and interfering reactions, electrodes of the first kind are limited to Ag, Bi, Cd, Cu, Hg, Pb, Sn, Tl, and Zn. Many of these electrodes, such as Zn, cannot be used in acidic solutions where they are easily oxidized by H^+.

Electrodes of the Second Kind An electrode of the first kind involving an M^{n+}/M redox couple will respond to the concentration of another species if that species is in equilibrium with M^{n+}. For example, the potential of a silver electrode in a solution of Ag^+ is given by

$$E = E^0_{Ag^+/Ag} - \frac{0,05916}{2} \cdot log\frac{1}{[Ag^+]} = +0,7996 - \frac{0,05916}{2} \cdot log\frac{1}{[Ag^+]} \quad (18)$$

If the solution is saturated with AgI, then the solubility reaction

$$AgI_{(s)} \rightleftharpoons Ag^+_{(s)} + I^-_{(aq)} \quad (19)$$

determines the concentration of Ag^+; thus

$$[Ag^+] = \frac{K_{SP,AgI}}{[I^-]} \quad (20)$$

where $K_{sp,AgI}$ is the solubility product for AgI.
Combining previous equations

$$E = +0,7996 - 0,05916 \cdot \frac{[I^-]}{K_{SP,AgI}} \quad (21)$$

shows that the potential of the silver electrode is a function of the concentration of I^-. When this electrode is incorporated into a potentiometric electrochemical cell

$$REF \| AgI_{sat'd}, I^-_{unk} | Ag_{(s)} \quad (22)$$

the cell potential is

$$E = K - 0,05916 \cdot \frac{1}{[I^-]} \quad (23)$$

where K is a constant that includes the standard-state potential for the Ag^+/Ag redox couple, the solubility product for AgI, the potential of the reference electrode, and the junction potential.
When the potential of an electrode of the first kind responds to the potential of another ion that is in equilibrium with M^{n+}, it is called an electrode of the second kind. Two common electrodes of the second kind are the calomel and

silver/silver chloride reference electrodes. Electrodes of the second kind also can be based on complexation reactions. For example, an electrode for EDTA is constructed by coupling a Hg^{2+}/Hg electrode of the first kind to EDTA by taking advantage of its formation of a stable complex with Hg^{2+}.

Redox Electrodes Electrodes of the first and second kind develop a potential as the result of a redox reaction in which the metallic electrode undergoes a change in its oxidation state. Metallic electrodes also can serve simply as a source of or a sink for, electrons in other redox reactions. Such electrodes are called redox electrodes. Note that the potential of a redox electrode generally responds to the concentration of more than one ion, limiting their usefulness for direct potentiometry.

Membrane Electrodes If metallic electrodes were the only useful class of indicator electrodes, potentiometry would be of limited applicability. The discovery, in 1906, that a thin glass membrane develops a potential, called a membrane potential, when opposite sides of the membrane are in contact with solutions of different pH lead to the eventual development of a whole new class of indicator electrodes called ion selective electrodes (ISEs). Following the discovery of the glass pH electrode, ion selective electrodes have been developed for a wide range of ions. Membrane electrodes also have been developed that respond to the concentration of molecular analytes by using a chemical reaction to generate an ion that can be monitored with an ion-selective electrode. The development of new membrane electrodes continues to be an active area of research.

Membrane Potentials Ion-selective electrodes, such as the glass pH electrode, function by using a membrane that reacts selectively with a single ion. Figure 7 shows a generic diagram for a potentiometric electrochemical cell equipped with an ion-selective electrode. The shorthand notation for this cell is

$$REF_{(samp)} \| A_{(samp)} | A_{int} \| REF_{(int)} \tag{24}$$

where the membrane is represented by the vertical slash (|) separating the two solutions containing analyte.

Two reference electrodes are used; one positioned within the internal solution, and one in the sample solution. The cell potential, therefore, is

$$E_{cell} = E_{ref(int)} - E_{ref(samp)} + E_{mem} + E_{lj} \tag{25}$$

where E_{mem} is the potential across the membrane.

Since the liquid junction potential and reference electrode potentials are constant, any change in the cell potential is attributed to the membrane potential. Interaction of the analyte with the membrane results in a membrane potential

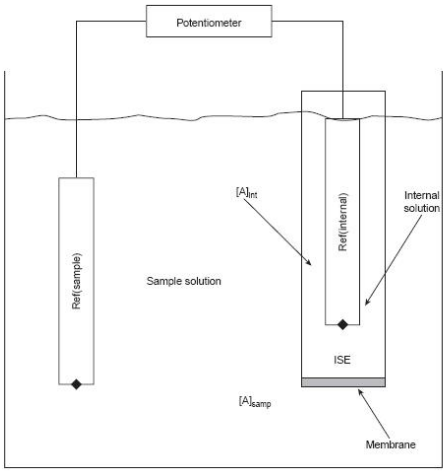

Figure 7: Electrochemical cell for potentiometry with an ion-selective-electrode

if there is a difference in the analyte concentration on opposite sides of the membrane. One side of the membrane is in contact with an internal solution containing a fixed concentration of analyte, while the other side of the membrane is in contact with the sample. Current is carried through the membrane by the movement of either the analyte or an ion already present in the membrane matrix. The membrane potential is given by a Nernst-like equation

$$E_{mem} = E_{asym} - \frac{RT}{zF} \cdot ln \frac{[A]_{int}}{[A]_{samp}} \tag{26}$$

where $[A]_{samp}$ and $[A]_{int}$ are the concentrations of analyte in the sample and the internal solution, respectively, and z is the analyte charge. Ideally, E_{mem} should be zero when the concentrations of analyte on both sides of the membrane are equal. The term E_{asym}, which is called an asymmetry potential, accounts for the fact that the membrane potential is usually not zero under these conditions. Rearranging previous equations and assuming a temperature of 25 ^{0}C, we can obtain

$$E_{cell} = K + \frac{0,05916}{z} \cdot log[A]_{samp} \tag{27}$$

where K is a constant accounting for the potentials of the reference electrodes, any liquid junction potentials, the asymmetry potential, and the concentration of analyte in the internal solution. Last equation is a general equation, and applies to all types of ion-selective electrodes.

Selectivity of Membranes Membrane potentials result from a chemical interaction between the analyte and active sites on the membrane surface.

Because the signal depends on a chemical process, most membranes are not selective toward a single analyte. Instead, the membrane potential is proportional to the concentration of all ions in the sample solution capable of interacting at the membrane active sites. General equation can be generalized to include the contribution of an interfering ion, J.

$$E_{cell} = K + \frac{0,05916}{z_A} \cdot log([I] + K_{I,J}[J]^{z_I/z_J}) \tag{28}$$

where z_I and z_J are the charges of the analyte and interferent, and $K_{I,J}$ is a selectivity coefficient accounting for the relative response of the interferent. The selectivity coefficient is defined as

$$K_{I,J} = \frac{[I]_E}{[J]_E^{z_I/z_J}} \tag{29}$$

where $[I]_E$ and $[J]_E$ are the concentrations of analyte and interferent yielding identical cell potentials. When the selectivity coefficient is 1.00, the membrane responds equally to the analyte and interferent. A membrane shows good selectivity for the analyte when $K_{I,J}$ is significantly less than 1,00. Selectivity coefficients for most commercially available ion-selective electrodes are provided by the manufacturer. If the selectivity coefficient is unknown, it can be determined experimentally. The easiest method for determining $K_{I,J}$ is to prepare a series of solutions, each of which contains the same concentration of interferent, $[J]_{add}$, but a different concentration of analyte. A plot of cell potential versus the log of the analyte concentration has two distinct linear regions (figure 8).

When the analyte concentration is significantly larger than $K_{I,J}[J]_{add}$, the

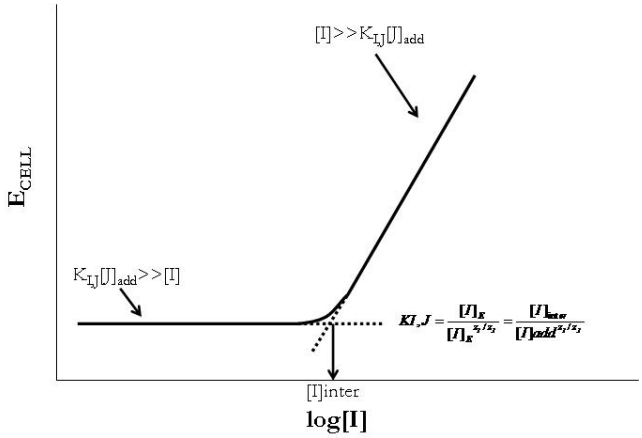

Figure 8: Plot of cell potential versus the log of the analyte concentration in the presence of a fixed concentration of interferent, showing the determination of the selectivity coefficient

potential is a linear function of log[I]. If $K_{I,J}[I]_{add}$ is significantly larger than

the analyte concentration, however, the cell potential remains constant. The concentration of analyte and interferent at the intersection of these two linear regions is used to calculate $K_{I,J}$.

Glass Ion-Selective Electrodes The first commercial glass electrodes were manufactured using Corning 015, a glass with a composition of approximately 22%Na_2O, 6% CaO, and 72% SiO_2. When immersed in an aqueous solution, the outer approximately 10 nm of the membrane becomes hydrated over the course of several hours. Hydration of the glass membrane results in the formation of negatively charged sites, G^-, that are part of the glass membrane silica framework. Sodium ions, which are able to move through the hydrated layer, serve as the counterions. Hydrogen ions from solution diffuse into the membrane and, since they bind more strongly to the glass than does Na^+, displace the sodium ions

$$H^+_{(aq)} + G^- \rightleftharpoons G^- - H^+_{(s)} + Na^+_{(aq)} \tag{30}$$

giving rise to the membrane selectivity for H^+. The transport of charge across the membrane is carried by the Na^+ ions. The potential of glass electrodes using Corning 015 obeys the equation

$$E_{cell} = K + 0,05916 \cdot log[H^+] \tag{31}$$

over a pH range of approximately 0.5-9. Above a pH of 9-10, the glass membrane may become more responsive to other cations, such as Na^+ and K^+. Replacing Na_2O and CaO with Li_2O and BaO extends the useful pH range of glass membrane electrodes to pH levels greater than 12. Glass membrane pH electrodes are often available in a combination form that includes both the indicator and the reference electrode. The use of a single electrode greatly simplifies the measurement of pH. An example of a typical combination electrode is shown in figure 9.

The response of the Corning 015 glass membrane to monovalent cations other than H^+ at high pH lead to the development of glass membranes possessing a greater selectivity for other cations. For example, a glass membrane with a composition of 11% Na_2O, 18% Al_2O_3, and 71% SiO_2 is used as a Na^+ ion-selective electrode. Other glass electrodes have been developed for the analysis of Li^+, K^+, Rb^+, Cs^+, NH_4^+, Ag^+, and Tl^+. Several representative examples of glass membrane electrodes are listed in table 1.

Since the typical thickness of the glass membrane in an ion-selective electrode is about 50 μm, they must be handled carefully to prevent the formation of cracks or breakage. Before a glass electrode can be used it must be conditioned by soaking for several hours in a solution containing the analyte. Glass electrodes should not be allowed to dry out, as this destroys the membrane hydrated layer. If a glass electrode has been allowed to dry out, it must be reconditioned before it can be used. The composition of a glass membrane changes over time, affecting the electrode performance; the average lifetime for a glass electrode is several years.

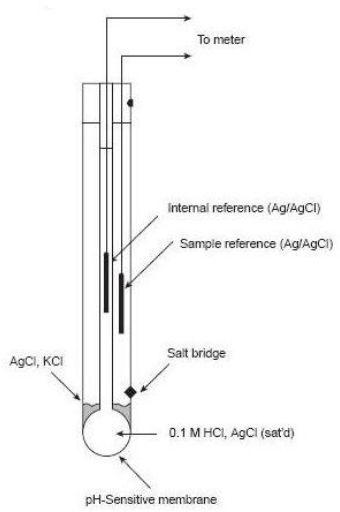

Figure 9: Schematic diagram of a combination glass electrode for measuring pH

Analyte	**Membrane Composition**	**Selectivity Coefficients**
Na^+	11%Na_2O, 18% Al_2O_3, 71%SiO_2	K_{Na^+/H^+}=1000 K_{Na^+/K^+}=K_{Na^+/Li^+}=10^{-3}
Li^+	15%Li_2O, 25% Al_2O_3, 60%SiO_2	K_{Li^+/Na^+}=0,3 K_{Li^+/K^+}=10^{-3}
K^+	27%Na_2O, 5% Al_2O_3, 68%SiO_2	K_{K^+/Na^+}=0,05

Table 1: Representative examples of Glass Membrane Ion-Selective Electrodes

Crystalline Solid-State Ion-Selective Electrodes Solid-state ion-selective electrodes use membranes fashioned from polycrystalline or single-crystal inorganic salts. Polycrystalline ion-selective electrodes are made by forming a thin pellet of Ag_2S or a mixture of Ag_2S and either a second silver salt or another metal sulfide. The pellet, which is 1-2 mm in thickness, is sealed into the end of a nonconducting plastic cylinder, and an internal solution containing the analyte and a reference electrode are placed in the cylinder. Charge is carried across the membrane by Ag^+ ions. The membrane potential for a Ag_2S pellet develops as the result of a difference in the equilibrium position of the solubility reaction

$$Ag_2S_{(s)} \rightleftharpoons 2Ag^+_{(aq)} + S^{2-}_{(aq)} \tag{32}$$

on the two sides of the membrane. When used to monitor the concentration of Ag^+ ions, the cell potential is

$$E_{cell} = K + 0,05916 \cdot log[Ag^+] \tag{33}$$

The membrane also responds to the concentration of S^{2-}, with the cell potential given as

$$E_{cell} = K - \frac{0,05916}{2} \cdot log[S^{2-}] \tag{34}$$

If a mixture of an insoluble silver salt and Ag_2S is used to make the membrane, then the membrane potential also responds to the concentration of the anion of the added silver salt. Thus, pellets made from a mixture of Ag_2S and AgCl can serve as a Cl^- ion-selective electrode, with a cell potential of

$$E_{cell} = K - 0,05916 \cdot log[Cl^-] \tag{35}$$

Membranes fashioned from a mixture of Ag_2S with CdS, CuS or PbS are used to make ion-selective electrodes that respond to the concentration of Cd^{2+}, Cu^{2+} or Pb^{2+}. In this case the cell potential is

$$E_{cell} = K + \frac{0,05916}{2} \cdot log[M^{2+}] \tag{36}$$

where $[M^{2+}]$ is the concentration of the appropriate metal ion. Several examples of polycrystalline, Ag_2S^-based ion-selective electrodes are listed in table 2.

The selectivity of these ion-selective electrodes is determined by solubility. Thus, a Cl^- ion-selective electrode constructed using a Ag_2S/AgCl membrane is more selective for Br^- ($K_{Cl^-/Br^-} = 10^2$) and I^- ($K_{Cl^-/I^-} = 10^6$) since AgBr and AgI are less soluble than AgCl. If the concentration of Br^- is sufficiently high, the AgCl at the membrane-solution interface is replaced by AgBr, and the electrode response to Cl^- decreases substantially. Most of the ion-selective electrodes listed in table 1 can be used over an extended range of pH levels. The equilibrium between S^{2-} and HS^- limits the analysis for S^{2-} to a pH range of 13-14. Solutions of CN^-, on the other hand, must be kept basic to avoid the release of HCN. The membrane of a F^- ion-selective electrode is fashioned from a single crystal of LaF_3 that is usually doped with a small amount of EuF_2 to enhance the membrane conductivity. Since EuF_2 provides only two F^- ions, compared with three for LaF_3, each EuF_2 produces a vacancy in the crystal lattice. Fluoride ions move through the membrane by moving into adjacent vacancies. The LaF_3 membrane is sealed into the end of a nonconducting plastic tube, with a standard solution of F^-, typically 0.1 M NaF, and a Ag/AgCl reference electrode.

The membrane potential for a F^- ion-selective electrode results from a difference

$$E_{cell} = K - 0,05916 \cdot log[F^-] \tag{37}$$

One advantage of the F^- ion-selective electrode is its freedom from interference. The only significant exception is OH^- ($K_{F^-/OH^-} = 0,1$), which imposes a maximum pH limit for a successful analysis.

Below a pH of 4 the predominant form of fluoride in solution is HF, which, unlike F^-, does not contribute to the membrane potential. For this reason, an

Analyte	**Membrane Composition**	**Selectivity Coefficients**
Ag^+	Ag_2S	$K_{Ag^+/Cu^{2+}} = 10^{-6}$ $K_{Ag^+/Pb^{2+}} = 10^{-10}$ Hg^{2+} interferes
Cd^{2+}	CdS/Ag_2S	$K_{Cd^{2+}/Fe^{2+}} = 200$ $K_{Cd^{2+}/Pb^{2+}} = 6$ Ag^+, Hg^{2+}, Cu^{2+} must be absent
Cu^{2+}	CuS/Ag_2S	$K_{Cu^{2+}/Fe^{3+}} = 10$ K_{Cu^{2+}/Cu^+}=1 Ag^+, Hg^{2+} must be absent
Pb^{2+}	PbS/Ag_2S	$K_{Pb^{2+}/Fe^{3+}} = 1$ $K_{Pb^{2+}/Cd^{2+}}$=1 Ag^+, Hg^{2+} must be absent
Br^-	$AgBr/Ag_2S$	$K_{Br^-/I^-} = 5000$ K_{Br^-/CN^-}=100 $K_{Br^-/Cl^-} = 5 \times 10^{-3}$ $K_{Br^-/OH^-} = 1 \times 10^{-5}$ S^{2-} must be absent
Cl^-	$AgCl/Ag_2S$	$K_{Cl^-/I^-} = 1 \times 10^6$ $K_{Cl^-/CN^-} = 1 \times 10^4$ $K_{Cl^-/Br^-} = 100$ $K_{Cl^-/OH^-} = 0,01$ S^{2-} must be absent
CN^-	AgI/Ag_2S	$K_{CN^-/I^-} = 100$ $K_{CN^-/Br^-} = 1 \times 10^{-4}$ $K_{CN^-/Cl^-} = 1 \times 10^{-6}$ $K_{CN^-/OH^-} = 1 \times 10^{-8}$ S^{2-} must be absent
I^-	AgI/Ag_2S	$K_{I^-/S^{2-}} = 30$ $K_{I^-/CN^-} = 0,01$ $K_{I^-/Br^-} = 1 \times 10^{-4}$ $K_{I^-/Cl^-} = 1 \times 10^{-6}$ $K_{I^-/OH^-} = 1 \times 10^{-7}$
SCN^-	$AgSCN/Ag_2S$	$K_{SCN^-/I^-} = 1000$ $K_{SCN^-/Br^-} = 100$ $K_{SCN^-/CN^-} = 100$ $K_{SCN^-/Cl^-} = 0,1$ $K_{SCN^-/OH^-} = 0,01$ S^{2-} must be absent
S^{2-}	Ag_2S	Hg^{2+} interferes

Table 2: Representative examples of Polycrystalline Ion-Selective Electrodes

analysis for total fluoride must be carried out at a pH greater than 4. Unlike ion-selective electrodes using glass membranes, crystalline solid-state ion-selective electrodes do not need to be conditioned before use and may be stored dry. The surface of the electrode is subject to poisoning, as described earlier for a Cl^- ISE in contact with an excessive concentration of Br^-. When this happens, the electrode can be returned to its original condition by sanding and polishing the crystalline membrane.

Liquid-Based Ion-Selective Electrodes Another approach to constructing an ion-selective electrode is to use a hydrophobic membrane containing a selective, liquid organic complexing agent. Three types of organic liquids have been used: cation exchangers, anion exchangers, and neutral ionophores. When the analyte concentration on the two sides of the membrane is different, a membrane potential is the result. Current is carried through the membrane by the analyte. One example of a liquid-based ion-selective electrode is that for Ca^{2+}, which uses a porous plastic membrane saturated with di-(n-decyl) phosphate. As shown in figure 10, the membrane is placed at the end of a nonconducting cylindrical tube and is in contact with two reservoirs. The outer reservoir contains di-(n-decyl) phosphate in di-n-octylphenylphosphonate, which soaks into the porous membrane. The inner reservoir contains a standard aqueous solution of Ca^{2+} and a Ag/AgCl reference electrode.

Calcium ion-selective electrodes are also available in which the di-(n-decyl)

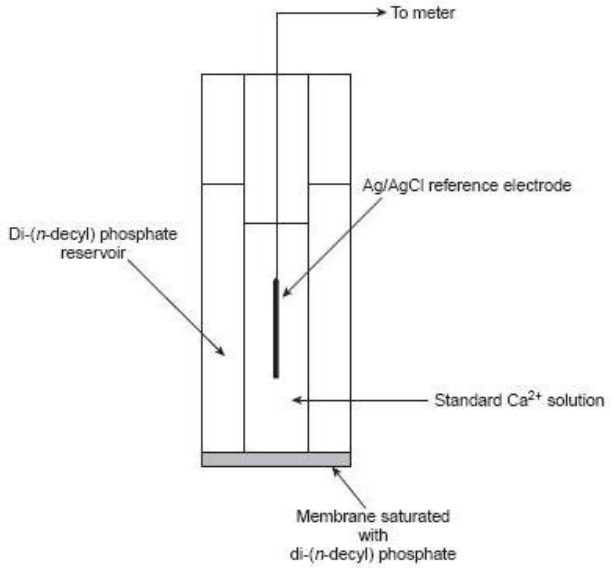

Figure 10: Schematic diagram of a Ca^{2+} liquid-based ion-selective electrode

phosphate is immobilized in a polyvinyl chloride (PVC) membrane, eliminating the need for a reservoir containing di-(n-decyl) phosphate. A membrane potential develops as the result of a difference in the equilibrium position of the complexation reaction

$$Ca^{2+}_{(aq)} + 2(C_{10}H_{21}O)_2PO_2^-(m) \rightleftharpoons Ca[(C_{10}H_{21}O)_2PO_2]_2(m) \tag{38}$$

on the two sides of the membrane, where (m) indicates that the species is present in the membrane. The cell potential for the Ca^{2+} ion-selective electrode is The selectivity of the electrode for Ca^{2+} is very good, with only Zn^{2+} showing greater selectivity. The properties of several representative liquid-based ion-selective electrodes are presented in table 3.

An electrode using a liquid reservoir can be stored in a dilute solution of

Analyte	**Membrane Composition**	**Selectivity Coefficients**
Ca^{2+}	di-(n-decyl) phosphate in PVC	$K_{Ca^{2+}/Zn^{2+}} = 1 - 5$ $K_{Ca^{2+}/Al^{3+}} = 0,90$ $K_{Ca^{2+}/Mn^{2+}} = 0,38$ $K_{Ca^{2+}/Cu^{2+}} = 0,07$
K^+	Valinomycin in PVC	$K_{K^+/Rb^+} = 0,9$ $K_{K^+/Cs^+} = 0,38$ $K_{K^+/Li^+} = 1 \times 10^{-4}$ $K_{K^+/Na^+} = 1 \times 10^{-5}$
Li^+	ETH 149 in PVC	$K_{Li^+/H^+} = 1$ K_{Li^+/Na^+}=0,05 $K_{Li^+/K^+} = 7 \times 10^{-3}$
NH_4^+	Nonactin and monactin in PVC	$K_{NH_4^+/K^+} = 0,12$ $K_{NH_4^+/H^+} = 16^{-3}$ $K_{NH_4^+/Li^+} = 4,2 \times 10^{-3}$ $K_{NH_4^+/Na^+} = 2 \times 10^{-3}$
ClO_4^-	$Fe(o\text{-}phen)_3^{3+}$ in p-nitrocymene with porous membrane	$K_{ClO_4^-/OH^-} = 1$ $K_{ClO_4^-/I^-} = 12 \times 10^{-3}$ $K_{ClO_4^-/NO_3^-} = 1,5 \times 10^{-3}$ $K_{ClO_4^-/Br^-} = 5,6 \times 10^{-4}$ $K_{ClO_4^-/Cl^-} = 2,2 \times 10^{-4}$
NO_3^-	tetradodecyl ammonium nitrate in PVC	$K_{NO_3^-/Cl^-} = 6 \times 10^3$ $K_{NO_3^-/F^-} = 9 \times 10^4$

Table 3: Representative examples of Liquid-Based Ion-Selective Electrodes

analyte and needs no additional conditioning before use. The lifetime of an electrode with a PVC membrane, however, is proportional to its exposure to aqueous solutions. For this reason these electrodes are best stored by covering the membrane with a cap containing a small amount of wetted gauze to maintain a humid environment. The electrode must then be conditioned before use

by soaking in a solution of analyte for 30-60 min.

Biosensors Potentiometric electrodes for the analysis of molecules of chemical importance can be constructed in a fashion similar to that used for gas-sensing electrodes. The most common class of potentiometric biosensors are the so-called enzyme electrodes, in which an enzyme is trapped or immobilized at the surface of an ion-selective electrode. Reaction of the analyte with the enzyme produces a product whose concentration is monitored by the ion-selective electrode. Potentiometric biosensors have also been designed around other biologically active species, including antibodies, bacterial particles, tissue, and hormone receptors. One example of an enzyme electrode is the urea electrode, which is based on the catalytic hydrolysis of urea by urease

$$CO(NH_2)_{2(aq)} + 2H_2O_{(l)} \rightleftharpoons 2NH^+_{4(aq)} + CO^{2-}_{3(aq)} \tag{39}$$

In one version of the urea electrode, shown in figure 11, an NH_3 electrode is modified by adding a dialysis membrane that physically traps a pH 7.0 buffered solution of urease between the dialysis membrane and the gas-permeable membrane ([2], [3]).

When immersed in the sample, urea diffuses through the dialysis membrane,

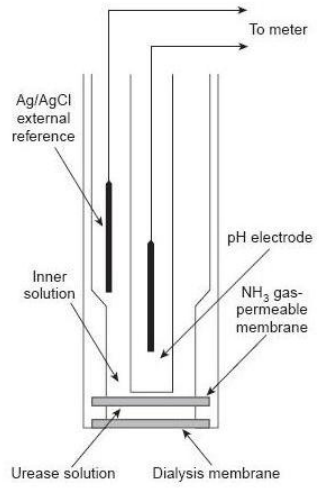

Figure 11: Schematic diagram of an enzyme-based potentiometric biosensor for urea in which urease is trapped between two membranes

where it reacts with the enzyme urease. The NH^+_4 that is produced is in equilibrium with NH_3:

$$NH^+_4(aq) + H_2O_{(l)} \rightleftharpoons H_3O^+_{(l)}) + NH_{3(aq)} \tag{40}$$

which, in turn, diffuses through the gas-permeable membrane, where it is detected by a pH electrode. The response of the electrode to the concentration of urea is given by

$$E_{cell} = K - 0,05916 \cdot [urea] \tag{41}$$

Another version of the urea electrode (figure 12) immobilizes the enzyme in a polymer membrane formed directly on the tip of a glass pH electrode ([4]). In this case, the electrode response is

$$pH = K \cdot [urea] \tag{42}$$

Several representative examples can be found in literature ([5], [6]), even if few

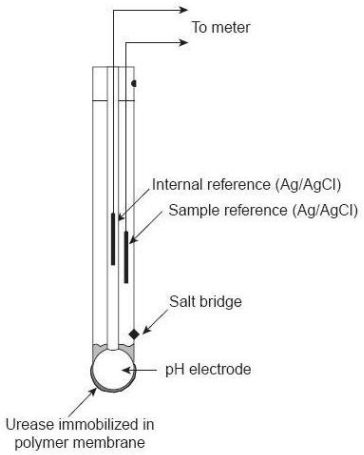

Figure 12: Schematic diagrams of a second enzyme-based potentiometric biosensor for urea in which urease is immobilized in a polymer matrix

potentiometric biosensors are commercially available.

Amperometric Sensors The most used voltammetric technique for sensorial applications is amperometry, in which a constant potential is applied to the working electrode, and current is measured as a function of time. Since the potential is not scanned, amperometry does not lead to a voltammogram. One important application of amperometry is in the construction of chemical sensors. One of the first amperometric sensors to be developed was for dissolved O_2 in blood, which was developed in 1956 by L.C. Clark. The design of the amperometric sensor is shown in figure 13 and is similar to potentiometric membrane electrodes.

A gas-permeable membrane is stretched across the end of the sensor and is separated from the working and counter electrodes by a thin solution of KCl.

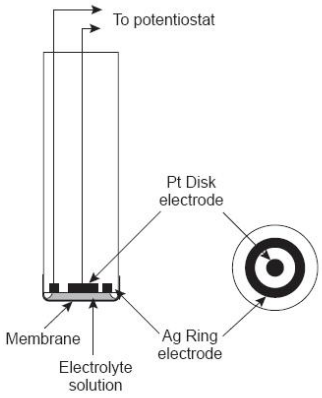

Figure 13: Clark amperometric sensor for the determination of dissolved O_2

The working electrode is a Pt disk cathode, and an Ag ring anode is the counter electrode. Although several gases can diffuse across the membrane, including O_2, N_2, and CO_2, only oxygen is reduced at the cathode.

$$O_{2(aq)} + H_3O^+_{(aq)} + 4e^- \rightleftharpoons 6H_2O_{(l)} \tag{43}$$

Another example of an amperometric sensor is the glucose sensor. In this case the single membrane in figure 13 is replaced with three membranes.
The outermost membrane is of polycarbonate, which is permeable to glucose and O_2. The second membrane contains an immobilized preparation of glucose oxidase that catalyzes the oxidation of glucose to gluconolactone and hydrogen peroxide.

$$\beta - D - glucose_{(aq)} + O_{2(g)} + H_2O_{(l)} \rightleftharpoons gluconolactone_{(aq)} + H_2O_{2(aq)} \tag{44}$$

The hydrogen peroxide then diffuses through the innermost membrane of cellulose acetate, where it is oxidized at a Pt anode.

$$H_2O_{2(aq)} + 2OH^-_{(aq)} \rightleftharpoons O_{2(g)} + 2H_2O_{(l)} + 2e^- \tag{45}$$

Figure 14 summarizes the reactions taking place in this amperometric sensor.

FAD is the oxidized form of flavin adenine nucleotide (the active site of the enzyme glucose oxidase), and $FADH_2$ is the active site reduced form. Note that O_2 serves as a mediator, carrying electrons to the electrode. Other mediators, such as $Fe(CN)^{3-}_6$, can be used in place of O_2. By changing the enzyme and mediator, the amperometric sensor in figure 14 is easily extended to the analysis of other substrates.
Other bioselective materials may be incorporated into amperometric sensors. For example, a CO_2 sensor has been developed using an amperometric O_2 sensor

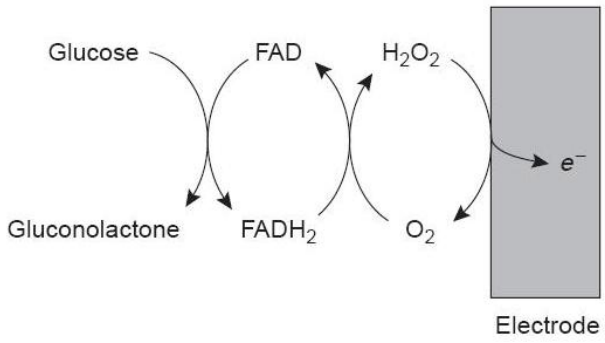

Figure 14: Schematic showing the reactions by which an amperometric biosensor responds to glucose

with a two-layer membrane, one of which contains an immobilized preparation of autotrophic bacteria ([7]). As CO_2 diffuses through the membranes, it is converted to O_2 by the bacteria, increasing the concentration of O_2 at the Pt cathode.

Detectors for HPLC As with gas chromatography, numerous detectors have been developed for use in monitoring HPLC separations ([8]). To date, the majority of HPLC detectors are not unique to the method, but are either stand-alone instruments or modified versions of the same.

Detectors for HPLC Another common group of HPLC detectors are those based on electrochemical measurements such as amperometry, voltammetry, coulometry, and conductivity. Effluent from the column passes over the working electrode, which is held at a potential favorable for oxidizing or reducing the analytes. The potential is held constant relative to a downstream reference electrode, and the current flowing between the working and auxiliary electrodes is measured. Detection limits for amperometric electrochemical detection are 10 $pg^{-1} \cdot$ ng of injected analyte.

Bibliography

[1] D.T. Sawyer, J.L. Roberts. Jr. Experimental Electrochemistry for Chemists. Wiley-Interscience: New York, 1974, p. 22

[2] D.S. Papastathopoulos, G.A. Rechnitz. Anal. Chim. Acta. 79 (1975) 17

[3] T.L.J. Riechel. Chem. Educ. 61 (1984) 640-642

[4] R. Tor, A. Freeman. Anal. Chem. 58 (1986) 1042-1046

[5] K. Cammann. Working with Ion-Selective Electrodes. Springer-Verlag: Berlin, 1977

[6] C.E. Lunte, W.R. Heineman. Electrochemical Techniques in Bioanalysis. In Steckham, E., ed. Topics in Current Chemistry, Vol. 143, Springer-Verlag: Berlin, 1988, 8

[7] I. Karube, Y. Nomura, Y. Arikawa. Trends in Anal. Chem. 14 (1995) 295-299

[8] D.J. Curran. Constant-Current Coulometry. Chapter 20 in Kissinger, P. T.; Heineman, W. R., eds. Laboratory Techniques in Electroanalytical Chemistry. Marcel Dekker, Inc.: New York, 1984, 539-568

Chapter 1

Sensor Array for liquid matrices: the Electronic Tongue

Introduction

Multisensor systems for liquid analysis based on chemical sensor arrays and pattern recognition, which are now widely known as *electronic tongues*, represent one of the most rapidly emerging and exciting fields of non-classical analytics during the last decade. This chapter presents an overview of the research and development of electronic tongue systems and describes various sensors, sensor arrays, and their numerous applications. A sound basis for electronic tongues was provided by the extensive development of well-known selective sensors, especially electrochemical, and biological inspirations originating from sensory systems of mammalians. So we will report the up-to-date achievements of various scientific groups working in this field, showing the performance of electronic tongues in the tasks of recognition (classification, identification, discrimination) of multicomponent media, also focusing on the possibility to correlate the output of an electronic tongue and human sensory assessments of food flavor made by taste panel, opening up an exciting possibility of measuring and quantifying the taste and flavor of foods. Application areas of the electronic tongue systems, including quality control of foodstuffs, clinical, industrial and environmental analysis, are surveyed, and finally future prospects for research and development of electronic tongues will be expressed.

1.1 The origins

Several definitions have been given, but scientific community does not totally agree in some aspects. The most accepted definition could be that an electronic

tongue is the combination of a sensor array with limited individual selectivity and an appropriate pattern recognition tool ([1]). All scientists do not always share this definition, as long as electronic tongues can use other chemometrics tools, as for example artificial neural networks. Sometimes disagreements appears in the sensing part of the electronic tongue; the edge between *electronic tongues* and *multiparametrical systems* is normally related to what is used as detector, and more important, who is giving the name to the analytical device. Another example of lexical discrepancy between scientists is the use of the term *taste sensor* by some research groups, normally located in Japan. Because of this subjective vision in this topic, we will try to summarize all documents found in literature, even when *electronic tongue* is not the given name.
Electronic Tongues, used for liquids, appeared as a natural consequence some year after the appearance of electronic noses, used in gas analysis and mainly developed in the 1980s, after the publication in 1982 of the seminar paper by Persaud and Dodd in Nature ([2]).
The idea to integrate several sensors in an array, starts from the Nikolsky equation which presents an additive term due to interferring ions if compared with Nernst equation.

$$E = E^0 + \frac{RT}{z_i F} \cdot ln[a_I + \sum K_{IJ} \cdot (a_J^{z_I/z_J})] \tag{1.1}$$

If an ISE is not highly selective, the value of its output (potential) will be determined by the simultaneous presence and the ratio of the contents of several ions or other species. The terms a_I and $\sum K_{IJ}(a_J^{z_I/z_J})$ may appear comparable and the electrode response becomes nonlinear. Although it is still possible to deal with a nonlinear calibration curve, more than one electrode is needed to find correctly the parameters of the equation for multiple analytes. Evidently, the number of electrodes should not be less than the number of analytes according to simple mathematical considerations.
In the mid-1980s, this reasoning led to the idea of applying an electrode array instead of a discrete ISE with the aim of improving the insufficient selectivity of the ISEs in the presence of interfering ions. This approach assumes that the behavior of each electrode of the array in multicomponent solutions can still be described by the Nikolsky equation. Thus, the system of Nikolsky equations should be solved to find ISE parameters such as standard potentials, selectivity coefficients, and/or slopes. The parameters found can be used subsequently for the prediction of the concentration of multiple analytes. Numerous methods can be applied for calculating the parameters of Nikolsky equation, including different regression techniques and even artificial neural networks (ANNs). Another approach that encouraged the development of chemical multisensor systems was an attempt to mimic the organization and performance of biological sensory systems, particularly the olfaction of mammalians (the sense of smell, [3]).
Olfaction was recognized long ago as the most effective sensing system owing to its high sensitivity and discrimination ability. The sense of smell is capable of distinguishing thousands of different volatile molecules, including some very similar ones such as stereoisomers. The perception threshold of humans for

some odorants can be as low as a few parts per trillion and it is even lower in animals ([4]). Evidently, all odorant substances are volatile but volatility (vapor pressure) and odor intensity are not proportional and some compounds with very low vapor pressure can be powerful odorants (e.g., musk) and vice versa. The relationship between a compound structure and the odor that it elicits is still unclear and compounds of very different chemical compositions may have similar odors.

However, a relation between fat solubility and odor intensity was postulated: the strongest odorants are both water and fat soluble ([5]). An impressive performance of the olfactory system is achieved owing to a wide set of non-specific or cross-sensitive receptors and processing of their signals in the neural system and in the brain. The detection of odor is performed by olfactory receptor neurons situated in mucus layer in the nostrils, where odorant molecules react with odorant- binding proteins the sensing layer of receptors. Since receptors are not selective, many of them respond to a given odor. This reaction results in an activity pattern which is transferred to the olfactory bulb, where primary signal processing is performed, and then to the higher level brain region for identification and recognition.

The sense of taste in mammalians is organized similarly to olfaction. Taste is perceived by non-specific taste buds, situated on the papillae of the tongue. Conventionally, the overall taste is correlated with a combination of four basic tastes: sweetness, sourness, bitterness, and saltiness. Sometimes another elementary taste characteristics are used, such as umami. Umami was firstly introduced by Japanese researchers and it is described as a delicious taste perceived in meat, cheeses, and mushrooms ([6]). Since taste and odor are often perceived simultaneously, the term flavor is widely used to describe their combination, especially when speaking about food.

The relationship between taste (flavor) and chemical composition is often not known precisely, especially for sweet substances. Another interesting and highly controversial issue is the interaction between different tastes ([5]). In most cases a desensitizing effect or threshold increase takes place when two substances eliciting different tastes are present simultaneously. A further effect is the sensitivity threshold decrease when substances present at non-perceptible concentrations can be felt if a contrasting taste substance is applied to the tongue. Perception thresholds of the human tongue to most of taste substances are much higher than those for olfaction with exception of alkaloids, such as quinine. However, differential taste and odor thresholds are comparable ([5]). Thus, the mammalian sense of taste function is similar to olfaction but is less developed, possibly because it is less related to the survival of living beings. Dr. Gardner made a very interesting review on this topic in 1994 ([7]).

Major complexity of water samples was probably the cause of this time delay in the electronic tongue appearance compared to electronic noses. First electronic tongues appeared in Japan and Russia: the Japanese group normally refer to electronic tongues under the name of taste sensor because of the analogy with human taste sense. In 2005, IUPAC recognized these new analytical devices and established the international nomenclature for potentiometric analysis of liquids

([8]). In this case, electronic tongue is defined as a multisensor system, which consist of a number of low selective sensors and used advanced mathematical procedures for signal processing based in pattern recognition and/or multivariate analysis.
The electronic tongues are appropriate in analytical problems where signal overlapping, due to different species, is present, and thus, direct calibration is not always possible. Even being this case, the calibration process is much more complex and time consuming, because of the huge number of standards or samples needed. Manual preparation and/or determination are, sometimes, the main impediment in using the electronic tongues as a good analytical approach. Mechanisation can simplify their operation and brings improvements in reproducibility. The use of electronic tongues as classification tool is, by far, the most explored approach. The analytical strategy is based on the measurements of a great number of samples covering the expected variability and afterwards, a visualization tool, such as Principal Components Analysis (PCA), if used for samples grouping, after which pattern recognition variants are used for classifications ([9] - [12]). Industrial applicability of the classifying electronic tongue is increasing each day, as a complement in industrial process monitoring, especially in agro-food industries ([13]).
The second variant of electronic tongues develops quantitative determinations. In this case, some specific analytes, presenting overlapping or interference signals, are simultaneously quantified from a direct measurement employing a sensor array featuring cross-response and appropriate multivariate calibration.

1.2 Cross-sensitivity

Cross-sensitivity of potentiometric sensors cannot be treated simply as a reverse value of the selectivity coefficient. The classical selectivity of ISEs was always considered in the framework of a thermodynamic approach, on the basis of certain sensing mechanisms (ion exchange) and for the situation when one primary and one interfering ion are present. Recently, equations describing the general sensor-mixed response were suggested ([14]). This approach takes into account the response of a polymer-based potentiometric sensor to any number of ions of different charges. It is based on the phase boundary potential model and assumes that the sensitivity mechanism is still ion exchange. The sensing mechanism, however, may be different or even variable, eg, some sensors would respond both to ionic and to non-ionic species in solutions. An adequate theoretical consideration of cross-sensitivity seems not to be possible at the current stage and much more experimental evidence and theoretical considerations of the sensing mechanisms of different materials to different substances, including nonionic ones, are needed. However, an empirical method of sensor cross-sensitivity assessment, which can be used to guide sensor choices in practical applications, was suggested ([15], [16]).
The first necessary step is the determination of a set of substances, for which

cross-sensitivity is to be studied, and a set of sensing materials. In most cases even very non-selective or cross-sensitive sensors would not respond to any ion or substance in solution, but presumably to a certain group of substances. The calculation of cross-sensitivity parameters was based on the sensitivity study of chalcogenide glass electrodes to a set of heavy metals ([15], [16]). Later the same parameters were successfully applied to the cross-sensitivity evaluation of other types of membrane materials on different sets of analytes ([17]). The experimental measurements used for cross-sensitivity estimation were simply calibrations of given sensors in individual solutions of the chosen set of compounds.
After the application of different fitting procedures and consideration of literature data, the following three parameters were chosen for the description of integral sensor response and cross-sensitivity. As the parameters involved are empirical ones, it is possible to suggest another version or set of them. However, these appeared to be sufficiently representative and successful.
The first is the *average sensor response slope* S, measured in solutions of the chosen set of substances:

$$S = \frac{1}{n} \sum S_i \tag{1.2}$$

where S_i is sensor response slope in solutions of each individual substance and n is the number of components in the set.
The second value is the *average signal-to-noise ratio* of a sensor (for all components of the set):

$$K = \frac{1}{n} \sum K_i = \frac{1}{n} \sum \frac{S_i}{s_i^2} \tag{1.3}$$

where S_i and s_i are response slope and its standard deviation in solutions of each substance.
The last parameter is termed the *non-selectivity factor*, because it describes the distribution of the sensitivity of a sensor to different components from the chosen set and is calculated as follows:

$$F = \frac{S}{s^2} \tag{1.4}$$

where S is the average slope (the first parameter) and s is its standard deviation. The average slope value is the main and the most important characteristic of integral response and, hence, cross-sensitivity of a sensor. The higher its value, the better is the overall sensitivity of the sensor to the substances from the set. An optimal range of the average slope could be estimated in each case on the basis of the following suppositions. Let us consider, e.g., a study of sensor sensitivity to a set of divalent ions. In this case, the sensor response slopes are likely to fall in the range from 0 to 29 mV/pX according to the Nernst equation. However, a super-Nernstian response may also be observed. Therefore, the average slope of a sensor close to 30 mV/pX is commonly related to a comparatively uniform distribution of sensitivity to the chosen set of divalent ions. A value of

S>30 mV/pX may be a result of a significantly super-Nernstian response to one of the ions. Thus, in this particular case the range of S from 25 to 30 mV/pX should be considered as the optimal one. The sensors displaying S>25 mV/pX display remarkable cross-sensitivity to all ions of the set and can be used for multisensor array analysis.
The average slope value is not the only valid response characteristic. At least two other measures appeared to be useful. To characterize the distribution of sensitivity for different components, the non-selectivity parameter F has been used.
F<<0.1 is typical for highly selective sensors with high sensitivity to the primary ion and very poor sensitivity to the other ions. An increase in F up to 0.1 is evidence for a smoother distribution, but the sensitivity to some components can still be low. A fairly uniform sensitivity distribution to most substances from the set is typical for sensors with F=1. Finally, values of F>0.5 characterize a reasonable distribution of sensitivity and significant cross-sensitivity to different species in complex solutions and thus may be considered as optimal for sensors designed for array applications.
The stability parameter is also important because, in preliminary experiments, a correlation between stability in individual ion solutions and that in complex liquids was found. The average signal-to-noise ratio K is a valuable estimate of sensor stability. The higher is K, the more reproducible is the sensor potential and the more stable is the electrochemical sensor behavior both in individual solutions and mixed liquid media. It was determined experimentally that values of K>2 could be used as a measure of reasonable sensor stability for array applications. In conclusion, it must be noted that the exact optimal values of cross-sensitivity parameters should be determined in each case individually. In particular, the value of the average slope can vary significantly. The parameters for cross-sensitivity estimation were developed and applied only for potentiometric chemical sensors. However, since no assumptions about the mechanism or theoretical description of sensor response were considered for cross-sensitivity parameter assessments, but only the experimental response value and its standard deviation, the same method could be applied for other types of sensors.

1.3 Data Processing: Multivariate Analysis

The other important aspect of multisensor analysis, apart from the sensor arrays, is the signal processing. The use of multivariate analysis methods together with sensor arrays has shown to be very powerful. Two main issues are dealt with, to search for a structure and correlation in the data or to make a model from a calibration set of data, which is then used to make predictions from test data.
Principal component analysis (PCA) is a mathematical transform which is used to explain variance in experimental data ([18]). The data matrix consists of a number of experiments, each consisting of a number of variables. PCA decomposes the data matrix into latent variables which successively account for

as much variance as possible. The loading vectors describe the direction of the principal components in relation to the original variables, and the score vectors describe the direction of the principal components in relation to the observations. A loading plot can be made, showing the relationships between the original variables and how much they influence the system. A corresponding score plot shows the relation between the observations or experiments, and groupings of observations in the score plot can be used for classifications. No prior knowledge about samples or variables is required, and the data structure is represented on as few latent variables as possible. A drawback is that it is difficult to give meaning to the components extracted.
To make models from calibration sets of data, different techniques can be used, e.g. projections to latent structures (PLS) and artificial neural nets (ANN). PLS is a statistical, linear model, in which principal component analysis is performed on both the dataset (e.g. the sensor signals) and the corresponding actual values (e.g. the concentrations, [19]).
A linear regression is then performed on each principal component between the dataset and the corresponding actual values, in order to obtain a useful regression model between these. The ANNs are especially valuable because of their adaptability to almost any mathematical transform. The models obtained are non-linear, thus being able to adapt to non-linear processes.
An ANN can be divided in different layers, an input layer consisting of input signals, one or more hidden layers and an output layer. A brief overview of some methods, which are most often used in this field, together with their main features, is shown in table 1.1.
Theoretical discussions of available methods and case studies of different sensor

Method	**Linear**	**Supervised**	**Advantage**	**Drawback**
PCA	Yes	No	Easy to interpret	Sensitive to the drift in the data
PLS	Yes	Yes	Statistical description of the results	Sensitive to the drift in the data
SOM	No	No	2D representation of the data of any dimensionality	Work as black box
BPNN	No	Yes	Easily deals with nonlinear data	Work as black box

Table 1.1: Overview of principal data-analysis methods

applications can be found in numerous books, manuals and papers, e.g. [20] - [22].

1.4 ET history: the first prototype

The first multisensor system for liquid analysis, which could be called an electronic tongue in the proper sense of the term, was a taste sensor (recently,

introduced in 1990 by Toko and co-workers ([23], [24]) of Kyushu University, Japan. The taste sensor consisted of eight potentiometric sensors with thick-film polymer membranes based on poly(vinyl chloride) (PVC). The membranes contained dioctyl phenylphosphonate (DOPP) as plasticizer and active substances called *lipids* by the authors, tetrahydrofuran being used as a solvent ([25] - [27]). Membrane compositions are given in table 1.2.

These membranes were used for the preparation of potentiometric sensors

Channel	**Lipid (abbreviation)**
1	Decyl alcohol (DA)
2	Oleic Acid (OA)
3	Dioctyl phosphate (DOP))
4	DOP:TOMA = 9:1
5	DOP:TOMA = 5:5
6	DOP:TOMA = 3:7
7	Trioctylmethylammonium chloride (TOMA)
8	Oleylamine (OAm)

Table 1.2: Representative examples of Liquid-Based Ion-Selective Electrodes

with a liquid inner filling. Potential values of the sensors were measured versus the conventional Ag/AgCl electrode. Potentiometric measurements were made using an eight-channel scanner connected to the sensors through a high-input impedance amplifier. The manipulations with the sensor array were done by a robot arm, the overall system performance being controlled by computer. A schematic diagram of the taste sensor is shown in figure 1.1.

The device was named a taste sensor because it was claimed to perceive the

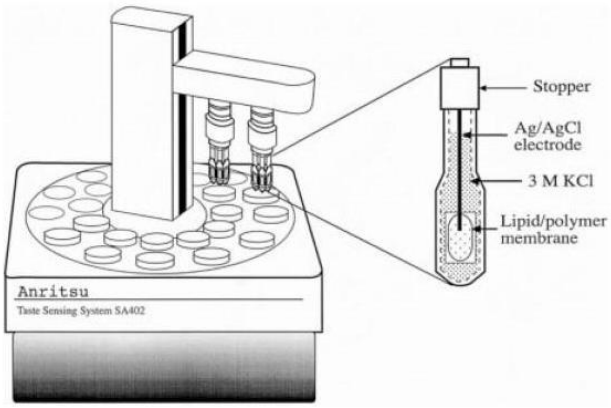

Figure 1.1: Taste-sensing system SA402, Anritsu

taste of food in the same manner as by humans. The sensors with PVC mem-

branes containing lipids are supposed to differentiate between tastes instead of detecting each substance selectively. This means that the sensor should respond similarly to substances eliciting similar tastes independently of their chemical structure.

The sensitivity of the taste sensor was studied in aqueous solutions of five basic taste substances: salty (NaCl, KCl, KBr), sour (HCl, citric and acetic acids), bitter (quinine), umami (monosodium glutamate) and sweet (sucrose) ([28],[29]). The taste sensor output exhibits different patterns for chemical substances which have different tastes, whereas it exhibits similar patterns for chemical substances with similar tastes. The sensor sensitivity (response slope) to sour and salty substances, i.e., HCl, organic acids, NaCl, KCl, and KBr, was about 50-60 mV/pX. These values correspond to the typical values known for ISEs and may be explained by the sensitivity to pH, alkali metal cations and halogen anions. The sensitivity to glutamate was found for one sensor and the slope was about 13 mV/pX. Also, the sensitivity of some sensors to quinine hydrochloride with a response slope of about 50 mV/decade was demonstrated. The reported sensitivity to another alkaloid, caffeine, was low, about 5 mV/pX. The sensitivity to natural sweet substances (sucrose) was very low. In contrast, some sensors responded to the change in concentration of the artificial sweetener aspartame with a slope of about 40 mV/pX. Therefore, in the cases when the sugar concentration was crucial, an enzymatic glucose-selective sensor was used together with the taste sensor ([30]).

The sensitivity of the device to astringent and pungent substances was investigated ([31], [32]). No sensitivity to pungent substances such as capsaicin, piperine, and allyl isothiocyanate was found. However, the taste sensor displayed a response to substances with an astringent taste: catechin, tannic acid, chlorogenic acid, and gallic acid. The astringency area was located between bitterness and sourness on principal component plots of the taste substances. Amino acids and dipeptides, which elicit complicated tastes from sour and bitter to sweet, were classified according to their tastes using the taste sensor ([33] - [36]). A principal component analysis (PCA) score plot of amino acids is shown in figure 1.2.

The strength of bitterness of the amino acid L-tryptophan was estimated in terms of quinine concentration.

The sensitivity to taste substances of polymer membranes of the same compositions as described above was studied using impedance measurements ([37], [38]). The impedance measurements were performed on thin-film membranes, which were prepared by dip-coating or by deposition of a Langmuir-Blodgett film. In contrast to the electric potential, the impedance of the membrane changed significantly in the presence of two umami substances simultaneously and sucrose. It was also found that impedance of the Langmuir-Blodgett polymer film increased in the presence of many bitter substances, which were both electrolytes and non-electrolytes.

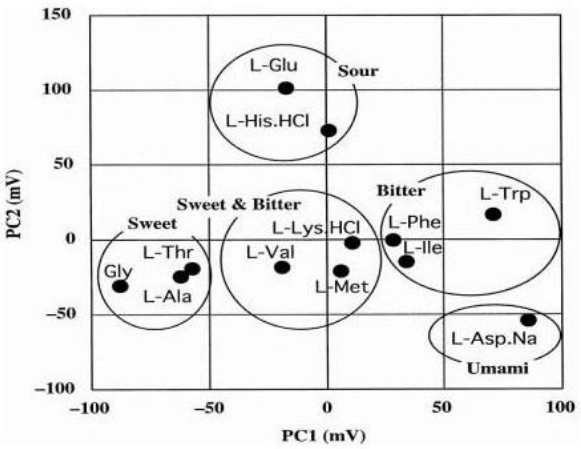

Figure 1.2: Discrimination of taste of amino acids using the taste sensor

1.5 Applications of ET systems

The main application area of electronic tongue systems is the analysis of foodstuffs and beverages in particular. The analysis of foodstuffs included different tasks: discrimination between different sorts, brands, and products of different quality, their classification, and quantitative determination of the content of various compounds. The most exciting application area of electronic tongues is taste quantification, which is understood as the assessment of taste (flavor) characteristics of a product using an electronic tongue and correlation of its response to human sensory perception. Since the different types of analysis were in many cases performed simultaneously and during the same experimental sessions, the discussion of electronic tongue applications will be arranged according the media analyzed.

1.5.1 Analysis of Beverages

Mineral waters

A large number of beverages and liquid foods have been analyzed using electronic tongue systems. Mineral waters represent relatively simple and, hence, ideal samples for analysis using the sensor systems.
The quality of drinking water varies due to the origin and quality of the raw water, untreated surface or ground water, but also due to efficiency variations in the drinking water production process. Problems can be related to occurrence of algae, bacteria, pesticides and herbicides, industrial contamination, etc. in the raw water. The character of the raw water, the biological activity at the

production plant as well as in the distribution net may all cause quality problems like bad odour/taste and/or unhealthiness. There are repeatedly controls done of the performance of the drinking water production process, but due to a rather low sampling frequency it is hard to register occasional changes. A method for monitoring variations in the raw water quality as well as the efficiency of separate process steps would therefore be of considerable value.
In [9] Martinez-Manez et al. reported the application of a potentometric sensor array for the analysis of six Spanish natural waters; dataset was completed by tap water (from Sagunto and Valencia) and by osmotised water.
Sensor array was composed of a wide range of different surfaces prepared in thick-film technology, namely RuO_2 (with resistivities of 10Ω/sq and $1M\Omega$/sq), C, Ag, Ni, Cu, Au, Pt, Al and small sticks of Sn, Pb and C (graphite), for a total of 12 electrodes which were used as active system for potentiometric measurements. Three masks were used for the sensor development, corresponding to three layers: namely, the conductive layer working as a conductor of the signal, the active layer and the upper protection layer.
Measurements were carried out using the operational amplifier OPA129P with high input impedance ($10^{15}\Omega$) in buffer configuration and an active pass-bass filter to avoid interferences from the electrical network; all the potential values were calculated referring to a *blank* value (25^0C, 10 mL of 0,1 M NaCl, 10 mL of phosphate buffer $pH = 7$ and 180 mL of distilled water) after a 5 minutes measure; data were finally analysed by PCA technique and the scores and the loadings plot with the first two latent variables is presented in figure 1.3.
As can be deduced from the figure, the PCA analysis is capable of discriminat-

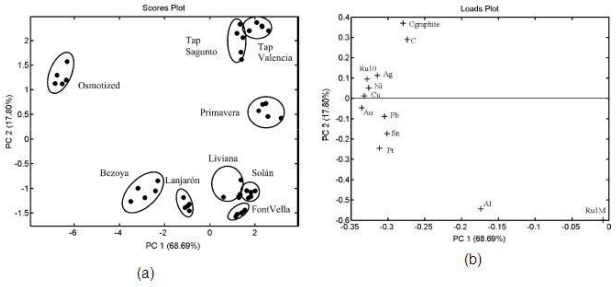

Figure 1.3: (a) Principal component analysis (PCA) scores plot for different waters. Data show from five different trials. PC axes are calculated to lie along lines of diminishing levels of variance in the data set; (b) Loads of each electrode in PCA analysis

ing between waters with a close chemical composition (figure 1.3). This is the case, for example, of Lanjaron and Font-Vella mineral waters or, for instance, the discrimination between osmotised and Lanjaron waters that, despite their very close value of conductivity, rH and pH, are clearly differentiated in the PCA plot.

Figure 1.3 show the loads of each electrodes in the PCA analysis. It can be observed that despite some electrodes which are far apart in the loads plot, many metallic electrodes show a strong correlation. Therefore it appeared advisable to make a thorough study using neuronal networks algorithms to look for a reduced set of electrodes.
A qualitative analysis of the different waters was performed using fuzzy ARTMAP neural networks. This consisted in a 9-category classification (nine different waters were tested). Prior to perform the analysis, the data matrix was normalised by subtracting its absolute minimum (e.g. a negative value) followed by the division by its absolute maximum. As a result of this process, every element in the normalised data matrix lay in [0, 1], which is a necessary condition to run the fuzzy ARTMAP network. Two different fuzzy ARTMAP models were built, which corresponded, either to the use of the 12 electrodes or to a restricted number of electrodes (according to loadings plot) and the confusion matrix is represented in table 1.3.

Another application is reported by Lvova et al. in [39]. Disposable all-

	a	b	c	d	e	f	g	h	i
Model 1									
a	5								
b		5							
c			5						
d				4	1				
e				1	3	1			
f					1	4			
g							5		
h								5	
i									5
Model 2									
a	5								
b		5							
c			5						
d				4	2				
e				1	3				
f						5			
g							5		
h								5	
i									5

Table 1.3: Confusion matrices for the two fuzzy ARTMAP classifiers built to discriminate between different waters; Model 1: built using 12 electrodes; Model 2: built using 7 electrodes. Samples: a: Primavera, b: Bezoya, c: Lanjaron, d: Livian, e: Solan, f: Font-Vella, g: Tap Valencia, h: Tap Sagunto, i: Osmotised

solid-state planar-type potentiometric electronic tongue has been developed

with the carbon paste electrode array screen-printed on a polymeric substrate. Highly cross-sensitive solvent polymeric membranes based on different matrices [poly(vinyl chloride) (PVC), aromatic polyurethane, and polypyrrole (Ppy)] and doped with common electroactive components for potentiometric measurements were deposited on the screen-printed carbon paste electrodes (SCPEs). The composition of sensor array is reported in table 1.4.

The potentiometric performance of each membrane was firstly examined in

Matrix	**Plasticizer**	**Ionophore**	**Additive**
PVC	DOA	TDDA	KTpClPB
ArPU	DOA	DODMA	NaTPB
PVC	o-NPOE	MnTPPCl	-
PVC	o-NPOE	ETH 1810	KTpClPB
PVC	DOA	ETH 2120/ ETH 129/ valinomicin/ nonactin	KTpClPB
PVC	DOS	Nonactin	-
PVC	o-NPOE	ETH 7075	ETH-500
PVC	DOA	-	-
Ppy	1-Methoxy-2-propanol	-	-
PVC	DOS	12-Crown-4-ether	-
PVC	DOS	ETH 2120	-
PVC	o-NPOE	ETH 1117	KTpClPB

Table 1.4: Composition of sensing membranes used in the electronic tongue array

0.,M Tris-H_2SO_4 (pH=7.2) by varying the concentration of different ions stepwise from 10^{-5} to 10^{-1}M at every 100 s. The same background electrolyte was used as a conditioning solution for the electronic tongue chips before and between the measurements of various beverage samples. It was then applied for the identification of eight commercial mineral waters and tap water in continuous flow injection mode and data were analysed by PCA. The scores plot is represented in figure 1.4.

It was found that the first two principal components, PC1 (55%) and PC2 (25%), account for the 80% of all system variance. The PC1 axis closely reflects the variations in pH of water samples, which is related to the degree of carbonation. The PC2 axis varies with the total mineral contents in water samples. Thus, in terms of human tasting, the PC1 may indicate sharp taste, while the PC2 bitter-salty tastes. The results suggest that the all-solid-state ET chips developed were very useful to discriminate the types of potable water samples. The third principal component, PC3 axis, accounts for 8% of system variance and was closely related to the variations in sensor performance with time, indicating the effective use life of the electronic tongue chips.

Quantitative analysis for the total inorganic components content was also performed for six mineral waters (e.g. Puriss, Sam Da Soo, Yakult, Dongwon Saemmul, Soon Soo, Cho Jung Su) and the results were compared with the

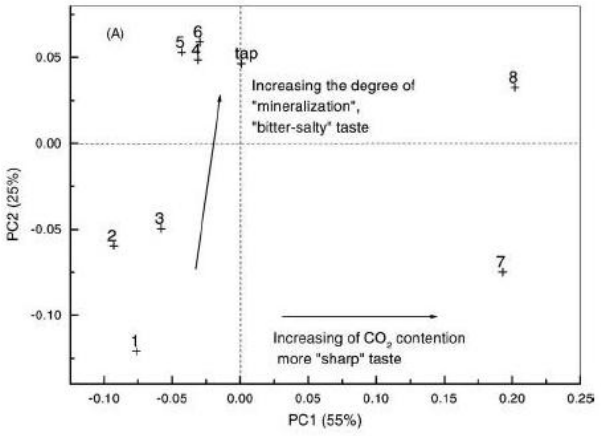

Figure 1.4: Principal component analysis (PCA) plots for potable water analysis obtained from the all-solid-state electronic tongue chips

values supplied by the bottlers, with leave-one-out cross-validation technique. PLS model results are given in figure 1.5.

Fruit juices

ET systems were also used as a classification tool for qualitative and quantitative analysis of fruit juices. One of the first applications is reported in [40]; Legin and co-workers performed different experiments on orange and grape juices. They firstly classified the different kinds of juices, then the quality monitoring of fruit juices was carried out in two steps:

- two identical packages of fruit juices were opened simultaneously and measured every hour during the first four hours; for 2 weeks, one vessel has been stored in refrigerator and the other one at room temperature. Measurements were taken two times a day to observe the differences in aging and spoilage processes;

- the first measurements were taken every hour for 5 hours after opening and later 6 times a day for a week; juice was stored in refrigerator.

Sensor array was composed of conventional ISEs (potassium-, chloride- and sodium-selective electrodes and pH glass electrode) and chalcogenide vitreous sensors, for a total of 21 electrodes. Data were finaly analyzed by PCA and different kinds of neural networks. Results are represented in figure 1.6.
It was found that during the first 4 hours after opening rapid evolution of fruit juice occurred, which could be clearly observed in PCA score plot (figure 1.6

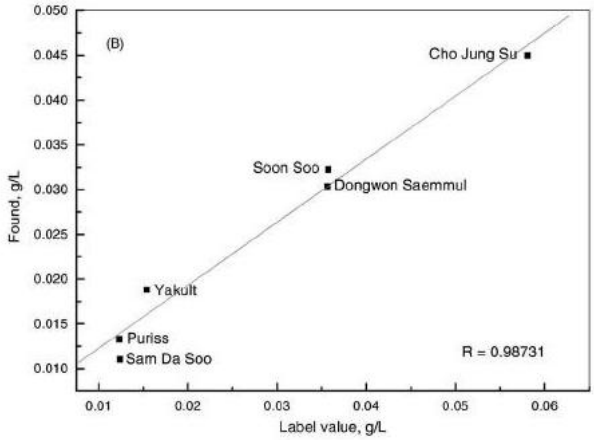

Figure 1.5: Correlation between the results from electronic tongue chip output and the values provide by the manufactures

(a)). During the first 5 hours after package opening were rather distant from each other, while the second data set (7−30 and 25−122 hours) was less evolving, thus indicating slow variations of juice integral composition. Figure 1.6 (b) shows the correlation between estimated and real time of juice storage. The most of points are close to the line which correspond to theoretical dependence, demonstrating good reliability of sensor array analysis.
Another application is represented by Ciosek et al. in [41], where they describe the application of an ion-selective-electrode array for the discrimination of several brands of apple juices. The membranes, prepared with standard ISE preparation method, contained appropriate ionophores, 20 - 50 mol% versus ionophore lipophilic salt, 61 wt.% plasticizer, and 31−33 wt.% high-molecular-weight PVC (table 1.5)
Sensors cross-sensitivity was firstly evaluated by calculating selectivity coefficients (Nicholsky equation) with separate solution method; array was then applied for the measure of juices; data were analysed by PCA technique and the scores plot of the first two principal components is represented in figure 1.7.

Coffee

Recognition of different sorts of coffee using the electronic tongue and especially the correlation of instrument output with human perception of coffee flavor are challenging and important tasks. All commercial brands of coffee are blends of different sorts of coffee beans. The quality of harvests differs from year to year but the same coffee brands must be prepared each year with a reproducible and familiar characteristic flavor. This procedure is performed by taste panels and,

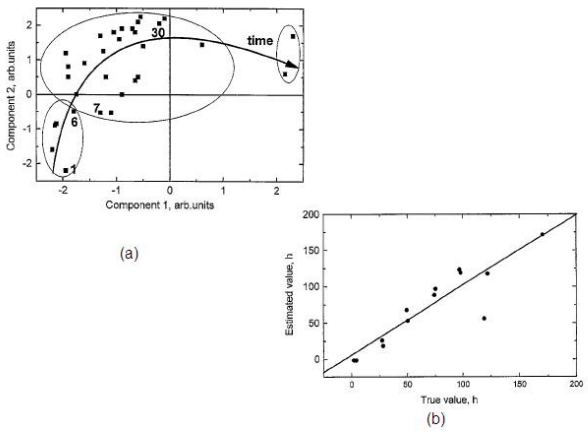

Figure 1.6: (a) The evolution with time of orange juice quality estimated by ET; (b) simulation of juice aging data with the help of artificial neural network

hence, is time consuming and expensive. The possibility of partially replacing humans in the coffee industry could have a large practical impact. Therefore, numerous attempts to use sensor systems for coffee analysis were carried out. Measurements with a taste sensor were performed on 10 brands of coffee of different origins, one of which was used as the standard, in [42]. Coffee recognition was performed using a potentiometric electronic tongue. Ten coffee samples were analyzed, consisting of seven individual sorts and three commercial brands. The measurements were performed on coffee brews which were prepared using a weighed amount of coffee and an exact water volume and cooled to room temperature. The electronic tongue was able to distinguish all coffee samples. The experiments made with different coffee concentrations and water compositions (distilled, distilled with sodium chloride and tap water) showed that the coffee samples were correctly distinguished in all cases. Coffee taste assessments made by a professional sensory panel were obtained from the manufacturer along with the coffee samples. Four parameters were evaluated: flavor, acidity, body and smell, which obviously characterize the taste, odor and flavor of the coffee. A PCA score plot of coffee sample recognition together with direction of change of coffee flavor parameters is shown in figure 1.8.

It was found that the first PC correlates with the flavor and smell of coffee. Then multivariate calibration was performed using a back-propagation neural network, taste panel scores being used as the reference data. Subsequently, the electronic tongue could correctly predict the sensory assessment values of all four flavor parameters.

Electrode type	Plasticizer	Lipophilic salt	Ionophore	Internal filling/ conditioning solution
Cl^-	o-NPOE	0.08 wt.% TDMAC	1 wt.% TPPClMn	0.01/0.001M NaCl
F^-	o-NPOE	0.18 wt.% TDAB	1.5 wt.% uranyl salophene	0.01/0.001M NaCl
NO_3^-	o-NPOE	-	3.5 wt.% TDMAC	0.01/0.001M NaCl
HCO_3^-	DOS 0.15 wt.% TDMAC	1 wt.% ETH 6010	0.1M NaH_2PO_4, 0.1M Na_2HPO_4, 0.01 NaCl/0.01M NaH_2PO_4, 0.01 NaCl/0.01M NaH_2PO_4, 0.01 M Na_2HPO_4, 0.001M NaCl	
K^+	o-NPOE	0.4 wt.% KTFPB	1 wt.% valinomycin	0.01/0.001M KCl
Na^+	o-NPOE	0.15 wt.% KTPClPB	1 wt.% ionophore X	0.01/0.001M NaCl
NH_4^+	BPPA	1 wt.% KTPClPB	2 wt.% nonactine	0.01/0.001M NH_4Cl
Ca^{2+}	DOS	0.8 wt.% KTPClPB	2 wt.% ETH 129	0.01/0.001M $CaCl_2$

Table 1.5: Solutions and components used for electrodes preparation

Milk and Dairy Products

Another widespread application area of electronic tongues is the analysis of fresh and fermented milk. The most important practical tasks are the discrimination of milk that has undergone different heat treatments, since the latter affects both milk flavor and nutritive value, and also monitoring of the milk souring process and bacterial growth.

A taste sensor was applied for measurements in milk focusing on the recognition of samples that had undergone different heat treatments and correlation of the system output with human perception ([43]). The measurements were performed on seven milk samples. Four milk characteristics were evaluated: richness, deliciousness, and cooked flavor estimated by tasters and whey-protein nitrogen index (WPNI), which defines the degree of protein denaturation due to the heating and which is determined by infrared spectroscopy. It was found that the response of the sensor containing trioctylmethylammonium chloride was correlated with the richness of milk taste with a correlation coefficient of 0.885. The response of the sensor containing decyl alcohol was correlated with WPNI with a correlation coefficient of 0.953. An attempt to distinguish milk samples which had been homogenized under different pressures and thus contained fat globules of different size was alsoperformed ([44]). However, the sensor responses were only slightly different in the milk samples and the potential changes were less than 0,5 mV.

Other applications, involving the study of milk samples that had undergone different heat treatments (ultra-high temperature (UHT) and pasteurized) from different manufacturers stored at room temperature and in a refrigerator using a potentiometric electronic tongue can be found in ([45], [46]). Devices were able in both cases to discriminate UHT and pasteurized milk samples and also the same type of milk produced by different manufacturers.

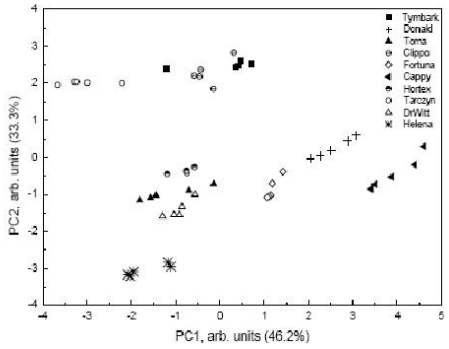

Figure 1.7: PCA plot of different brands of apple juices

Alcoholic Beverages

ET applications have been often focused on qualitative and quantitative analysis of alcoholic beverages, such as wines both white and red ones and several articles can be found ([47]-[50]), but applications on strong alcoholic drinks can be found too, due to the their diffusion all around the world.
An example is given by [51]. Legin and co-workers applied an ET system to the analysis of ten brands of vodka (obtained from a big Moscow distillery, produced using two types of spirit of different purity, three types of water and containing different additives such as citric acid, sugar, dried milk, sodium acetate, etc.), six samples of ethanol (four samples of alimentary ethanol of three grades allowed for vodka production and two types of synthetic ethanol) and six samples of eau-de-vie (obtained from Martel). Sensor array used for measurements in the spirits comprised 20 potentiometric sensors, with both chalcogenide glass and PVC plasticized membranes, showing high cross-sensitivity to organic substances. Some results are given in figure 1.9.
Developed system was able to successfully distinguish among different samples, detecting the presence of contaminants in vodka in concentrations exceeding allowed levels, distinguishing synthetic and alimentary grain ethanol as well as alimentary ethanol of different grades and samples of eau-de-vie produced by different distillation technologies and samples kept in contact with different types of oak.

Analysis of Vegetable Oils

Applications on an untypical foodstuff for chemical sensor analysis, vegetable oil, can be found, e.g. in [52]. Since the oil is not conductive, a special procedure of

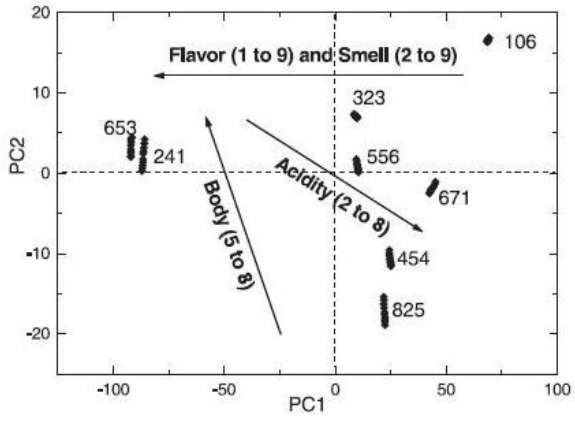

Figure 1.8: PCA score plot of different sorts of coffee

oil extraction by an organic solvent was elaborated, the resulting extract being used for the measurements. Soybean, rapeseed, and corn refined and olive mixed with vegetable, olive extra virgin, and sunflower unrefined oils were studied. The electronic tongue could distinguish all vegetable oils, including oils very close in composition such as olive extra virgin and olive refined. The electronic tongue also reliably detected the rancidity in oils.

Analysis of Biological Liquids

Application of chemical sensors for analysis of blood, blood plasma and other biological liquids started in 1970 along with the rapid development of different types of ion-selective electrodes (for example, [53] and references therein). These activities resulted in the development of ion sensors for K^+, Na^+, Ca^{2+}, Cl^- and other species with reliable characteristics and reasonable lifetime ([54]). Some of them have been successfully applied in commercial blood analysers and similar instruments.

However, since the mid 1980s the progress in this field became significantly slower due to an obvious lack of new sensing materials and new ideas. A possible revival and enhancement of potentiometric methods in analysis of biological liquids can be related to the development of multisensor systems based on the sensor array approach together with data processing using pattern recognition methods.

The first work dealing with multisensor approach for liquids appeared in 1985 ([55]). Since that time there were several publications concerned with the application of sensor arrays and multidimensional data processing for the determination of inorganic ions. Authors of [56] and [57] used various regression methods for processing of the complex signal from a sensor array comprising five ion-

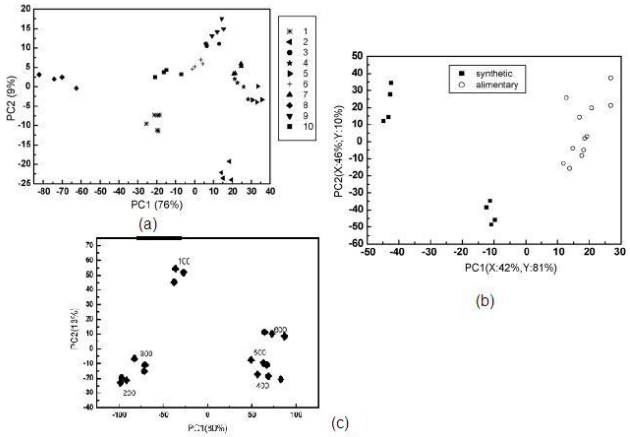

Figure 1.9: (a) Discrimination of 10 vodka brands produced by Moscow distillery; (b) Discrimination of two samples of synthetic and four samples of alimentary grain ethanol; (c) Discrimination of six samples of eau-de-vie

selective sensors in binary solutions of Na^+ and K^+ and found that both ions can be determined with an error of 0,4% for Na^+ and 5.3% for K^+.
In later studies attention has been paid to the application of artificial neural networks for fitting of data produced by ion-selective sensors ([58] - [60]). These first attempts were not developed into an analytical method of clinic analysis of biological liquids. However, there are some problems that are to be solved using the multisensor approach: the enhancement of the range of determined components, the problem of Ca/Mg selectivity during simultaneous determination, measuring of content of carbonate ions and related species, pH determination without silicate glass ion sensors, etc.

1.5.2 Analysis of non-liquid Food

Fruits and Vegetables

Although electronic tongues were primarily designed for the analysis of liquids, they could also be applied for measurements in suspensions, purees, and other watersolid mixtures or homogenates. A sample preparation is a necessary step in this case and it can be performed in different ways. Products with a high water content such as fruits and some vegetables can be crushed and the measurements can be performed on the resulting pulp. Other products with lower water content, e.g., flesh food, should first be minced and then mixed with distilled water.
Recognition of different tomato varieties was performed with a taste sensor ([61]). The measurements were performed on crushed tomato pulp. For quantification of tomato taste, the taste sensor was first calibrated with canned tomato

juice, to which four basic taste substances, NaCl, citric acid, monosodium glutamate, and glucose, were added. The experimental data were processed by PCA and then the measurements on several tomato varieties (without additives) were projected on to the principal axes, which represented a kind of taste map. The resulting taste assessment agreed well with human perception.
A taste sensor was applied to measurements on another non-liquid foodstuff, miso, which is Japanese fermented soybean paste ([62]). Chemical parameters (e.g., titratable acidity) during the miso fermentation process are measured by conventional analytical methods, while ripeness and taste quality are estimated by humans. In the present study, the possibility of replacing part of the routine analysis by simpler measurements using a sensor system was evaluated. It was found that the taste sensor output changed linearly with time of miso fermentation (figure 1.10 (a)) whereas changes in sensor responses in ripe miso during the storage were smaller (figure 1.10 (b)). The responses of the sensors with membranes containing dioctyl phosphate and oleylamine were correlated with total acidity of miso, the correlation coefficients being 0,87 and 0,88, respectively.

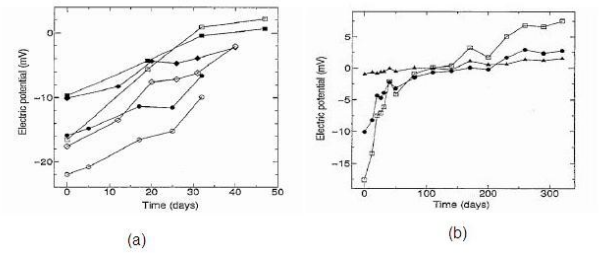

Figure 1.10: Changes in response of sensors 1 and 8 for komi-miso, mugi-miso, and awase-miso with length of fermentation. Circles denote changes for komi-miso, squares for mugi-miso and diamonds for awase-miso; solid symbols denote changes of sensor 1 and open symbols for sensor 8

Flesh Food

The applicability of the electronic tongue to flesh food analysis was demonstrated on the examples of fish and pork liver recognition ([52]). The measurements were made in a homogenate prepared by stirring chopped fish with distilled water. It was found that the system was capable of distinguishing between a sample of freshwater fish and two samples of seawater fish. The measurements were performed on fish samples which had been stored in a freezer and at room temperature.The electronic tongue could easily detect and monitor fish spoilage (figure 1.11).
In this work twelve samples of pork liver taken from animals of the same gender and age and similar breeding conditions were evaluated using the electronic tongue. Sample preparation was performed in the same way as for fish. Liver

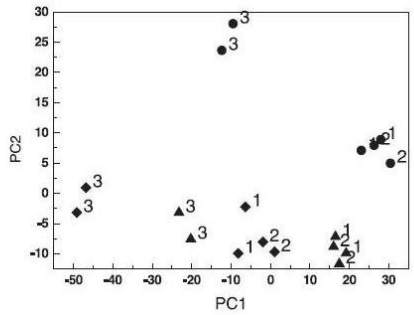

Figure 1.11: Discrimination of fresh and spoiled samples of seawater and freshwater fish

samples from different animals were reliably discriminated by the instrument. Furthermore, the liver from healthy animals was clearly separated from the liver from sick animals. Also, it was found that the electronic tongue could distinguish between samples of pork liver from animals fed with an anti-stress drug before slaughter and control animals which did not receive any medication.

Bibliography

[1] M. Holmber, M. Eriksson, C. Krantz-Kulcker, T. Artutsson, F. Winquist, A. Lloyd-Spetz, I. Lundstrom. Sensors anc Actuators B. (2004) 213

[2] K. Persaud, G. Dodd. Nature. 299 (1982) 352

[3] J.W. Gardner, P.N. Bartlett (eds.). Sensors and Sensory Systems for an Electronic Nose. NATO ASI Series E: Applied Sciences; Dordrecht: Kluwer, 1992, Vol. 212

[4] W. Gopel, Ch. Ziegler, H. Breer, D. Schild, R. Apfelbach, J. Joerges, R. Malaka. Biosens. Bioelectron. 13 (1998) 479-493

[5] G.F. Stewart, M.A. Amerine. Introduction to Food Science and Technology. New York: Academic Press, 1973

[6] Y. Kawamura, M.R. Kare. Umami: a Basic Taste. New York; Marcel Dekker, 1987.

[7] J.W. Gardner, P.N. Bartlett. Sensors and Actuators B. 18 (1994) 211

[8] Y. Vlasov, A. Legin, A. Rudnitskaya, C. Di Natale, A. D ′ Amico. Pure Appl. Chem. 77 (11) (2005) 1965

[9] R. Martinez-Manez, J. Soto, E. Garcia-Breijo, L. Gil, J. Ibanez. J. Llobet. Sensors and Actuators B. 104 (2005) 302

[10] P. Ivarsson, S. Holmin, N.E. Hojer, C. Krantz-Kulcker, F. Winquist. Sensors and Actuators B. 76 (2001) 449

[11] A. Riul Jr., H.C. de Sousa, R.R. Malmegrin, D.S. dos Santos Jr., A.C.P.L.F. Carvalho, F.J. Fonseca, O.N. Oliveira, L.H.C. Mattoso. Sensors and Actuators. 98 (2004) 77

[12] V. Parra, A.A. Arrieta, J.A. Fernandez-Escudero, M. Iniguez, J.A. de Saja, M.L. Rodriguez-Mendez. Analytical Chimica Acta. 563 (1/2) (2006) 229

[13] A.K. Deisingh, D.C. Stone, M. Thompson. International Journal Food. Sci. Technology. 39 (6) (2004) 587

[14] M. Nagele, E. Bakker, E.Pretsch. Anal. Chem. 71 (1999) 1041-1048

[15] A. Legin, Yu. Vlasov, A. Rudnitskaya, E. Bychkov. Sens. Actuators. 34 (1996) 456-461

[16] Yu. Vlasov, A. Legin, A. Rudnitskaya. Sens. Actuators. 44 (1997) 532-537

[17] A. Legin, A. Rudnitskaya, A. Smirnova, L. Lvova, Yu. Vlasov. J. Appl. Chem. (Russia). 72 (1999) 114-120

[18] S. Wold, K. Esbensen, P. Geladi. Chemomet. Intelligent Laboratory Syst. 2 (1987) 37

[19] P. Geladi, B.B. Kowalski. Anal. Chim. Acta. 185 (1986) 1

[20] Neural Computing. Pittsburgh, PA: Neural Ware, 1997

[21] K. Esbensen, S. Schonkopf, T. Midtgaard, D. Guyot. Multivariate Analysis in Practice. Norway: Camo ASA, 3rd edn., 1998

[22] H. Martens, T. Naes. Multivariate Calibration. New York: Wiley, 1989

[23] K. Toko, K. Hayashi, M. Yamanaka, K. Yamafuji in: Technical Digest of 9th Sensor Symposium. 1990, pp. 193-196

[24] K. Hayashi, M. Yamanaka, K. Toko, K. Yamafuji. Sensors and Actuators B. 2 (1990) 205-213

[25] K. Toko. Mater. Sci. Eng. C 4 (1996) 69-82

[26] K. Toko. Meas. Sci. Technol. 9 (1998) 1919-1936

[27] K. Toko. Sens. Actuators B. 64 (2000) 205-215

[28] K. Oohira, K. Toko, H. Akiyama, H. Yoshihara, K. Yamafuji. J. Phys. Soc. Jpn. 64 (1995) 3554-3561

[29] K. Hayashi, K. Toko, M. Yamanaka, H. Yoshihara, K. Yamafuji, H. Ikezaki, R. Toukubo, K. Sato. Sens. Actuators. 23 (1995) 55-61

[30] S. Iiyama, Y. Suzuki, S. Ezaki, Y. Arikawa, K. Toko. Mater. Sci. Eng. C. 4 (1996) 45-49

[31] S. Iiyama, K. Toko, T. Matsuno, K. Yamafuji. Chem. Sens. 19 (1994) 87-96

[32] S. Iiyama, S. Ezaki, K. Toko, T. Matsuno, K. Yamafuji. Sens. Actuators B 24 (1995) 75-79

[33] Kikkawa, Y., Toko, K., Matsuno, T., Yamafuji, K., Jpn. J. Appl. Phys. 32 (1993) 5731-5736

[34] K. Toko, T. Fukusaka. Sens. Mater. 9 (1997) 171-176

[35] T. Nagamori, K. Toko in: Digest of Technical Papers of Transducers 1999, Sendai,Japan, 62-65

[36] K. Toko, T. Nagamori. Trans. IEE Jpn. E 119 (1999) 528-531

[37] H. Akiyama, K. Toko, K. Yamafuji. Jpn. J. Appl. Phys. Part 1. 35 (1996) 5516-5521

[38] K. Toko, H. Akiyama, K. Chishaki, S. Ezaki, T. Iyota, K. Yamafuji. Sens. Mater. 9 (1997) 321-329

[39] L. Lvova, S.S. Kima, A. Legin, Yu. Vlasov, J.S. Yang, G.S. Chaa, H. Nam. Analytica Chimica Acta. 468 (2002) 303-314

[40] A. Legin, A. Rudnitskaya, Yu. Vlasov, C. Di Natale, F. Davide, A. D'Amico. Sensors and Actuators B. 44 (1997) 291-296

[41] P. Ciosek, Z Brzozka, W. Wroblewski. Sensors and Actuators B. 103 (2004) 76-83

[42] T. Fukunaga, K. Toko, S. Mori, Y. Nakabayashi, M. Kanda. Sens. Mater. 8 (1996) 47-56

[43] K. Toko, T. Iyota, Y. Mizota, T. Matsuno, T. Yoshioka, T. Doi, S. Iiyama, T. Kato, K. Yamafuji, R. Watanabe. Jpn. J. Appl. Phys., Part 1 34 (1995) 6287-6291

[44] C. Di Natale, R. Paolesse, A. Macagnano, A. Mantini, A. D'Amico, A. Legin, L. Lvova, A. Rudnitskaya, Yu. Vlasov. Sensors and Actuators B. 64 (2000) 15-21

[45] A. Legin, A. Rudnitskaya, L. Lvova, Yu. Vlasov, A. D'Amico, C. Di Natale, R. Paolesse in: Proceedings of 5th Italian Conference on Sensors and Microsystems, Lecce, Italy; Singapore: World Scientific, 2000, pp. 263-269

[46] A. Legin, A. Rudnitskaya, Yu. Vlasov, C. Di Natale, E. Mazzone, A. D'Amico in: Proceedings of International Conference Eurosensors XIII, The Hague, The Netherlands; 1999, pp. 1017-1020

[47] L. Rong, W. Ping, H. Wenlei. Sensors and Actuators B 66 (2000) 246-250

[48] A. Rudnitskaya, I. Delgadillo, A. Legin, S.M. Rocha, A.-M. Costa, T. Simoes. Chem. and Intell. Lab. Systems 87 (2007) 50-56

[49] S. Buratti, S. Benedetti, M. Scampicchio, E.C. Pangerod. Analytica Chimica Acta 525 (2004) 133-139

[50] C. Di Natale, R. Paolesse, M. Burgio, E. Martinelli, G. Pennazza, A. D'Amico. Analytica Chimica Acta. 513 (2004) 49-56

[51] A. Legin, A. Rudnitskaya, B. Seleznev, Yu. Vlasov. Analytica Chimica Acta. 534 (2005) 129-135

[52] Yu. Vlasov, B. Seleznev, A. Ivanov, A. Rudnitskaya, A. Legin in: Proceedings of 5th Italian Conference on Sensors and Microsystems, Lecce, Italy; Singapore: World Scientific, 2000

[53] J. Havas. Ion and Molecule-Selective Electrodes in Biological Systems, Akademiai Kiado, Budapest, Hungary, 1985

[54] E.J. Fogt, Clin. Chem. 36(8(B)) (1990) 1573

[55] M. Otto, J.D.R. Thomas, Anal. Chem. 57 (1985) 2647

[56] K. Beebe, B. Kowalski, Anal. Chem. 60 (1988) 2273

[57] K. Beebe, D. Uerz, J. Sandifer, B. Kowalski, Anal. Chem. 60 (1988) 66

[58] W.E. van der Linden, M. Bos, A. Bos, Anal. Proc. 26 (1989) 329

[59] M. Bos, A. Bos, W.E. van der Linden, Anal. Chim. Acta. 233 (1990) 31

[60] M. Bos, A. Bos, W.E. van der Linden, Anal. Chim. Acta. 233 (1995) 31

[61] Y. Kikkawa, K. Toko, K. Yamafuji. Sens. Mater. 5 (1993) 83-90

[62] T. Imamura, K. Toko, S. Yanagisawa, T. Kume. Sensors and Actuators B. 37 (1996) 179-185

Chapter 2

Tetra-pyrrolic compounds as Chemical Interactive materials

Introduction

The sensor performances in term of sensitivity, reproducibility, and selectivity strictly depend on the properties of the sensing materials. For this reason great effort has been made to develop sensing materials with improved properties ([1]). From this point of view, the exploitation of organic compounds as sensing materials is particularly advantageous. The progress made in designing synthetic receptors ([2]) allows the orientation of the sensor selectivity toward different classes of compounds via modulation of weak interactions occurring between the sensing material and the analytes.
Among the different classes of receptors developed, porphyrins and metalloporphyrins represent one of the most promising, because of the richness of their properties, their stability, and the development of the chemistry of these macrocycles that allows the possibility to modulate their properties by synthetic modifications or by changing the coordinated metal. In these applications porphyrins mimic their functions in biological systems, where they are able, for example, to reversibly bind oxygen. Since generally target analytes are also good ligands for metal ions, porphyrins represent a perfect match for the properties required to sense materials.
For this reason research in this area has experienced significant growth in the last decade and porphyrin based chemical sensors are now going to be as famous as those based on related phthalocyanines. In this chapter we want to highlight their exploitation when used as CIM in in potentiometric chemical sensors, devoted to detecting analytes in liquid phase.

2.1 Biological role of Porphyrins in nature

Porphyrins (figure 2.1) and related tetrapyrrolic pigments occur widely in nature, to provide natural systems with brilliant colors and play very important roles in various biological processes.
Heme (figure 2.2), the iron(II) protoporphyrin-IX complex, is the prosthetic group in hemoglobins and myoglobins responsible for oxygen transport in red blood cells, and oxygen storage in living tissues. Heme is also located in the

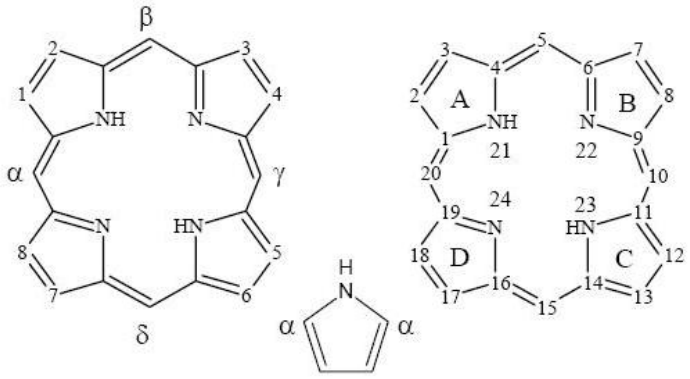

Figure 2.1: Structure and numeration of Porphyrin (IUPAC and Fisher)

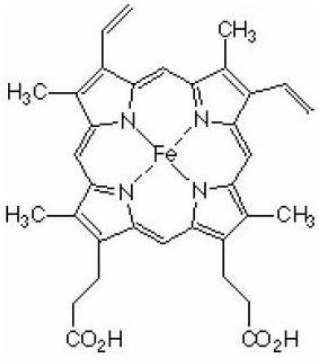

Figure 2.2: Heme (an iron-porphyrin) is the part of hemoglobin coordinating O_2 and CO

enzyme peroxidase, which catalyzes the oxidation of substrates whit hydrogen peroxide. The related enzyme catalase, also containing heme, catalyzes the breakdown of hydrogen peroxide to water and oxygen. Other heme-containing proteins include the cytochromes, which serve as one-electron carriers in the electron transport chain. Reduction of a pyrrolic unit on the porphyrin ring

leads to a class of porphyrin derivatives termed chlorines. Chlorophylls (e.g. chlorophyll-a), found abundantly in green plants, are classified in this category and play an essential role in the process of plant photosynthesis. Further saturation of another pyrrole unit on chlorins provides another type of porphyrin derivative termed bacteriochlorins, in which the saturated pyrrole units are diagonally opposite to each other. One of the vitamins, vitamin B_{12}, also contains a porphyrin-like unit called corrin, a reduced form of corrole. Porphyrins are also found in other systems such as the oxygen-carrying pigment chlorocruorin from Sabella starte indica ([3]) and in oil shales ([4]).

2.2 A brief history of Porphyrin chemistry

Thudichum ([5]) developed the first preparation of a porphyrin in 1867 by treatment of haemoglobin with concentrated acid. A few years later by a similar route, Hoppe-Seyler ([6]) obtained a purple substance which he called hematoporphyrin. However, these procedures failed to provide a pure sample of porphyrin.
Approximately 30 years later, Nencki isolated the first pure sample of porphyrin ([7]), preparing hematoporphyrin hydrochloride from isolated hemin. These initial studies marked the beginning of porphyrin chemistry, which now includes many disciplines of science and medicine and continues to flourish.
Porphyrins (figure 2.1) possess a basic skeleton consisting of four pyrrole units linked by four methane bridges. This skeletal structure was first proposed by Kuster in 1912 ([8]). However, it was suggested by both Fischer and Willstatter that such a large ring system would not be very stable; they proposed other structures containing smaller ring systems. The debate over the actual structure of a porphyrin continued until 1926 when Fischer successfully synthesized etioporphyrin-I by the first totally synthetic pathway ([9]).
Shortly thereafter, Fischer completed the synthesis of octamethylporphyrin ([10]) by two distinctly different methods. These preparations led to the acceptance of the structure initially proposed by Kuster as the basic structure of porphyrins. By 1975, almost all metals and some semimetals had been combined with a porphyrin ligand. These elements are shown in the so-called periodic table of metalloporphyrins. The development of this periodic table took place in five stages ([11]):

- **Stage I**: Metallo-porphyrins provided by nature - Mg (in the chlorophylls); Fe (in the hemes); Ni, V (mineral oils), Cu (*Turacus indicus*), Mn (blood), Zn (yeast mutants), Co (vitamin B_{12});

- **Stage II**: Recognition of hemin and chlorophyll as species containing the -N_4FeCl- and -N_4Mg- coordination groups, respectively, by Richard Willstatter in 1913 in his famous book on chlorophyll ([12]). In the decade before, one had learned to insert Fe, Co, Mn, Cu, Zn, Ni and Sn into porphyrins ([11]) and Mg into chlorophyll ([12]);

- **Stage III**: Culmination of Hans Fischer work ([13], [14]) in 1940 which was reviewed by Treibs ([15]). At that time, Metallo-porphyrins containing Na, K, Mg, Zn, Cd, Hg, Cu, Ag, Ni, Pd, Pt, Co, Fe, Mn, Al, Ga, In, Tl, V, Ge, Sn, Pb, As and Sb were known ([11]); Li, Be, and Cr had been combined with phtalocyanine by Linstead ([16]);

- **Stage IV**: Publication of Falk monograph on porphyrins and metallo-porphyrins ([17]) in 1964. Here, the *further coordination*, i.e. the addition, elimination and substitution of axial ligands received a thorough evaluation. New metals at this stage were Li, Rb, Cs, Be, Ca, Sr, Ba, Si and Au ([11]);

- **Stage V**: The present time is characterized by the application of the recent achievements in X-ray cristallography ([18], [19]) and coordination chemistry ([11], [20] - [23]), to the porphyrin field. A large variety of coordination types have been detected and the periodic table of metallo-porphyrins has been completed to the present stage. New metals since 1964 are Sc, Y, La, all the lanthanoids, Ti, Zr, Hf, Th, Nb, Ta, Cr, Mo, W, Tc, Re, Ru, Os, Rh, Ir and Bi, i.e. mainly the early transition metals and the noble metals which could not be introduced by the classical methods. Even a phosphorus porphyrin seems to exist.

2.3 General properties of porphyrins

All porphyrins are derived from the cyclic porphyrin (figure 2.1), consisting of four pyrrole units connected by four methane (meso) carbons. The porphyrin macrocycle is an aromatic system containing 22π electrons of which 18 are involved in any one delocalization pathway. Porphyrins obey Huckels rule of aromaticity (4n+2p electrons, where n=4). The aromatic character of porphyrins is also evident in their NMR spectra.
H-NMR spectroscopy of porphyrins shows that the N-H protons appear at d $\approx$-5 ppm (upfield from TMS), indicative of NHs located in an anisotropic aromatic shielding cone ([24]). Whereas the methine protons appear at $\approx$ 10 ppm, a d-value indicating a highly deshielding environment resulting from the aromatic ring current. All visible absorption spectra of porphyrins display the following characteristic spectra (figure 2.3):

- **B band**: An exceedingly intense band (referred to as the *Soret band*, [25]) appears between 380 and 420 nm. It is the origin B (0,0) of the second excited singlet state and has molar extinction generally from 2 to $4 \times 10^5 M^{-1}$ cm^{-1}. This is characteristic of a highly conjugated porphyrin macrocycle. Better resolved spectra sometimes show another band $\approx$ 1250 cm^{-1} to the blue; it is attributed to addition of one mode of vibrational excitation and is denoted B(1,0);

- **Q bands**: There are several weaker absorptions at longer wavelengths between 500 and 700 nm: four visible bands are seen (sometimes called

satellite bands). The lower-energy band (sometimes called α) is the electronic origin $Q_{x,y}(0,0)$ of the lowest-energy excited singlet state. The higher-energy band (sometimes called β) includes one mode of vibrational excitation and is denoted $Q_{x,y}(1,0)$; it is actually a merging of several different vibrations. It was originally identified as a vibration on the basis of the relative constant energy gap between $Q_{x,y}(1,0)$ and $Q_{x,y}(0,0)$. The $Q_{x,y}(1,0)$ band has molar extinction coefficient in a narrow range between 1,2 and $2 \times 10^4 M^{-1}cm^{-1}$, in fact they are not allowed by selection rules.

All these bands are interpreted as (π, π^*) in origin. The nomenclature (Q and B bands) was originally given by Platt ([26]); B implies a strongly allowed excited state and Q a quasi-allowed one.
The basic porphyrin ring, as shown in figure 2.1, provides the electronic heart of a porphyrin. The ring is structured with a basic fourfold symmetry, including four nitrogen atoms directed toward the center. This electronic heart is responsible for porphyrin-type optical spectra, which are then perturbed to a greater or lesser extent by various chemical modifications to the basic structure. Variations of the peripheral substituents on the porphyrin ring often cause minor changes in the intensity and wavelength of these absorptions. Protonation of two inner imine nitrogen atoms or insertion a metal into the porphyrin cavity also changes the visible absorption spectra. These absorptions can often be very helpful in elucidating certain structural features on a porphyrin. X-ray structural determinations of both Metallo-porphyrins and free-base porphyrins have basically shown the core porphyrin to be planar, a fundamental requirement for perfect aromaticity ([27]). Measurements of heats of combustion and thermodynamics also indicate the existence of aromatic stabilization energy ([28]).
The porphyrin ring is very stable on both concentrated acid and base, and the macrocycle can act both as an acid and a base. Strong bases such as alkoxides remove the two central protons ($Pk_a \approx 16$) on the inner nitrogen atoms of a porphyrin to form a dianion. However, trifluoroacetic acid easily protonates the two free pyrrolenine nitrogen atoms ($Pk_b \approx 9$) to form a dication.
Porphyrins also undergo a number of chemical reactions typical of aromatic compounds. For example, electrophillic substitution reaction such as nitration, halogenation, acetylation, and formylation are often performed on porphyrins. Only the meso carbons and the β-pyrrolic carbons participate in these reactions. The α -pyrrolic carbons rarely take part in any kind of reaction.
Porphyrins are also capable of being metallated and demetallated. Almost every metal in the periodic chart has been inserted into the porphyrin macrocycle but most typically are: Fe, Zn, Cu, and Ni, which can be inserted into the porphyrin cavity by using simple metal salts ([11]). Demetallation can usually be achieved by treatment with acids of various strengths.

2.4 Metallo-porphyrins classification

The various kinds of metallo-porphyrins can be classified according to either their stoichiometry or geometry or both ([11], [29]). The region extending to

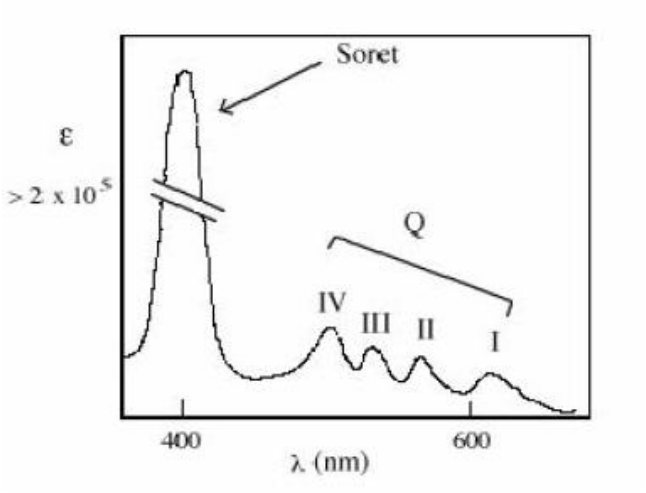

Figure 2.3: Typical UV-Visible absorption spectrum of a Porphyrin

the peripheral carbon atoms is called the *equatorial plane* and contains the four nitrogen atoms (figure 2.1). Hence, the formation and disruption of the metal-to-nitrogen bonds in a metalloporphyrin are the subject of the equatorial coordination chemistry of metallo-porphyrins. The equatorial stoichiometry - the ratio of metal atoms to porphyrin ligands - then generates the various classes of metallo-porphyrins $M_h(P)_k$ which are shown in the first column of table 2.1.

2.5 The role of the Metal ion coordinated in the inner core

Porphyrins have been widely used as CIMs for electrochemical sensors, because of their richness in coordinating several ions and of the possibility to fine tune the selectivity by introducing peripheral substituents or, mainly, by changing the metal ion coordinated in the central core of the structure.

2.5.1 The role of the metal oxidation state in the metal carrier

The higher the charge of the metal ion in the metal carrier MX_mL_n, the more sluggishly it will react, for simple electrostatic reasons; the anions X^- and the negatively polarized ligands L are more strongly attracted by the metal ion if it carries a high positive charge; a high charge impedes the deconvolution of the metal carrier. Therefore, it is advisable to use metal carriers that have the metal in its lowest conveniently accessible oxidation state. Metal carbonyls

Classes generated by equatorial stoichiometry	**Character of the $[M_h(P)_k]$ moiety**	**Types generated by stereochemistry**
Class I M(P)	**Monometallic**[b] Mononuclear $h = k = 1$	A,B, figure 2.4 C, D, figure 2.5 E, H, figure 2.6
Class II $M(P)_2$	**Semimetallic**[c] $h = 1, k = 2$	K, figure 2.7
Class III $M_2(P)$	**Bimetallic**[c] $h = 2, k = 1$	L-O, figure 2.7
Class IV $[M(P)]_2$	**Monometallic**[c] Binuclear[d] $h = k = 2$	AA-CC, figure 2.9 EE, figure 2.9 GG, figure 2.9
Class V $M_3(P)$, $M_4(P)$	**Polymetallic**[e] $h = 3, 4; k = 1$	R-I, figure 2.10
Class VI $M_h(P)_k$	**Polynuclear**[f] $h = 2; k = 2$	DKD, BCB, CCC figure 2.11 C_x, G_x, figure 2.12

Table 2.1: Classification of metallo-porphyrins $[M_n(P)_kZ_l]$[a]; [a] Metal ion, (P) porphyrin ligand, Z donor ligand atom; [b] The term monometallic specifies the M:(P) ratio, namely $h : k = 1 : 1$; [c] Semimetallic: $h : k = 0,5 : 1$; bimetallic: $h : k = 2 : 1$; [d] Binuclear regarding metal; [e] h:k $\approx$ 2:1; [f] Some of these polynuclear complexes are monometallic: $h = k$

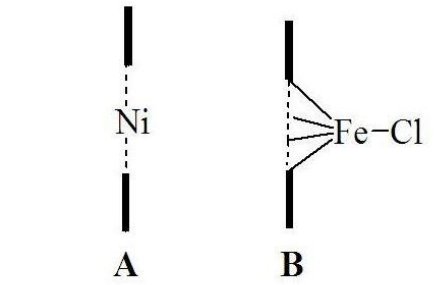

Figure 2.4: Coordination types, e.g., octaethylporphinatonickel(II), short formula Ni(OEP), type A, and hemin, FeCl(Proto), type B. The bar graphs are shown together with the usual representations of the square-planar coordination groups of (a) the square-planar NiN_4 system in A, and (b) the square-pyramidal FeN_4Cl system in B. In the latter, the Fe(III) ion is not coplanar with the porphyrin plane; in such a case, the bar graph shows all bonds extending from the metal ion

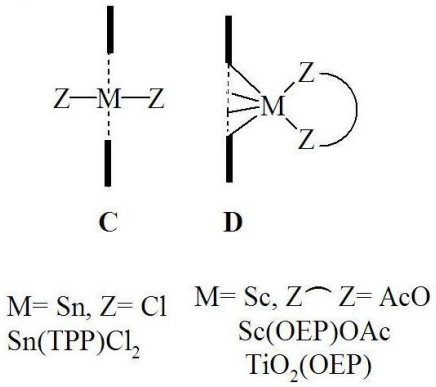

Figure 2.5: Coordination types of a general metalloporphyrin $M(P)Z_2$ where Z represents a monodentate ligand atom of any charge. C is a trans configuration; D a cis configuration with respect to the porphyrin plane. C is exemplified by dichloro(tetraphenylporphinato)tin(IV), $Sn(TPP)Cl_2$, and D by acetato(octaethylporphinato)scandium(III), Sc(OEP)OAc. D has so far only been realized with uninegative, bidentate chelating ligands, e.g., OAc^-. ZZ is the general symbol for a bidentate chelating ligand

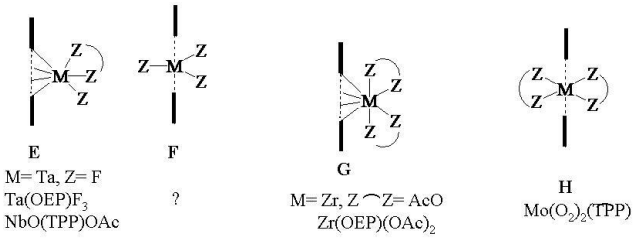

Figure 2.6: Bar graphs E-H of hepta- and octacoordinate monometallic Metalloporphyrins $M(P)Z_3$ or $M(P)Z_4$

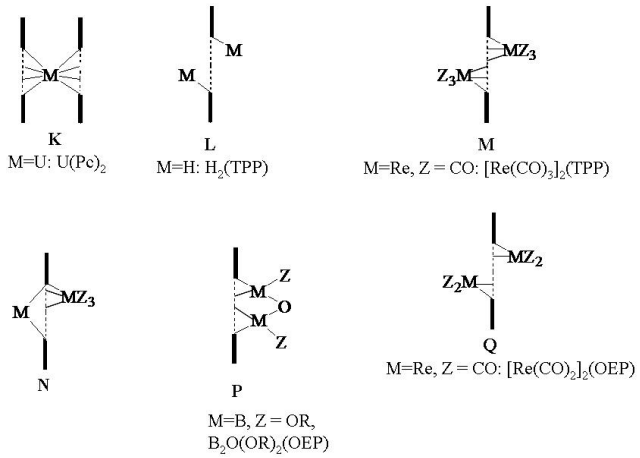

Figure 2.7: Bar graphs of a semimetallic porphyrin $M(P)_2$ (K) and some bimetallic porphyrins M_2P) (N-Q)

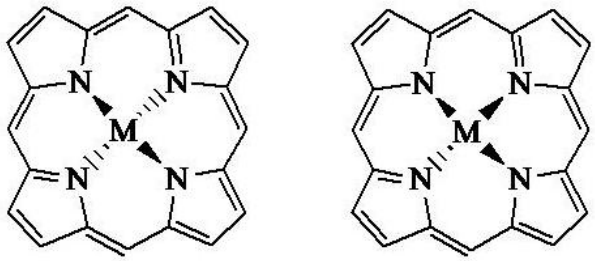

Figure 2.8: Two constitutional isomers, 3a and 3b, of bimetallic porphyrins $M_2(P)$

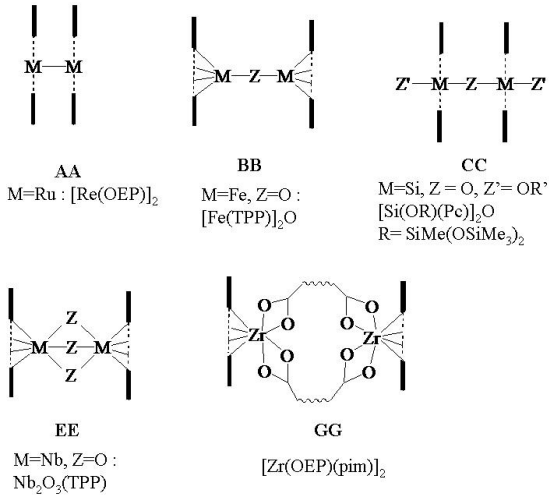

Figure 2.9: Bar graphs of binuclear Metallo-porphyrins $[M(P)]_2Z_l$, AA, BB, CC, EE and GG. They are derived from the corresponding mononuclear, monometallic porphyrins A, B, C, E and G

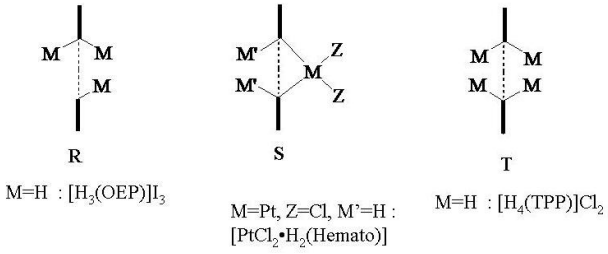

Figure 2.10: Bar graphs of polymetallic porphyrins $M_3(P)$ and $M_4(P)$

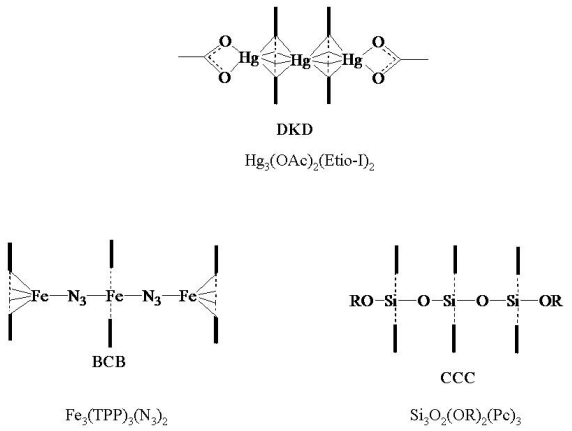

Figure 2.11: Bar graphs DKD, BCB and CCC of some trinuclear Metallo-porphyrins

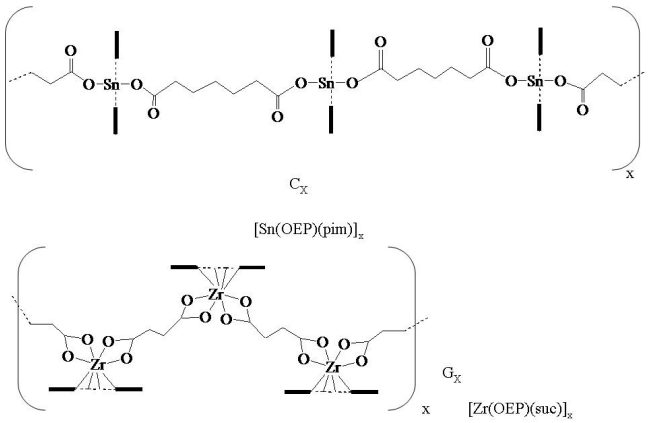

Figure 2.12: Bar graphs C_x and G_x of some polynuclear Metallo-porphyrins

are, therefore, a good choice. Most metalations starting from divalent metal ions proceed rather quickly under comparatively mild conditions, whereas the incorporation of metal ions with charges between +3 and +5 requires prolonged heating.
Of course, preference for certain high or low coordination numbers by the various metal ions also plays a role. For a given oxidation state, the metal ion preferring a low coordination number will be more easily inserted.

2.5.2 The *stable oxidation states* of metal ions in metallo porphyrins

The central metal ions in metallo-porphyrins display in most cases those oxidation states which are normal for these ions; sometimes, however, unusual oxidation states occurr under aerobic conditions, and, therefore, a change of oxidation state very easily occurrs in the course of a metalation reaction. The oxidation states which are adopted in the presence of air, i.e. of water and oxygen, are for convenience called *stable* states.
Some unusual, but stable, oxidation states are the following: Mo(V), W(V), Mn(III), Re(V) and Os(VI). These belong to metals that have several oxidation states available, being both higher and lower than the stable ones; in this case, it is thought that the stable but unusual state is selected because its ionic radius gives the best fit to the steric requirements of the porphinato ligands ([11], [29], [30]). The optimum of the ionic radius r_i, lies between 0,60 and 0,69 A for an ion which is coplanar with the porphyrin ([11]). The same olds for the choice between the two or more common oxidation states that are taken by some other metal ions: V(IV), Cu(II), Au(III), Sn(IV), Sb(V). V(V) is too small, while Cu(I), Au(I), Sn(II) and Sb(III) are too big for the hole in the porphyrin plane.
There are, however, some cases which cannot be explained by ionic radii alone. For some ions, the radius of the ion in the stable state seems too large, although it has been shown that the metal is coplanar with the porphryin, e.g. for Ag(II), where Ag(III) should be the stable state. Here, the ionic radius tabulated may not be appropriate. In the earlier papers of the autor ([11], [30]), only effective ionic radii have been used; these are valid for the coordination number $N = 6$ and metal oxides. Ionic radii of other sources do not fit the picture, as in the case with Ag(II). A useful compilation of ionic radii from various sources has been published by Shannon and Prewitt ([31]).
If, however, the proper effective ionic radius of Ag(II) were known, it might still turn out to be too big. This is also suspected for Ru(II), Os(II) and Pt(II). The high degree pf covalent bonding in the porphyrin complexes of the noble metals may make the ionic radius a completely inappropriate quantity. On the other hand, one can argue that the oxidation state of these metal ions is effectively raised be metal-to-porphyrin back-bonding; the decrease in electron density caused at the metal due to the back-donation then results in a shrinkage of the metal ion. There is a ample evidence for metal-to-porphyrin back-bonding in porphyrin complexes containing the metal ions.
Furthermore, the overlage Pb(II) and Bi(III) do not follow the ionic radius role,

although Pb(IV) and Bi(V) would fit much better. Here, the inertness of the s^2 subshell obviously stabilizes the lower oxidation state, while for the lighter homologues, Sn(II) and Sb(III) the opposite obtains.

2.5.3 Central metals of group Ia (alkali metals)

In this and the following sections, the special chemistry of metallo-porphyrins will be summarized using the general terminology described before. This section deals with the group Ia metals ([32] - [36]). The group Ib metals are treated together with the VIIIa metals because most of their complexes are more similar to the latter, with the M(II) oxidation state predominating.
Stoichiometrical data predict that alkali metal porphyrins belong to the bimetallic mononuclear species of typ L, M or Q (figure 2.7) with the assumed constitution 3b (figure 2.8). No elemental analysis were performed on the alkali metal porphyrins; thus, it is not clear wheter they will crystallize as type L without axial ligands or M or Q, where Z may be donor sites of the solvent molecules. Because of the low charge-to-radius ratio and the low electronegativity, all complexes show class V stability. Thus they can only be kept in very rigorously dried solutions, mostly in presence of an excess of metal alkoxide.
In most cases, the alkali metals are inserted by a combination of methods, e.g. by heating NaOMe with the porphyrins in absolute pyridine ([32]-[37]). Their porphyrin chemistry is little explored because of their lability.
Notable are the transmetalation studies ([36]). It is reasonable that the more adhesive metal ion M^+ replaces more weakly bound ions in

$$M_2(TPP) + 2M'J \rightarrow M'(TPP) + 2MJ \tag{2.1}$$

This has been shown for the pairs $M/M' = Na/Li$ and K/Na in pyridine at room temperature, whereas for $M/M' = Li/Na$ and Na/K in pyridine, no reaction occurred. Some divalent ions, M(II)=Zn(II), Hg(II), displace Li in pyridine at room temperature according to equation:

$$Li_2(TPP) + M(OAc)_2 \rightarrow M(TPP) + 2LiOAc \tag{2.2}$$

whereas Pb(TPP) is not attached by LiI. An excess of metal salt was administrated in all cases.

2.5.4 Central metals of groups IIa and IIb (alkaline earth and zinc metals)

The study of the alkaline earth metal ions and the zinc metal ions in porphyrin systems is of great importance in conjunction with the role of the magnesium ion in chlorophyll, which has been investigated by Katz ([38]).
Most of the the representative metallo-porphyrins have to be prepared in basic media because of their acid lability, which is expressed by stability classes IV and V. Only Zn(II) can be inserted in acetic acid as solvent, and its porphyrin derivatives are easy to handle.

Be(II) porphyrins have never been identified with certainty ([39]). As regards their chemistry, the group II metallo-porphyrins can be grouped in three classes:

- Mg and Zn;
- Cd/Hg;
- Ca, Sr and Ba.

The latter, e.g. Ca(OEP) are so labile that their chemistry is difficult to study.

Magnesium and Zinc The ionic radii of Mg(II) and Zn(II) are a little too large to fit nicely into the porphyrin hole. Thus, their porphyrin complexes have a strong preference to show the square-pyramidal coordination type B with an exoplanar metal ion. This is important for the self-association of chlorophyll molecules ([38]). Mg is the lightest central metal ion to allow type B. A light metal is necessary to remove all heavy atom effects in the energy transmission between chlorophyll molecules. The low electronegativity, furthermore, gives Mg (χ=1,31) and Zn (χ=1,65) a close relationship. Therefore, both have approximately the same, and within a large variety of central metals, the most favorable influence on the hydrogenation of porphyrins to chlorins ([29], [40]). However, the ejection of an electron from the porphyrin molecule is easier with Mg(II) than with Zn(II) ([41]). Electron ejection may be important for the closing of the isocyclic ring in chlorophyll and for photosynthesis ([40]). Thus, the specific coordination properties, the low mass and its good influence on the biosynthesis of chlorophyll, as well as the electron transport phenomena during photosynthesis, make Mg an ideal choice of nature for its purpose.

Cadmium and Mercury Because of their large diameter, Cd(II) (0,95A) and Hg(II)(1,02A) form rather unstable metallo-porphyrins. It is not understood why Hg(OEP) crystallizes a bare complex A, whereas Cd(OEP)Py B is easily obtained from the same solvent. Nevertheless, Hg(II) in porphyrins shows a remarkable tendency to increase its coordination number to 6, 7 or 8.

2.5.5 Central metals of groups VIa and VIIa

Apart from manganese which is known in porphyrins since the beginning of this century, the metals of groups VIa and VIIa had been introduced into a porphyrin only a few decased ago. In the next section, only Mn-porphyrins chemistry will be treated, since it was used as ionophore in the applications described in this Thesis.

Complexes containing Manganese Manganese porphyrins have been extensively studied because they had been thought to play a role in photosynthesis ([42]) and are easily prepared from Mn(II) with standard methods. The Mn(Proto-DME)-X(H_2O), where $X = F, Cl, Br, I, N_3, OCN, NCS$, has been investigated by Boucher ([43]) who has also reviewed the state of knowledge in Mn-porphyrins up to 1972 ([44]). As Mn(II) porphyrins easily autoxidize to Mn(III) porphyrins, it was suspected, and recently proved ([45], [46]) that they might act as oxygen carriers. Dioxygen is reversibly bound by Mn(TPP)Py or Mn(TPP) below -76 ^{0}C according to the following equation

$$Mn(TPP)Py \rightleftharpoons Mn(TPP) \rightleftharpoons Mn(TPP)O_2 \tag{2.3}$$

Because in Mn(TPP) the metal is exoplanar ([18], [45]) and as well in Mn(TPP)-(1-MeIm) which is closely related to Mn(TPP)Py, the dioxygen molecule must enter the Mn(TPP) moiety from the same side as the leaving Py ligands. As a corollary, the oxygen molecule cannot be bound trans to the Py ligand.

2.5.6 Central metals of groups VIIIa and Ib

The section devoted to iron porphyrins and its relatives is, of course, based upon a broad experience described in a very large number of papers, many of which deal with physical or biological aspects. This section will be centered on the typical topics of coordination chemists, while other aspects will not be considered in detail.

Iron porphyrins With respect to the large number of papers that have been contributed to che chemistry of iron porphyrins, it seems appropriate to summarize the present knowledge. The historical development may be taken from the books of Willstatter ([12]), Fischer ([11], [13]) and Falk ([17]). The recent impact of inorganic chemistry on biochemistry has caused an enormous revival in this field. Caughey ([47] - [50]) has presented pioneering work in the identification of axial ligands of iron porphyrins and their influence on the physical and chemical properties of the compounds. The iron porphyrins are subdivided arbitrarily according to their historical names:

- hemes (Fe(II) compounds Fe(P)L_n, d^6 electronic configuration, any neutral axial ligands L;
- hemochromes (Fe(II) compounds Fe(P)L_2, two equal donor molecules L as axial ligands;
- hemins Fe(III) compounds, Fe(P)X, d^5 electronic configuration, X univalent anion, and adducts Fe(P)X(L);
- hematins (binuclear Fe(III) complexes $[Fe(P)_2O]$;
- hemichromes (cationic or anionic Fe(III) complexes $[Fe(P)L_2]^+$ or $[Fe(P)X_2]^-$.

For further classifications of iron porphyrins, whose chemistry is very complex and cannot be presented here, we suggest [51].

Cobalt porphyrins At the present, Co(II) is the only metal ion that may replace Fe(II) in hemoglobin or myoglobin without causing a lethal mutation to the function of these macromolecules ([52]). Furthermore the redox triplets $Co(I)/Co(II)/Co(III)$ and $Rh(I)/Rh(II)/Rh(III)$ lend themselves as model for vitamin B_{12} in which the first triplet plays an important role ([53]). For this reason, many contributions have been made to the chemistry of cobalt and rhodium porphyrins, although most of these investigations are either physicochemical in nature or they report structural data.
The paramagnetic bare Co(II) porphyrins, Co(P) (A) are easily accessible and show a variety of axial ligation reactions yielding Co(P)L (B) and Co(P)LL′. Penta- and hexacoordinate adducts Co(P)L and Co(P)L_2 can be formed with axial bases like $L = Py, (1 - MeIm), Pip, AsMe_3, PR_3 and PMe_2Ph.$

Nickel, Palladium, Platinum, Copper, Silver and Gold porphyrins Ni(II), Pd(II), Pt(II), Cu(II), Ag(II) and Au(III) are found in the porphyrin system in the square-planar configuration A. This is due to their low spin d^8 or their d^9 electronic configurations in which the filled d_z^2 orbital normally repels and axial ligand approaching the metal ion. Thus, the chemistry of these complexes shows only a few notable features. Nevertheless, these metal ions are very useful for comparative investigations just because they prefer to exist as bare species.
The optical spectra of these metallo-porphyrins indicate a reinforce in metal-to-porphyrin back-bonding. This may be caused by the better penetration to the porphyrin ligand of the d orbitals with high quantum numbers. Furthermore, the metal ion may be squeezed within the porphyrin hole as it gets heavier and, thus, larger. The compression of the ion is effectively reduced when electron density flows away to the porphyrin π^* levels. This is the reason why these ions are coplanar with the porphyrin ([18]), although the radii of the heavier ones are probably largen than the optimum, 0,64 A, at the oxidation state under consideration.
It is known from the structural studies ([11], [18], [29]), that the diamagnetic Ni(II) ion is a little too small for the porphyrin hole. For this reason, Ni(II) porphyrins can be forced to add one or even two axial ligands L in solution when a large excess of L is present ([54], [55]).
Redox chemisty of the nickel and coper group metallo-porphyrins is easy to investigate. The d^8 configuration of Ni(II) and Pd(II) is so stable within the porphyrin that oxidation and reduction of Ni(OEP) and Pd(OEP) ([56], [57]), and probably like-wise of Pt(Etio-I) ([58]), solely involve the porphyrin π-system.
The rather good fit of Cu(II) and Ag(II) into the porphyrin hole may explain the facts that no Cu(I) porphyrins are known and that Ag(I) porphyrins are disproportionated. It seems to be a general phenomenon that the higher oxidation state of a metal is stabilized with respect to the lower one when the diameter

of the ion in the higher oxidation state fits better into the porphyrin hole.

2.6 Porphyrin-based Electrochemical sensors

2.6.1 Potentiometric Sensors

Among the different examples of porphyrin based chemical sensors, their exploitation as ionophores in the development of ion selective electrodes (ISE) is probably one of the most popular. These electrodes (figure 2.13) are generally comprised of a polymeric membrane, where the sensing materials are dispersed, an internal filling solution and an electrode for the electrical connection to the external circuit.

Such sensors respond to the activity of target ions by an intrinsic ion exchange

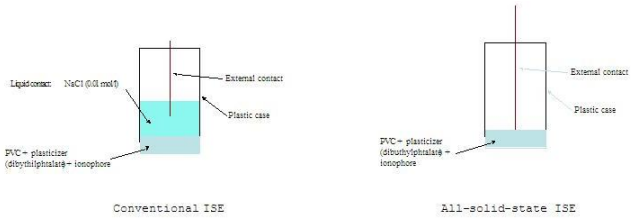

Figure 2.13: General structure of ISEs

mechanism between the organic polymeric phase and the aqueous phases. In table 2.2 we report the detection limits of some porphyrin based ISEs reported in the literature.

The basic theory describing the working mechanism of such a sensor has been developed ([59]), but the contribution of the different constituents (e.g. ionophore, additives, etc.) is still a matter of further researches. The membrane, usually comprised of a PVC disk, has ion-exchange properties that depend on the ionic sites present in the polymeric structure. The sensor responds to the activities of the ions present in the sample and the selectivity depends on the relative solubility of the ions into the polymeric membrane solvent (plasticizer). It is the ionophore that drives the selectivity of the sensor toward the target analyte. Under certain conditions ([59]), the response of the ISE to the target analyte concentration follows the Nernst equation

$$E = E^0 + \frac{RT}{zF} \cdot ln(a_i) \tag{2.4}$$

The developed coordination chemistry of metallo-porphyrins has attracted interest for their exploitation in the development of anion-selective sensors. In the absence of metallo-porphyrins, there are no specific interactions and the selectivity of ISE depends on the anion lipophilicities and results in the so-called

Porphyrin	**Analyte**	**Membrane**	**Ionic additive**	**Detection limit** (mol/L)	**Ref.**
CoTPPCl	NO_2^-	$PVC/o-NPOE$		$7{,}9\times10^{-6}$	[63]
		PU	-	10^{-5}	[74]
		PU	TDMAC	10^{-5}	
		PVC	TDMAC	10^{-5}	
InOEPCl	Cl^-	PU		10^{-4}	[59]
		PU	TDMAC	10^{-2}	
		PU	KTFPB	3×10^{-5}	
		PVC	KTFPB	3×10^{-5}	
		$SR/o-NPOE$	-	$2{,}5\times10^{-4}$	[75]
		SR	DBS	10^{-4}	
GaOEPCl	F^-	PVC	KTFPB	$3{,}2\times10^{-4}$	[74]
		PU	-	10^{-3}	
		PU	KTFPB	$6{,}3\times10^{-4}$	
MnOEPCl	Cl^-	$SR/o-NPOE$	o-NPOE	$7{,}9\times10^{-4}$	[75]
		SR	DBS	$1{,}3\times10^{-3}$	
MnTPPCl	Cl^-	$SR/o-NPOE$	o-NPOE	$3{,}2\times10^{-4}$	[75]
		SR	DBS	$1{,}6\times10^{-3}$	
	SCN^-	PVC/DOP	NaTPB	5×10^{-8}	[69]
$ZrOEPCl_2$	F^-	$PVC/o-NPOE$	KTFPB	$3{,}2\times10^{-5}$	[71]
$ZrTPPCl_2$	F^-	$PVC/o-NPOE$	KTFPB	10^{-5}	[71]
$SnTPPCl_2$	salycilate	$PVC/o-NPOE$	NaTFPB	10^{-4}	[68]
	salycilate	$PVC/o-NPOE$	-	$1{,}6\times10^{-4}$	
OMoTPP(OEt)	salycilate	$PVC/o-NPOE$	NaTFPB	10^{-5}	[68]
UPFP	acetate	$PVC/o-NPOE$	TDDMACl	3×10^{-5}	[71]
MnPPIXCl-PS	I^-	$PVC/o-NPOE$	-	10^{-5}	[72]
TSPP	I^-	polypyrrole	-	10^{-6}	[83]
TAPP	Zn^{2+}	PVC/AP	OA	3×10^{-5}	[82]
PPIXDME	Zn^{2+}	PVC/DOP	NaTPB	$1{,}5\times10^{-5}$	[81]

Table 2.2: Sensing properties of porphyrin-based ISEs

Hofmeister series:

$$ClO_4^- > SCN^- > Sal^- > I^- > NO_3^- > Br^- > NO_2^- > Cl^- > HCO_3^- > \\ > F^- > CH_3CO_2^- > SO_4^{2}- > HPO_4^{2-} > H_2PO_4^- > PO_4^{3-} > OH^- \quad (2.5)$$

The presence of metalloporphyrin in the membrane induces deviations on this series, which depend in large part on the coordination of the anion to the metalloporphyrin. After the first report by Chaniotakis co-workers [[60]], the importance of coordination interactions has been demonstrated, in terms of both the nature of the central metal and the substituents present in the porphyrin ring ([61], [62]). Metallo-porphyrins can act as neutral or charged ion carriers, depending on the oxidation state of the coordinated metals. While coordinated metals in a +2 oxidation state lead to neutral carriers, and metals in a +4 oxidation state lead to charged carriers, with metals in a +3 oxidation state can give either neutral or charged carriers, depending on both the coordination number of the metal and the nature of the incoming axial ligand (neutral or anionic, [63]). The performances of metalloporphyrin based ISEs depend also on the addition on lipophilic ionic additives, such as tri(phenyl)borate or trialkylammonium salts, which improve the potentiometric behavior of the resulting sensors, in terms of selectivity and long-term stability. The nature of the positive effect of these additives has been studied in detail and both the nature and the amount of the ionic additive to be added for the membrane compositions can be rationally predicted ([64], [65]). Furthermore, the origin of the so-called *super-Nernstian* behavior reported for several metalloporphyrin-based ISEs has recently been clarified ([66]). These non-Nernstian responses are characteristic of anion-selective electrodes based on Mn(III), Sn(IV), In(III), and Ga(III) porphyrins and are derived from a monomer-dimer equilibrium occurring in the PVC membrane. The occurrence of this equilibrium and the degree of dimerization, have been demonstrated by ultraviolet-visible spectroscopy, following the blue-shifted Soret band characteristic of the hydroxy-bridged dimer. Furthermore In and Ga complexes of picketfence porphyrins, which do not dimerize, showed slightly sub-Nernstian slopes. A theoretical model based on the dimerization equilibrium was shown to be able to predict the super-Nernstian behavior of the resulting ISEs. Different metallo-porphyrins have been proposed in recent years for the development of ISEs devoted to the detection of various analytes ([63] - [70]). A free base TPP modified with appended urea group (figure 2.14) has been proposed as ionophore to develop an ISE for acetate and it was demonstrated to be able to measure the concentration of acetic acid in vinegar samples ([71]).

Among the shortcomings observed with these metalloporphyrin-PVC based ISEs, one of the most important is their reduced long-term stability because of the ionophore leaching from the membrane. To avoid this problem, a covalent binding of the porphyrin to the polymeric matrix has been proposed ([72], [73]). This immobilization effectively overcame the problem of ionophore leaching but also contributed to reducing the interference of lipophilic anion, such as salicylate, because of size exclusion from the polymeric matrix. This steric effect also

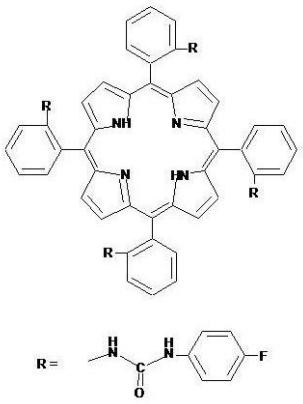

Figure 2.14: Molecular structure of urea-functionalized TPP

prevented the super-Nernstian behavior due to metalloporphyrin dimerization and the resulting Mn(III) porphyrin showed a Nernstian behavior to iodide.
Although PVC is the most widely used membrane, some examples of different matrices have been proposed for particular applications. Malinowska and co-workers have studied the potentiometric behavior of ISEs based on In(III), Ga(III), and Co(III) porphyrin complexes encapsulated in PU membranes, in comparison with that observed with conventional PVC ISEs ([74]). The same sensing mechanism is observed in both membranes, although the presence of endogeneous cationic sites in PU, instead of anionic sites as in PVC, strongly influences the potentiometric response if no lipophilic salt additives are added.
Silicon rubber has also been proposed for the development of all-solid-state ISEs ([75]). In these devices the membrane is directly attached to the electrode surface, without the presence of the internal solution (figure 2.13).
Mn(III) and In(III) porphyrins encapsulated in SR matrices were used to develop chloride selective electrodes, suitable for the measure of chloride in clinical samples. Silicon rubber is necessary for the development of all-solid-state sensors because of its adhesion properties to the electrode surfaces. It was necessary to add plasticizers in order to obtain potentiometric responses. In(III)OEPCl gave the best results as ionophore, because of reduced interference from salicylate, and an InOEPCl based ISE was demonstrated to be suitable for serum chloride measurement.
Other than inorganic anions, metalloporphyrin based ISEs have been exploited for the measurement of particular target analytes, such as aminoacids ([76] - [79]).
Free base porphyrins have also been used as ionophores for cation selective electrodes ([80], [81]) although cation sensing is far less developed than anion detection. TPP and TTP encapsulated in PVC membranes have been used to develop Ni(II)-selective sensors ([80]), although only moderate selectivity was

effectively achieved. More recently two examples of Zn(II)-selective electrodes have been reported in the literature ([81], [82]) In the first example the PP-IX dimethyl ester was encapsulated into a PVC membrane, along with sodium tetraphenylborate and dioctyl phtalate as plasticizer ([81]). The resulting Zn-ISE showed fast response time, good long-term stability, pH range $2,1-4,0$, and a working concentration range of 10^{-5} to 10^{-1} mol/L. The second sensor was developed using T(2-APP) as ionophore in PVC membrane ([82]). This ISE showed good selectivity toward other metal ions in a pH range $3,0-6,0$ and it was successfully applied for the determination of Zn in pharmaceutical samples.
The development of ISEs that do not include a polymeric support has also been investigated. Alternate deposition of water soluble anionic TSPP and cationic polypyrrole was used to obtain the deposition of a multilayer film onto a 2-aminothiol modified silver electrode ([83]). This chemical modified electrode (CME) was used as iodide ISE, showing a Nernstian behavior and detection limit of 10^{-6} mol/L, with fast response time and low resistance. An interesting approach for the development of all-solid-state ISEs has been the modification of the electrode surfaces by an electropolymerization technique ([84] - [86]) T(2-APP) and the related TETMAPP were used as precursors to deposit polymeric films onto the surfaces of different electrodes.
Free base and Fe(III), Ni(II), Co(II), and Cu(II) complexes of T(2-APP) were deposited by an electropolymerization technique onto the surfaces of different metal electrodes ([84]). The films obtained were not conductive, probably because of the three−dimensional, spongelike structure of the polymeric film. They were tested as ISEs for the detection of different anions and, in the case of the free base, both anions and cations. It is interesting to note that useful potentiometric data were obtained when the electrode was positively polarized at positive potential before use, so inducing positive charge on the film. These ISEs generally showed sub−Nernstian slopes for iodide ions, with detection limits ranging from 10^{-4} to 10^{-3} mol/L. However, different parameters influenced the responses of these ISEs and for this reason it was sometimes difficult to give a rationale for the results obtained. In the case of the electropolymerized electrodes developed by Volf and co−workers ([85]), the anion selectivity pattern shown was attributed to coordination interactions in the case of polymeric films containing Metallo-porphyrins, and to ion−exchange polyporphyrin free base. When applied to the determination of amino acids ([86]), a remarkable selectivity for cysteine was observed.

2.6.2 Amperometric and Voltammetric Sensors

The working mechanisms of these devices are based on the well known ability of Metallo-porphyrins to catalyze oxidation or reduction of different substrates. Thin films of Metallo-porphyrins have been deposited onto electrode surfaces to develop chemical modified electrodes (CME) and the electrocatalytic action of the developed CMEs has been used for the detection of different analytes. Particular attention has been devoted to the detection of NO, starting from

the seminal paper of Malinski and Taba ([87]). NiTMHPP (figure 2.15) was deposited by the electropolymerization technique to give conductive films onto the surface of carbon fiber electrodes.

An additional layer of Nafion was necessary to avoid the interference of anion

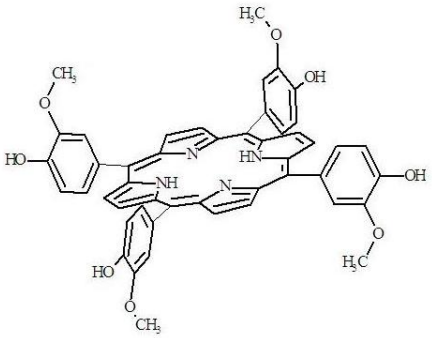

Figure 2.15: Molecular structure of TMHPP

present in real matrices, such as nitrite. A major advantage of this approach was the extremely small dimension in which the electrodes can be fabricated. The sensor is miniaturized by thermal sharpening of the electrode carbon fiber. The diameter of the carbon fiber is reduced to 500 nm and the fiber is mounted into a truncated needle (figure 2.16, [88]).

The tip of the fiber (500 nm length) is coated with the poly-NiTMHPP by

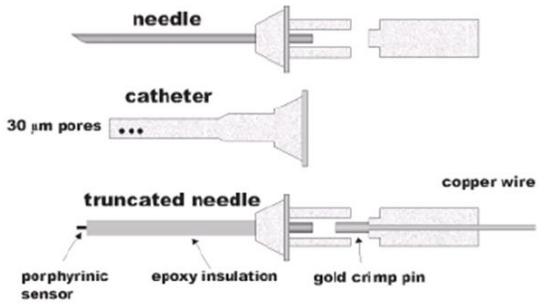

Figure 2.16: Sketch of the NiTMHPP−based nanoelectrode used for NO measurement

electropolymerization and then an additional layer of Nafion is added by a dipping technique. The resulting CMEs were demonstrated to be useful for the detection of NO in biological samples, because the developed nanosensors in-

duced minimal damage for biological tissues, so allowing both in vitro and in vivo measurements ([87] - [90]). In table 2.3 we report examples of detection limits of some sensors reported in the literature.

Furthermore the small size of these sensors was necessary to allow the mon-

Porphyrin	**Detection limit, nmol/L**	**Additional layer**	**Ref.**
NiTHMPP	10	Nafion	[87]
	1,5		[89]
	27	Nafion+o−PD	[96]
	85	eugenol	[95]
	1		[90]
	0,5	Nafion, AAO polylisine	[97]
CoTPPCl	1,2	Nafion	[89]
MnTCPPCl	100	Poly−pyrrole	[89]

Table 2.3: Porphyrin−based NO sensors

itoring of transient concentration of NO produced in physiological processes, because the half−life of this reactive molecule is very short in biological samples. While the miniaturization and the exploitation of these nanosensors has been greatly improved, the exact mechanism of electrochemical NO detection by the poly-NiTMHPP sensors is still unclear. In the first reports by Malinski and Taba and coworkers the electrocatalytic role of the coordinated Ni(II) ion has been involved for the oxidative reaction of NO, and coordination of NO and formation of the Fe−nitrosyl complex [Fe(III)P]NO was confirmed by cyclic voltammetry and spectroscopic data by Bedioui and co−workers ([91]). On the other hand the same authors showed that in the case of Ni complexes the coordination of NO to the metalloporphyrin is probably not involved in the electrocatalytic process ([92]). The hypothesis that the role of the porphyrin layer could not be related to the axial coordination chemistry of the Ni ion was later confirmed, showing that the non-metalated poly−TMHPP coated CME presented the same electroctalytic activity toward NO detection ([93]). The same authors showed that the thickness of the porphyrin layer influenced the efficiency of the NO detection, and a tentative oxidation mechanism, where the porphyrin polymer acted as a three-dimensional structure, was proposed ([94]). The external Nafion has been added to increase the selectivity toward interfering anions present in biological matrices, such as nitrite, which cannot diffuse through the Nafion layer. On the other hand Nafion can increase the interference of cation species of biological relevance, such as catecholamines. For this reason, Ciszewski and Milczarek proposed the exploitation of electropolymerized eugenol as external layer, in order to preserve the selectivity toward anions and to reduce the interference of cationic species ([95]). Pontie and co−workers developed a NO multilayer microelectrode composed of a poly−NiTMHPP layer, Nafion, and o-phenylenediamine ([96]). The developed sensor showed a detection limit as low as 40 nmol/L, a NO concentration expected in some biological

system. Mitchell and Michaelis reported a composite multilayer electrode having poly-NiTHMPP as sensing material and layers of Nafion, acorbic acid oxidase, and either polylisine or polypyridinium to preclude interferences by physiological concentrations of both anionic and cationic electroactive species ([97]). The resulting microdevice was used for in situ NO detection, showing a NO detection limit of 8 nmol/L for in vitro and 173 nmol/L for in vivo tissue sample analyses. Several Metallo-porphyrins were later exploited to develop CMEs devoted to the determination of different analytes ([98] - [100]). Reducing anions such as nitrite and sulfite has been determined by dip coating modified glassy carbon electrodes with a tetraruthenated cobalt porphyrin (figure 2.17, [98]).

These electrodes showed excellent performance for the determination of ni-

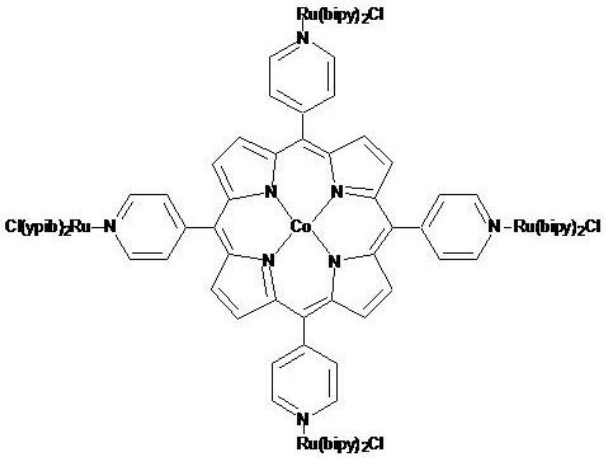

Figure 2.17: Molecular structure of the cobalt complex of tetraruthenated-TPP

trite and sulphite, even at ppb level, both in conventional and in flow injection conditions. The same authors developed modified glassy carbon electrodes by deposition of an electrostatically assembled film of the tetraruthenated cobalt porphyrin and Zn(II)TSPP ([99]). These electrodes were successfully exploited for nitrite detection in flow injection analysis with a detection limit of 10^{-5} mol/L. The same electrode can be used for nitrate ion detection after reduction to nitrite in a reductor column containing copperized cadmium. Graphite electrodes functionalized by cobalt(II)TPP permitted the detection of a wide range of different organohalides, including compounds that are industrial pollutants ([100]). A further advantage of these electrodes was the absence of interference from oxygen.

2.6.3 Porphyrin-based Electronic Tongues

The excellent performance of Metallo-porphyrins in vapour phase chemical sensors led to the exploration of the development of liquid phase sensors based

on Metallo-porphyrins as sensing material, where the metallo-porphyrins were immobilized into PVC membranes. The developed electrodes were integrated in an array to develop an electronic tongue based on potentiometric sensors ([101], [102]). The developed electronic tongue was integrated with a metalloporphyrin-QMB based electronic nose in the fields of clinical and food analysis. In this way it was possible to extract information from both the liquid and the headspace of the analyzed matrix, resulting in a net increase of performances. This is the first approach to develop a complete artificial sensorial system. More recently CMEs were fabricated by the electropolymerization of different metal complexes of TMHPP on glassy carbon electrodes, using the cyclic voltammetric method. The resulting electrodes were used as potentiometric sensors and demonstrated higher resolution and stability than the corresponding PVC based electrodes. These CMEs were assembled in an array configuration and utilized to analyze several samples. In particular, this array was able to discriminate compounds, each one used as a model of the five classical tastes. These preliminary results were a basic step for the development of porphyrin based taste sensor systems for a variety of applications.

Bibliography

[1] J. W. Grate. Chem. Rev. 100 (2000) 2627

[2] J.-M. Lehn. Supramolecular Chemistry. WileyVCH, Weinheim, 1995; J. L. Atwood J.-M. Lehn. Comprehensive Supramolecular Chemistry. Pergamon Press, Oxford, 1996

[3] R. Lemberg, J.Falk. Biochem.J. 49 (1951) 674

[4] D.T. Lash. Energy and Fuels. 7 (1993) 166

[5] J.L.W. Thudichum. Report Med.Off. Privy Council. 1867, Appendix 7-10, 152

[6] M. Nencki, N. Sieber. Arch. Exptl. Path. Pharmakol. 18 (1884) 401

[7] M. Nencki, J. Z. Zaleski. Z. Physiol. Chem. 34 (1901) 997

[8] W. Kuster. Z. Physiol. Chem. 82 (1912) 463

[9] H. Fisher, J. Klarer. Liebigs Ann. Chem. 440 (1926) 181

[10] H. Fisher, B. Wallach. Liebigs Ann. Chem. 468 (1926) 98

[11] J.W. Buchler in Porphyrins and Metallo-porphyrins. Smith, K. M. Ed.; Elsevier: Amsterdam, 1975; 157-231

[12] R. Willstatter, A. Stoll. Untersuchungen uber Chlorophyll-Methoden und ergebnisse. Springer-Verlag, Berlin and New York, 1913

[13] H. Fischer, H. Orth. Die chemie des pyrrols. Vol. II, part 1. Akad. Verlagsges, Leipzig, 1937

[14] H. Fischer, A. Stern. Die chemie des pyrrols. Vol. II, part 1. Akad. Verlagsges, Leipzig, 1940

[15] A. Treibs. Das Leben und Wirken von Hans Fischer. Hans Fischer Gesellschaft, Munchen, 1971

[16] F.H. Moser, A.L. Thomas. Phtalocyanine compounds. Van Nostrand-Reinhold, Princeton, New Jersey, 1963

[17] J.E. Falk. Porphyrins and Metallo-porphyrins. Elsevier: Amsterdam, 1964

[18] W.R. Scheidt, Vol. III, Chap. 10

[19] J.L. Hoard in Porphyrins and Metallo-porphyrins. Smith, K. M. Ed.; Elsevier: Amsterdam, 1975; 317-381

[20] P. Hambright. Coord. Chem. Rev. 6 (1971) 247

[21] P. Hambright in Porphyrins and Metallo-porphyrins. Smith, K. M. Ed.; Elsevier: Amsterdam, 1975; 233-279

[22] D. Ostfeld, M. Tsutsui. Acc. Chem. Res. 7 (1974) 52

[23] M. Tsutsui, G.A. Taylor in Porphyrins and Metallo-porphyrins. Smith, K. M. Ed.; Elsevier: Amsterdam, 1975; 279-317

[24] D. C. Becker, B. R. Bradley, C. J. Watson. J. Am. Chem. Soc. 83 (1961) 3743

[25] J. L. Soret. Compt. Rend. 97 (1883) 1267

[26] J.R.Plat in Radiation Biology. A. Hollaender ed., Vol III, Chapter 2. McGraw- Hill, New York, 1956

[27] J. L. Hoard in Porphyrins and Metallo-porphyrins. Smith, K. M. Ed.; Elsevier: Amsterdam, 1975; 317

[28] A. Stern, G. Klebs. Ann. Chem. 500 (1932) 91

[29] J.W. Buchler, L. Puppe, K. Rohbock, H.H. Schneehage. Ann. N.Y. Aca. Sci. 206 (1973) 116

[30] J.W. Buchler, L. Puppe, K. Rohbock, H.H. Schneehage. Chem. Ber. 106 (1973) 2710

[31] R.D. Shanon, C.T. Prewitt. Acta Crystallogr. Sect. B 25 (1969) 925

[32] G.D. Dorough, J.R. Miller, F.M. Huennekens. J. Am. Chem. Soc. 73 (1951) 4315

[33] J.B. Allison, R.S. Becker. J. Phys. Chem. 67 (1963) 2675

[34] R. Rothemund, A.R. Menotti. J. Am. Chem. Soc. 70 (1948) 1808

[35] R.Hill. Biochem. J. 19 (1925) 341

[36] J.W. Barnes, G.D. Dorough. J. Am. Chem. Soc. 72 (1950) 4045

[37] J.H. Fuhrhop, K.M. Smith in Porphyrins and Metallo-porphyrins. Smith, K. M. Ed.; Elsevier: Amsterdam, 1975; 757

[38] J.J. Katz. Vol. V, Chapt. 9

[39] R.S. Becker, J.B. Allison. J. Phys. Chem. 67 (1963) 2669

[40] H. Scheer, Vol. II, Chapt.1

[41] J.-H. Fuhrhop, D. Mauzerall. J. Am. Chem. Soc 91 (1969) 4174

[42] M. Calvin. Rev. Pure Appl. Chem. 15 (1965) 1

[43] L.J. Boucher. J. Am. Chem. Soc. 90 (1968) 6640

[44] L.J. Boucher. Coord. Chem. Rev. 7 (1972) 289

[45] B. Gonzalez, J. Kouba, S. Yee, C.A. Reed, J.F. Kirner, W.R. Scheidt. J. Am. Chem. Soc. 97 (1975) 3247

[46] C.J. Weschler, B.M. Hoffman, F. Basolo. J. Am. Chem. Soc. 75 (1975) 5278

[47] J.O. Alben, W.H. Fuchsman, C.A. Beaudreau, W.S. Caughey. Biochemistry 7 (1968) 624

[48] W.S. Caughey in Inorganic Biochemistry. G.I. Eichhorn, ed. Vol. 2, p.797

[49] W.S. Caughey, C.H. Barlow, D.H. O′Keefe, M.C. O′Toole. Ann. N.Y. Acad. Sci. 206 (1975) 2676

[50] D.H. O′Keefe, C.H. Barlow, G.A. Smythe, W.H. Fuchsman, T.H. Moss, H.R. Lilienthal, W.S. Caughey. Bioinorg. Chem. 5 (1975) 125

[51] The Porphyrins, Structure and Synthesis, Part A. Vol. 1. D. Dolphin Ed. Academic Press, 1978

[52] C.A. Spilburg, B.M. Hoffman, D.H. Petering. J. Biol. Chem. 247 (1972) 4219

[53] J.M. Pratt. Inorganic chemistry of vitamin B_{12}. Academic Press, New York, 1972

[54] R.J. Abraham, P.F. Swinton. J. Chem. Soc. B (1969) 903

[55] B.D. McLees, W.S. Caughey. Biochemistry. 7 (1968) 642

[56] J.-H. Fuhrhop. Angew. Chem. 86 (1974) 363

[57] J.-H. Fuhrhop, K. Kadish, D.G. Davis. J. Am. Chem. Soc. 95 (1973) 5140

[58] A. Stanienda. Z. Physi. Chem. 229 (1964) 259

[59] E. Bakker, P. Buhlmann, E. Pretsch. Chem. Rev. 97 (1997) 3083

[60] N. A. Chaniotakis, A. M. Chasser, M. E. Meyerhoff, J. T. Groves. Anal. Chem. 60 (1988) 185

[61] D. Gao, J. Gu, R.-Q. Yu, G.-D. Zheng. Anal. Chim. Acta. 302 (1995) 263

[62] E. Bakker, E. Malinowska, R.D. Schiller, M. E. Meyerhoff. Talanta. 41 (1994) 881

[63] E. Malinowska, M.E. Meyerhoff. Anal. Chim. Acta. 300 (1995) 33

[64] U. Schaller, E. Bakker, U.E. Spichiger, E. Pretsch. Anal. Chem. 66 (1994) 391

[65] S. Amemiya, P. Buhlmann, E. Pretsch, B. Rusterholz, Y. Umezawa. Anal. Chem. 72 (2000) 1618

[66] E.D. Steinle, S. Amemiya, P. Buhlmann, M. E. Meyerhoff. Anal. Chem. 72 (2000) 5766

[67] P. Buhlmann, E. Pretsch, E. Bakker. Chem. Rev. 98 (1998) 1593

[68] E. Malinowska, J. Niedziolka, E. Rozniecka, M.E. Meyerhoff. J. Electroanal. Chem. 514 (2001) 109

[69] J. H. Khorasani, M. K. Amini, H. Motaghi, S. Tangestaninejad, M. Moghadam. Sens. Actuators B 87 (2002) 448

[70] E. Malinowska, L. Gorski, M. E. Meyerhoff. Anal. Chim. Acta. 468 (2002) 133

[71] S. Amemyia, P. Buhlmann, Y. Umezawa, R.C. Jagessar, D.H. Burns. Anal. Chem. 71(1999) 1049

[72] K.-C. Oh, K.-A Kim, I.R. Paeng, D. Baek, K.-J. Paeng. J. Electroanal. Chem. 468 (1999) 98

[73] K.-C. Oh, S.M. Lim, I.R. Paeng, D. Baek, K.-J. Paeng. J. Electroanal. Chem. 506 (2001) 42

[74] E. Malinowska, J. Niedziolka, M.E. Meyerhoff. Anal. Chim. Acta. 432 (2001) 67

[75] I.J. Yoon, J.H. Shin, I.R. Paeng, H.Nam, G.S. Cha, K.-J. Paeng. Anal. Chim. Acta. 367 (1998) 175

[76] M. K. Amini, S. Shahrokhian, S. Tangestaninejad. Anal. Chem. 71 (1999) 2502

[77] M. K. Amini, S. Shahrokhian, S. Tangestaninejad. Analyst. 124, (1999) 1319

[78] X.-B. Zhang, C.-C. Guo, J.-B. Xu, G.-L. Shen, R.Q. Yu. Analyst. 125 (2000) 867

[79] I.H.A. Badr, M.E. Meyerhoff, S.S.M. Hassan. Anal. Chim. Acta. 321 (1996) 11

[80] V.K. Gupta, A. K. Jain, L. P. Singh, U. Khurana. Anal. Chim. Acta. 355 (1997) 33

[81] V.K. Gupta, A. Kumar, R. Mangla. Sens. Actuators B 76 (2001) 617

[82] A.R. Fakhari, M. Shamsipur, K. Ghanbari. Anal. Chim. Acta. 460 (2002) 177

[83] C. Sun, J. Zhao, H. Xu, Y. Sun, X. Zhang, J. Shen. Talanta. 46 (1998) 15

[84] E. M. Bruti, M. Giannetto, G. Mori, R. Seeber. Electroanalysis. 11 (1999) 565

[85] R. Volf, T.V. Shishkanova, P. Matejka, M. Hamplova, V. Kral. Anal. Chim. Acta 381 (1999) 197

[86] R. Volf, T.V. Shishkanova, V. Kral. J. Incl. Phen. Macroc. Chem. 35 (1999) 111

[87] T. Malinski, Z. Taba. Nature. 358 (1992) 676

[88] T. Malinski in The Porphyrin Handbook. K.M. Kadish, K.M. Smith, R. Guilard, Eds.). Vol. 6, p. 231. Academic Press, New York, 2000

[89] F. Bedoui, N. Villeneuve. Electroanalysis. 15(2003) 5 and references therein

[90] T. Malinski, J. Nanobashvili, I. Huk. Eur. Surg. 34 (2002) 79

[91] F. Bedioui, S. Trevin, V. Albin, M. G. G. Villegas, J. Devynck. Anal. Chim. Acta. 341 (1997) 177

[92] S. Trevin, F. Bedioui, J. Devynck. Talanta. 43 (1996) 303

[93] A. Ciszewski, E. Kubaszewski, M. Lozinski. Electroanalysis. 8 (1996) 293

[94] A. Ciszewski, G. Milczarek, E. Kubaszewski, M. Lozinski. Electroanalysis. 10 (1998) 628

[95] A. Ciszewski, G. Milczarek. Electroanalysis. 10 (1998) 791

[96] M. Pontie, F. Bedioui, J. Devinck. Electroanalysis. 11 (1999) 845

[97] K.M. Mitchell, E.K. Michaelis. Electroanalysis. 10 (1998) 81

[98] K. Araki, L. Angnes. C.M.N. Azevedo, H.E. Toma. J. Electroanal. Chem. 397 (1995) 205

[99] J.R. Caetano da Rocha, L. Angnes, M. Bertotti, K. Araki, H.E. Toma. Anal. Chim. Acta. 452 (2002) 23

[100] D. J. Dobson , S. Saini. Anal. Chem. 69 (1997) 3532

[101] C. Di Natale, R. Paolesse, A. Macagnano, A. Mantini, A. D'Amico, A. Legin, L. Lvova, A. Rudnitskaya, Y. Vlasov. Sens. Actuators B. 64 (2000) 15

[102] C. Di Natale, R. Paolesse, A. Macagnano, A. Mantini, A. D'Amico, M. Ubigli, A. Legin, L. Lvova, A. Rudnitskaya, Y. Vlasov. Sens. Actuators B. 69 (2000) 342

Chapter 3

Preliminary studies on suitable CIMs for chemical sensors

Introduction

Conventional approaches to chemical sensors have traditionally made use of a *lock-and-key* design, wherein a specific receptor is synthesized in order to strongly and highly selectively bind the analyte of interest ([1] - [3]). A related approach involves exploiting a general physico-chemical effect selectively towards a single analyte, such as the use of the ionic effect in the construction of a pH electrode. In the first approach, selectivity is achieved through recognition of the analyte at the receptor site, and in the second, selectivity is achieved through the transduction process in which the method of detection dictates which species are sensed. Such approaches are appropriate when a specific target compound must be identified in the presence of controlled backgrounds and interferences. However, this type of approach requires the synthesis of a separate, highly selective sensor for each analyte to be detected. In addition, this type of approach is not particularly useful for analyzing, classifying or assigning human value judgments to the composition of complex vapor mixtures such as perfumes, beers, foods, mixtures of solvents, etc.
An emerging strategy that is complementary to the conventional chemical sensing approach, involves the use of sensor arrays. The utilization of sensor arrays is inspired by the superb performance of biological olfactory systems in odor detection, identification, tracking and location tasks. Recent work has shown that the mammalian olfactory system contains approximately 1000 different olfactory receptor genes and that, upon odor stimulation, responses from many receptors are sent to the olfactory bulb and then onto the olfactory cortex for processing ([4] - [7]). Furthermore, recent experiments have shown that the ol-

factory receptors are not highly selective toward specific analytes; in fact, one receptor responds to many analytes and many receptors respond to any given analyte ([5], [7], [8]). Pattern recognition methods are thus thought to be a dominant mode of olfactory signal processing in the broadly responsive portion of the olfactory system of higher mammals.
In the array approach, the strict lock-and-key design criterion of traditional sensing devices is abandoned. Instead, in this alternative sensor architecture, an array of different sensors is used, with every element in the sensor array chosen to respond to a number of different chemicals or classes of chemicals. The elements of such an array need not to be individually highly selective toward any given analyte, so this stressing constraint on sensor design is relaxed. Instead, the collection of sensors should contain as much chemical diversity as possible, so that the array responds to the largest possible cross-section of analytes. In practice, most chemical sensors suffer from some interference by responding to chemical species that are structurally or chemically similar to the desired analyte. This interference is an inevitable consequence of the *lock* being able to fit a number of imperfect *keys*. Differentially responsive arrays take advantage of this interference or *cross reactivity* by deliberately attempting to use the nonspecific response patterns for analyte recognition. In this design, identification of an analyte cannot be accomplished from the response of a single sensor element; a distinct pattern of responses produced over the collection of sensors in the array, can provide a fingerprint that allows classification and identification of the analyte. The pattern can be obtained from equilibrium or kinetic responses with the latter often providing additional discriminating power.
For these reasons, different materials, both organic (such as porphyrinoids) and inorganic (metallic wires), have been studied, focusing on their response mechanism and their cross-sensitivity.
For a better description, only chemical properties of different sensors will be discussed in this chapter, while all applications involving them, will be deeply discussed in next chapter.

3.1 Metallic electrodes

The first studied materials have been metallic wires, since they can be easily found in local markets at low prices, with several compositions (alloys) which allow the fine tuning of cross-sensitivity. Furthermore, their shape can be easily modified, allowing the nice fitting of sensors in the used system configuration.
An attention has been turned to the exploitation of metallic wires (so-called first kind electrodes) as potentiometric sensors for multicomponent analysis. Metallic wires have been widely used recently for the voltammetric multicomponent analysis; an electronic tongue was developed at Linkoping University: it was based on the pulsed voltammetry of an array of different metal electrodes; it was finally applied for the analysis of liquid samples. The utility of such device has been shown for monitoring the quality of water in a production plant for drinking water ([9]), monitoring mold growth in liquids ([10]) and discrimina-

tion between the different rinses from household washing machine runs with four different prerequisites ([11]). At the same time, there are still few reports on the application of potentiometric metallic sensors for multivariate analysis in electronic tongues: metallic wires were used in multisensor array for discrimination of vinegars ([12]), both wires and conducting surfaces in thick-film technology were utilized as potentiometric electrodes for qualitative analysis of naturalwaters ([13], [14]).
Seven metallic wires were used, namely:

- Iron (Fe);
- Platinum (Pt);
- Copper (Cu);
- Brass (Zinc and Copper alloy);
- Stainless steel;
- Aluminium (Al);
- Tin (Sn).

Evaluation of potentiometric properties of sensors was evaluated in electrochemical cell REF | analysed solution | sensor array.
Potential values of sensors included in array, were calculated by measuring the potential differences between electrodes and the conventional reference electrode (standard calomel electrode, AMEL, Italy) using a PC equipped high-impedance input 8-channel A/D converter (Smartronix, Rome, ITALY). Potentiometric performances of each membrane were examined by varying the concentration of different ions stepwise in a concentration range from 10^{-5}M to 10^{-1}M with measurement cycle of 100 sec. A magnetic stirrer was used during all the measure time to avoid concentration gradients into the solution. Slopes were calculated for linear ranges of sensors calibration curves and listed in table 3.1.

All sensors showed anionic response towards most of the analyzed solutions, but a very poor reproducibility in calibration repetitions was found. Standard deviation values of all sensor responses are represented in figure 3.1.

The reasons of such a low reproducibility during several repetitions of the same measurement or calibration, are still not clear, since the sensing mechanism of metallic electrodes has still not been completely clarified; we focused on three possible causes, trying to reduce their influence:

- metals oxidation;
- influence of immersed sensor surface;
- development of a magnetic field by the stirrer rotation.

	NaCl	**$NaNO_3$**	**$NaNO_2$**	**$CaCl_2$**	**NaSCN**	**CH_3CO_2Na**
Fe	$-214,6 \pm 81$	$-141,7 \pm 114$	$-5,8 \pm 11,8$	$-248,1 \pm 7,7$	$-310,0 \pm 22,4$	$-26,9 \pm 11$
Pt	$-41,2 \pm 0,6$	$-20,4 \pm 11,1$	$-21,9 \pm 10,1$	$-54,3 \pm 11,1$	$-45,5 \pm 4,3$	$-16,5 \pm 3,4$
Cu	$-43,4 \pm 28,8$	$-2,1 \pm 1,1$	$-19,7 \pm 6,7$	$-55,4 \pm 21,0$	$-93,4 \pm 7,7$	$-26,9 \pm 2,0$
Brass	$-50,5 \pm 39,3$	$-3,5 \pm 2,6$	$-27,3 \pm 11,7$	$-53,5 \pm 28,8$	$-88,0 \pm 0,3$	$-33,6 \pm 9,4$
Steel	$-85,8 \pm 1,4$	$-9,8 \pm 8,5$	$-5,7 \pm 15,8$	$-102,3 \pm 36,5$	$-20,3 \pm 1,9$	$-15,1 \pm 4,0$
Al	$-9,7 \pm 13,7$	$-4,8 \pm 1,2$	$+19 \pm 2,4$	$+24,6 \pm 8,0$	$-3,3 \pm 12,9$	$-15,2 \pm 4,3$
Sn	$-24,7 \pm 0,5$	$-14,5 \pm 3,0$	$-39,9 \pm 7,8$	$-26,5 \pm 8,0$	$-36,9 \pm 8,2$	$-48,1 \pm 8,9$
	$NaHCO_3$	**$NaClO_4$**	**KCl**	**NH_4Cl**	**KI**	**$Pb(NO_3)_2$**
Fe	$-61,4 \pm 19,3$	$-93,2 \pm 33,0$	$-229,8 \pm 82,0$	$-229,8 \pm 82,0$	$-243,0 \pm 57,9$	$-84,9 \pm 44,5$
Pt	$-47,5 \pm 9,4$	$-17,2 \pm 1,3$	$-44,6 \pm 10,5$	$-57,6 \pm 3,4$	$-18,2 \pm 7,0$	$-7,7 \pm 0,9$
Cu	$-48,5 \pm 15,9$	$-18 \pm 0,9$	$-50,4 \pm 18,4$	$-61,4 \pm 15,6$	$-68,5 \pm 3,3$	$+6,3 \pm 1,8$
Brass	$-59,2 \pm 21,1$	$+22,7 \pm 1,3$	$-47,9 \pm 33$	$-49,7 \pm 30,7$	$-65,0 \pm 0,9$	$+5,2 \pm 0,8$
Steel	$-460,0 \pm 34,9$	$-18,6 \pm 5,0$	$-96,9 \pm 31,1$	$-104,7 \pm 11,3$	$-19,3 \pm 5,1$	$-1,6 \pm 10,9$
Al	$-81,1 \pm 15,1$	$-4,0 \pm 0,5$	$+7,5 \pm 6,2$	$+5,4 \pm 10,1$	$+43,0 \pm 11,1$	$-1,3 \pm 1,3$
Sn	$-53,9 \pm 46,5$	$-31,4 \pm 10,7$	$-30,9 \pm 7,7$	$-41,4 \pm 22,0$	$-42,5 \pm 9,4$	$-22,3 \pm 27,1$
	Na_3PO_4	**CH_3CO_2Cd**	**$Cu(NO_3)_2$**	**NaSal**	**$CoCl_2$**	**$MgCl_2$**
Fe	$-17,3 \pm 7,5$	$-86,3 \pm 29,3$	$-30,7 \pm 21,1$	$+21,4 \pm 22,6$	$-126,3 \pm 10,8$	$-239,5 \pm 31,9$
Pt	$-83,8 \pm 15,5$	$-19,7 \pm 8,6$	$-15,4 \pm 9,3$	$-13,8 \pm 0,9$	$+20,3 \pm 3,4$	$-39,4 \pm 2,2$
Cu	$-59,1 \pm 14,0$	$-19,7 \pm 12,0$	$+23,7 \pm 0,5$	$-28,7 \pm 3,1$	$-13,7 \pm 0,2$	$-61,9 \pm 12,3$
Brass	$-63,7 \pm 31,8$	$-15,7 \pm 8,7$	$+28,0 \pm 3,0$	$-30,0 \pm 6,9$	$-14,3 \pm 0,5$	$-50,1 \pm 29,8$
Steel	$-633,0 \pm 221,7$	$-34,8 \pm 24,9$	$+90,8 \pm 9,0$	$-11,6 \pm 21,9$	$-144,4 \pm 42,0$	$-324,8 \pm 57,3$
Al	$-120,0 \pm 6,6$	$-3,2 \pm 2,8$	$+27,9 \pm 41,0$	$-4,6 \pm 0,9$	$+12,8 \pm 1,1$	$+14,1 \pm 17,8$
Sn	$-212,5 \pm 51,5$	$-41,8 \pm 19,2$	$+8,8 \pm 66,4$	$-10,9 \pm 22,2$	$-19,7 \pm 7,2$	$-34,6 \pm 9,2$

Table 3.1: Standard calibrations of metallic electrodes: response slope towards standard laboratory analytes. All values are given in mV/decade

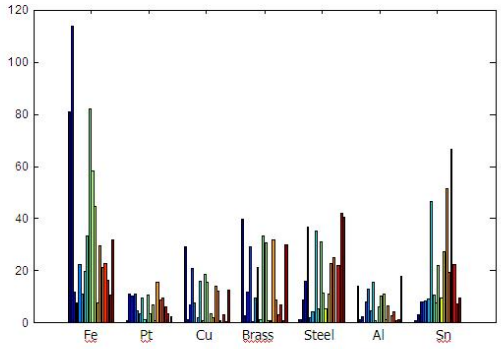

Figure 3.1: Standard deviation values (expressed in mV) of metallic sensor responses

3.1.1 Formation of metal oxide layer on the sensor surface

It is well known that some metals, e.g. iron or copper, are very sensitive to oxidation reactions and, in case of contact, a layer of metal oxide easily forms on the sensor surface. To verify the influence of such a layer, we studied the sensor response reproducibility in a background solution for a period of 3 weeks, waiting until the stabilization and using the reached potential value for the creation of a *temporal profile*. Each day, the sensor surface was previously cleaned by *sand paper* to remove the metal oxide layer; just in four days pre-treatment was not performed. The response profile for iron is given in figure 3.2.

It can be seen how the previous mechanical cleaning of the sensor surface,

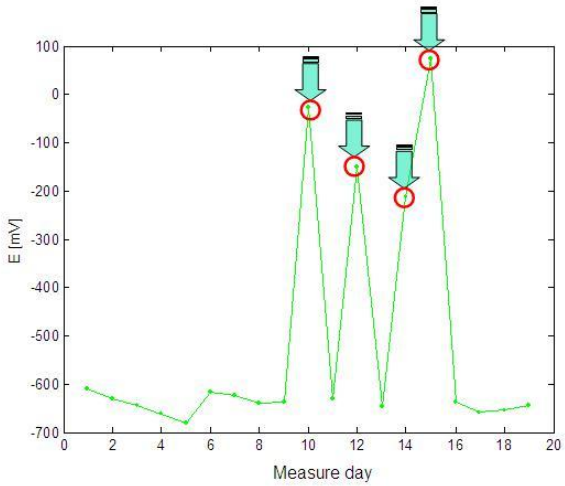

Figure 3.2: Sensor surface oxidation influence for iron electrode. Response has been measured for a period of 3 weeks in the same background solution and sensor was previously cleaned by sand paper

improves the better sensor response stability in a background solution during all the measurement period; it is also confirmed by days 10, 12, 14 and 15, when pre-treatment was not performed and when the related potential values are very different from the other ones.

3.1.2 Influence of the magnetic stirrer

In all applications involving chemical sensor measurements in static mode, the solution to be analysed, must be shake to avoid the formation of concentration gradients of the analytes. The common way to homogenize the solution in laboratory measurements, is the utilization of a magnetic stirrer which generates a rotating field; the magnetic anchor on the basis of the becker, containing the solution, rotates with the same speed (expressed in $1/min$). The rotation

rate is a parameter which has to be chosen very carefully in measurements involving chemical sensors, because it should be enough high to guarantee the homogenization of the solution, but, at the same time, it should also allow the sensing layer to reach a stable equilibrium with analytes; furthermore, when using metallic electrodes, the high rotation rate produced by a higher magnetic field, causes the temporary magnetization of the sensor surface.
To check the magnetic influence on the sensor response, a measurement on a background solution (NaCl 10^{-2}M) was performed; the rotating speed was changed according to the following protocol, waiting until the complete response stabilization after each change.

- 0 rpm (turn per minute);
- 50 rpm (turn per minute);
- 0 rpm (turn per minute);
- 200 rpm (turn per minute);
- 0 rpm (turn per minute);
- 350 rpm (turn per minute);
- 0 rpm (turn per minute);
- 50 rpm (turn per minute).

A typical calibration which was obtained is shown in figure 3.3 The stirring rate showed a strong influence, maninly for Iron, Brass, Copper, Steel and Tin; a typical *wave response* has been noticed, consequence of the continuous changes in rotation speed, which cause un-reversible sensor responses: in fact, the potential value obtained when the stirrer is switched off, strongly depend on what was done before, with a *memory effect* of the system. It can be noticed more easily in the zoom on Copper, Steel and Tin response (figure 3.4).

3.1.3 Influence of the immersed surface

The equilibrium potential of metallic electrode depends on the concentration of a primary ion in solution according to the well-known Nernst equation. For metallic electrode operating in open circuit potentiometric mode, anodic and cathodic partial exchange currents corresponding to the oxidation and reduction processes on surface, are equal with the opposite magnitudes and a net current on the electrode is, hence, equal to zero. In reality, in the absence of the primary ion, the apparent steady-state potential of metallic electrode immersed in analyzed solution is determined by several concurrent electrochemical processes. The overall electrode potential change can be explained by mixed

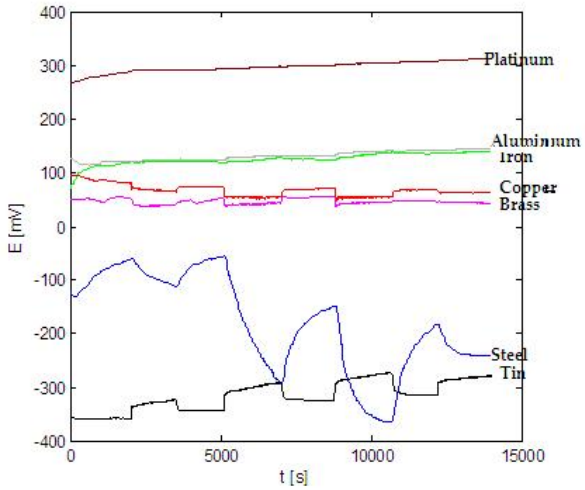

Figure 3.3: Influence of the magnetic stirrer. Rotational rate was changed several times and related potentials were acquired

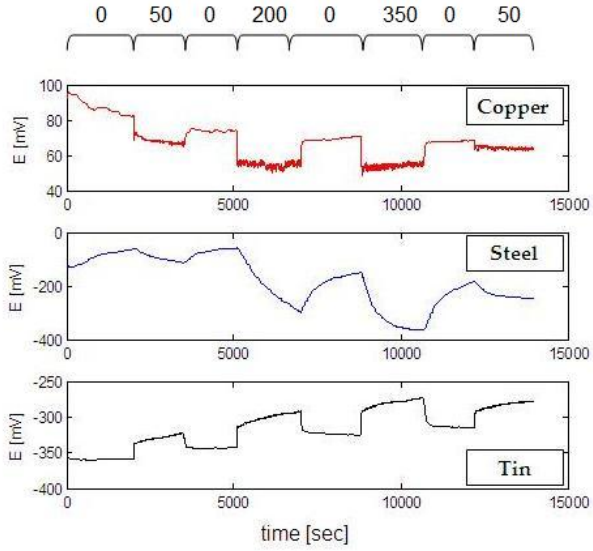

Figure 3.4: Zoom on copper, steel and tin response related to different stirring rates

potential phenomenon, discussed by several authors ([15], [16]). Mixed (or corrosion) potential is considered to occur when a non-equilibrium state exists at the electrode surface involving two or more electrochemical processes.
Typically different oxidation and reduction reactions take place on the electrode simultaneously. Moreover, the material of metallic wire can undergo complexes formation, physisorption or chemisorption/desorption processes of a number of chemical species, coming from electrode reaction or complexation products or other solution constituents.
All the above mentioned processes strictly depend on the immersed surface of the electrode; to check that influence, we studied the potential variations when sensors were used in different configurations (A: completely immersed, B: partially immersed), to evaluate a reproducible method to perform measurements. Sensor response was measured in a buffer solution (MES, 2-[N-Morpholino] ethane sulphoric acid, 0,01M pH=5.5); mean potential values for sensors are shown in figure 3.5. A high influence of immersed surface was noticed, mainly

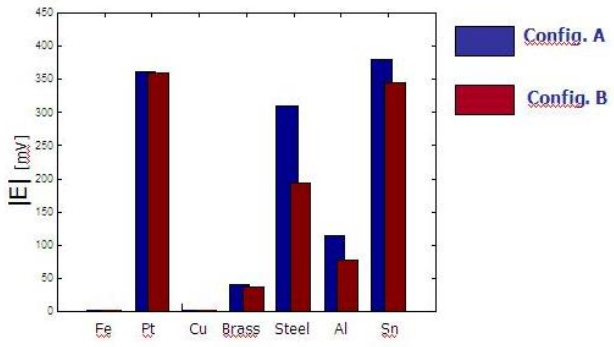

Figure 3.5: Mean potential values for metallic sensors when immersed in different configurations

for steel, aluminium and tin, with differences of over 50 mV when sensors were partially or totally immersed.

3.1.4 New measure strategy

After the preliminary considerations on parameters affecting sensor response reproducibility, a new measure protocol was evaluated, to check if their influence could be reduced:

- calibrations were performed in buffered background solution (MES 0,01M pH=5,5);
- concentration range was $10^{-3} - 10^{-1}$ M;
- magnetic stirrer was switched on (200 rpm) for 5 seconds after the injection and then switched off;

- successive injection were performed every 100 seconds;
- sensors were mechanically cleaned by sand paper after each calibration;
- sensors were stored in air at the end of each day.

Calibrations were repeated several times, focusing on the most representative salts, according to previous results (table 3.1), namely NaCl (calibrations were also repeated using distilled water as background solution), $NaHCO_3$ and $NaNO_2$; chloride ion response was also studied with higher accuracy: in fact super-Nernstian or near-Nernstian responses were obtained, for most electrodes; in all the concentration range, more points were collected to evaluate a more precise calibration curve.
Calibration curve slopes are shown in table 3.2.

From a comparison with calibrations performed in distilled water with first

	NaCl	**$NaNO_3$**	**$NaHCO_3$**
Fe	$-16,0 \pm 6,1$	$-18,0 \pm 13,9$	$-36,5 \pm 3,4$
Pt	$-10,8 \pm 6,4$	$-31,0 \pm 6,0$	$+162,6 \pm 7,2$
Cu	$-66,9 \pm 5,8$	$-62,6 \pm 1,6$	$+1,7 \pm 5,8$
Brass	$-91,1 \pm 6,3$	$-100,6 \pm 64,0$	$+8,5 \pm 1,0$
Steel	$-213,2 \pm 15,6$	$-26,4 \pm 6,7$	$-24,5 \pm 3,4$
Al	$-1,0 \pm 2,0$	$-87,0 \pm 6,0$	$+5,0 \pm 5,3$
Sn	$-24,4 \pm 3,3$	$-90,2 \pm 1,9$	$-33,5 \pm 3,9$

Table 3.2: Standard calibrations of metallic electrodes with new measure strategy: response slope towards standard laboratory analytes. All values are given in mV/decade

strategy, a sensitivity reduction, probably due to the presence of MES (which acts as interferring ion) and a higher reproducibility have been noticed; in particular a dramatic reduction in standard deviation values have been obtained, thus indicating that the news introduced in new calibration protocol, improved the system performances.
New measure strategy was also applied for the study of the response towards chloride ion, which induced super- or near-Nernstian response in most all sensors. Calibrations were performed in distilled water and potentials were measured at 10^{-3}M, $10^{-2,5}$M, 10^{-2}M, $10^{-1,5}$M, 10^{-1}M and $10^{-0,7}$M. Response slopes in solutions of KCl and NaCl are shown in table 3.3.

Slopes confirmed the influence of MES as interferring ion, with all sensitivities showing higher values, in particular for iron and tin, whose response varied from cationic to anionic. Distilled water as background solution, on the other side, induced unstable potentials, with a more noisy signal during calibration. At higher concentrations all sensors showed a well defined potential, with differences during several repetitions (at least 15 for all salts) in the order of few milliVolts.

	NaCl	KCl
Fe	$-107,0 \pm 16,6$	$-111,3 \pm 11,2$
Pt	$-29,7 \pm 9,9$	$-23,6 \pm 4,0$
Cu	$-88,9 \pm 6,5$	$-94,4 \pm 65,9$
Brass	$-90,6 \pm 9,9$	$-93,2 \pm 3,2$
Steel	$-137,1 \pm 29,0$	$-146,2 \pm 27,0$
Al	$-11,8 \pm 10,3$	$-5,3 \pm 7,2$
Sn	$-60,9 \pm 13,7$	$-83,4 \pm 8,9$

Table 3.3: Standard calibrations of metallic electrodes towards chloride ions: further investigations. All values are given in mV/decade

3.1.5 Conclusions

The sensing properties of metallic electrodes were analyzed by calibrating them in solutions of several standard laboratory salts, showing very high sensitivity towards most of them, but with low reproducibility in several repetitions during the measurement period and noisy signals. Our study was focused on the recognition of some parameters affecting the sensor response, evaluating a new calibration protocol with improved performances in term of stability and long-time reproducibility; calibrations performed in *controlled* conditions showed better results.
In particular:

- **iron** electrode showed a slow response dynamic: the time between two successive injections (100 seconds) was often not enough to reach the signal stabilization, while all other sensors showed stable potentials after 60-70 seconds. This behavior may be ascribed to the elevate reactivity shown by the sensor;

- **platinum** electrode showed low sensitivity towards most ions, with a particular behavior response, which still is object of further investigations: in all calibrations, except KI and Na_3PO_4, sensor showed cationic response between 10^{-3}M and 10^{-2}M and anionic between 10^{-2}M and 10^{-1}M. Improvements added in the new calibration protocol did not improve sensor performances;

- **copper** and **brass** electrode showed high sensitivity towards most anions, with response close to theoretical Nernstian value for chloride and iodide ions; in particular response towards chloride was very reproducible, with variations of only 2mV in solutions of Cl^- 0,1M;

- **steel** sensor reproducibility was not satisfactory and very noisy signal in all calibrations was observed, thus indicating the non-equilibrium situation; only at high concentrations (0,1M) a reproducible potential is obtained. Sensor showed high sensitivity towards solution pH;

- **aluminium** sensor showed partial cationic response, even if the reproducibility is not satisfactory with both calibration protocols;

- **tin** electrode stabilization, before all the calibrations, was strongly affected by drift which did not allow reproducible measures; sensing performances greatly improved when the second measure protocol was applied.

3.2 Porphyrinoid-based electrodes

In the past few years there has been an explosion of research activity in the area of chemically modified electrodes. This area of research has attracted such interest because of potential applications to electrocatalysis, electrosynthesis and photosensitization. Most of the methods that have been used to modify electrodes have involved covalent attachment to the electrode surface. In addition to covalent attachment, polymeric films have been recently used to modify electrodes. These polymeric films have been formed by casting the film on an electrode surface ([21] - [23]), using radio-frequency plasmas ([24]) and electropolymerization ([25] - [27]).

3.2.1 Solvent polymeric membranes

The key components of both types of sensors are lipophilic complexing agents capable of reversibly binding ions. They are usually called ionophores or ion carriers, thus reflecting the fact that these compounds also catalyze ion transport across hydrophobic membranes.
The essential part of a carrier-based ISE is the ion-sensitive solvent polymeric membrane, physically a water-immiscible liquid of high viscosity that is commonly placed between two aqueous phases, i.e. the sample and the internal electrolyte solution. It contains various constituents, commonly an ionophore (ion carrier) and a lipophilic salt as ion exchanger. The sensor responds to the activity of the target ion and usually covers an extraordinarily large sensitivity range, from about 1 to 10^{-6} M. Its selectivity is related to the equilibrium constant of the exchange reaction of target and interfering ions between the organic and aqueous phases. It strongly depends on the ratio of complex formation constants of these ions with the ionophore in the membrane phase; ionophores are in their uncomplexed (or unassociated) form either charged or electrically neutral.
According to literature proposed methods, membranes are composed of ionophore (1 wt.%), polymeric matrix (usually PVC, 33wt.%) and plasticizer (66-67 wt.%). In some case, blank membranes (with no ionophore) have been proposed: for a ligand free ISE membrane based on an ion exchanger that is incapable of specific interactions, the selectivities are determined by the difference between the standard free energies of the ions in the aqueous and organic phases, which is only influenced by the plasticizer. The selectivity sequence obtained with such membranes is always the same. The potentiometrically obtained values ([28], [29])

nicely correlate with those measured by voltammetry on liquid-liquid interfaces ([30]). It is usually named after Hofmeister, who, in 1888 at the Pharmacological Institute in Prague, studied the effect of various salts on the coagulation of egg proteins and aimed at finding correlations with their diuretic and laxative properties ([31]). The sequences he obtained for some cations and anions were later shown to agree with those of the free energies of hydration of the ions.

3.2.2 Electro-polymer based membranes

Electrodes coated with electroactive polymers have been intensively researched over the past several years. Besides providing avenues for fundamental studies of the electroactive materials ([32]), coated electrodes can have applications in energy storage, electrocatalysis, photosensitization, electrochromics, electroanalysis and controlled ion release ([33], [34]). The electroactive polymers include those prepared by electropolymerization of aniline ([35]), phenol ([36]) and pyrrole ([37]) and their derivatives; the electropolymerization chemistry of these monomers and the electrochemical, electrical and physicochemical properties of their polymer films have been reported in the literature.
Attachment of Metallo-porphyrins to electrodes is attractive on several grounds. These molecules exhibit a rich electron-transfer chemistry, are ingredients of biopolymers, can often be manipulated by axial ligation to the central metal ion and are potentially good catalysts and photosensitizers. Previous immobilization studies of porphyrins and phthalocyanines have relied on chemisorption ([38]) vapor deposition ([39]) and condensation reactions of porphyrin side chains with functionalized electrodes ([40]). Polymeric porphyrin films have been obtained by amidization or esterification of a methyl acryl polymer and subsequent adsorption of the polymer-porphyrin solution ([41]) and by the uptake of charged porphyrins by ion-exchange polymer coatings ([42]). Macor and Spiro used a different approach by oxidatively electropolymerizing metal/protoporphyrin IX complexes via the vinyl substituents on the porphyrin periphery ([43]). Following previous experiences with amino-substituted ruthenium phenanthroline complexes ([44]), Bettelheim and co-workers recently investigated and reported on the oxidative electropolymerization of $tetrakis(o-aminophenyl)porphyrin$ ($H_2(o-NH_2)TPP$) and some of its metalated derivatives ([20], [47]). The electropolymerized $poly-Co(o-NH_2)TPP$ films are effective catalysts for the electroreduction of dioxygen in aqueous solution and in general the electropolymerized porphyrin films have proved to be stable, adherent and electroactive at the expected potentials ([47]).
They also reported a broadened electrochemical and spectroscopic study of porphyrin electro-oxidative polymerization using amino-, dimethylamino- and hydroxy-substituted tetraphenylporphyrins, their cobalt and nickel complexes and a newly synthesized porphyrin, tetrakis$(p-N-pyrrolylphenyl)porphyrin$ ($H_2(p-pyr)TPP$) that was designed to electropolymerize via polypyrrole-like coupling ([37]).

3.2.3 Sensor array for the prostate tumor detection

An array composed of eight sensors was developed (table 3.4), for the analysis of human urines, to detect prostate tumor.

5,10,15,20-tetra(4-hydroxy 3-methoxy phenyl) porphyrin (VanPorph, figure

Membrane	**Ionophore**	**Polymer**	**Plasticizer**	**Ionic additive**
1	VanPorph	-	-	-
2	ZnVanPorph	-	-	-
3	VanPorph	PVC	DOS	-
4	-	PVC	DOS	TDACl
5	CoVanPorph	-	-	-
6,8	(NH_2)-TPP	-	-	-
7	Hemin	-	-	-

Table 3.4: Composition of sensor array membranes for the detection of prostate tumor

3.6) and related metal complexes, hemin (figure 3.7) and 5-(4-AminoPhenyl)-10,15,20-tri(phenyl) porphyrin ($(NH_2)-TPP$, figure 3.8) were synthesized according to literature methods ([48]). Poly(vinyl chloride) (PVC), plasticizer bis(2-ethylexyl) sebacate (DOS), Tetrahydrofurane (THF) and tetra dodecylammonium chloride (TDACl) were purchased from Fluka (Ronkonkoma, NY). All aqueous solutions were prepared with distilled water; salts of highest purity were available from Fluka (Buchs, Switzerland).

Array is composed of sensors based on electro-polymerized membranes (no. 1, 2, 5-8), PVC-based membrane (no. 3) and a blank membrane (no. 4). PVC-

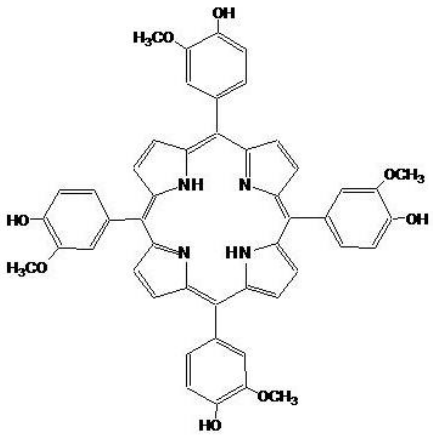

Figure 3.6: $5,10,15,20-tetra(4-hydroxy3-methoxyphenyl)porphyrin$ (VanPorph) structure

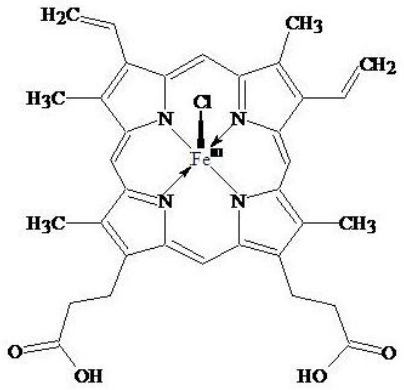

Figure 3.7: Hemin structure

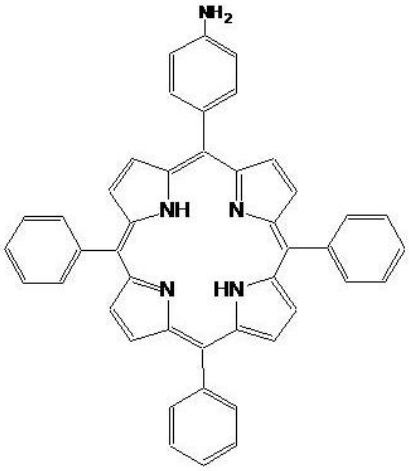

Figure 3.8: $5-(4-AminoPhenyl)-10,15,20-tri(phenyl)porphyrin$ (H_2NH_2TPP) structure

membranes were prepared according to standard method (already described in previous sections), using tetra-hydro furane (THF) as solvent.
The deposition of regular films of Vanillin Porphyrin and Hemin was performed by electro-polymerization on the sensor surfaces, in a 3-electrodes cell, using a commercial potentiostat (AMEL, mod. 7050), Standard Calomel Electrode as reference electrode (AMEL, mod. 303/SCG/6) and platinum wire (diameter 0,7 mm) as counter electrode, starting from a solution of porphyrin dissolved in basic media (NaOH 1M, $porphyrin : solvent = 3mg : 4mL$); ($NH_2$)-TPP deposition was performed in analogue conditions, but from acidic solution (HCl

37 wt.% and MeOH). In particular, no references in literature, report about hemin molecules electro-deposition on platinum sensors.
Interesting results were obtained from the cyclic voltammetry used for the electro-polymerization of porphyrins; in analogy with literature references, a non-conductive layer was obtained for vanillin porphyrin deposition, shown by a decreasing peak value in the current flowing through the cell. On the other hand, the choice of amino group- modified porphyrins, allowed the evaluation of a conductive film. In figure 3.9 a a well defined reduction peak can be observed at a potential of $\approx 0,9V$, thus indicating the formation of the porphyrin layer; in the zoom, the arrow clearly indicates the increasing in current peak, thus indicating the increasing layer conductance.

Chemical properties were evaluated by calibrating sensors towards standard

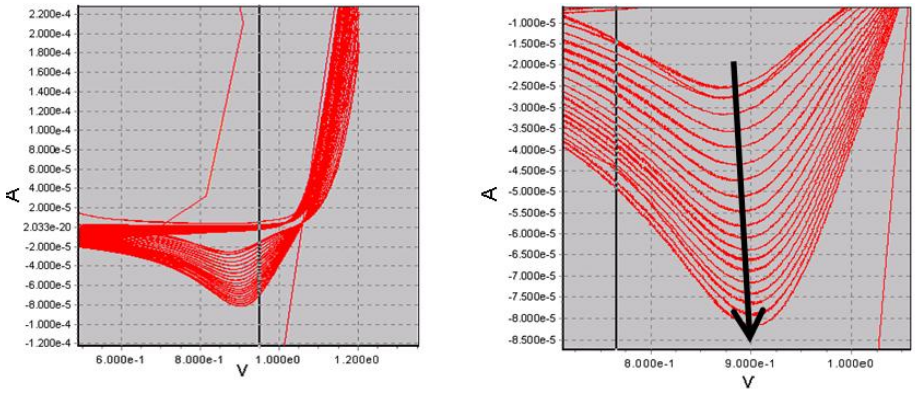

Figure 3.9: Cyclic voltammetry plot related to NH_2-TPP deposition. It shows an increasing peak in reduction phase at $\approx 0,9V$

laboratory salts; calibrations were performed in the range between 10^{-6} and 10^{-1} M and slopes, calculated in the linear range, are shown in table 3.5. Buffer solution (MES 10^{-2}M + NaOH, $pH = 5,5$) was used as background to avoid pH influence on response.

All studied membranes showed a good stability in background solution and a high reproducibility in *baseline* potential, with errors in the order of few milli-Volts.
Membranes based on vanillin porphyrin (no. 1 and 3, both deposed by electro-polymerization and PVC-based) as M.A.C. (Membrane Active Material), showed a similar selectivity pattern, characterised by a partial cationic selectivity except for iodide ion. Such response is related to the molecule structure, with several $-OH^-$ groups, which reversibly and weakly bind positive charged molecules.
The introduction in the molecule core of a metal ion (Zn, membrane no. 2 and Co, membrane no.5), changed the selectivity from partially cationic to anionic, in particular to iodide ion, with response of $-22,2$ and $-37,7$ $mV/decade$ respectively.

Membrane	**NaCl**	**KI**	**LiCl**	**NaBr**	**CH_3CO_2Na**
1	$+3,2 \pm 0,4$	$-53,8 \pm 4,6$	$+1,7 \pm 0,4$	$+2,7 \pm 0,7$	$-5,2 \pm 1,4$
2	$-8,3 \pm 0,2$	$-22,2 \pm 3,4$	$-6,8 \pm 0,8$	$-6,9 \pm 1,9$	$-4,1 \pm 0,5$
3	$+6,7 \pm 0,6$	$-7,3 \pm 8,8$	$+6,8 \pm 0,8$	$+9,7 \pm 3,1$	$+3,9 \pm 0,6$
4	$-34,9 \pm 0,8$	$-45,9 \pm 7,2$	-	$-45,6$	$-1,9 \pm 0,4$
5	$+0,3 \pm 0,3$	$-37,7 \pm 5,8$	$+0,9 \pm 0,4$	$+0,3 \pm 0,4$	$-7,2 \pm 0,2$
6, 8	$-12,4 \pm 1$	$-41,1 \pm 4,4$	$-11,5 \pm 0,8$	$-12,6 \pm 1,2$	$-14,3 \pm 1,9$
7	$-9,2 \pm 1$	$-2,6 \pm 3,7$	$+6 \pm 0,6$	$-8 \pm 0,1$	$-1,6 \pm 0,4$
Membrane	**$NaNO_3$**	**$NaNO_2$**	**$NaClO_4$**	**$MgCl_2$**	**NaF**
1	$+4 \pm 1,9$	$+1,7 \pm 1,6$	$+1,3 \pm 1$	$+2,8 \pm 0,9$	$+0,8 \pm 0,7$
2	$-2,3 \pm 1,6$	$-3,5 \pm 1,3$	$-1,8 \pm 1,2$	$-10,5 \pm 1,9$	$-3 \pm 1,2$
3	$+13,1 \pm 1$	$+11,4 \pm 4,6$	$-3,2 \pm 5,9$	$+5,6 \pm 1,9$	$+6,7 \pm 4,9$
4	$-40,22$	$-53,0$	$120,2 \pm 18$	–	$-1,8$
5	$+1 \pm 1,7$	$-0,5 \pm 1,2$	$-1 \pm 0,5$	$+0,2 \pm 0,1$	$+0,2 \pm 0,3$
6, 8	$-26,5 \pm 2,8$	$-21,9 \pm 7,3$	$-15,4 \pm 5,1$	$-16,2 \pm 0,1$	$-9,4 \pm 2$
7	$-4 \pm 0,5$	$-5,4 \pm 1,2$	$-4,9 \pm 1,1$	$-12,1 \pm 1,8$	$+2 \pm 1,2$

Table 3.5: Calibration towards standard laboratory salts of the PVC- and electropolymer-based sensor array for the detection of prostate tumor; response slopes are calculated in the linear range and given in mV/decade

Blank membrane, only based on classical ion exchanger (TDACl), showed a pattern selectivity close to theoretical Hofmeister series, obtained for quaternary ammonium salts (Q.A.S.).
Hemin sensor has shown anionic response towards all studied ions, with selectivity pattern very different from Hofmeister series and chloride as primary ion.
Amino-TPP-based sensor, showed high selectivity towards iodide ion, with response close to theoretical Nernstian-slope and nitrate and nitrite ions (with responses of $-26,5$ and $-21,9$ respectively), while low selectivity coefficient were found for chloride, fluoride and perchlorate ions.
All metallo-porphyrins normally show high selectivity towards H^+ ions, so all calibrations were performed in buffered solution, namely MES 10^{-2}M, adjusting pH to 5,5 by NaOH injections. Sensors were also calibrated to pH variations, starting from the commonly used solution, named *universal buffer* (citric acid $6,7 \times 10^{-3}$M, boric acid $11,4 \times 10^{-3}$M and NaH_2PO_4 10^{-2}M). Solution pH was then increased by NaOH 1M additions and controlled by commercial pH glass electrode. Calibration plot is shown in figure 3.10, while response slopes, calculated in all range for sensors no. $1-5$ and 7 and ranges $2-9$ and $9-11$ for sensors no. 6 and 8 are shown in table 3.6.

All membranes based on porphyrins were sensitive to pH variations with response close to theoretical value for membranes no. 1, 5, 6 and 8, while blank membrane showed a low influence (response of $-5,6 mV/decade$). NH_2-TPP sensor showed low sensitivity until $pH = 9$ with slope of $-10,4 mV/decade$, which increased at higher values.

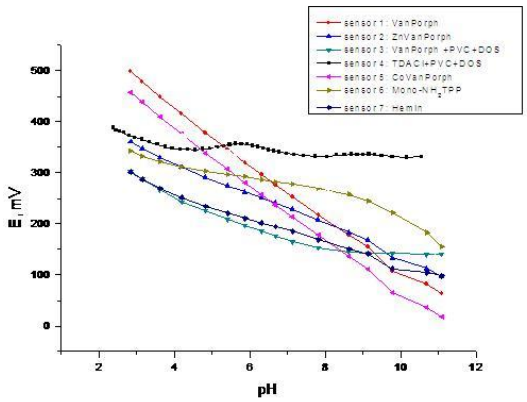

Figure 3.10: Sensor pH response in range $2,5 - 10,5$

Membrane	**Range**	**Response slope**
1	All	$-53,9 \pm 1,2$
2	All	$-31,2 \pm 0,3$
3	All	$-19,2 \pm 0,7$
4	All	$-5,6 \pm 1,0$
5	All	$-54,2 \pm 0,8$
6, 8	$2 - 9$	$-10,4 \pm 4,6$
	$9 - 11$	$-51,8 \pm 9,9$
7	All	$-23,7 \pm 0,3$

Table 3.6: Sensor pH response slopes

3.2.4 Sensor array for the detection of gases dissolved in solution

In the measure of gases in mixtures, a lot of variables affecting Electronic Nose sensor response, are present. One of the most important, in term of influence, is the relative humidity, since water molecules, polar, can interact with the sensitive molecules of the membrane. Strategy for Electronic Nose measurements, normally utilizes inert gases (such as N_2) previously dried or humidity traps. Starting from these limits, a new idea was developed, in order to overcome Electronic Nose humidity problems by measuring gases dissolved in water by means of an Electronic Tongue system. Sensor array was composed of four different membranes, each one deposited twice to verify deposition technique reproducibility; compositions are shown in 3.7.

5-(4-Amino phenyl)-10,15,20-tri(phenyl) porphyrin ($(NH_2)-TPP$, figure 3.8),

Membrane	**Ionophore**	**Polymer**	**Plasticizer**
1, 2	Tris(NH_2)-TPP	-	-
3, 4	(NH_2)-TPP	PVC	DOS
5, 6	Bis(NH_2)-TPP	PVC	DOS
7, 8	Tris(NO_2)-TPP	PVC	DOS

Table 3.7: Composition of sensor array membranes for the detection of dissolved gases in liquids

5,15-di(4-Amino phenyl)-10,20-di(phenyl) porphyrin ($Bis(NH_2)-TPP$, figure 3.11), 5,10,15-tris(4-Amino Phenyl)-20-phenyl Porphyrin ($Tris(NH_2)-TPP$, figure 3.12) and 5,10,15-tri(4-nitro Phenyl)-20-phenyl porphyrin ($Tris(NO_2)-TPP$, figure 3.13) were synthesized according to literature methods ([48]). Poly (vinyl chloride) (PVC), plasticizer bis(2-ethylexyl) sebacate (DOS) and Tetrahydrofurane (THF) were purchased from Fluka (Ronkonkoma, NY). All aqueous solutions were prepared with distilled water; salts of highest purity were available from Fluka (Buchs, Switzerland).

Plasticized membranes (no. $3-8$) were prepared according to standard method; no ionic additives were added, in order to evaluate the ionophore response. Electro-polymerized membranes, no. 1 and 2, were prepared in a 3−electrode cell, using a commercial potentiostat (AMEL, mod. 7050), Standard Calomel Electrode as reference electrode (AMEL, mod. 303/SCG/6) and platinum wire (diameter 0,7 mm) as counter electrode, starting from a solution of $7,5mg$ of porphyrin dissolved in $10mL$ of HCl 1M and $15mL$ of pure MeOH. Response slopes were calculated in linear range and values are given in table 3.8.

Membranes no. 1 and 2 showed anionic response towards all studied ions, with the highest sensitivity towards iodide ions ($-26,8mV/decade$); all the obtained results are very close to those obtained depositing the same porphyrin in other applications (see previous section), thus indicating a good control in deposition

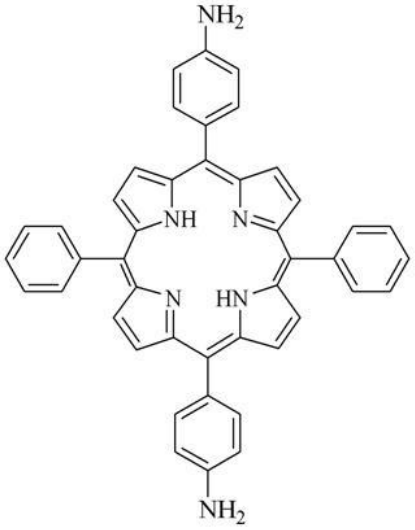

Figure 3.11: $5,15-di(4-AminoPhenyl)-10,20-di(phenyl)porphyrin$ ($(Bis-NH_2)-TPP$) structure

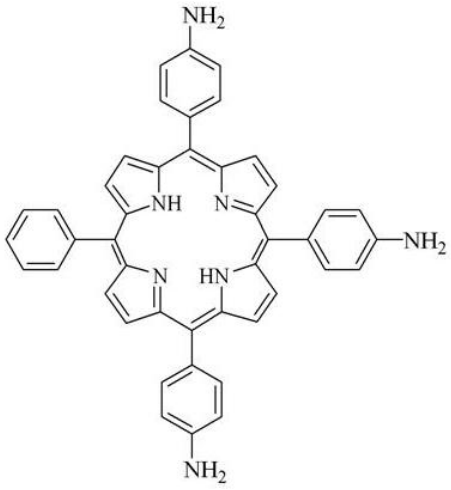

Figure 3.12: $5,10,15-tri(4-NH_2Phenyl)-20-phenylPorphyrin$ ($Tris(NH_2)-TPP$) structure

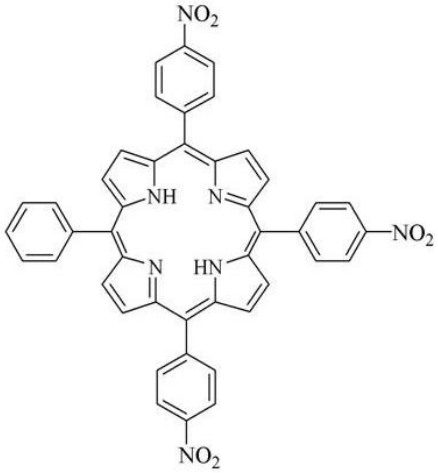

Figure 3.13: $5,10,15 - tri(4 - NO_2Phenyl) - 20 - phenylporphyrin$ $(Tris(NO_2) - TPP)$ structure

Membrane	**NaCl**	**NaF**	**$NaNO_3$**	**$NaNO_2$**	**NaBr**	**KCl**
1	$-7,3 \pm 3,4$	$-2,2 \pm 1,2$	$-5,3 \pm 2,2$	$-5,3 \pm 4,3$	$-4,5 \pm 0,4$	$-5,6 \pm 2,5$
2	$+3,7 \pm 3,2$	$+5,8 \pm 2,2$	$+5,3 \pm 1,5$	$+7,4 \pm 3,9$	$-2,3 \pm 1,5$	$+11,5 \pm 1,0$
3	$+14,5 \pm 3,9$	$+18,9 \pm 0,6$	$+15,0 \pm 1,9$	$+19,0 \pm 4,5$	$+19,5 \pm 2,4$	$+20,6 \pm 0,9$
4	$+34,6 \pm 1,5$	$+37,2 \pm 3,9$	$+33,0 \pm 2,1$	$+53,5 \pm 1,5$	$+43,3 \pm 2,1$	$+43,3 \pm 3,2$
Membrane	**LiCl**	**KI**	**$NaCH_3CO_2$**	**NaSal**	**NaSCN**	**$NaClO_4$**
1	$-8,8 \pm 0,4$	$-26,8 \pm 4,3$	$-1,4 \pm 0,8$	$+0,8 \pm 0,1$	$-7,4 \pm 4,3$	$-2,4 \pm 0,7$
2	$+9,1 \pm 2,8$	-	-	$-3,2 \pm 2,9$	$-7,4 \pm 1,5$	-
3	$+21 \pm 0,2$	$+15,9 \pm 0,8$	$+25,2 \pm 1,7$	$20,0 \pm 2,9$	$+21,1 \pm 0,7$	$+18,9 \pm 0,3$
4	$+38,6 \pm 3,0$	$+37,4 \pm 1,9$	$+47,2 \pm 2,4$	$+43,8 \pm 1,1$	$+43,8 \pm 1,1$	$+40,9 \pm 0,7$
Membrane	**Na_2SO_4**	**$MgCl_2$**	**$CaCl_2$**	**$CoCl_2$**	**$Cu(NO_3)_2$**	**$AlCl_3$**
1	-	$-12,1 \pm 1,8$	$-5,4 \pm 0,2$	$-9,9 \pm 0,6$	$+9,4 \pm 0,9$	$+7,8 \pm 2,4$
2	$+8,3 \pm 2,5$	$+5,4 \pm 5,2$	$+2,0 \pm 1,8$	$+5,7 \pm 1,0$	$+15,7 \pm 6,3$	$+36,4 \pm 5,8$
3	$+21,4 \pm 0,9$	$+14,3 \pm 7,3$	$+9,9 \pm 1,6$	$16,9 \pm 2,8$	$+12,6 \pm 5,3$	-
4	$+47,1 \pm 3,7$	-	$+9,92 \pm 2,5$	$-2,2 \pm 0,9$	$+17,9 \pm 1,5$	$+7,2 \pm 6,5$

Table 3.8: Calibration towards standard laboratory salts of the sensor array for the detection of gases dissolved in liquids; response slopes are calculated in the linear range and given in mV/decade

technique parameters which allow reproducible membranes.
Membranes based on amino-TPP based PVC membrane (no. 3 and 4) showed cationic response, with sub-Nerstian slopes in all solutions.
Membranes no. $5-8$ had similar selectivity patterns, with the highest responses for sensors based on nitro-substituted porphyrins, with response close to teorethical value in the case of sodium and potassium ions ($+53,5$ and $+43,3$ $mV/decade$ in solutions of $NaNO_2$ and KCl, respectively).
Selectivity coefficients for all membranes were calculated, according to primary ion (respectively I^-, Al^{3+} and Na^+). Separate solution method was applied:

$$logK_{I/J}^{POT} = \frac{z_i F[E(J) - E(I)]}{2,303RT} + log(\frac{a_I(I)}{a_J(J)^{z_I/z_J}}) \tag{3.1}$$

Selectivity coefficients are shown in figure 3.14, for membranes no. 1 and 2 (anionic response) on the left and for membranes no. $3-8$ (cationic response) on the right. It is possible to see how all studied membranes showed a pattern se-

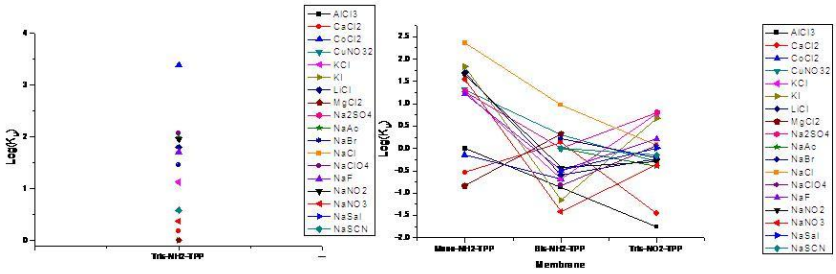

Figure 3.14: Selectivity coefficients: membranes with anionic response (no.1 and 2, left) and with cationic response (no. $3-8$, right)

lectivity very different from classical Hofmeister series, caused by the porphyrin which induces such behavior. In particular, membranes no. 1 and 2 showed a high sensitivity towards cobalt ion with selectivity coefficients higher than 1,5 than all other ions. Membranes with plasticized amino-substituted porphyrins showed similar patterns with low influence from second group metals; amino-substituted porphyrin, on the other hand, showed similar sensitivity towards first group metals, but not neglectable influence from cobalt ion.

3.2.5 PVC-based sensor array for the analysis of *Verdicchio* white wines

Sensor array is fastly becoming a promising way to perform chemical qualitative and quantitative analysis on several liquid matrices, such as drinkable or waste waters, soft and alcoholic drinks, ...
A sensor array, composed of 12 PVC-based membranes, was developed, in order to analyse different samples of white wines, of *Verdicchio D.O.C.* quality, but

produced in different years and coming from different cantinas. Array composition is reported in table 3.9.
$5,10,15,20-tetra(phenyl)porphyrin$ (TPP, figure 3.15) and related metal com-

	Ionophore (wt%)	**Plasticizer**	**Lipophilic additive (wt%)**
1	H_2TPP (1)	DOS	-
2	Co(III)TPPBr (1)	o-NPOE	-
3	Co(II)TPP-O-$(CH_2)_6$-CH_3 (1)	o-NPOE	-
4	Co(II)TPP-O-$(CH_2)_6$-CH_3 (1)	DOS	TpClPBK (0,4)
5	-	TOP	-
6	-	DOS	TDACl (0,4)
7	Pt(II)TPP (1)	DOS	-
8	Pt(II)TPP (1)	DOS	TDACl (0,4)
9	Pt(II)TPP (1)	DOS	TDACl (1,6)
10	Pt(IV)TPPCl_2 (1)	o-NPOE	-
11	Pt(IV)TPPCl_2 (1)	o-NPOE	TDACl (0,4)
12	Pt(IV)TPPCl_2 (1)	o-NPOE	TDACl (1,6)

Table 3.9: Composition of PVC-based membranes for the analysis of different samples of Verdicchio wines

plexes of Co and Pt, were synthesized according to literature methods ([48]).
Poly(vinyl chloride) (PVC), plasticizers o-nitrophenyl octyl ether (o-NPOE), bis(2−ethylexyl) sebacate (DOS), tris(2−ethylexyl) phosphate (TOP), lipophilic additives potassium tetrakis(4−chlorophenyl) borate (TpClPBK) and tetra dodecylammonium chloride (TDACl), tetrahydrofurane (THF) were purchased from Fluka (Buchs, Switzerland).
Tris[hydroxymethyl]aminomethane (TRIS) and 2-[N-Morpholino]ethanesulforic acid (MES) were from Sigma Chemical Co. (St. Louis, MO, U.S.A.).
All aqueous solutions were prepared with distilled water, salts of highest purity were available from Fluka. Membranes of 100 mg weight were prepared according to the common procedure:

- 1 mg of ionophore, lipophilic additive (if needed) and 33 mg of PVC were weighted on analytical balances and placed in a test-tube;
- all components were dissolved in 1 mL of THF;
- plasticizer was added;
- mixture was cast on Glassy Carbon (GC, AMEL, Italy) working electrodes;
- solvent was allowed to evaporate overnight.

Potentiometric properties of freshly prepared electrodes were evaluated after 24 hours soaking in 0,01M NaCl solution. Potentials of sensors were measured

versus double junction saturated calomel electrode (AMEL, Italy), using a PC equipped high-impedance input 8−channel A/D converter (Smartronix, Rome, ITALY).
Sensor responses was examined in solutions of standard laboratory salts, by varying the concentration of salt in a range from 10^{-5}M to 10^{-1}M stepwise by addition of standard solutions 1M to the 0,01M TRIS-HCl, $pH = 7,2$ or 0,01M MES-NaOH, $pH = 5,5$ background every 100 sec (at least 3 replicas of every calibration were performed).
Membrane response towards pH variations, has been evaluated in universal buffer solution (citric acid 6,7 mM, boric acid 11,4 mM, NaH_2PO_4 10^{-2}M) with initial $pH = 2,5$, by additions of 1M NaOH, to $pH = 10,5$; AMEL glass pH electrode (model 411/CGG/6) was used to control pH.
Slopes were calculated for linear ranges of sensors calibration curves and used the for cross-sensitivity parameter evaluations (tables 3.10 and 3.11).
In general, H_2TPP based membrane no. 1, showed partial cationic response in

	NaCl	**NaBr**	**LiCl**	**$NaNO_3$**	**$NaNO_2$**	**$NaCH_3CO_2$**
1	$+11,0 \pm 6,0$	$+13,0 \pm 1,0$	$+9,0 \pm 1,0$	$+10,0 \pm 2,0$	$-1,0 \pm 2,0$	$+4,0 \pm 1,0$
2	$+13,0 \pm 3,0$	$+14,0 \pm 1,0$	$+4,0 \pm 1,0$	$+13,0 \pm 1,0$	$-31,0 \pm 3,0$	$+14,0 \pm 1,0$
3	$-10,0 \pm 6,0$	$-12,0 \pm 6,0$	$-14,0 \pm 3,0$	$-12,0 \pm 3,0$	$-21,0 \pm 3,0$	$-7,0 \pm 1,0$
4	$+37,0 \pm 10,0$	$+45,0 \pm 3,0$	$+32,0 \pm 3,0$	$+32,0 \pm 1,0$	$+30,0 \pm 2,0$	$+39,0 \pm 1,0$
5	$+17,0 \pm 5,0$	$+22,0 \pm 2,0$	$+21,0 \pm 1,0$	$+3,0 \pm 4,0$	$+31,0 \pm 2,0$	$+21,0 \pm 1,0$
	KCl	**KI**	**Na_2SO_4**	**$CaCl_2$**	**$MgCl_2$**	**pH**
1	$+24,0 \pm 1,0$	$-15,0 \pm 2,0$	$+6,0 \pm 4,0$	$+8,0 \pm 1,0$	$+7,0 \pm 1,0$	$-25,0 \pm 0,5$
2	$+19,0 \pm 2,0$	$-49,0 \pm 6,0$	$+9,0 \pm 1,0$	$+17,0 \pm 2,0$	$-1,0 \pm 0,5$	$-37,0 \pm 1,0$
3	$+3,0 \pm 1,0$	$-32,0 \pm 7,0$	$-6,0 \pm 7,0$	$-14,0 \pm 2,0$	$-17,0 \pm 2,0$	$-10,0 \pm 5,0$
4	$+42,0 \pm 5,0$	$+42,0 \pm 3,0$	$+40,0 \pm 6,0$	$+23,0 \pm 5,0$	$+2,0 \pm 3,0$	$-9,0 \pm 2,0$
5	$+21,0 \pm 4,0$	$+10,0 \pm 3,0$	$+24,0 \pm 3,0$	$+5,0 \pm 1,0$	$+5,0 \pm 3,0$	$-18,0 \pm 2,0$

Table 3.10: Calibration towards standard laboratory salts of the sensor array for the analysis of Verdicchio wines using TRIS-HCl, $pH = 7,2$, as background solution; response slopes are calculated in the linear range and given in mV/decade

analyzed salts, with slope varying in range $4 - 24$ mV/decade. The absence of lipophilic cationic additive TDA^+ in the composition of membrane 2 evoked the partial cationic influence (11−19 mV/decade) in solutions of high concentrations of all studied salts except nitrite and iodide ions for which the sub-Nernstian slopes of -31 ± 3 and -49 ± 6 mV/decade correspondingly have been detected in all concentration range.
While membrane 3 based on Co(II)TPP-O-$(CH_2)_6$-CH_3 showed a partial anionic response with slopes in range $10 - 17$ mV/decade in all studied salt solution, an addition of lipophilic anionic $TpClPB^-$ particles (membrane no. 4) led to the partial cationic sensitivity towards almost all analyzed cations, particularly for ammonium chloride solution, 40 ± 3 mV/decade and alkali ions (45 ± 3 mV/decade in solutions of NaBr and 42 ± 3 mV/decade in solutions of KI and KCl). Dummy TOP-plasticized membrane no. 5 showed a cationic response

	NaCl	**NaBr**	**$NaHCO_3$**	**$NaNO_3$**	**$NaNO_2$**	**$NaClO_4$**
6	$-35,0 \pm 1,0$	$-46,0 \pm 1,0$	$-50,0 \pm 2,0$	$-40,0 \pm 2,0$	$-53,0 \pm 2,0$	$-120,0 \pm 7,0$
7	$-48,0 \pm 1,0$	$-58,0 \pm 3,0$	$-68,0 \pm 4,0$	$-53,0 \pm 1,0$	$-7,0 \pm 11,0$	$-40,0 \pm 11,0$
8	$-9,0 \pm 11,0$	$-7,0 \pm 6,0$	$-21,0 \pm 2,0$	$-7,0 \pm 11,0$	$-35,0 \pm 3,0$	$53,0 \pm 1,0$
9	$-24,0 \pm 3,0$	$-50,0 \pm 1,0$	$-50,0 \pm 1,0$	$-36,0 \pm 3,0$	$-41,0 \pm 4,0$	$-117,0 \pm 9,0$
10	$-40,0 \pm 1,0$	$-48,0 \pm 6,0$	$-54,0 \pm 8,0$	$-41,0 \pm 4,0$	$-19,0 \pm 9,0$	$-44,0 \pm 5,0$
11	$-35,0 \pm 3,0$	$-46,0 \pm 2,0$	$-50,0 \pm 1,0$	$-43,0 \pm 1,0$	$-42,0 \pm 1,0$	$-72,0 \pm 7,0$
12	$-33,0 \pm 6,0$	$-39,0 \pm 4,0$	$-42,0 \pm 5,0$	$-41,0 \pm 2,0$	$-41,0 \pm 2,0$	$-39,0 \pm 6,0$
	NaGlu	**NaSal**	**Na_2SO_4**	**NaF**	**NaSCN**	**pH**
6	$-9,0 \pm 2,0$	$-59,0 \pm 4,0$	-19	$-1,8$	$-42,3$	$-6,0 \pm 1$
7	$-10,0 \pm 3,0$	$-19,0 \pm 15,0$	$+1,0 \pm 4,0$	$-8,0 \pm 6,0$	$-44,0 \pm 5,0$	$-9,0 \pm 2,0$
8	-	$-44,0 \pm 1,0$	$-4,0 \pm 1,0$	$-2,0 \pm 1,0$	$-38,0 \pm 6,0$	$-35,0 \pm 3,0$
9	$-10,0 \pm 2,0$	$-48,0 \pm 10,0$	$-8,0 \pm 2,0$	$-2,0 \pm 1,0$	$-49,0 \pm 1,0$	$-13,0 \pm 4,0$
10	$-9,0 \pm 1,0$	$-30,0 \pm 11,0$	$+1,0 \pm 1,0$	$-5,0 \pm 2,0$	$-45,0 \pm 4,0$	$-8,0 \pm 2,0$
11	-	$-53,0 \pm 7,0$	$+6,0 \pm 5,0$	$-1,0 \pm 1,0$	$-50,0 \pm 9,0$	$-34,0 \pm 5,0$
12	-	$-54,0 \pm 8,0$	$+8,0 \pm 7,0$	$-3,0 \pm 4,0$	$-45,0 \pm 18,0$	$-27,0 \pm 6,0$

Table 3.11: Calibration towards standard laboratory salts of the sensor array for the analysis of Verdicchio wines using MES-NaOH, pH 5,5, as background solution; response slopes are calculated in the linear range and given in mV/decade

towards all cations, slope varied in a range $3 - 42$ mV/pX.
Membranes based on Pt-porphyrins showed anionic responses, with higher slopes of Pt(IV)TPPCl_2 based membranes no. 10, 11 and 12 towards anions and selectivity different from Hofmeister pattern for Quaternary Ammonium Salts. An addition of lipophilic cationic additive improved anionic response (membranes no. 8, 9, 11 and 12): the optimal content of TDACl was found 40 mol% relative to ionophore ([45]). It was found, that the better operating conditions for porphyrin-based PVC solvent polymeric membranes can be reached in acidic media (0,01M MES-NaOH $pH = 5.5$) where a partial protonation of porphyrins can occur, which favor an ionophore-analyte complexation. This fact is favorable for porphyrin-based sensor application for acidic samples analysis as wine is.
Since there is not a well established method for the evaluation of sensors cross-sensitivity, we have used the method introduced in [46], which suggest the evaluation of 3 parameters: an *average sensor response slope* S, a *signal-to-noise* ratio K and a *non-selectivity factor* F describing the distribution of sensor sensitivity to different analytes. The higher are these values, the more cross-sensitive is a sensor; they are shown in table 3.12.

	Average slope S	**Signal-to-noise ratio K**	**Non-selectivity factor F**
1	13,8	0,96	0,050
2	26,7	0,79	0,020
3	14,0	4,68	0,020
4	25,9	0,72	0,010
5	10,9	0,21	0,020
6	45,6	5,60	0,046
7	24,9	0,45	0,069
8	36,9	9,90	0,069
9	40,7	3,70	0,045
10	32,1	1,50	0,109
11	43,4	2,70	0,116
12	38,3	1,07	0,158

Table 3.12: Cross-sensitivity parameters of sensor array applied for the analysis of Verdicchio wines

3.2.6 PVC-based sensor array for the detection of sophisticating substances in white wines

An array composed of 16 PVC-based membranes was developed in order to detect some analytes in white wines, mimicking wine defects, namely SO_2, H_2S and CH_3CO_2H. The membrane composition is given in table 3.13.

5,10,15,20-tetra(phenyl)porphyrin (TPP, figure 3.15) and related metal complexes of Mn, Fe, Cu and Rh, 5,10,15-tri(phenyl)corrole (TPC, figure 3.16) and related metal complexes of Mn, Fe and Cu, Mn and Zn complexes of 5,10,15,20-tetra(4-butyl phenyl) porphyrin (MnButTPP, figure 3.17), iron and nickel complexes of 2,3,17,18-tetra(ethyl)-7,8,12,13-tetra(methyl)corrole ($Et_4Me_4FeCorrCl$, figure 3.18), phosporus complex of 2,3,8,12,17,18-hexa(ethyl)-7,13-di(methyl) porphyrin (PO(EMC), figure 3.19), 2,3,17,18-tetra(ethyl)-7,8,12,13-tetra(methyl)-a,c-biladiene dihydro bromide (Biladiene, figure 3.20) and zinc complex of 5-furanyl-2,3,7,8,13,17-hexa(ethyl)-12,18-di(methyl)porphyrin (Zn(DEHMP-Fu), figure 3.21) were synthesized according to literature methods ([48]. Poly(vinyl chloride) (PVC), plasticizer bis(2-ethylexyl) sebacate (DOS) and Tetrahydrofurane (THF) were purchased from Fluka (Ronkonkoma, NY). All aqueous solutions were prepared with distilled water; salts of highest purity were available from Fluka (Buchs, Switzerland).

All plasticized membranes were prepared according to standard method, dissolving ionophore ($1mg$), polymer ($33mg$) and plasticizer ($66mg$) in 1,5mL of THF.

Membranes potentiometric properties were evaluated in solution od standard laboratory salts, by varying stepwise the concentration from 10^{-6}M to 10^{-1}M; slopes were calculated in linear range and shown in table 3.14.

Membranes showed sub-Nerstian response towards all studied ions, except for

Membrane	Ionophore	Polymer	Plasticizer
1	MnTPP	PVC	DOS
2	MnButTPP	PVC	DOS
3	MnTPC	PVC	DOS
4	CuTPC	PVC	DOS
5	TPC	PVC	DOS
6	FeTPP	PVC	DOS
7	TPP	PVC	DOS
8	FeTPC	PVC	DOS
9	CuTPP	PVC	DOS
10	$Et_4Me_4FeCorrCl$	PVC	DOS
11	PO(EMC)	PVC	DOS
12	$Et_4Me_4NiCorr$	PVC	DOS
13	RhOHTPP	PVC	DOS
14	ZnButTPP	PVC	DOS
15	Biladiene	PVC	DOS
16	Zn(DEHMP-Fu)	PVC	DOS

Table 3.13: Composition of sensor array membranes for the detection of sophisticating substances in wines

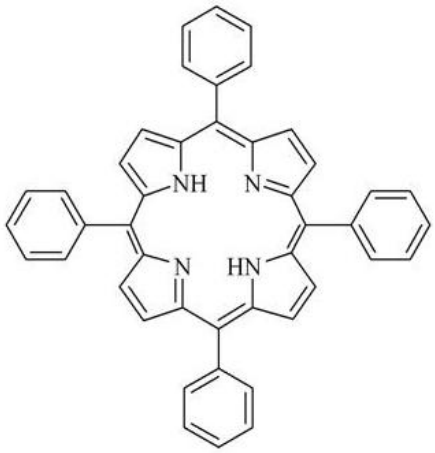

Figure 3.15: $5, 10, 15, 20 - tetra(phenyl)porphyrin$ (TPP)structure

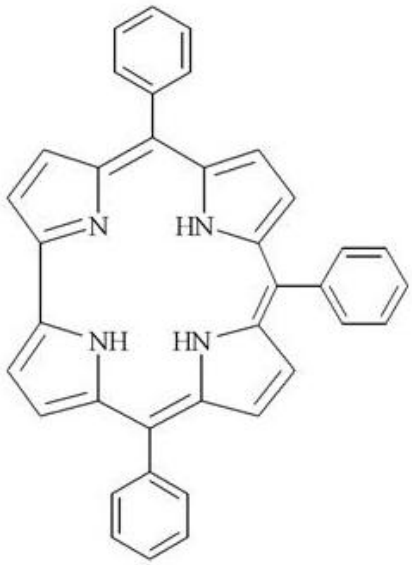

Figure 3.16: $5,10,15-tri(phenyl)corrole$ (TPC) structure

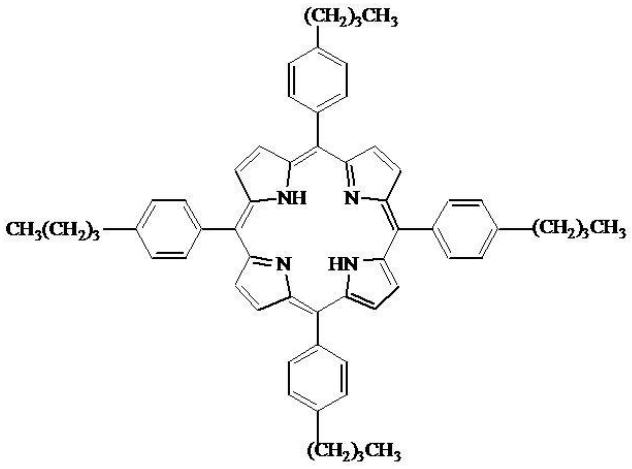

Figure 3.17: $5,10,15,20-tetra(4-butylphenyl)porphyrin$ (ButTPP) structure

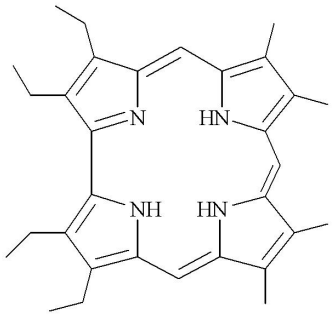

Figure 3.18: $2,3,17,18 - tetra(ethyl) - 7,8,12,13 - tetra(methyl) corrole$ (Et_4Me_4Corr) structure

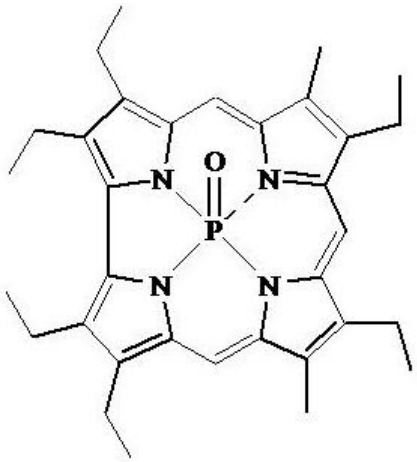

Figure 3.19: phosporus complex of $2,3,8,12,17,18 - hexa(ethyl) - 7,13 - di(methyl)$ *porphyrin* (PO(EMC)) structure

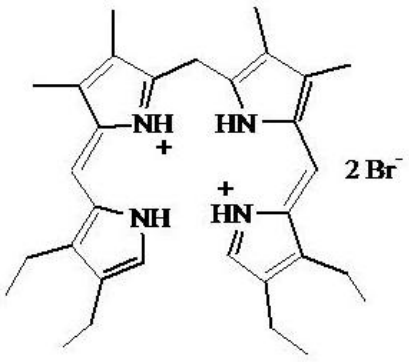

Figure 3.20: $2,3,17,18-tetra(ethyl)-7,8,12,13-tetra(methyl)-a,c-biladiene\ di(hydro)\ bromide$ (Biladiene) structure

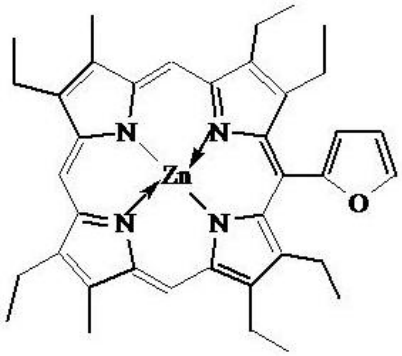

Figure 3.21: zinc complex of $5-furanyl-2,3,7,8,13,17-hexa(ethyl)-12,18-di(methyl)porphyrin$ (DEHMP-Fu) structure

Membrane	**$NaNO_2$**	**NaSal**	**NaGlu**	**NaSCN**	**$NaClO_4$**	**Na_2SO_4**
1	$-40,6 \pm 2,7$	$-60,1 \pm 1,7$	$-21,3 \pm 0,3$	$-60,4 \pm 2,6$	$-39,2 \pm 0,4$	$-16,8 \pm 0,9$
2	$-0,8 \pm 4,0$	$-37,7 \pm 7,2$	$-13,0 \pm 1,0$	$-42,7 \pm 3,6$	$-11,0 \pm 0,9$	$-10,6 \pm 0,7$
3	$-18,7 \pm 0,7$	$-27,3 \pm 0,3$	$-16,8 \pm 2,3$	$-29,4 \pm 1,2$	$-8,8 \pm 1,5$	$-14,5 \pm 1,5$
4	$-10,7 \pm 3,9$	$+14,6 \pm 1,8$	$+7,0 \pm 1,0$	$+1,6 \pm 1,8$	$-0,9 \pm 1,6$	$+4,3 \pm 0,6$
5	$-20,2 \pm 4,0$	$-18,9 \pm 0,2$	$+7,2 \pm 0,9$	$-30,3 \pm 0,2$	$-3,7 \pm 1,7$	$+7,8 \pm 0,1$
6	$-26,4 \pm 2,4$	$-14,3 \pm 1,9$	$+11,2 \pm 4,0$	$-15,0 \pm 7,1$	$-3,0 \pm 1,0$	$+3,4 \pm 0,5$
7	$+50,5 \pm 9,6$	$+13,2 \pm 3,9$	$+11,2 \pm 4,3$	$+33,3 \pm 2,7$	$+7,2 \pm 6,7$	$+8,6 \pm 3,2$
8	$-19,4 \pm 1,1$	$-34,6 \pm 2,0$	$-17,3 \pm 1,6$	$-25,9 \pm 2,6$	$-11,2 \pm 1,5$	$-13,9 \pm 1,2$
9	$+14,5 \pm 2,2$	$-22,7 \pm 0,9$	$-13,1 \pm 0,2$	$-15,8 \pm 0,5$	$-16,6 \pm 0,4$	$+1,3 \pm 2,9$
10	$-38,6 \pm 0,8$	$-41,7 \pm 1,5$	$-19,7 \pm 2,3$	$-43,7 \pm 5,1$	$-15,0 \pm 1,6$	$-6,5 \pm 1,6$
11	$+4,5 \pm 4,1$	$+21,2 \pm 2,2$	$+14,9 \pm 0,3$	$+9,8 \pm 0,2$	$+10,3 \pm 0,6$	$+15,9 \pm 1,7$
12	$+19,2 \pm 6,0$	$+23,7 \pm 2,1$	$+22,0 \pm 1,6$	$+13,2 \pm 0,9$	$+17,4 \pm 1,6$	$+17,0 \pm 0,4$
13	$+19,4 \pm 3,4$	$+41,5 \pm 3,6$	$+24,8 \pm 1,9$	$+16,2 \pm 1,8$	$+23,8 \pm 1,0$	$+21,0 \pm 1,3$
14	$-39,8 \pm 2,1$	$-16,1 \pm 2,4$	$-20,9 \pm 2,1$	$-28,5 \pm 1,5$	$-18,7 \pm 0,7$	$+1,7 \pm 2,0$
15	$+5,2 \pm 0,1$	$+11,7 \pm 0,5$	-	$+6,4 \pm 1,5$	$+10,9 \pm 1,8$	$+14,8 \pm 1,7$
16	$+20,0 \pm 2,8$	$+6,5 \pm 1,0$	$+19,6 \pm 0,9$	$+4,1 \pm 1,1$	$+17,2 \pm 3,9$	$+10,1 \pm 0,5$
Membrane	**NaCl**	**NaF**	**KI**	**$NaCH_3CO_2$**	**KCl**	**$NaNO_3$**
1	$-26,7 \pm 1,3$	$-28,7\pm,2$	$-14,5 \pm 9,5$	$-33,0 \pm 4,0$	$-17,0$	$-16,0$
2	$-10,9 \pm 0,7$	$+9,9 \pm 5,4$	$-4,2 \pm 1,0$	$-40,0 \pm 11,0$	$-5,8$	$-2,0$
3	$-8,5 \pm 1,1$	$-16,8 \pm 0,4$	$-9,1 \pm 1,9$	$-34,0 \pm 9,0$	$-2,2$	$-0,3$
4	$+4,0 \pm 0,6$	$+14,7 \pm 0,6$	$+13,1 \pm 5,6$	$+11,7 \pm 0,7$	$+1,1$	$+11,4$
5	$-8,6 \pm 1,0$	$-23,2 \pm 0,4$	$-8,4 \pm 5,0$	$-22,9 \pm 2,9$	$-6,4$	$-7,5$
6	$+18,0 \pm 0,2$	$-26,9 \pm 1,5$	$-23,0 \pm 15,7$	$-15,2 \pm 0,3$	$+18,6$	$+25,5$
7	$+9,9 \pm 4,3$	$+34,6 \pm 1,5$	$+27,5 \pm 11,6$	$+65,0 \pm 5,0$	$+12,2$	$+15,4$
8	$-7,7 \pm 0,8$	$+3,6 \pm 1,5$	$+6,8 \pm 6,0$	$-30,0 \pm 10,0$	$+1,4$	$-0,52$
9	$-0,5 \pm 1,4$	$-12,4 \pm 1,9$	$+5,9 \pm 1,2$	$-21,9 \pm 1,0$	$+10,6 \pm 0,3$	$+2,5 \pm 1,8$
10	$-12,0 \pm 1,2$	$-30,4 \pm 0,8$	$-67,7 \pm 1,7$	$-43,5 \pm 12,7$	$-12,2 \pm 2,8$	$+3,9 \pm 1,6$
11	$+4,6 \pm 2,0$	$+9,5 \pm 2,8$	$+8,8 \pm 0,2$	$+12,5 \pm 2,9$	$+10,2 \pm 1,6$	$+4,0 \pm 2,8$
12	$+26,7 \pm 3,1$	$+15,7 \pm 1,1$	$+15,6 \pm 0,3$	$+23,7 \pm 7,9$	$+18,1 \pm 2,9$	$+19,8 \pm 6,7$
13	$+23,0 \pm 4,2$	$+25,9 \pm 1,0$	$+31,1 \pm 1,2$	$+34,3 \pm 11,6$	$+20,0 \pm 0,7$	$+19,4 \pm 1,9$
14	$-10,0 \pm 1,0$	$-29,8 \pm 2,4$	$-36,0 \pm 2,3$	$-38,5 \pm 0,2$	$-4,0$	$-3,6 \pm 0,5$
15	$+10,4 \pm 3,3$	$+8,2 \pm 2,3$	-	–	$-48,2 \pm 11,0$	$+12,3 \pm 0,4$
16	$+13,7 \pm 1,1$	$+18,0 \pm 0,7$	$+18,7 \pm 0,7$	$+26,0 \pm 2,3$	$+22,2 \pm 0,7$	$+14,5 \pm 3,7$

Table 3.14: Calibration towards standard laboratory salts of the PVC-based sensor array for the detection of sophisticating substances in white wines; response slopes are calculated in the linear range and given in mV/decade

the most lipophilic ions such as Sal^- or SCN^-, when near-teorethical value of $-60,1$ and $-60,4 mV/decade$ in the case of membrane no. 1, were respectively obtained.
Free-base TPP based membrane (membrane no. 7) showed, as reported in literature, cationic response in almost all solutions with the highest response in solution of sodium acetate ($+60,5 mV/decade$). On the other side, membrane based on free-base corrole had different selectivity pattern, with mostly anionic response and high sensitivity towards fluoride, salicilate and nitrite ions.
Membranes based on manganese complexes of ionophore, showed anionic response towards all ions, with the highest response obtained for membrane no. 1 (MnTPP); high sensitivity towards Sal^- and SCN^- was received. Analogue membrane (no. 3, MnTPC) showed a similar selectivity pattern, but with lower slope values. The introduction of alchilic chain $(CH_3)_3CH_2$ in the ionophore molecule (membrane no. 2), did not vary the general response of membrane, but lower performances, if compared with membrane no. 1, were obtained.
In the case of copper metal ion, expected anionic response was obtained for membrane based on CuTPP (no. 9) with selectivity pattern close to Hofmeister series, while for membrane no. 4 (CuTPC), it was obtained only for ClO_4^- and NO_2^-.
For FeTPP based membrane (no. 6), anionic response was received with high sensitivity towards F^- ($-26,9 mV/decade$), I^- ($-23,0 mV/decade$) and NO_2^- ($-26,4 mV/decade$); a change in response slope, with anionic response at lower concentration and cationic at higher ones, seems to suggest a fast saturation of sensitive sites in membrane, probably allowing the migration of negatively charged ions from organic phase to water; this kind of response is matter of further investigations. When iron metal ion was coordinated to corrole (FeTPC, membrane no. 8), membrane showed different response pattern, with the highest sensitivities towards Glu^- ($-17,3 mV/decade$) and SO_4^{2-} ($-13,9 mV/decade$).
Membranes based on functionalized corroles showed different responses according to the oxidation state of the central metal: in the case of iron (membrane no. 10) anionic response with super-Nernstian response towards iodide ion ($-67,7 mV/decade$) was obtained; nickel corrole based membrane (no. 12) showed cationic response towards all salts, with slope varying in the range $13,2 - 26,7 mV/decade$.
ZnButTPP based membrane (no. 14) showed a selectivity pattern very different from classical Hofmeister series, with anionic response and high sensitivity towards not lipophilic ions such as fluoride ($-29,8 mV/decade$) and acetate ($-38,5 mV/decade$).
Finally, membranes no. 11, 13 and 15 showed prevalently cationic response towards most of salts.

3.2.7 PVC- and electropolymer-based sensor array for the detection of sophisticating substances in white wines

A second sensor array was developed, for the detection of sophisticating substances in wines, mimicking defects, namely sulphur dioxide, sulphidric and acetic acids.
It was composed of six different membranes, both deposited by solvent casting (PVC-based membranes) and by electro-polymerization on the platinum sensor surface. Membrane compositions are given in table 3.15.
Iron and manganese complexes of 5-(4-amino phenyl)-10,15,20-tri(phenyl) por-

Membrane	Ionophore	Polymer	Plasticizer
1	CoTris(NH_2)-TPP	-	-
2	Fe(NH_2)-TPP	-	-
3	Mn(NH_2)-TPP	-	-
4, 5	CuTris(NH_2)-TPP	-	-
5	ZnTPP	PVC	DOS
6	$ZnBr_2Mes_2TPP$	PVC	DOS

Table 3.15: Composition of sensor array membranes for the detection of sophisticating substances in wines

phyrin ($(NH_2) - TPP$, figure 3.8), cobalt and copper complexes of 5,10,15-tris(4-Amino phenyl)-20-phenyl porphyrin ($Tris(NH_2) - TPP$, figure 3.12), zinc complexes of 5,10,15,20-tetra(phenyl)porphyrin (TPP, figure 3.15) and 5,15-di(mesithyl)-10,20di(bromide) porphyrinate (Br_2Mes_2TPP, figure 3.22) were synthesized according to literature methods ([48]).
Poly(vinyl chloride) (PVC), plasticizer bis(2-ethylexyl) sebacate (DOS) and

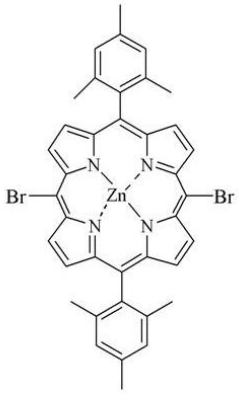

Figure 3.22: 5,15-di(mesithyl)-10,20di(bromide) porphyrinate structure

Tetrahydrofurane (THF) were purchased from Fluka (Ronkonkoma, NY). All aqueous solutions were prepared with distilled water; salts of highest purity were

available from Fluka (Buchs, Switzerland).
Analytical grade CH_2Cl_2 (Carlo Erba) and tetrabutylammonium perchlorate (TBAP, Fluka) were used as received.
All plasticized membranes were prepared according to standard method, dissolving ionophore ($1mg$), polymer ($33mg$) and plasticizer ($66mg$) in 1,5mL of THF.
The deposition of regular films of amino-substituted porphyrins was performed by electro-polymerization on the sensor surfaces, in a 3−electrodes cell, using a commercial potentiostat (AMEL, mod. 7050), Standard Calomel Electrode as reference electrode (AMEL, mod. 303/SCG/6) and platinum wire (diameter 0,7 mm) as counter electrode, starting from a solution of porphyrin ($1mM$), supporting electrolyte (TBAP, $0,1M$) in CH_2Cl_2.
100 layers of porphyrin were deposited on each sensor, by cyclically varying the potential between $-0,2V$ and $+1,4V$ with $250mV/sec$ as scan rate.
All cyclic voltammetry plots showed the formation of a conductive film, with an increasing value of the current flowing through the cell in successive scans. Deposition plots for membrane no. 1 (figure 3.23), no. 2 (figure 3.24), no. 3 (figure 3.25) and no. 4 (figure 3.26) are shown. In each graph, the reduction peak indicating the formation of porphyrinic film is indicated. Potentiometric

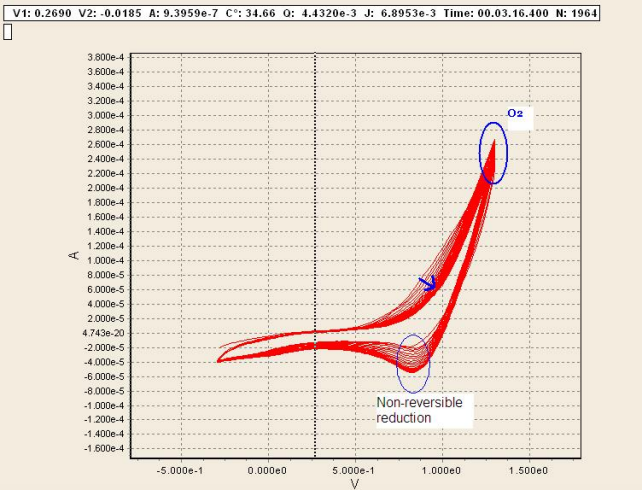

Figure 3.23: Cyclic voltammetry plot for CoTris(NH_2)-TPP deposition

properties of membranes were firstly evaluated by calibration towards several standard laboratory salts in concentration range between 10^{-6}M and 10^{-1}M, by varying stepwise concentration every 100 seconds. Response slopes for each calibration were calculated in the response linear range and are shown in table 3.16.

Membranes no. 1 and 3 showed similar response pattern, with low sensitivity towards all analysed cations; anionic response was only obtained for iodide ion

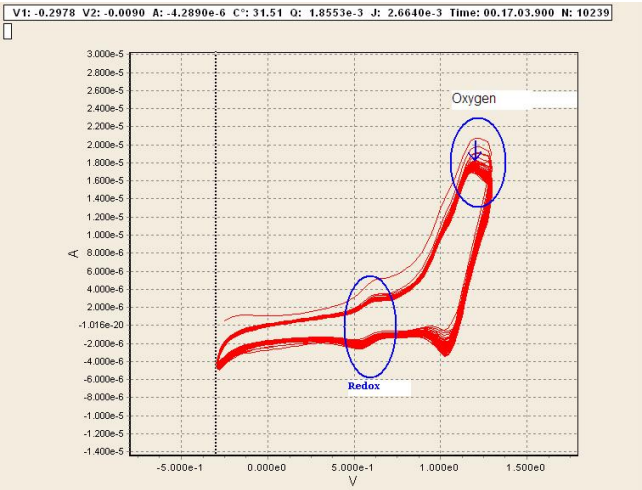

Figure 3.24: Cyclic voltammetry plot for $Fe(NH_2)$-TPP deposition

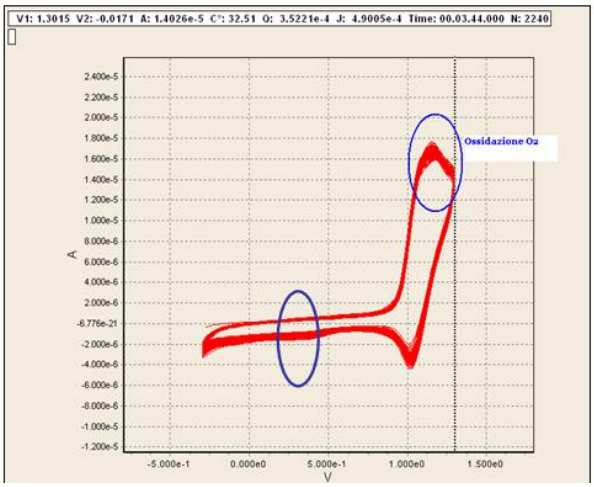

Figure 3.25: Cyclic voltammetry plot for $Mn(NH_2)$-TPP deposition

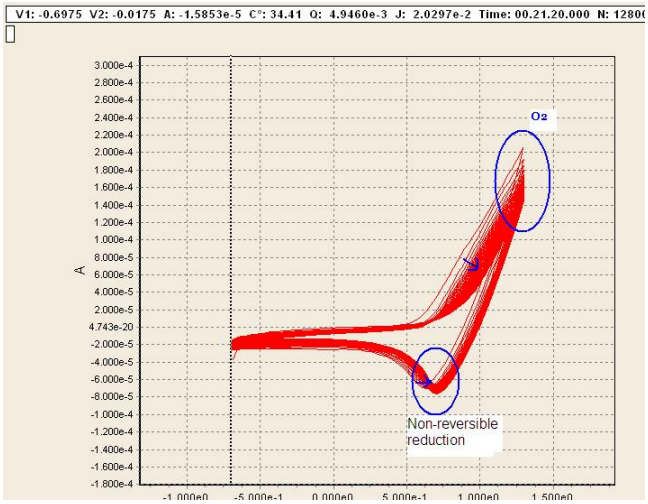

Figure 3.26: Cyclic voltammetry plot for CuTris(NH_2)-TPP deposition

Membrane	KI	NaBr	NaCl	$NaClO_4$	$NaNO_2$	$NaNO_3$	NaSCN
1	$-27,1 \pm 4,8$	$+3,9 \pm 3,9$	$+3,9 \pm 0,4$	$+9,3 \pm 1,4$	$+7,1 \pm 2,4$	$+11,1 \pm 0,2$	$+5,6 \pm 0,3$
2	$-40,1 \pm 4,5$	$-23,6 \pm 3,8$	$-10,3 \pm 2,0$	$-6,3 \pm 3,3$	$-17,8 \pm 2,8$	$-0,6 \pm 8,2$	$-23,5 \pm 1,4$
3	$-41,2 \pm 2,1$	$-3,1 \pm 1,7$	$+3,7 \pm 0,5$	$+10,6 \pm 1,6$	$+3,2 \pm 2,1$	$+10,0 \pm 1,7$	$-11,9 \pm 2,6$
4	$-46,9 \pm 2,8$	$-18,2 \pm 5,5$	$-10,9 \pm 5,7$	$-16,5 \pm 2,2$	$-17,2 \pm 3,8$	$-2,3 \pm 1,0$	$-29,3 \pm 2,7$
5	$+9,2 \pm 3,9$	$-0,2 \pm 2,0$	$+5,9 \pm 0,9$	$-4,3 \pm 2,3$	$-5,4 \pm 3,1$	$+7,6 \pm 0,8$	$-6,9 \pm 0,7$
6	$-10,2 \pm 3,9$	$-6,6 \pm 1,6$	$-3,6 \pm 1,0$	$-6,1 \pm 2,7$	$-11,5 \pm 3,3$	$+2,8 \pm 0,5$	$-14,7 \pm 2,9$

Table 3.16: Calibration towards standard laboratory salts of the PVC- and electropolymer-based sensor array for the detection of sophisticating substances in white wines; response slopes are calculated in the linear range and given in mV/decade

($-27,1 mV/decade$ and $-41,2 mV/decade$ respectively).
Anionic response was obtained towards all salts for $Fe(NH_2) - TPP$ and $CuTris(NH_2) - TPP$ based membrane (no. 2 and 4), with the highest sensitivity towards I^- ($-40,1$ $mV/decade$ and $-46,9 mV/decade$), Br^- ($-23,6$ $mV/decade$ and $-18,2$ $mV/decade$) and SCN^- ($-23,5$ $mV/decade$ and $-29,3$ $mV/decade$).
PVC-based membranes no. 5 and 6, showed anionic response towards most of salts, but with lower performances in terms of response slopes, with mean slope values varying in the range $0,2 - 6,9$ and $3,6 - 14,7$ mV/decade, respectively.
Selectivity patterns for all studied membranes, presented high deviations from classical Hofmeister series and partial selectivity towards all ions, thus indicating an ideal utilization in array configuration.

3.2.8 Evaluation of the best deposition conditions for amino-substituted porphyrins

Amino-substituted TPP electrodeposition has been studied since 1987 ([20]), when Bettelheim and co-workers reported the electro-polymerization of tetra (amino-phenyl) porphyrin. From that moment, researchers mainly focused on tetra-substituted amino porphyrins, because a more symmetrical and regular film can be obtained, since it has been shown that amino group acts as polymerization centre between one molecule and the phenyl group of an adjacent one.
A few years ago, researchers attention was also focused on TPP containing one, two or three amino groups in different positions of phenyl group, since they were proved to lead to the formation of sensitive films which could give good performances when used in sensor array.
Starting from Bettelheim work ([20]), all other works involving such molecules, utilized the proposed parameters, but no further investigations on their influence on sensing properties were performed. In fact, in [20] they concluded that the complex current/potential patterns shown for cyclic voltammetry plots for amino-substituted porphyrins, vary somewhat with potential scan limits and rate, but they did not pursued a detailed analysis of the growth patterns.
Electropolymerization is suggested to take place, when amino group is in para-position of phenyl group, in two different organic solvents:

- porphyrin ($1mM$) and TBAP ($0,1M$) as supporting electrolyte in CH_2Cl_2, with potential varying between 0 and $+1,0$ V versus Ag/AgCl reference electrode with scan rate of 200mV/second;

- porphyrin ($1mM$) and TEAP (Et_4NClO_4 $0,1M$) as supporting electrolyte in CH_3CN, with potential varying between 0 and $+1,1$ V versus Ag/AgCl reference electrode with scan rate of 200mV/second.

Starting from these values, we performed an intensive study of the deposition conditions which lad to the better sensing properties, in terms of response stabil-

ity and reproducibility and sensitivity. Several complexes of 5-(4-aminophenyl)-10,15,20-tri(phenyl) porphyrins (figure 3.8) were deposited in different conditions on platinum sensor surface; the chemical properties of obtained membranes were evaluated by calibrations towards three standard laboratory salts, namely NaCl (normally used for sensors soaking), KI (in preliminary studies amino-substituted porphyrin based membranes showed high sensitivity towards iodide ion) and $NaClO_4$. Response slope (calculated in response linear range) and cyclic voltammetry parameters (scan rate, potential range and number of cycles) are shown in tables $3.17 - 3.24$. In each table, the best conditions are marked by bigger letters.
A new sensor array was then developed, according to found parameters and potentiometric performances were evaluated by calibrations to standard laboratory salts, in concentration range varying from 10^{-6}M to 10^{-1}M, with distilled water as background solution. Slopes were calculated in response linear range and are shown in table 3.25. A better response at higher concentrations

Scan rate $[mV/sec]$	**Cycles**	**Potential range** $[V]$	**NaCl**	**KI**	**$NaClO_4$**
50	20	$-0,3 \rightarrow +1,3$	$-21,3 \pm 10,5$	$-42,7 \pm 11,1$	$+7,5 \pm 5,3$
250	100	$-0,3 \rightarrow +1,3$	$-2,8 \pm 2,2$	$-36,5 \pm 3,8$	$+3,9 \pm 1,1$
250	100	$-0,5 \rightarrow +0,9$	$-9,3 \pm 5,9$	$-38,9 \pm 2,8$	$+4,3 \pm 3,8$
250	100	$-0,9 \rightarrow +1,0$	$-4,3 \pm 3,0$	$-38,5 \pm 3,9$	$+3,3 \pm 2,4$

Table 3.17: Deposition parameters and calibration response slopes for nickel complex of $5-(4-aminophenyl)-10,15,20-tri(phenyl)porphyrin$

Scan rate $[mV/sec]$	**Cycles**	**Potential range** $[V]$	**NaCl**	**KI**	**$NaClO_4$**
100	10	$-0,3 \rightarrow +1,3$	$+3,9 \pm 3,2$	$-46,2 \pm 4,2$	$+6,9 \pm 3,5$
250	100	$-0,3 \rightarrow +1,4$	$-1,9 \pm 3,9$	$-27,8 \pm 3,0$	$-1,0 \pm 2,3$
250	100	$-0,6 \rightarrow +0,9$	$-4,6 \pm 2,4$	$-46,2 \pm 3,3$	$-1,7 \pm 1,7$
250	100	$-0,3 \rightarrow +1,3$	$-13,0 \pm 1,6$	$-35,6 \pm 4,4$	$-6,5 \pm 3,4$

Table 3.18: Deposition parameters and calibration response slopes for molibdenum complex of $5-(4-aminophenyl)-10,15,20-tri(phenyl)porphyrin$

was found: membrane potential standard deviation decreased until few milliVolts when concentration was higher than 10^{-2}M (in particular for membranes no. 1, 2 and 4), thus indicating a possible utilization of such sensors as highly selective electrodes for some analytes. High sensitivity towards phosphate ion was obtained for most of membranes with slopes varying in the range between $-44,7mV/decade$ (membrane no. 4) and $-90,0mV/decade$ (membrane no. 2); in particular membranes no. 2, 3 and 7 showed super-Nernstian values.
Free-base amino porphyrin showed cationic response (due to the central metal absence coordinating anions) towards all cations, with partial anionic sensitivity

Scan rate $[mV/sec]$	**Cycles**	**Potential range** $[V]$	**NaCl**	**NaSCN**	**$NaNO_2$**
100	100	$-0,3 \rightarrow +1,3$	$+18,4 \pm 3,3$	$+19.8 \pm 2,1$	$+23,3 \pm 2,4$
400	100	$-0,3 \rightarrow +1,3$	$+9,2 \pm 2,4$	$+4,4 \pm 2,1$	$+9,5 \pm 3,4$
100	100	$-0,3 \rightarrow +1,3$	$-4,2 \pm 6,2$	$-13,9 \pm 6,3$	$-1,0 \pm 2,3$
250	100	$-0,3 \rightarrow +1,3$	$-3,4 \pm 3,6$	$+3,5 \pm 2,4$	$+4,9 \pm 1,3$

Table 3.19: Deposition parameters and calibration response slopes for free-base $5-(4-aminophenyl)-10,15,20-tri(phenyl)porphyrin$

Scan rate $[mV/sec]$	**Cycles**	**Potential range** $[V]$	**NaCl**	**NaSCN**	**$NaNO_2$**
250	250	$-0,3 \rightarrow +1,3$	$-7,7 \pm 3,2$	$-14,2 \pm 4,2$	$-3,5 \pm 2,6$
100	100	$-0,3 \rightarrow +1,3$	$-5,0 \pm 1,5$	$+0,8 \pm 1,0$	$+2,5 \pm 2,1$
250	100	$-0,3 \rightarrow +1,3$	$-11,9 \pm 3,8$	$-16,0 \pm 0,9$	$-1,8 \pm 2,9$
250	250	$-0,3 \rightarrow +1,3$	$-8,9 \pm 1,3$	$-6,9 \pm 0,9$	$-9,6 \pm 1,9$

Table 3.20: Deposition parameters and calibration response slopes for zinc complex of $5-(4-aminophenyl)-10,15,20-tri(phenyl)porphyrin$

Scan rate $[mV/sec]$	**Cycles**	**Potential range** $[V]$	**NaCl**	**KI**	**NaSCN**
100	20	$-0,3 \rightarrow +1,3$	$+5,8 \pm 2,9$	$-43,3 \pm 9,1$	$-19,9 \pm 2,6$
250	20	$-0,3 \rightarrow +1,3$	$+6,7 \pm 3,9$	$-15,5 \pm 7,0$	$-6,7 \pm 5,2$
250	100	$-0,3 \rightarrow +1,3$	$+6,3 \pm 5,2$	$-22,9 \pm 5,4$	$-15,2 \pm 8,0$
400	100	$-1,0 \rightarrow +1,0$	$+11,1 \pm 2,2$	$-35,3 \pm 9,8$	$+3,8 \pm 8,5$

Table 3.21: Deposition parameters and calibration response slopes for manganese complex of $5-(4-aminophenyl)-10,15,20-tri(phenyl)porphyrin$

Scan rate $[mV/sec]$	**Cycles**	**Potential range** $[V]$	**NaCl**	**KI**	**$NaClO_4$**
50	50	$-0,3 \rightarrow +1,3$	$-9,4 \pm 7,3$	$-21,9 \pm 11,4$	$-21,0 \pm 6,6$
250	100	$-0,3 \rightarrow +1,3$	$+1,7 \pm 3,5$	$+1,7 \pm 7,1$	$-4,3 \pm 4,9$
400	100	$-0,5 \rightarrow +1,5$	$+3,3 \pm 4,8$	$-25,1 \pm 11,2$	$-19,9 \pm 5,9$
400	200	$-0,5 \rightarrow +1,5$	$-14,0 \pm 3,6$	$-35,4 \pm 1,7$	$-32,4 \pm 5,8$

Table 3.22: Deposition parameters and calibration response slopes for copper complex of $5-(4-aminophenyl)-10,15,20-tri(phenyl)porphyrin$

Scan rate $[mV/sec]$	**Cycles**	**Potential range** $[V]$	**NaCl**	**KI**	**NaSCN**
50	20	$-0,3 \rightarrow +1,3$	$-15,3 \pm 2,9$	$-46,8 \pm 17,7$	$-17,8 \pm 7,3$
250	20	$-0,3 \rightarrow +1,3$	$+1,6 \pm 3,7$	$-7,7 \pm 3,0$	$-7,2 \pm 5,7$
250	100	$-0,3 \rightarrow +1,3$	$+1,7 \pm 6,5$	$-26,0 \pm 4,3$	$-13,9 \pm 5,6$
250	100	$-0,5 \rightarrow +1,5$	$+6,7 \pm 3,5$	$-32,8 \pm 2,7$	$-5,2 \pm 6,8$

Table 3.23: Deposition parameters and calibration response slopes for cobalt complex of $5-(4-aminophenyl)-10,15,20-tri(phenyl)porphyrin$

Scan rate $[mV/sec]$	**Cycles**	**Potential range** $[V]$	**NaCl**	**KI**	**NaSCN**
100	20	$-0,5 \rightarrow +1,5$	$+11,2 \pm 3,7$	$-56,1 \pm 4,4$	$-2,7 \pm 3,4$
250	100	$-0,5 \rightarrow +1,5$	$+13,4 \pm 3,4$	$+10,8 \pm 2,3$	$+11,8 \pm 6,7$
400	100	$-1,0 \rightarrow +2,0$	$+5,5 \pm 2,3$	$-29,3 \pm 3,8$	$-10,7 \pm 6,8$
600	200	$-1,0 \rightarrow +2,0$	$-1,3 \pm 3,3$	$-33,8 \pm 3,0$	$-19,8 \pm 9,6$

Table 3.24: Deposition parameters and calibration response slopes for iron complex of $5-(4-aminophenyl)-10,15,20-tri(phenyl)porphyrin$

Membrane	**NaCl**	**$NaHCO_3$**	**Na_2SO_4**	**Na_3PO_4**	**$NaNO_3$**	**NaSCN**
1: $Zn(NH_2)$-TPP	$-13,0 \pm 7,2$	$+9,6 \pm 7,0$	$+16,0 \pm 7,0$	$+1,2 \pm 10,6$	$+13,2 \pm 4,3$	$-26,5 \pm 0,5$
2: $Cu(NH_2)$-TPP	$-4,4 \pm 9,4$	$-25,0 \pm 15,0$	$+3,6 \pm 7,5$	$-90,0 \pm 3,3$	$-1,8 \pm 5,0$	$-21,2 \pm 7,0$
3: $Co(NH_2)$-TPP	$-1,3 \pm 7,9$	$-24,9 \pm 18,9$	$+1,5 \pm 9,7$	$-67,3 \pm 8,6$	$+0,2 \pm 7,0$	$-31,2 \pm 10,8$
4: (NH_2)-TPP	$+3,5 \pm 3,3$	$+0,3 \pm 8,6$	$+5,8 \pm 5,7$	$-44,7 \pm 17,0$	$+9,7 \pm 7,4$	$-11,6 \pm 12,7$
5: $Mn(NH_2)$-TPP	$-2,6 \pm 5,3$	$-1,2 \pm 15,3$	$+5,2 \pm 8,7$	$-1,9 \pm 9,3$	$+4,5 \pm 5,7$	$-1,7 \pm 3,4$
6: $Ni(NH_2)$-TPP	$-5,4 \pm 5,7$	$-16,2 \pm 18,9$	$+2,8 \pm 5,5$	$-55,2 \pm 12,6$	$-2,8 \pm 3,2$	$-14,4 \pm 6,2$
7: $Mo(NH_2)$-TPP	$-8,2 \pm 7,3$	$-40,8 \pm 18,5$	$+2,1 \pm 7,1$	$-108,0 \pm 14,1$	$+1,3 \pm 6,5$	$-33,9 \pm 7,8$
8: $Fe(NH_2)$-TPP	$-8,4 \pm 4,8$	$-21,7 \pm 21,0$	$+1,2 \pm 4,1$	$-67,0 \pm 17,4$	$-4,9 \pm 1,6$	$-13,5 \pm 4,2$

Table 3.25: Calibration towards standard laboratory salts of the sensor array based on amino-substituted porphyrins; response slopes are calculated in the linear range and given in mV/decade

towards SCN^-.
Membrane no.1 showed both cationic and anionic response, depending on the involved ions, with the highest sensitivity towards tiocyanate and chloride ions; membranes no. 2 and 6 mainly responded to HCO_3^- and SCN^- with low influence from Cl^- and NO_3^-. $Mn(NH_2) - TPP$ based membrane (no. 5) showed low sensitivities towards most ions, while membrane no. 7 was influenced by HCO_3^- and SCN^-, with responses of $-40,8$ and $-33,9 mV/decade$, respectively.

3.2.9 Conclusions

Several membranes, all based on porphyrinoids as active material, were studied. Chemical and cross-sensitivity properties were evaluated by calibrations towards standard laboratory salts, by varying stepwise ionic concentration between 10^{-6}M and 10^{-1}M. Sensor response slopes, according to Nernst equation, were calculated in the linear range and discussed, focusing on sensitivity (sub-, near- or super-Nernstian values, both anionic and cationic) and on the influence from other ions in solutions.
Ionophores were immobilized in the membrane by two different techniques:

- PVC-based membranes: standard method, commonly used, is based on the integration of the ionophore into a polymeric support; the response of membranes just based on polymer and plasticizer, normally follow the so-called Hofmeister series, where sensitivity is due to ion lipophilicity; the use of porphyrins and their analogs in membranes, is able to induce a different behavior, with the possibility to fine tuning the selectivity towards some ions;

- electro-polymerized membranes: ionophore can be deposited directly on the sensor surface, bu using the oxidative reaction of some peripheral substituents, which can act as polymerization centre between two adjacent molecules. The obtained membrane showed lower sensitivity than PVC-based one; at the same time, improved stability in long-term period was noticed; furthermore, electro-polymerization technique allowed selective deposition of ionophore on the contacted area. Our research was mainly focused on metal complexes of amino-substituted porphyrins, which have been studied from 1980s as sensitive material; the deposition parameters influence (such as number of cycles, scan rate and potential range in cyclic voltammetry) has been deeply studied and the best conditions for each complex have been found.

3.3 Features selection optimization and drift compensation

Due to the unavoidable fluctuations of chemical, physical and biological quantities, any property of a given sensing material experiences fluctuations that

represent the origin of the electrical noise, evaluated as the root mean square value of the fluctuations. Sensors, whatever their complexity may be, manifest noise at their output with a given signal to noise ratio. This noise is one of the reasons that the resolution cannot approach the zero value; another direct reason is the sensitivity value limitation.
Concerning the drift, we can define it as a slow unpredictable change of the sensor output, undefined from the statistical point of view, which is superimposed to both the signal and noise levels. Its origin may be correlated to the aging of the sensing material (release of internal stresses, slow residual diffusion processes) and of the electronic components that interact with chemical, physical and biological quantities present in the environment. Its presence can be detected usually through a long time observation and can be considered another reason of the loss of accuracy of the sensor.
In this section, the application of several data analysis methods will be discussed, for the evaluation of a new protocol of feature selection for the long-term discrimination between two substances and for the reduction of drift influence on the sensor response.
The array described in previous section (table 3.25), was applied for a 2 months measurements campaign; two substances, namely KI and $NaHCO_3$, were chosen as markers and the evolution of sensor response towards these analytes was then analized by principal component analysis (PCA) and partial least squares - discriminant analysis (PLS-DA). Salts were analyzed in two different concentrations (10^{-4} and 10^{-2}M) for 150 seconds and potentials were firstly divided in 4 classes; dataset was chronologically divided in two sub-dataset, for training model and for testing ($training : test$=70% : 30%, 50% : 50% and 30% : 70%).

3.3.1 Target analytes clustering: application of PLS-DA

Measure time is a crucial parameter, whose importance is often neglected; membrane should have the necessary time to reach chemical equilibrium with analytes in solution, but longer times can lead to active sites saturation (generally evidenced by an inversion of response nature, from cationic to anionic or viceversa) or to ionophore molecules lacks from organic phase (PVC-based membranes).
In order to evaluate the optimal measure time, 6 features were extracted for each measure, namely the potential value after 30, 60, 90 and 120 seconds from the beginning and after membrane response stabilization (150 seconds). PLS-DA model was created for each dataset and the system performances were evaluated by calculating the correct classification percentage. Percentages for all models are given in table 3.26.
The PLS-DA models application, showed that the best discrimination among considered classes, was obtained for 120 seconds, with mean correct classification percentage of 90,82% in training phase and 83,33% in test.
After first results, another approach was used, to identify the most discriminating features among all studied values. The analysis of the matrix comprising

Feature: TRAINING	70%:30%	50%:50%	30%:70%	100%:0%	Mean %
30 sec.	86,42%	83,82%	82,63%	83,76%	84,16%
60 sec.	92,59%	83,82%	82,63%	83,76%	84,16%
90 sec.	92,59%	88,97%	88,95%	90,40%	90,23%
120 sec.	92,59%	90,44%	89,47%	90,78%	90,82%
150 sec.	93,83%	90,44%	83,16%	87,10%	88,63%
Feature: TEST	**70%:30%**	**50%:50%**	**30%:70%**	**100%:0%**	**Mean %**
30 sec.	65,79%	71,85%	82,71%	-	73,45%
60 sec.	72,63%	86,67%	86,42%	-	81,90%
90 sec.	80,00%	84,44%	85,18%	-	83,20%
120 sec.	82,10%	85,19%	82,72%	-	83,33%
150 sec.	81,58%	80,74%	86,42%	-	82,91%

Table 3.26: Percentage of correct classification when different features were used for data analysis

all the studied features was firstly studied and the performances are shown in table 3.27.

Study clearly showed better discriminating performances, evidenced by higher

Feature: TRAINING	70%:30%	50%:50%	30%:70%	100%:0%	Mean %
All features	97,53%	91,91%	91,58%	92,99%	93,50%
Feature: TEST	**70%:30%**	**50%:50%**	**30%:70%**	**100%:0%**	**Mean %**
All features	75,79%	83,70%	93,83%	-	84,44%

Table 3.27: Percentage of correct classification when different features were used for data analysis

correct classification percentages, if compared with all matrix composed of single features (30, 60, 90, 120 or 150 seconds, respectively). Furthermore, from the analysis of misclassified samples, we were able to see how the system mostly confused samples at lower concentrations; just focusing on high concentration samples, we could reach a percentage of over 96% in training and 88% in test. Next step has been characterized by the reduction of chosen features, to create a robust but light model, with improved performances obtained avoiding ridundant information. Feature selection was performed on the basis of the correlation coefficient between all the analyzed features and the matrix indicating the sample class; in this way, only the most discriminative features, for chosen purpose, can be chosen. Coefficients corresponding to chosen classes, are shown in figure 3.27.

A first features reduction led to the choice of 23 features; number was then decreased to 9, by choising only the most $2-3$ discriminative features for each class. System performances are shown in table 3.28.

Better performances were obtained when the most discriminative features were chosen, according to the class division index; the optimum value was reached in

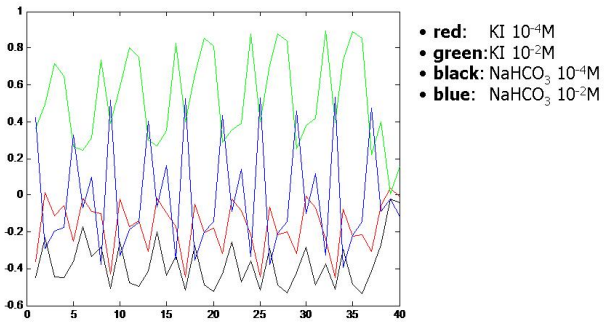

Figure 3.27: Correlation coefficients between all features and the classes matrix

Feature: TRAINING	70%:30%	50%:50%	30%:70%	100%:0%	Mean %
23 features	95,06%	94,12%	94,21%	93,36%	94,19%
9 features	86,42%	86,76%	84,21%	88,56%	86,49%
Feature: TEST	**70%:30%**	**50%:50%**	**30%:70%**	**100%:0%**	**Mean %**
23 features	75,26%	86,67%	92,59%	-	84,84%
9 features	71,58%	77,04%	92,59%	-	80,40%

Table 3.28: Percentage of correct classification when a reduced number of features was used for data analysis, namely 23 and 9, according to correlation coefficients

correspondance of 23 features (94,19% and 84,84% in training and test, respectively), while a further reduction (9 features) led to lower percentages of correct classification (86,49% and 80,40% in training and test, respectively), thus indicating a lack in system performances.
The last approach for the measure optimization and feature selection, has been characterized by the choice of the most discriminative features (on the basis of the correlation coefficient study) in training phase for each model and the successive application of chosen features in test. This approach did not improved system performances and correct classification percentages of 86,91% and 78,82% in training and test, respectively, were obtained.

3.3.2 Measurement drift compensation: application of PCA

Feature selection is a crucial parameter, in order to obtain comparable information from chemical sensors in middle- and long-time period; in fact, a non-neglectable component of the response is due to drift that unpredictably modifies the sensor potential, leading to mistakes in prediction in data analysis.
This problem is still unsolved and techniques, to reduce the drift component of the response, must be evaluated in single cases. In this section, the operations for drift reducing will be discussed in detail.
According to sensor lower detection limit, the recognition performance limits were mainly due to low concentration samples, which were confused each other from the system. In order to obtain information on the response evolution through the time, we just focused our attention on the classes corresponding to high concentration samples, KI (10^{-2}M, label 4) and $NaHCO_3$ (10^{-2}M, label 6). As for PLS-DA analysis, different strategies in feature selection were followed and the whole dataset was chronologically divided in two parts, for model training and test.
We firstly analysed matrices composed of sensor potentials after 30, 60, 90, 120 and 150 seconds from the measure beginning, using 3 different dataset divisions for training and test: $70\%_{training} : 30\%_{test}$, $50\%_{training} : 50\%_{test}$ and $30\%_{training} : 70\%_{test}$. PCA scores plot are represented in figures 3.28 - 3.32.

A high influence of drift can be noticed in all graphs, not depending from the dimensions of the training dataset; the formation of well defined clusters is not allowed and samples follow a straight direction during the campaign period. Also the values obtained by applying the built model, lay in a different portion of the graph, indicating low system discrimination power on unkown samples.
Also the analysis with all the features, did not allow an evident reduction of drift influence; a better definition of the clusters corresponding to KI and $NaHCO_3$, can be seen in figure 3.33, even if a correlation with the time is still evident, mainly when model is built by a reduced dataset and then applied to a large set of unknown samples.
Following the same strategy used for PLS-DA analysis, a reduction of features was performed; matrix composed of 23 features (features reduction, from 40 to 23, has been performed basing on correlation coefficients; see previous section

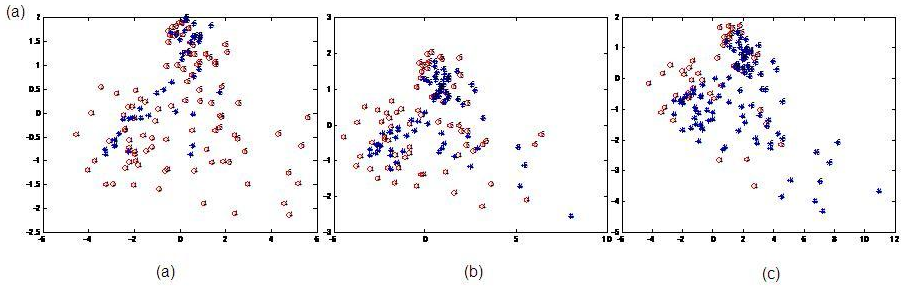

Figure 3.28: PCA scores plots of Electronic Tongue means after 30 seconds of measure; samples used for model training are shown by red circles, those for test by blue stars; label 4 indicates KI 10^{-2}M samples, label 6 $NaHCO_3$ 10^{-2}M ones; (a) 70% of dataset for training, 30% for test, (b) 50% of dataset for training, 50% for test, (c) 30% of dataset for training, 70% for test

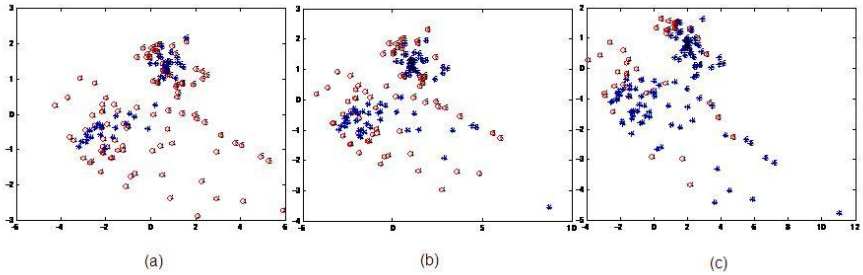

Figure 3.29: PCA scores plots of Electronic Tongue means after 60 seconds of measure; samples used for model training are shown by red circles, those for test by blue stars; label 4 indicates KI 10^{-2}M samples, label 6 $NaHCO_3$ 10^{-2}M ones; (a) 70% of dataset for training, 30% for test, (b) 50% of dataset for training, 50% for test, (c) 30% of dataset for training, 70% for test

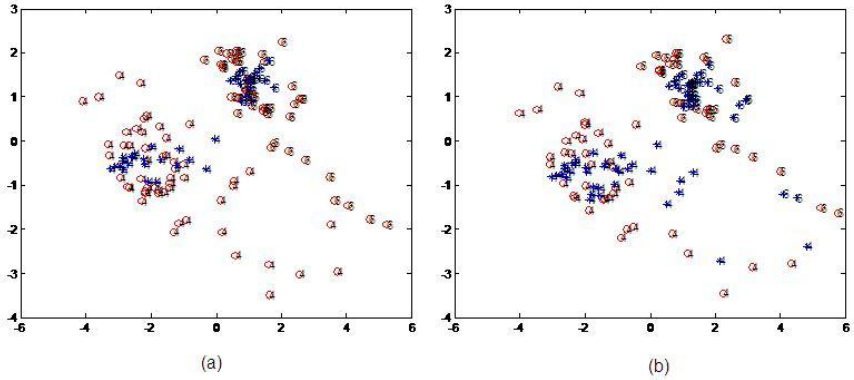

Figure 3.30: PCA scores plots of Electronic Tongue means after 90 seconds of measure; samples used for model training are shown by red circles, those for test by blue stars; label 4 indicates KI 10^{-2}M samples, label 6 $NaHCO_3$ 10^{-2}M ones; (a) 70% of dataset for training, 30% for test, (b) 50% of dataset for training, 50% for test

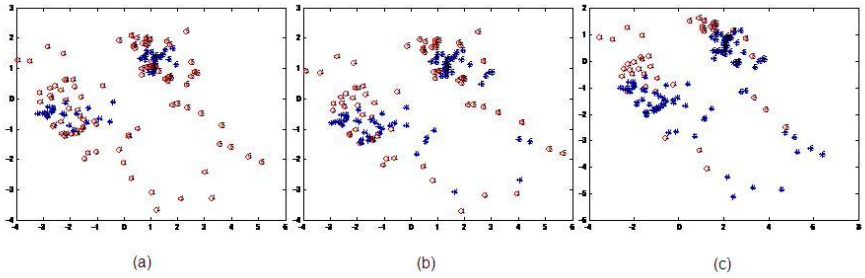

Figure 3.31: PCA scores plots of Electronic Tongue means after 120 seconds of measure; samples used for model training are shown by red circles, those for test by blue stars; label 4 indicates KI 10^{-2}M samples, label 6 $NaHCO_3$ 10^{-2}M ones; (a) 70% of dataset for training, 30% for test, (b) 50% of dataset for training, 50% for test, (c) 30% of dataset for training, 70% for test

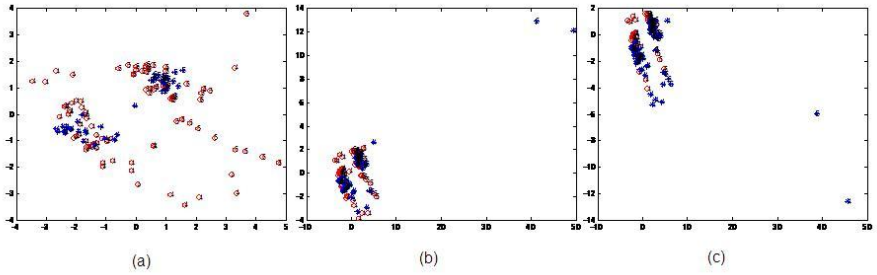

Figure 3.32: PCA scores plots of Electronic Tongue means after 150 seconds of measure; samples used for model training are shown by red circles, those for test by blue stars; label 4 indicates KI 10^{-2}M samples, label 6 $NaHCO_3$ 10^{-2}M ones; (a) 70% of dataset for training, 30% for test, (b) 50% of dataset for training, 50% for test, (c) 30% of dataset for training, 70% for test

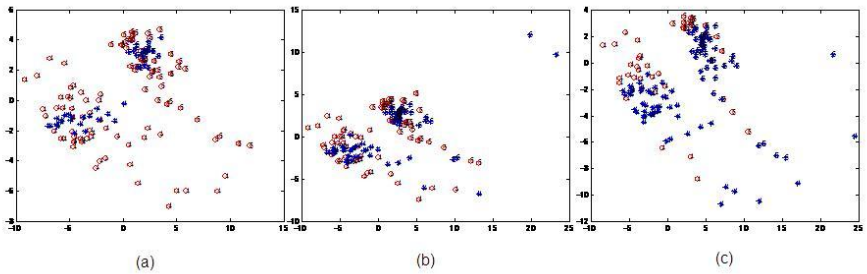

Figure 3.33: PCA scores plots of Electronic Tongue means using all features; samples used for model training are shown by red circles, those for test by blue stars; label 3 and 4 indicates KI (10^{-4}M and 10^{-2}M) samples, label 5 and 6 $NaHCO_3$ (10^{-4}M and 10^{-2}M) ones; division of dataset for training and test is indicated

for more detailed information); PCA scores plot (figure 3.34), did not show appreciable improvements in drift influence reduction, even if a better resolution in clustering can be observed. In this case, also samples at low concentration (label 3 and 5) were analysed; as suggested by PLS-DA analysis, overlap between samples no. 3 and 5 was noticed, due to low sensor sensitivity at low concentrations. A new approach for drift compensation was performed: new

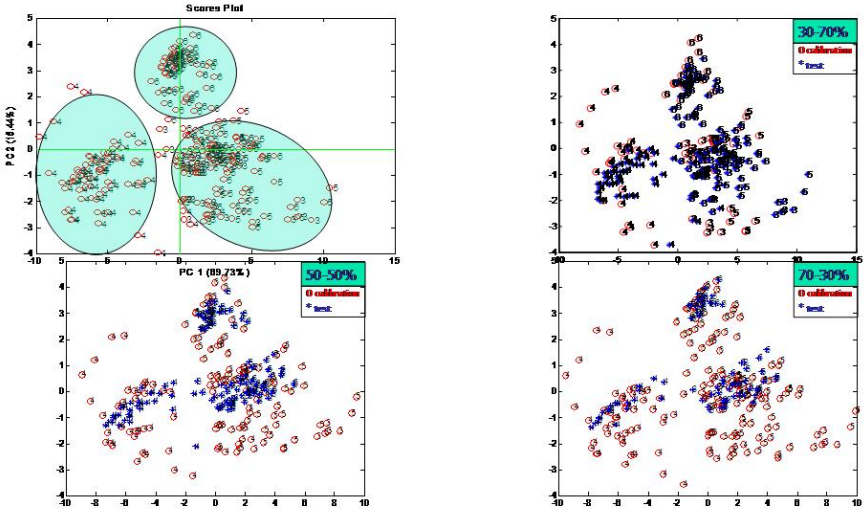

Figure 3.34: PCA scores plots of Electronic Tongue means using a reduced number of features (23), chosen on the basis of correlation coefficients; samples used for model training are shown by red circles, those for test by blue stars; label 4 indicates KI 10^{-2}M samples, label 6 $NaHCO_3$ 10^{-2}M ones; (a) 70% of dataset for training, 30% for test, (b) 50% of dataset for training, 50% for test, (c) 30% of dataset for training, 70% for test

correlation coefficients versus a vector indicating the measure day were calculated and features minimizing this relation were chosen; this features group was then intersected with those found before, leading to 4 features. PCA scores plot is shown in figure 3.35. Good results, with well defined clusters, both for training and test samples, was only obtained when a robust model was built (with 70% of whole dataset, figure 3.35 (a)), while, when training was performed with 50% and 30% of data (figures 3.35 (b) and (c), respectively), strongly drifted from originary clusters.
Differential approach was used to build scores plot shown in figures 3.36 and 3.37. Dataset was built by using, for each sensor and measure, the difference between the potential after 150 and 90 (figure 3.36) or 120 seconds (figure 3.37) respectively. Also these features were strongly influenced by drift and test samples, mainly for KI, individuated a defined cluster, but separate from the one formed in training. In particular the ΔV of the last 60 seconds brought to de-

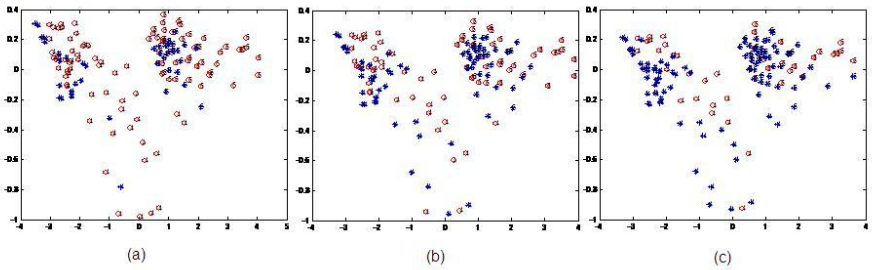

Figure 3.35: PCA scores plots of Electronic Tongue means using a reduced number of features (4), which, at the same time, maximize the correlation with the discrimination index and minimize the influence of time; samples used for model training are shown by red circles, those for test by blue stars; label 4 indicates KI 10^{-2}M samples, label 6 $NaHCO_3$ 10^{-2}M ones; (a) 70% of dataset for training, 30% for test, (b) 50% of dataset for training, 50% for test, (c) 30% of dataset for training, 70% for test

fined clusters, thus confirming the results previously obtained by PLS-DA, in which the potential after 120 seconds result more discriminative than the other features. Better results were obtained when linear normalization on potentials

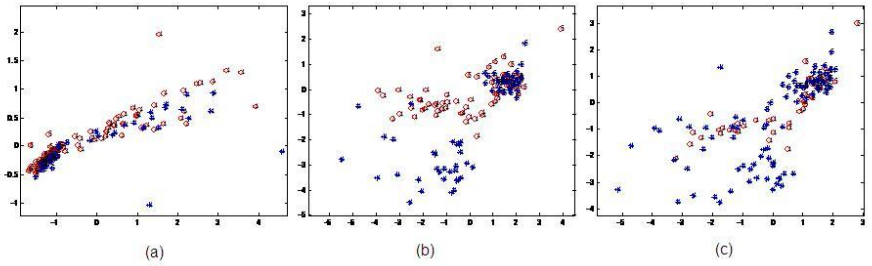

Figure 3.36: PCA scores plots of Electronic Tongue means using the potential variation between 90 and 150 seconds; samples used for model training are shown by red circles, those for test by blue stars; label 4 indicates KI 10^{-2}M samples, label 6 $NaHCO_3$ 10^{-2}M ones; (a) 70% of dataset for training, 30% for test, (b) 50% of dataset for training, 50% for test, (c) 30% of dataset for training, 70% for test

were performed: potential of generic sensor x, V_x, is substituted by $V_x / \sum_{i=1}^{n} V_i$, in array composed of n sensors. Both matrices composed of responses after 120 seconds (figure 3.38) and 150 seconds (figure 3.39) have been analysed, leading to well defined clusters. In particular, in figure 3.38, drift influence is almost completely neglectable and two clusters, comprising all similar samples, can be

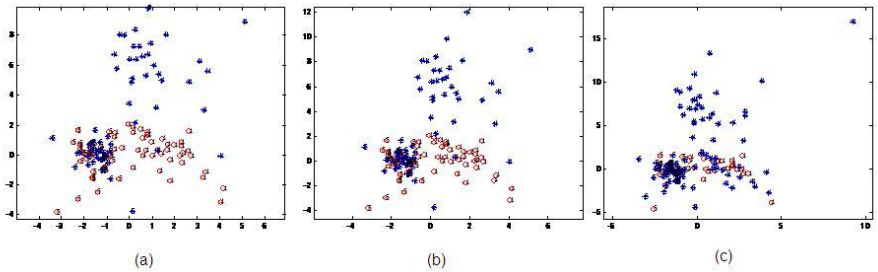

Figure 3.37: PCA scores plots of Electronic Tongue means using the potential variation between 120 and 150 seconds; samples used for model training are shown by red circles, those for test by blue stars; label 4 indicates KI 10^{-2}M samples, label 6 $NaHCO_3$ 10^{-2}M ones; (a) 70% of dataset for training, 30% for test, (b) 50% of dataset for training, 50% for test, (c) 30% of dataset for training, 70% for test

noticed; also test scores lay on the same plot region, minimizing the differences due to sensor performances degradation.

Since the best results were obtained by linear normalization of dataset, we

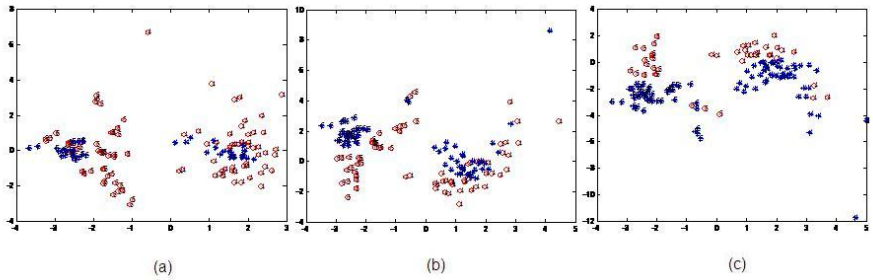

Figure 3.38: PCA scores plots of Electronic Tongue means using the potential variation between 120 and 150 seconds; samples used for model training are shown by red circles, those for test by blue stars; label 4 indicates KI 10^{-2}M samples, label 6 $NaHCO_3$ 10^{-2}M ones; (a) 70% of dataset for training, 30% for test, (b) 50% of dataset for training, 50% for test, (c) 30% of dataset for training, 70% for test

hypotised a linear behavior of sensor response drift. Let us imagine two sensors, x and y, the response at the generic moment t is

$$V_x = V_{0,x} + k_x \times t \tag{3.2}$$

$$V_y = V_{0,y} + k_y \times t \tag{3.3}$$

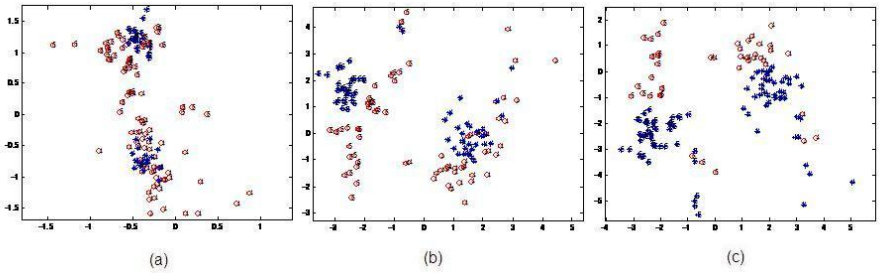

Figure 3.39: PCA scores plots of Electronic Tongue means using the potential variation between 90 and 150 seconds; samples used for model training are shown by red circles, those for test by blue stars; label 4 indicates KI 10^{-2}M samples, label 6 $NaHCO_3$ 10^{-2}M ones; (a) 70% of dataset for training, 30% for test, (b) 50% of dataset for training, 50% for test, (c) 30% of dataset for training, 70% for test

where k_x and k_y represent the potential variation in time ($\partial V/\partial t$). If the sensor potential vary with similar rate ($k_x \approx k_y$), the term caused by drift can be reduced by subtracting, i.e. V_x from the other potentials:

$$V_y - V_x = (V_{0,y} - V_{0,x}) + (k_y - k_x) \times t \approx V_{0,y} - V_{0,x} \tag{3.4}$$

Following the linear variation hypotesis, the difference between each potential and the first one, was used as feature:
The scores plot is shown in figure 3.40 where potentials at 120 seconds (accord-

Feature 1	**Feature 2**	**... ... ...**	**Feature n-1**
$V_2 - V_1$	$V_3 - V_1$	... ...	$V_n - V_1$

Table 3.29: Hypotizing a linear variation of drift, the difference between each sensor and the first one, was used as feature

ing to previous results, both obtained by PLS-DA and PCA) were used. The well defined clustering verifies the hypotesis of linear drift, since two distinct regions contain all KI and $NaHCO_3$, samples, both from model training and test. Furthermore, the new feature, allowed the utilization of a lower number of measures for model construction: in fact, drift reduction, can be noticed also in figure 3.40 (c), obtained by using only the 30% of dataset for model building and then applying it on the other 70%.

3.3.3 Conclusions

Drift is a still un-solved problem generally affecting sensor measurements in middle- or long-time period; in particular chemical sensors produce a response which is highly influenced by drift: for this reason, many applications in which

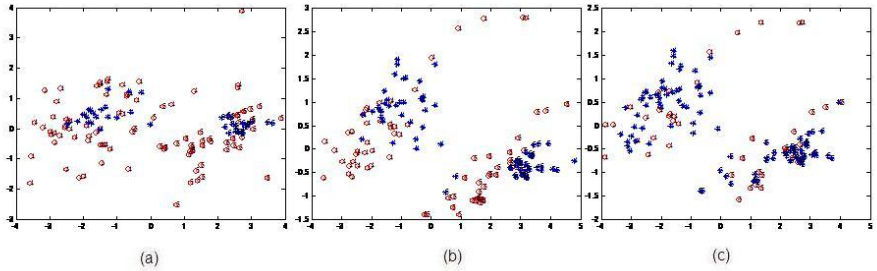

Figure 3.40: PCA scores plots of Electronic Tongue means using the difference between each potential at 120 seconds and the first sensor response; samples used for model training are shown by red circles, those for test by blue stars; label 4 indicates KI 10^{-2}M samples, label 6 $NaHCO_3$ 10^{-2}M ones; (a) 70% of dataset for training, 30% for test, (b) 50% of dataset for training, 50% for test, (c) 30% of dataset for training, 70% for test

sensor arrays are used to obtain qualitative or quantitative information, present many limits, since sensor calibration is needed before the measurement.
A first approach on the optimization of measurement strategy, has been performed on the basis of the correlation coefficients between the means of an Electronic Tongue system and two defined substances, chosen as markers. Optimum measure time (enough to reach stability but avoiding active sites saturation or ionophore lacks from membranes) was found, on the basis of the study of correlation coefficients and PLS-DA analysis.
Drift influence reduction on potentials, in a time range of 2 months, has been performed by selecting different features from each measure; a linear trend for drift seems to affect sensor responses and a strategy to reduce it, by differential approaches has been realized.

Bibliography

[1] R. Elghanian, J.J. Storhoff, R.C. Mucic, R.L. Letsinger, C.A. Mirkin. Science 277 (1997) 1078

[2] W. Gopel. Mikrochim. Acta. 125 (1997) 179

[3] W. Gopel. Microelectron. Eng. 32 (1996) 75

[4] L.B. Buck, R. Axel. Cell 65 (1991) 175

[5] B. Malnic, J. Hirono, T. Sato, L.B. Buck. Cell 96 (1999) 713

[6] R. Axel. Sci. Am. 273 (1995) 154

[7] H. Breer, I. Wanner, J. Strotmann. Behav. Genet. 26 (1996) 209

[8] D. Lancet, N. Ben-Arie. Curr. Biol. 3 (1993) 668

[9] C. Krantz-Kulcker, M. Stenberg, F. Winquist, I. Lundstrom. Anal. Chim. Acta. 426 (2001) 217-226

[10] C. Soderstrom, H. Boren, F. Winquist, C. Krantz-Kulcker. Int. J. Food Microbiol. 83 (2003) 253-261

[11] P. Ivarsson, M. Johansson, N.E. Hojer, C. Krantz-Kulcker, F. Winquist, I. Lundstrom. Sens. Actuators B. 108 (2005) 851-857

[12] L. Lvova, G. De Angelis, C. Montieri, T. Primadei, E. Martinelli, E. Mazzone, A. Pede, R. Paolesse, C. Di Natale, A. D'Amico. Proceedings of the 3rd IEEE Sensors Conference. Vienna, Austria, October 23-27, 2004, p. 71

[13] R. Martinez-Manez, J. Soto, E. Garcia-Breijo, L. Gil, J. Ibanez, E. Llobet. Sens. Actuators B. 104 (2005) 302-307

[14] L. Lvova, E. Martinelli, E. Mazzone, A. Pede, R. Paolesse, C. Di Natale, A. D'Amico. Talanta. 70 (2006) 833-839

[15] J. Koryta, J. Dvorak, V. Bochakova. Electrochemistry. Methuen and Co., London (1970) 318

[16] P.B. Hahn, D.C. Johnson, M.A. Wechter, A.F. Voigt. Anal. Chem. 46 (1974) 553-558

[17] R.W. Catrall, H. Freiser, Coated-wire ion-selective electrodes, Anal. Chem. 43 (1971) 1905-1906

[18] J. Bobacka. Anal. Chem. 71 (1999) 4932-4937

[19] E. Bakker, E. Malinowska, R.D. Schiller, M.E. Meyerhoff. Talanta. 41 (1994) 881-890

[20] A. Bettelheim, B.A. White, S.A. Raybuck, R.W. Murray. Inorg. Chem. 26 (1987) 1009-1017

[21] N. Oyama, F.C. Anson. J. Am. Chem. SOC. 101 (1979) 739

[22] N. Oyama, F.C. Anson. J. Am. Chem. SOC. 101 (1979) 3450

[23] A. Merz, A.J. Bard. J. Am. Chem. SOC. 100 (1978) 3222

[24] R. Nowak, F.A. Schuitz, M. Umana, H. Abruna, R.W.J.Murray. Nectroanal. Chem. 94 (1978) 219

[25] H.L. Landrum, R.T. Salmon, F.M. Hawkridge. J. Am. Chem. Soc. 99 (1977) 3154

[26] J.F. Stargardt, F.M. Hawkridge. H.L Landrum. Anal. Chem. 50 (1878) 930

[27] M.C.Pham, P.C. Lacaze, J.E. Dubois. Electroanal. Chem. 86 (1978) 147

[28] U. Schaller, E. Bakker, U.E. Spichiger, E. Pretsch. Talanta. 41 (1994) 1001

[29] U. Schaller. Diss ETH Zurich 10948 (1994)

[30] P. Vanysek. Electrochemistry on Liquid/Liquid Interfaces. Springer: Berlin, 1985

[31] F. Hofmeister. Arch. Exp. Pathol. Pharmakol. 24 (1888) 247

[32] C.P. Andrieux, J.M.O. Bouchiat, J.M. Saveant. J. Electroanal. Chem. Interfacial Electrochem. 169 (1984) 9

[33] R.W. Murray. Annu. Rev. Mater. Sci. 14 (1984) 145

[34] R.W. Murray. Electroanal. Chem. 13 (1984) 191-368

[35] A.F. Diaz, J.A. Logan. J. Electroanal. Chem. Interfacial Electrochem. 111 (1980) 111

[36] P. Mourcel, M.-C. Pham, P.-C. Lacaze, J.-E. Dubois. J. Electroanal. Chem. Interfacial Electrochem. 145 (1983) 467

[37] R.A. Bull, F.-R. Fan, A.J. Bard. J. Electrochem. SOC. 130 (1983) 1636

[38] A. Bettelheim, R.J.H. Chan, T. Kuwana. J. Electroanal. Chem. Interfacial Electrochem. 99 (1979) 391

[39] H. Tachikawa, L. Faulkner. J. Am. Chem. SOC. 100 (1978) 4379

[40] C.P. Jester, R.D. Rocklin, R.W. Murray. J. Electrochem. Soc. 127 (1980) 1979

[41] A. Bettelheim, R.J.H. Chan, T. Kuwana. J. Electroanal. Chem. Interfacial Electrochem. 110 (1980) 93

[42] D.A. Buttry, F.C. Anson. J. Am. Chem. SOC. 106 (1984) 59

[43] K.A. Macor, J.G. Spiro. J. Am. Chem. Soc. 105 (1983) 5601

[44] C.D. Ellis, C.D. Margerum, R.W. Murray, T. Meyer. J. Inorg. Chem. 22 (1983) 1283

[45] L. Lvova, G. Verrelli, M. Stefanelli, S. Nardis, R. Paolesse, C. Di Natale, A. D'Amico, S. Makarychev-Mikhailov. Journal of Porphyrins and Phthalocyanines. 10 (2006) 480

[46] Yu. Vlasov, A. Legin, A. Rudnitskaya. Sens. Actuators B 44 (1997) 532-537

[47] B.A. White, R.W. Murray. J. Electroanal. Chem. Interfacial Electrochem. 189 (1985) 345

[48] R. Paolesse in The Porphyrin Handbook. K.M. Kadish, K.M. Smith, R. Guilard, Editors, , vol. 2, Academic Press, New York (2000)

Chapter 4

Application of Electronic Tongue systems for the analysis of liquid matrices

Introduction

Recent trends in the analytical chemistry field, take direction opposed to those that invest efforts in the development of quasi-specific instruments. The new approach departs from the use of general-purpose devices, combined with computer processing stages, which could probably grasp looks or composition of a sample and transmit us information about it ([1]). These new strategies are based on the use of sensor arrays with a generic cross response to a wide spectrum of analytes; with those, we can obtain different aspects of information about the sample. Afterwards, the use of multivariate calibration tools is used to extract the sought results from the data generated by the devices ([2]). This strategy is already known, for analyte detection on aqueous samples, as electronic tongue or for gases or headspace samples, as electronic nose. The used terminology suggests that this approximation is bioinspired on animal taste or olfaction senses, where a few receptors can respond to a large variety of substances. With taste, only generic information is used, like sweet, bitter, salted or acid; additionally, this approach entails an advanced data treatment mechanism next applied by the brain, in order to finally recognize, quantify or classify between different substances. An interesting application of this new concept is the use of chemometric tools for multivariate calibration and multiple analyte recognition simultaneously, which is a good strategy for multiparametric determination without interference removal ([3], [4]). A second interesting application is their use inspired in the human brain to classify the nature of a sample. For this purpose, principal component analysis (PCA) and partial least squares (PLS) are employed as data treatment. The use of non-selective poten-

tiometric sensors arrays in combination with PCA, starts to be an analytical alternative for sample classification or identification, especially in food analysis ([5]). After we presented the chemical and cross-sensitivity properties of several sensor array based both on metallic alloys and organic compounds as sensing material, in this chapter, all the applications of Electronic Tongue systems will be discussed in detail and results will be presented.

4.1 Detection of prostate tumor

4.1.1 Introduction

The importance of the odour in relation to human health was understood and used by ancient medicine as a diagnostic tool for preliminary interpretation of diseases. Nowadays electronic-nose devices are able to perform odour images which can be used to detect diseases by analysing the headspace of different body fluids.
In early studies urine has proven to be an useful mean to monitor the patients health-state. One of these studies has shown that patients with kidney disorders produce characteristic volatile compounds, which can be a useful mean for both the diagnosis and control of renal dialysis ([6]). In another work, samples from patients with urinary tract infections were identified correctly in 90-99% of cases compared with traditional culture techniques ([7]).
Prostate cancer is the most common non-skin cancer in America: 1 in 6 men will be diagnosed and the older you are, the more likely you are to be diagnosed with prostate cancer.
Although only 1 in 10,000 under age 40 will be diagnosed, the rate shoots up to 1 in 39 for ages 40 to 59 and 1 in 14 for ages 60 to 69. In fact, about 65% of all prostate cancers are diagnosed in men over the age of 65. Although genetics might play a role in deciding why one man might be at higher risk than another, social and environmental factors, particularly diet and lifestyle, likely have an effect as well. The exact relationship between obesity and prostate cancer remains unclear, but there is no doubt that obesity can have a negative effect on outcomes. Research has shown that prostate-specific antigen (PSA) test results in obese men can be lower despite the presence of disease, potentially leading to a delay in diagnosis and treatment; recovery from surgery tends to be longer and more difficult; and the risk of dying from prostate cancer can be higher.
The purpose of screening for cancer is to detect the cancer at its earliest stages, before any symptoms have developed. Some men, however, will experience symptoms that might indicate the presence of prostate cancer. Since these symptoms can also indicate the presence of other diseases or disorders, these men will undergo a more thorough work-up. Typically, men whose prostate cancer is detected through screening, are found to have very early-stage disease that can be treated most effectively.
Screening for prostate cancer can be performed quickly and easily in a physician

office using two tests: the PSA (prostate-specific antigen) blood or urine test and the digital rectal exam (DRE). PSA is a protein produced by the prostate and released in very small amounts into the bloodstream. When there is a problem with the prostate, such as when prostate cancer develops and grows, more and more PSA is released, until it reaches a level where it can be easily detected in biological liquids such as blood or urines. There is no specific normal or abnormal PSA level: the higher a mans PSA level, the more likely it is that cancer is present. But since various factors (such as age) can cause PSA levels to fluctuate, one abnormal PSA test does not necessarily indicate a need for other diagnostic tests; when PSA levels continue to rise over time, other tests may be needed. However, PSA can also be elevated if other prostate problems are present, such as BPH or prostatitis and some men with prostate cancer have low levels of PSA. This is why both the PSA and DRE are used to detect the presence of disease.
During a DRE, the physician inserts a gloved, lubricated finger into the rectum and examines the prostate for any irregularities in size, shape and texture. Often, the DRE can be used by urologists to help distinguish between prostate cancer and non-cancerous conditions such as BPH.

4.1.2 Experimental, results and discussion

In this section, the application of the array described in table 3.4, implemented by commercial pH glass electrode, for the detection of PSA level in urines, will be described. The sensorial approach in the detection of such a pathology, would be very important in medicine, since it allows fast, low-cost and non-invading method for preliminary diagnosis.
Samples have been provided by *Urology ward* of *Policlinico Tor Vergata*; they were both characterized by an elevate PSA value (cancers or other infections) and coming from healty patients; they were stored in refrigerator at 4^0C and then measured the same day of analysis, after a 10 minutes conditioning at room temperature.
Sensors have been soaked in NaCl 10^{-2}M for membrane recovery at the end of each measure day; since urines are an aggressive ambient for chemical sensors, samples have been previously diluted in distilled water, used as background solution ($50mL_{H_2O} : 5mL_{sample}$) and analysed for 10 minutes; 3 repetitions were performed in raw order during the day. Data were collected by using a PC equipped high-impedance input 8-channel A/D converter (Smartronix, Rome, ITALY) and analyzed by PLS-DA technique.
Since PLS is a supervised technique, samples were previously divided in 3 classes:

- class 0: healty patient;
- class 1: prostate tumor;
- class 2: other prostate pathologies.

In fact, first dataset division was performed on the basis of 2 classes (tumor and non-tumor cases); sensor array discriminating power was highly affected by the displacement in dataset sizes (25% of samples were from patients suffering of tumor, 75% were from healty patients or suffering from other pathologies). Optimum number of latent variables was chosen on the basis of *leave-one-out-cross-validation* (LOOCV) error (figure 4.1); leave one out technique was chosen since a low number of samples (16 patients) was available. Similar results were

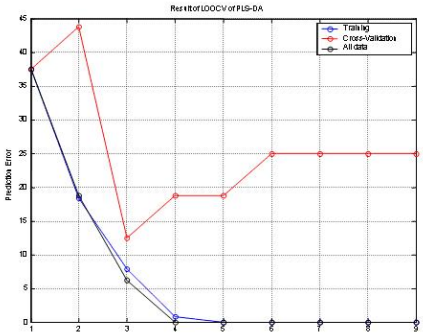

Figure 4.1: Leave-One-Out-Cross-Validation (LOOCV) error trend in PLS-DA

obtained both when all data were considered (black curve) or when a reduced dataset was used (blue curve). To avoid overfitting problem, typical in multivariate data analysis methods, optimization of latent variables had to be performed by cross-validation (red curve). It was found that the use of 3 latent variables led 87,5% of sample to be correctly classified. Scores plot of analysed data is shown in figure 4.2. The projection of the first two latent variables, containing

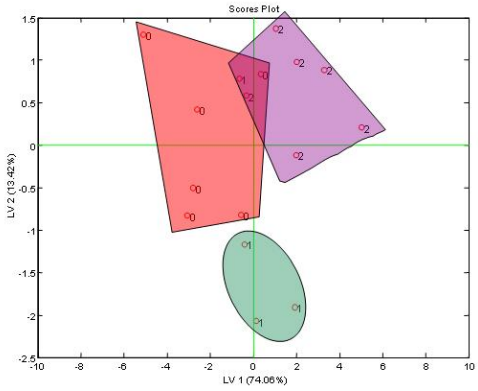

Figure 4.2: PLS-DA scores plot of the first two latent variables for sensor array application for prostate tumor detection

the most part of total variance (87,48%), allows enough high discrimination between samples owning to different classes, with a clear distinction of urines from patients suffering of tumor (class 1) and non-tumor cases (class 0 - healty and class 2 - other pathologies). A misclassified sample from class 1 can be noticed in the plot region between samples 0 and 2.
Sensor array discriminating power was also confirmed by confusion matrix (table 4.1). It is a square matrix with the number of raws (and columns) is equal to the number of chosen classes and shows the number of samples correctly assigned by the system to owning class (numbers on main diagonal) or misclassified. There were only two misclassified samples, namely no. 7, owning to class

5	1	0
1	3	0
0	0	6

Table 4.1: PLS-DA confusion matrix of urine samples analysed by sensor array for prostate tumor detection

0 and assigned to class 1 and no. 16 (from class 1 to class 0). The percentage of correct classification of 87,5% has been obtained; detailed values for each class have been calculated and reported in table 4.2.

83,3%	16,7%	0
25,0%	75,0%	0
0	0	100,0%

Table 4.2: PLS-DA correct classification percentages of urine samples analysed by sensor array for prostate tumor detection

4.1.3 Conclusions

Developed Electronic Tongue system, composed of both PVC-based and electropolymerised membranes, has been applied for the analysis of urine samples, coming from healty patients and from patients suffering from prostate tumor or other pathologies (both cases are characterised by high PSA value). Analysis were performed on 16 samples and comparative analysis were performed by *Policlinico Tor Vergata* with independent standard methods.
Samples were previously divided in 3 classes (according to pathology) and analysed after dilution with distilled water. Data were collected and analysed by PLS-DA technique; leave-one-out cross-validation technique was used to find the optimum number of latent variables. Interesting results were obtained and a correct classification percentage of 87,5% was obtained.
If such results will be confirmed in applications involving a higher number of samples or improved by coupling with other systems (e.g. Electronic Noses), the presence of prostate pathologies could be diagnosed with sensorial approach, which allows faster, low cost and non-invading analysis.

4.2 Detection of gases dissolved in liquids

4.2.1 Introduction

In the measurement of gases in gaseous mixtures, a huge number of variables affecting the performances of the used device, in particular in the case of Electronic Nose systems, is present.
Among the most important parameters, we can consider:

- the flux pressure, which mechanically interact with molecules adsorbed on electronic noses quartz and increase friction during micro-balances vibration;
- the temperature, which can sensibly vary during the measure time;
- the humidity; water molecules are an ineliminable presence in the measure chamber and, since their polarity, show a high cohesion with surfaces; for these reasons, molecules interact with sensing layer and quartz surface, altering vibration frequency and, so, the micro-balance performances. To reduce the problem, measures in controlled conditions must be performed, e.g. by humidity traps, even if their performances fastly decrease with time.

The strategy was then based on the EN limits, by using a potentiometric sensor array for the detection of gases dissolved in a liquid matrix. This, should solve the above mentioned problems, since liquids have thermic capacity higher than gases (higher capability to absorb temperature variations with possibility to keep physical status about constant during measure time); furthermore, gases are fluxed into the liquid matrix and, after a transient period, the concentration becomes homogeneus (thus eliminating the pressure influence); finally, humidity problem would be eliminated, since the measure is performed in liquid media.

4.2.2 Experimental, results and discussion

In this section, the application of the array described in table 3.7, implemented by commercial pH glass electrode, for the detection of dissolved gases in liquids, will be described in detail.
4 gases were studied, namely:

- SO_2,from reaction:

$$Na_2SO_3 + 2HCl \rightleftharpoons 2NaCl + SO_2 + H_2O \tag{4.1}$$

- CO_2 from reaction:

$$K_2CO_3 + 2HCl \rightleftharpoons 2KCl + CO_2 + H_2O \tag{4.2}$$

- CO (from tank);
- NH_3 (from tank).

Gases were fluxed into 200 mL of distilled water for 180 seconds with a pressure of 2,5 atm; samples were divided in sealed plastic bottles of 50 mL, for repetitions and measured immediately after opening, to avoid concentration changes in solution.
Buffer solution (MES 10^{-2}M and NaOH, $pH = 5,5$) was used as background, since it reduces pH influence and maintains an acidic ambient, where porphyrins performances are higher (partial protonation can occurr). It was also used as conditioning solution between two successive measurements, to restore chemical properties of membranes and to reduce memory effect. The difference of membrane potential between a reference measure and the successive sample analysis was used as feature and data were analysed by PCA. PCA biplot of the first two principal components is shown in figure 4.3.
A preliminary study on loadings, evidenced how the sensors characterised by

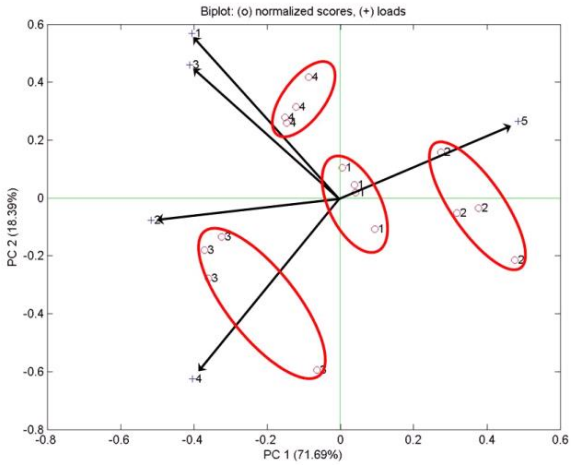

Figure 4.3: PCA biplot of the first two principal components for the detection of different gases dissolved in water

the same membrane, individuated similar directions on the PCA plot, thus indicating a good reproducibility of deposition technique. To avoid redundant information, the mean value of similar sensors was used (4 couples of sensors); sensor array was then completed by pH glass electrode.
The 90,08% of the total variance is represented. A clear distintion between all gases can be noticed, thus indicating good discrimination; furthermore, high reproducibility of sensor potentials, evidenced by low intra-cluster variance, was shown.
Loadings analysis showed that membranes no. 2 and 4 (PVC-based membrane

with $(NH_2) - TPP$ and $Tris(NO_2) - TPP$, respectively) and no. 5 (pH glass electrode), had similar directions, thus evidencing a strong influence of pH solution on the response of such sensors. Among this direction, the distinction of samples of SO_2 (label 3), CO (label 1) and NH_3 (label 2) was mostly evidenced; samples were, in fact, characterised by pH values of 3,3, 5,5 and 10,5, respectively.
The distinction between CO and CO_2 samples, characterised by similar pH (5,5), was mostly due to sensors no. 1 and 3 (based on electro-polymerized $Tris(NH_2) - TPP$ and plasticized $Bis(NH_2) - TPP$, respectively) responses. Their response was not influenced by pH, since near-orthogonal loading direction was obtained.

4.2.3 Conclusions

An innovative approach for the detection of gases was reported, by dissolving them in a liquid background and analyzing by means of an Electronic Tongue system, based on electro-polymerized and PVC-based membranes. The new strategy started from limits which actually affect the measurements performed by Electronic Nose systems, in particular humidity, flux pressure and temperature; all mentioned problems could be solved by using a liquid media.
Array was composed by five sensors: four different membranes (deposited twice to test the reproducibility of deposition technique) and commercial pH electrode. Four gases, namely SO_2, CO_2, CO and NH_3 were analysed by dissolving in buffer background, used as reference solution. Potential variations between reference and sample solution were finally analysed by principal components analysis (PCA).
A clear distinction between all samples was noticed, with good reproducibility among different repetitions. Clustering between SO_2, CO_2 and NH_3 was mostly based on pH variations (sensors no. 2 and 4), while sensors no. 1 and 3 did not result affected by pH (loadings in orthogonal direction if compared with pH sensor loading) and were useful to discriminate between CO and CO_2 samples. This approach seems to be promising, since it would allow the detection of gases by means of an Electronic Tongue system. Data fusion with Electronic Noses for the analysis of the same sample headspace, could be a powerful tool in the chemical analysis, but further investigations are needed.

4.3 Analysis of Verdicchio white wines by metalloporphyrins PVC-based membranes

4.3.1 Introduction

Recently a significant constant wine market growth has been registered all around the world. In the last period, several research efforts have been focused on the analysis of wines applying chemical sensor arrays.

Thus, in [8], Parra et al., reported the application of voltammetric hybrid ET, composed of phtalocyanines-based carbon paste electrodes (CPEs) and gold electrodes covered by polypyrrole doped with several counterions, for the detection of forbidden adulterants in wines, used to improve wine organoleptic characteristics. The same authors developed an array of CPEs modified with three rare-earth bisphthalocyaninate compounds and successfully applied it for the discrimination of different Spanish red wines, prepared from the same grape variety but from different geographic areas and with different ageing times, from 4 to 36 months ([9]). In [10], Riul Jr. et al., showed the capability of an array of gold interdigitated sensors modified with LB films of conducting polymers/lipids and chitosan, to correctly distinguish different types of red wines, according to the vintage, vineyard, brand and storage conditions of the sample, using Principal Component Analysis (PCA) and Neural Networks as data analysis techniques. An ET composed of 28 potentiometric sensors was exploited to classify 160 Port wine samples of different ages (from 2 to 70 years, [11]); the ET predicted the Port wine age with an accuracy similar to that obtained using chemical analysis data.
The multiparametric analyser based on ISFET sensors for process control in the wine industry is reported in [12]. Authors developed high sensitive and stable pH, calcium and potassium sensors capable to measure the saturation point of ion-exchange resins, used to control the tartaric stabilization of wines in real time.
Previously our group reported an application of potentiometric ET system composed of porphyrin-based sensors for identification of beverages made of two different source materials: grape and barley ([13]); simultaneously a scale of beverages alcoholic degree in ethanol concentration units was evolved. The alcoholic strength of several commercial sorts of wine, beers, grappa and whiskey was successfully evaluated according to the evolved scale.
However while many papers are related to the application of chemical sensor arrays for red wine analysis ([14] - [16]), only few works are related to the white wines analysis, although its consumption is growing during the last period ([30]). Moreover, the spoilage processes propagate even faster in white wines especially if the production or storage conditions were affected, making the development of a rapid, not expensive analytical procedure of strong importance.
The sensor array described in table 3.9, was applied both for the classification and quantitative analysis of *Verdicchio D.O.C.* Italian dry white wines produced by nine cantinas. Peculiar parameters of white wines (namely alcoholic degree, volatile acidity, SO_2, L-Malic Acid, L-Lactic Acid and Total Polyphenols) individuated by standard analytical methods were compared with the values evaluated by metalloporphyrin-based ET. The developed procedure allows the monitoring of the acetic acid amount in wines and hence to control wine volatile acidity, so indicating the initial steps of wine spoilage process.

4.3.2 Experimental, results and discussion

All analyzed samples of Italian white wines were of *Verdicchio D.O.C.* quality, available in local stores (Rome, Italy); Verdicchio is a particular kind of wine produced in the middle eastern Italy, in Marche region. Following wines from nine cantinas produced in 4 subsequent years have been analysed: 1999- *San Sisto*, 13,5 vol.%; 2001 - *Monte Schiavo*, 12 vol.%; 2002 - *Casal de' Cavalieri*, 12,5 vol.%; 2002 - *Caldirola*, 12 vol.%; 2002 - *Sartarelli*, 13 vol.%; 2002 - *Fazi Battaglia*, 13 vol.%; 2003 - *Piersanti*, 12 vol.%; 2003 - *Moncaro*, 12 vol.%; 2003 - *Sant'Ignazio*, 13 vol.%.

All wines were measured immediately after opening the bottle; measurement procedure included no sample pretreatment. Initially, after open the bottle, wine was replaced in a plastic containers of 100mL volume with a minimum headspace over the sample. A fresh portion of each wine was measured every time for about 300 seconds, potential readings were collected automatically every 2 seconds. The samples were analyzed in 3 replicas in random order; sensors were conditioned in *artificial wine solution* (5 g/L of tartaric acid, 123 g/L of ethanol, 0,3 g/L of isobutyl alcohol, 0,06 g/L of isoamyl alcohol, pH=3,2) between measurements.

For quantitative analysis, peculiar parameters of white wines (table 4.3 have been analysed in certified laboratory (Institute of Agrarian Enology - *Istituto Enologico Agrario di C. Vinciguerra e C.*, Marino, RM, Italy) according to EEC recommended methods ([17]) and compared by regression methods with response of sensor array.

Principal component analysis (PCA) was applied for wines identification. Par-

	Alcoholic Degree	Volatile Acidity	SO_2	Malic Acid	Lactic Acid	Total Polyphenols	Total Polyphenols
	vol.% $\pm 0,19$	g/L $\pm 0,08$	mg/L ± 15	g/L $\pm 0,05$	g/L $\pm 0,05$	UV	F-C Index
Caldirola	11,72	0,27	90	1,05	0,18	21,6	4,76
Casal de' Cavalieri	12,65	0,34	80	0,31	1,82	8,81	5,74
Fazi Battaglia	12,20	0,31	96	1,70	0,80	9,24	6,92
Piersanti	12,31	0,27	90	0,86	0,53	8,91	6,48
Moncaro	12,19	0,22	77	1,06	0,16	8,12	6,70
San Sisto	13,01	0,46	93	0,36	0,87	9,67	6,62
Sant'Ignazio	12,95	0,40	61	0,26	1,13	6,53	4,98

Table 4.3: Wine parameters obtained by independent chemical analysis

tial Least Regression (PLS) method was applied in order to correlate ET system output with results received by certified methods; data were used without any preprocessing and scaling and validation was performed using either cross-validation or test set validation (especially for classification task). The RMSEP

(Root Mean Square Error of Prediction), slope and correlation coefficient of predicted versus measured correlation line was used to evaluate the efficiency of applied regression model. Data treatment was performed with commercial Unscrambler (v. 9,1, 2004, CAMO PROCESS AS, Norway) and Matlab (V.7,0,4, MathWorks, USA) software.

In the present work we continue the recently started evaluation of cobalt- and platinum-tetraphenylporphyrinates (MeTPP)-based polymeric film sensors in order to utilise them for wine discrimination purpose. As it was shown previously, the sensitivity of Co(III)- and Pt(II)TPP towards aliphatic alcohols decreases in a following order ([12]): ethanol > methanol > isobutyl alcohol; while in [18] and [19] the response of 5,10,15,20-tetraphenyl porphyrin (H_2TPP) and its Co(II) complexes-based sensors, towards the changes in acetic acid, ethanol, ammonia, NaCl, HCl, quinine, glucose, monosodium glutamate, dissolved SO_2 and H_2S content was evolved.

Basing on evaluated cross-sensitivity parameters (table 3.12), an array composed of highly cross-sensitive membranes has been developed and applied for qualitative and quantitative analysis of Verdicchio dry white wines. Sensors with following membranes were included in the array (table 3.9: H_2TPP-based membrane no. 1, Co(III)TPPBr-based membrane no. 2, Co(II)Por-based membrane no. 4, dummy membrane no. 5, Pt(II)TPP-based membrane no. 8 and Pt(IV)TPPCl_2-based membranes no. 11 and 12).

A PCA discrimination of five Verdicchio wines (Monteschiavo, Sartarelli, Fazi Battaglia, Casal de′ Cavalieri and Piersanti, table 4.3) and artificial solution mimicking wine composition has been performed; the score plot is reported in figure 4.4.

The score plot shows 99% of total variance (PC1 94%, PC2 4%, PC3 1%)

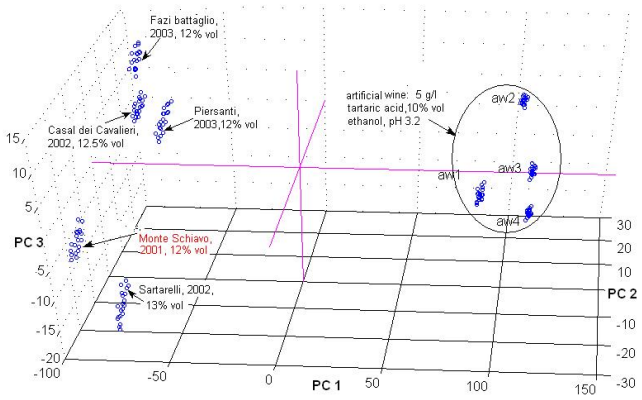

Figure 4.4: PCA score plot for discrimination of five Verdicchio Italian white wines evaluated by porphyrins-based ET. On graph: aw - artificial wine of composition: tartaric acid 5 g/L , ethanol 123 g/L, isobutyl alcohol 0,3 g/L, isoamyl alcohol 0,06 g/L, pH=3,2, number of replicas n=4

and a clear distinction between all analyzed samples can be seen. Along the PC1 axis, two well separated clusters, corresponding to the analysed wines and artificial wine can be observed. Moreover, two sub-clusters in Verdicchio wines group may be evolved: one contains wines *Monteschiavo* and *Sartarelli* (on the top) and the other wines *Fazi Battaglia*, *Casal de′ Cavalieri* and *Piersanti*. According to the information on samples, provided by manufacturers, this distinction may be attributed to the age of wines: in fact wines of the second group are older then other wine samples. The highest discriminative ability (and the largest loading values) was shown by sensors with membranes based on H_2TPP (no. 1), Co(II)TPP-R (no. 3), dummy membrane no. 5 plasticised with TOP, TDACl based membrane no. 6 and Pt(IV)TPPCl_2 based membrane no. 11.
The array was then applied for the analysis of another group of seven Verdicchio wines, coming from cantinas Caldirola, Casal de′ Cavalieri, Fazi Battaglia, Piersanti, Moncaro, San Sisto and Sant′Ignazio, for which both discriminative analysis according to the year of wine production, as far as quantitative evaluation of several wine components by regression methods have been performed. In figure 4.5, a Partial Least Squares-Discriminant Analysis (PLS-DA) plot of first tree latent variables represent classification of Verdicchio wines according to the year of production. PLS-DA is an extension of supervised PLS technique. Prior to analysis Verdicchio wine samples have been divided in three different classes: years 1999, 2002 and 2003. Then discriminating plane has been found in order to separate the classes of observations on the basis of the X-variables sensor responses according to an Y-vector that encodes the year of production in a set of categorised variables, denoted as positive and negative (1 and 0 values, respectively). A high capability of porphyrin-based ET system to classify the Verdicchio wines in 3 groups corresponding to the year of production can be observed.

On the second stage of the study the possibility to determine the amounts of SO_2, polyphenols, malic and acetic acids in Verdicchio dry white wines by means of metalloporphyrin-based ET system was studied. Sulphur dioxide is employed in wines as an antiseptic and antioxidant from the ancient times, but according to the nowadays legal limits for Italian wines, it should not exceed $200mg/L$ ([20]). Malic acid is an important parameter especially for white wines; its high amount in wine (may reach $0{,}5g/100mL$) represents the cool years or regions of grapes cultivation. The phenols in wine give an astringent test, may cause the pungent odors and may indicate special flavoring or other adulterating agents added to the wine.
PLS results of correlation for total dissolved SO_2, total polyphenols and malic acid content determined by ET system and compared to the values evaluated according to EEC certified analytical methods ([17], table 4.3) are shown in figure 4.6(A-C). It can be seen that a satisfactory correlation between predicted and measured values is reached in the calibration step for all tree analytes, while some deviations can be noticed in the validation phase mainly for samples no. 1, 3 and 7.

Volatile acidity (VA) is an important determination used by winemakers as wine spoilage marker; it is expressed as $g_{CH_3CO_2H}/100mL_{wine}$ since the acetic

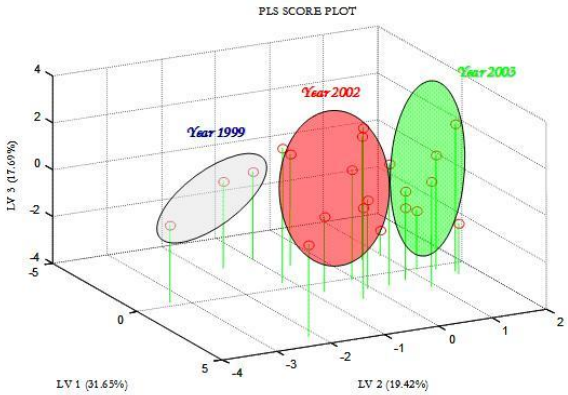

Figure 4.5: PLS-DA plot for Verdicchio dry white wines: classification for year of production

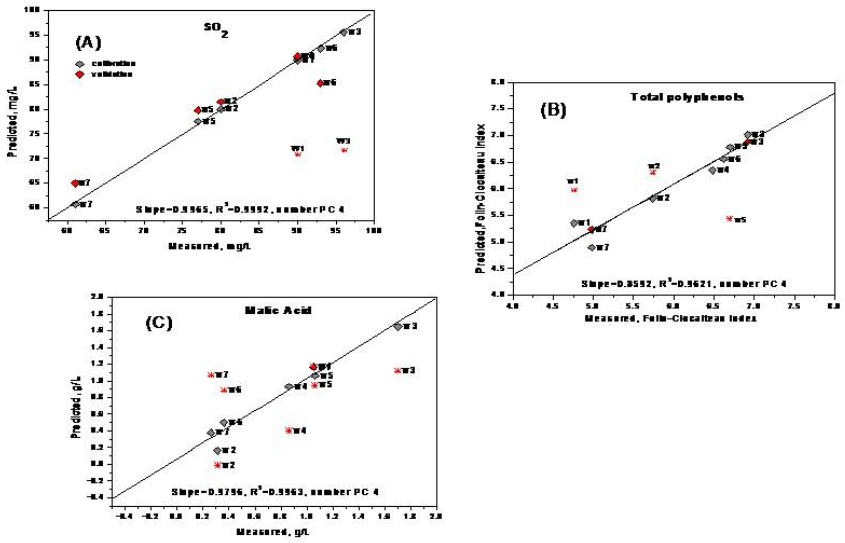

Figure 4.6: Results of porphyrin-based ET application in Verdicchio white wines for determination of: (A) SO_2 content, PLS model: Slope 0,9965, R^2 0,9992, number of PCs 4; (B) Total Polyphenols (versus Folin-Ciocalteau index), PLS model: Slope 0,8592, R^2 0,9922, number of PCs 4; (C) Malic Acid, PLS model: Slope 0,9797, R^2 0,9963, number of PCs 4; Wine samples: w1 - Caldirola, 2002; w2 - Casal de′ Cavalieri, 2002; w3 - Fazi Battaglia, 2002; w4 - Piersanti, 2003; w5 - Moncaro, 2003; w6 - San Sisto, 1999; w7 - Sant′Ignazio, 2003

acid is the organic acid mainly affecting VA. The VA maximum amounts permitted in white wines are 0,120, 0,110, 0,250 and 0,090 $g/100mL$ for USA, France and Italian domestic and export market respectively ([17]). Small quantities of acetic acid are formed in wine during normal, bacteria-free alcoholic fermentation; normally this amount is within $0,03 - 0,06$ $g/100mL$ range and not noticeable to taste or smell. Once wines reach 0,07 $g/100mL$ to just under $0,100g/100mL$, a spoilage process becomes noticeable due to a sweet, sour vinegary smell and taste. Under this conditions the spoilage organisms, particularly *Acetobacter*, are present and indicate that wine conditions may support the growth and activity of other spoilage yeast and bacteria and turn wine to vinegar. At low levels, acetic acid can enhance the flavor of a wine, while at higher levels (over 0,100 $g/100mL$) this flavor can dominate and flaw the wine. That is why the accurate and rapid determination of acetic acid amount is necessary.
Acetic acid amount can be detected following the classical steam evaporation method ([20]). Moreover several sensor applications have been developed for this purpose during the last years ([21] - [23]).
Here we applied porphyrin-based ET system for acetic acid content evaluation in white dry Verdicchio D.O.C. Italian wines. In figure 4.7, the result of Multi Linear Regression (MLR) yielded a root mean square error of calibration (RMSEC) and prediction (RMSEP) values of 0,000917 and 0,001743 mg/L respectively which are lower then the value permitted for VA determination error recommended by EEC (0.08 g/L). The correlation coefficients for the calibration and validation were 0,9943 and 0,9799 respectively.

The generated MLR calibration model was then applied to acetic acid con-

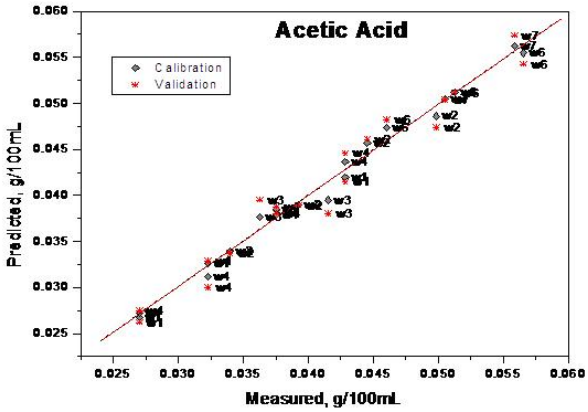

Figure 4.7: Acetic acid content in Verdicchio wines. Data treated by MLR, Calibration: Slope 0,9888, R^2 0,9943, RMSEC 0,000917, Validation: Slope 0,9857, R^2 0,9799, RMSEP 0,001743. The wines notations are the same as in figure 4.6 caption

tent determination in real Verdicchio wines. The results of prediction are given in table 4.4. Calibration models were constructed basing on 10 times diluted training samples; the predicted acetic acid concentrations in $g/100mL$ were back calculated to get the actual concentration of acetic acid in undiluted wine in g/L. As can be seen, the relative error of acetic acid content determination lies within the range $0,9 - 17,5\%$, which is satisfactory for an express monitoring of wine spoilage process initiation.

Cantina	**Found by EEC recommended method**	**Predicted by ET system**	**Relative Error %**
Caldirola	0,270	0,262	3,0
Casal de′ Cavalieri	0,340	0,337	0,9
Fazi Battaglia	0,310	0,360	16,1
Piersanti	0,270	0,274	1,5
Moncaro	0,220	-	-
Caldirola	0,460	0,482	4,8
Caldirola	0,400	0,470	17,5

Table 4.4: Results of quantitative data analysis on Verdicchio wine samples

4.3.3 Conclusions

Cross-sensitivity properties of potentiometric PVC solvent polymeric membranes doped with Co- and Pt -porphyrinates have been evaluated. Sensors with high cross sensitivity were incorporated in the ET sensor array and applied for the discrimination of Italian dry white wines *Verdicchio* of D.O.C. quality. It was found that porphyrin-based ET system was able to identify all analyzed *Verdicchio* wine samples on the base of the production year and to distinguish between real wines and an artificial solution, used as conditioning solution.
Along with good discriminating ability, the system has showed an adequate predictive power for several white wine components, previously evaluated by independent chemical analysis. Thus, the possibility of quantitative detection of total SO_2, Total Polyphenols, Malic and Acetic Acids content using ET system has been found.
Porphyrin-based all-solid-state ET system hence, may be a promising rapid and inexpensive analytical instrument for quality assessment and quantitative analysis for such delicate beverages as white dry wines.

4.4 Sensor array for the automatic control of must fermentation process

4.4.1 Introduction

Slow and/or incomplete consumption of sugars by *Saccharomyces cerevisiae* during grape must fermentation is a persistent problem in wine production. Stuck fermentations can be attributed to a variety of factors, including availability of nutrients, presence of toxic substances, temperature, pH variation and poor ethanol tolerance of the yeast ([24]). The rate of fermentation strongly depends on the ability of yeast cells to transport sugars. Environmental and physiological stress leads to a decrease in transport activity. Early identification and correction of the problem is vital to prevent stuck fermentations and the adaptive response of the yeast (loss of cellular transport activity) to adverse conditions requires the readjustment of the medium before irreversibility of adaptation occurs ([25] - [28]). Thus, it is desirable to develop diagnostic methods for close monitoring of alcoholic fermentation performance. In red wine production, pomace extraction is achieved by different protocols and techniques for pumping-over, fermentation time, timing and intensity of must aeration, sulfiting, temperature control and mass homogenization. These factors affect yeast viability and, therefore, may influence the alcoholic fermentation.
For example, pumping-over plays a major role in pomace extraction and secondary effects can also occur. By mixing the mass, homogeneity of the temperature throughout the tank is achieved, together with an increase in dissolved oxygen necessary to improve the yeast fermentation process ([29]).
In this section, the application of an array of potentiometric sensors, for the control of the must fermentation process, will be described.

4.4.2 Experimental, results and discussion

All the experiments have been conducted in the framework of the Italian project *ELEN-TOOL (on-line measurement tool for automatic control of must fermentation process in wine industry).*
An array based on potentiometric sensors, with platinum surface on which metal complexes of vanillin porphyrin (figure 3.6) were deposited by electropolymerization, has been developed.
The deposition of regular films of Vanillin Porphyrin was performed by electropolymerization on the sensor surfaces, in a 3-electrodes cell, using a commercial potentiostat (AMEL, mod. 7050), Standard Calomel Electrode as reference electrode (AMEL, mod. 303/SCG/6) and platinum wire (diameter 0,7 mm) as counter electrode, starting from a solution of porphyrin dissolved in basic media (NaOH 1M, $porphyrin : solvent = 3mg : 4mL$); in analogy with literature references, a non-conductive layer was obtained, shown by a decreasing peak value in the current flowing through the cell.
The array was integrated in an automatic system, connected to silos containing red wine must; samples were analysed every 4 hours for 5 minutes by means of

the developed Electronic Tongue and a QMB-based Electronic Nose, developed by our University.
After preliminary tests in laboratory, with calibration towards standard salts, system was applied in the cantina *Ermacora* in Cormons (Udine, Italy), for the control of *Cabernet-Franc* must. Data were collected and automatically sent to our processors for data analysis, for a period of 1 month (19^{th} October - 19^{th} November 2004).
Data from ET and EN systems were compared with data obtained from classical laboratory analysis performed by local patented laboratory Brava. 10 parameters, commonly chosen as markers by winemakers during fermentation process, were studied, namely volatile and total acidity ($g_{CH_3CO_2H}/L$), reducing sugars (%), alcohol, total polyphenols ($mg_{catechins}/L$), colour intensity, colour tone, anthocyans (mg/L), malic and lactic acid (g/L).
The chemical profile of the process, according to measure day, is shown in figure 4.8. In the plot, showing 83,73% of total variance, 4 fermentation steps can be

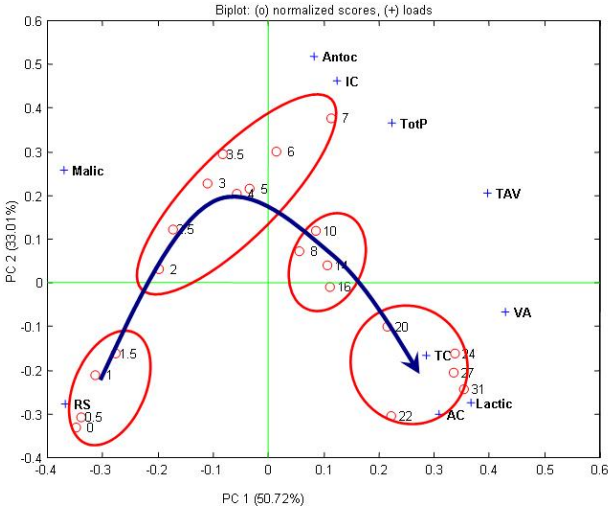

Figure 4.8: Chemical profile of fermentation process, obtained by data coming from classical laboratory analysis

identified:

- 1^{st} and 2^{nd} day;
- from day 2 to 7;
- from day 8 to 16;
- from day 17 to day 31.

The influence of each parameter (loading) is also shown.
Electronic Tongue data were deeply analysed (figure 4.9): it is evident how there

are two periods in which data were out-of-scale; this non-sense behavior was due to problems in the fluidic system (pumps and valves) and data from days 5 to 13 and 23 to 25 were not used for data analysis. Data were firstly analysed by

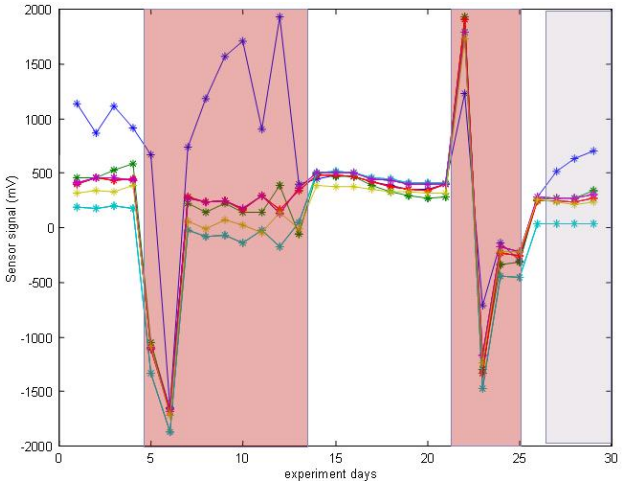

Figure 4.9: Electronic Tongue signal during measurement period of Cabernet-Franc must. Two periods, in which array provided out-of-scale signals, is related to fluidics problems

Principal Component Analysis (PCA), in order to obtain qualitative information on fermentation process. Scores plot is shown in figure 4.10. It represents the 88,02% of the total variance and a high correlation with chemical profile obtained from classical analysis, can be found, showing the capability of the developed system to closely follow the fermentation process. In fact, according to useful data, the same clusters can be identified, namely days 1 and 2, 4 to 7 and 14 to 16. Only the sample from day 25 was misclassified, probably due to non-linearities in model building.
A quantitative correlation with parameters chosen as markers, was evaluated by PLS technique, showing a high correspondence between the data from sensorial system and real values. Plots for all parameters are shown in figure 4.11.

4.4.3 Conclusions

Sensor array, based on chemically modified platinum sensors with electropolymerised metal complexes of vanillin porphyrin, was developed.
It was firstly used in laboratory test, with calibrations towards standard salts, showing high cross-sensitivity coefficients.
It was then applied for the control of the fermentation process of Cabernet-Franc must, by automatic connection to silos in cantina *Ermacora* in northern Italy. 10 parameters, commonly used by winemakers to control fermentation process,

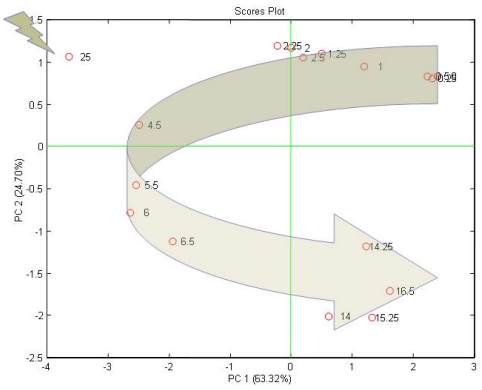

Figure 4.10: Chemical profile of fermentation process, obtained by data coming from Electronic Tongue data

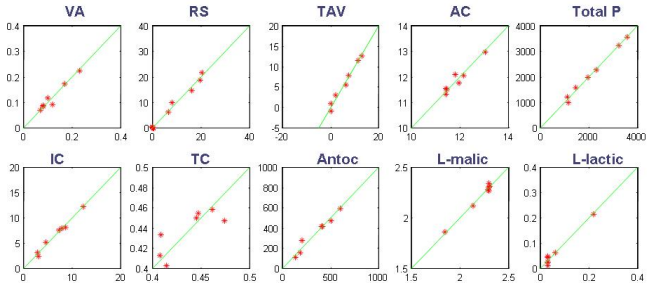

Figure 4.11: Analytical profile regression for chosen parameters: data from Electronic Tongue were compared with data from standard analysis

were evaluated by analysis performed by standard methods in patented laboratory; they were then compared with data coming from sensor array.
Not all data could be used, according to some problems in fluidics, which could not be able to provide in correct way the sample into measure chamber. Useful data were finally analysed by PCA for qualitative information and PLS for quantitative correlation with real values of chosen parameters.
PCA scores plot showed a chemical profile during the period of measure, very close to the one obtained with studied parameters, evidencing the same clusters, according to the day from fermentation beginning; PLS plots showed a high capability of the system to exactly predict the amount of each parameter.

4.5 Detection of sophistications in white wines - *GoodFood* integrated european project

4.5.1 Introduction

Recently, a significant constant wine market growth has been registered all around the world ([30]). In fact, the latest International Organization of Vine and Wine (OIV) report, issued in March 2007, showed wine consumption rising slightly in European countries (1.4% in total), while for countries outside the European Union, the growth was even more consistent. For instance, consumption in the United States rose by 3.1%, in Argentina by 1.2%, 2 % in South Africa, by 1.7% in Australia and by 6.5% in New Zealand ([31]). In order to ensure uniformity within a brand and to avoid falsifications, an accurate product control is strictly required for wine industry. The utility of chemical sensor arrays working in the liquid phase for this purpose has been shown recently ([32], [33]).
Furthermore, wine is a complex solution, whose global composition is due to more than 600 components, which characterised the different qualities. Factors affecting the good taste and smell of a wine, are in great number, but, if just one of them is lower then expectations, final product of lower quality can be obtained.
Some of the components which give the organoleptic characteristics of wines, are already present in the grapes, while others grow during the fermentation, maturation and wine aging. Neo-formed products mainly come from sugars and, in minor part, from nitrogenous compounds.
In this section, the applications of several sensor arrays for the detection of some analytes, mimicking wine defects, in white wines, will be discussed in detail. In particular, SO_2, H_2S and acetic acid, in different concentrations were analysed, both in synthetic solutions and in real white wines.
Application of platinum-based sensors, modified with PVC-based and electropolymerized membranes, will be presented. Wines were then analysed also by means of a miniaturised Electronic Tongue, based on silicium wafers, obtained by litographic technique; 3 different configurations will be shown.

Finally, the innovative coupling of a miniaturised sensor array based on electropolymerized amino-substituted porphyrins, with a micro-separation column, will be discussed.

Sulphur Dioxide - SO_2

The year 1487 marked a turning point in the history of good winemaking. In that year, a Prussian royal decree officially permitted the use of the wine additive sulfur dioxide for the first time. Not that it hadn't been used before then: in fact, to help preserve their wines during transport, Dutch and English wine traders regularly burnt sulfur candles inside barrels before filling them; it was a trick that they learned from the Romans who conducted the same practice over a millennia before.

Today, the use of the additive SO_2 is an almost universally accepted winemaking practice. Although it is naturally produced in small amounts by wine yeast during alcoholic fermentation, most of the SO_2 found in wines has been put there by the winemaker. It is added at most stages of the white winemaking process, from crushing through to bottling. It is used less liberally during red winemaking, but with an almost mandatory addition being made following the completion of the malolactic fermentation of these wines. It is added in the form of a powder or it is directly fed into the wine as a gas from a dosing gun.

Many would be aware that sulfur dioxide can cause severe allergic reactions in some people. So why do winemakers use it? Put simply, it is very difficult to make wines that have an aging potential beyond a few months if sulfur dioxide is not used during winemaking. A big statement but true.

Sulfur dioxide plays two important roles. Firstly, it is an anti-microbial agent and as such is used to help curtail the growth of undesirable fault producing yeasts and bacteria. Secondly, it acts as an antioxidant, safeguarding the wine fruit integrity and protecting it against browning. Despite its chemical simplicity, SO_2 can take on a few different forms in a wine. One form is called molecular SO_2. When in this form, it is around 500 times more effective in killing wine microbes than when in any of the other forms that it can take ([34]). Luckily for us, the desirable yeasts that undertake wine fermentation are more resistant to SO_2 than most of the spoilage yeasts.

When dissolved in wine, SO_2 can also exist in what is called an ionised form. This form has the greatest antioxidant effect. In reality, SO_2 is not that keen to react directly with oxygen, but it does readily combine with other oxidising agents that are formed in the presence of oxygen. In conjunction with molecular SO_2 which plays a further role of *knocking out* the naturally occurring enzymes in grapes that cause wines to brown (called polyphenoloxidases), SO_2 is a powerful force in keeping wines fresher longer.

One less known but important property of SO_2, is its ability to bind with acetaldehyde. This compound has an unpleasant smell of bruised apple or rank sherry and is produced when wines undergo some oxidation. When the SO_2 and acetaldehyde molecules bind to each other, the resultant substance is odourless.

The SO_2 effectively strips the wine of its oxidative character.
When present in excess, it can cause a healthy ferment to stop before the yeast has converted all the grape sugar to alcohol. Furthermore, as the bacteria responsible for malolactic fermentation are particularly sensitive to SO_2, excessive amounts will almost certainly block its onset. This lack of resistance to SO_2 by malolactic bacteria can be very handy when a winemaker is attempting to make a wine that does not benefit from malo, such as a crisp fruity Riesling or a Rose. However, malo is a defining component of the style of most full bodied dry white and nearly all red wines. Therefore, having excessive SO_2 present at the time when malo would normally occur is particularly undesirable.
When SO_2 is greatly in excess, it can also produce a pungent aroma in white wines, considered by most to be a fault. The aroma is best described as that of a match that has just been struck. Many people have trouble smelling the sulfurous aroma of SO_2, but instead perceive it as a irritation of the membranes of the nose. High SO_2 can also render the palate of the wine harsh, metallic and frequently bitter.

Hydrogen sulfide - H_2S

In minute quantities, reduced-sulfur compounds may be important to the desiderable and characteristic fragrance of wine. They also can be the source of revolting off-odors. The same compounds may induce both responses, depending on the concentration.
One of the most well-known reduced-sulfur compounds is hydrogen sulfide (H_2S). At much above the sensory treshold, H_2S produces a rotten-egg odor. The origin of H_2S can be very diverse because of its pivotal role in the metabolism of sulfur compounds. It may be generated from sulfate found in grape tissue, sulfite derived from SO_2, amino acid degradation and elemental sulfur fungicidal sprays.
During fermentation organic sulfur compounds do not appear to be significant sources of hydrogen sulfide. Its primary source during fermentation is elemental sulfur, especially in colloidal form. Elemental sulfur is derived mainly from its use in the control of powdery mildew. Consequently, the application of sulfur is not recommended 6 weeks prior to harvesting. This interval is usually adequate to avoid sulfur application significantly contributing to reduced-sulfur odor production. However, data from Thomas et al. suggest that sulfur derived from its use as fungicide is tipically insufficient to produce significant amount of H_2S, at least during fermentation. Its conversion to H_2S appears to be non-enzymatic, resulting from the reduction from sulfur particles touching yeast cells. Other sulfur-containing fungicides, such as captan, mancozeb and dichlofuanid, may contribute to H_2S production if applied late in the season. Reducing substances in yeast cells are presumed to be involved, but yeast-strain selection is unlikely to affect H_2S production via this non-enzymatic route. Nevertheless, strain selection can be of value in minimizing the enzymatic reduction of sulfite to hydrogen sulfide. H_2S produced during fermentation declines spontaneously

during maturation. Its oxidation to sulfur is spurred by the production of a strong oxidant (hydrogen peroxide) in the presence of small amounts of oxygen and o-diphenols.
Unless hydrogen sulfide is removed from wine promptly, it can react with other wine materials and form mercaptan, which can then be oxidized into disulfides (mercaptan and disulfide also produce very disagreeable odors). Most people can detect less than 1 ppm of H_2S, so very small quantities of hydrogen sulfide can completely spoil a fine wine.
In smaller amounts, hydrogen sulfide can give wines a Askunk or Arotten cabbage odor. In even smaller quantities, it may not produce a recognizable odor, but it often destroys the fruity nose of the wine.
Sometimes, hydrogen sulfide is encountered during fermentation even when the grapes contain no residual sulfur. Here the problem occurs because the yeast runs short of some needed material. Hydrogen sulfide can be produced when yeast lacks micro-nutrients or vitamins including pantothenic acid; a common cause of stinking fermentations is a lack of nitrogen and mild cases of H_2S can often be cured by adding a small quantity of diammonium phosphate (DAP) to the fermentation.
Many winemakers add extra nitrogen, micro-nutrients and pantothenic acid to their fermentations specifically to avoid the production of hydrogen sulfide gas.
Hydrogen sulfide can also be produced when wine is left on the gross lees for long times. Winemakers avoid this problem by promptly racking new wines off the gross lees or by periodically stirring the wine when long lees contact times are desired.
Hydrogen sulfide should be removed promptly because it becomes more difficult to remove the longer it stays in the wine. Home winemakers often use the following procedure to remove hydrogen sulfide from wine:

- about 50 milligrams per liter of sulfur dioxide is added to the wine when fermentation is complete;
- wine is then aerated by racking with a great deal of splashing and bubbling to blow off the H_2S gas;
- sulfur dioxide in the wine then converts the remaining hydrogen sulfide back into elemental sulfur and the sulfur settles to the bottom of the storage container;
- after a week or two, the wine should be racked or filtered to remove the elemental sulfur or the smell may reappear.

Aeration is often effective in treating mild cases of hydrogen sulfide. However, aeration must be used with some caution. Aeration may oxidize mercaptan in the wine into disulfide and disulfide is as stinky as H_2S and more difficult to remove.
Some home winemakers rack their stinky wine through a clean piece of copper screen or they place a few copper pennies in the wine container. Copper converts the hydrogen sulfide gas into copper sulfide, which is not soluble in wine

and it settles to the bottom of the tank.
After a few days, the winemaker racks or filters the wine off the copper sulfide residue; but, placing copper metal in wine can cause other problems: wine has a low pH and the acid may dissolve too much copper which may be deposited in the wine and since copper is a heavy metal, it should be used with care.

Acetic Acid - CH_3CO_2H

The formation of the vinegary characters were the result of the growth of acetic acid bacteria. There are a number of these, but the most destructive ones in wine are *Acetobacter aceti*, *Acetobacter pasteurianus* and to a lesser extent, *Gluconobacter oxydans*. These bacteria are found on the surfaces of grapes (particularly these latters) and the others are common residents on winery equipment and in used oak barrels. They all have one thing in common: they are aerobic bacteria, needing lots of oxygen to proliferate. They are microscopic single celled critters which have enzymes embedded in their cell walls. These enzymes work to oxidise alcohol into the vinegary smelling acetic acid. Other enzymes also convert alcohol, but this time through a complex set of reactions, into the solvent like compound ethyl acetate.
Acetic acid bacteria were first recognized as causing wine spoilage in the XIX century. Their ability to oxidize ethanol to acetic acid bot induces wine spoilage and is vital to commercial vinegar production. Although acetic acid synthesis during vinegar production has been extensively investigated, the action of acetic acid bacteria on grapes and in must and wine, has escaped scrutiny.
Alcohol is the primary energy source for most of the acetic acid bacteria. When the grape is damaged by birds or after being infected with moulds such as Botrytis, the juicy parts of the grape are exposed to the air. The grape skin is home to natural populations of yeasts which ferment the exposed juice producing alcohol. The Acetobacters then use this alcohol to produce acetic acid. When you crush these sorts of grapes, the resultant juice will have a high viable population of Acetobacter and also a higher than normal level of acetic acid.
Most acetic infections occur in the winery. The bacteria enjoy living in wines that are both low in acidity and sulfur dioxide. But the key ingredient for their growth is oxygen: it is absorbed by wine every time it is racked or transferred between storage containers; it is also slowly absorbed into the wine through the gaps between the staves in oak barrels. More damaging is when the level of wine in the barrel falls due to evaporation and this lost wine is not regularly replaced; it will be replaced by air resulting in an ideal environment for acetic acid bacteria to grow. In fact, it is probably true that the most likely time for any wine to become acetic is during its barrel storage, either due to the barrel being ullaged or its sulfur dioxide levels not being maintained or both.
Minimising oxygen pick-up combined with a good protective level of sulfur dioxide are the two most important winemaking strategies employed to avoid acetic acid build-up in wine. While sounding simple to do, there are some complicating factors: oxygen is a necessary ingredient in the natural reactions which soften

tannins and stabilise the colour of red wines; wine yeasts also find it difficult to undertake clean and completed ferments if the oxygen levels in the juice are very low. So in many wines, having close to absolute zero dissolved oxygen is not the answer.
Lastly poor bottling practices can also result in acetic wines. Filtration prior to bottling is known to reduce the number of viable acetic acid bacteria. Membrane filtration, in which the wine is passed through a filter which has holes smaller than the acetic acid bacteria themselves, is particularly effective. However once again, if the wine picks up excessive air when it is being bottled then there is a possibility of the wine spoiling after bottling.

4.5.2 Qualitative and quantitative analysis of synthetic white wines - Sensor configuration 1

Introduction

In the last decades an increasing demand to control the quality of different matrices, such as food and beverages, has been noticed. One of the most promising ways to perform fast and low cost analyses is related to the use of arrays of cross-selective chemical sensors, which have been usually called *Electronic Nose* (headspace analysis) and *Electronic Tongue* (solution analysis).
Another focal point of research attention is the realization of miniaturized devices, because they can allow significant improvements in performances and a dramatic reductions of sample consumption ([35], [36]). This purpose can be reached by the integration of chemical sensors technology with the silicon technology. In fact, the use of silicon-based techniques allows the construction of chemical sensors of reduced dimensions, also nano-dimensioned ones ([37]), with the possibility to strongly vary the geometry of sensitive layer on the surface. Both these aspects are even more challenging for the development of sensor arrays working in the liquid phase, because the so called electronic tongues have been far less studied than the corresponding electronic nose systems.

Sensors preparation

The fabrication of microelectrodes was carried out on a 3" polished silicon wafer, (100)-oriented, with 500 nm of thermal grown oxide. For each wafer, two different geometries of platinum microelectrodes may be processed, 12 devices for each layout; two masking levels and about 25 fabrication steps were required for complete devices fabrication. Present work focused on performance of solid miniaturized thin film platinum microelectrodes, locally passivated with sputtered silicon nitride.
Microelectrodes fabrication started with a first platinum deposition by RF Sputtering equipment. The dielectric passivation of this microelectrodes was implemented by a layer of sputtered silicon nitride deposited in a reactive environment of Ar/N with the substrate heated at 300 ^0C during deposition.

Implemented fabrication process required following fabrication steps:

- First lithographic process for resist patterning, with specific lift-off resist profile;
- Sputtering deposition of 200 nm platinum thin film;
- Lift-off process to remove metal on unwanted areas;
- 300 nm silicon nitride thick wafer passivation;
- Second lithographic process for reactive dry etching of silicon nitride;
- Dry etching of nitride layer for vias opening;
- Resist mask ashing;
- Oxygen plasma cleaning, dicing and breaking of single array die.

Figure 4.12 shows typical silicon wafer during fabrication process and a flow chart of main fabrication steps.
Dry etching process of silicon nitride, in order to remove passivation from ac-

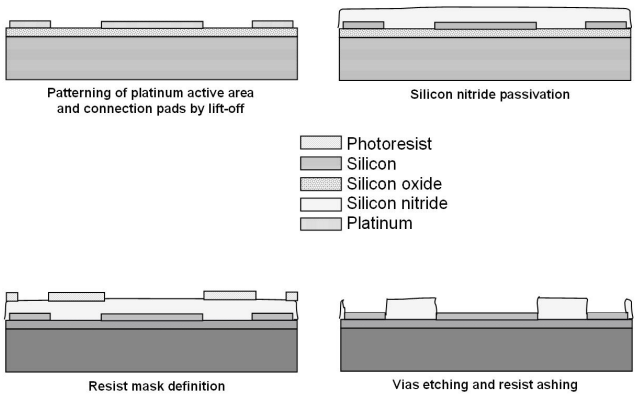

Figure 4.12: Two different microelectrodes geometries onto 3″ Si wafer (left); schematic of microelectrodes fabrication run (right)

tive area of electrodes, was carried out by means of a Plasmalab 80 RIE reactor with chamber pressure of 30 mTorr, 20 sccm reactive gases flow, SF_6/O_2 90:10 mixture; the RF power density supplied to reactor plate has set to about 0.5 W/cm^2.
Figure 4.13 shows final devices after dicing process; nevertheless final die dimensions are quite large and were introduced for a preliminary investigation of device performance; further integration and dimension reduction may be easily

obtained with a new set of photolithographic masks. Further optimization of silicon nitride deposition process and passivation process in general is under development, since exposure of nitride to acid or basic solutions may cause oxidation of the surface and modification of insulation properties ([38]).

Figure 4.13: Final diced devices for potentiometric measurements

Measurement set-up

The geometry of sensor surface is represented in figure 4.14.

Sensors are based on a silicon wafer and by lithographic techniques, three different deposition pads on the surface were obtained. Each sensors was $15mm$ long, $7,5mm$ large and $100\mu m$ high; in this study, the deposition has been performed on the central pad whose deposition area was $4,5mm \times 5mm$ (red area). Measures were performed in a flow injection cell, represented in figure 4.15. The cell had external dimensions of $80mm \times 40mm \times 30mm$; during the measures, a peristaltic pump provided a flow rate of few mL per minute. Distilled water was used to clean sensors during each measure and the typical trend of the response curve is reported in figure 4.16, when the different phases of cleaning and measure can be observed.

Results and discussion

Membranes, whose composition and selectivity properties have been described in tables 3.13 and 3.14, have been deposited on miniaturised sensors, based on silicium wafer and applied for qualitative and quantitative analysis of synthetic

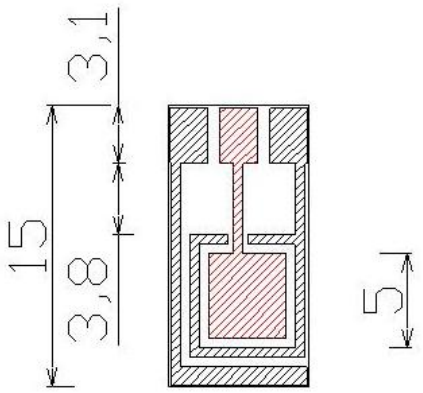

Figure 4.14: Structure of miniaturized sensor surfaces. PVC-based membrane deposition has been performed on the central pad (red area); dimensions are reported in mm

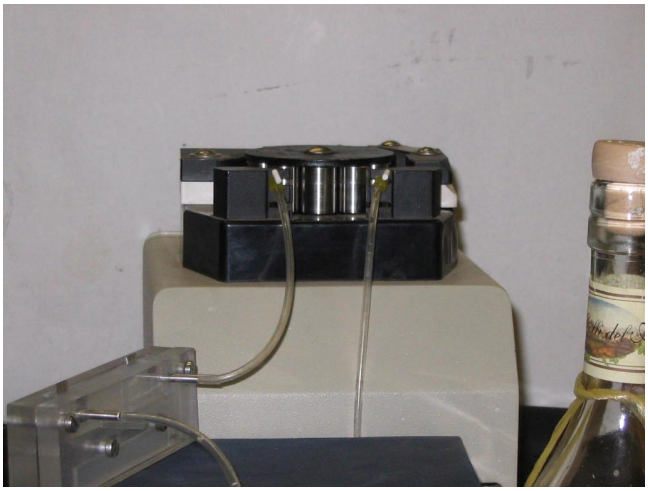

Figure 4.15: Experimental set-up, composed of measurement cell and a peristaltic pump which provided the sample flow

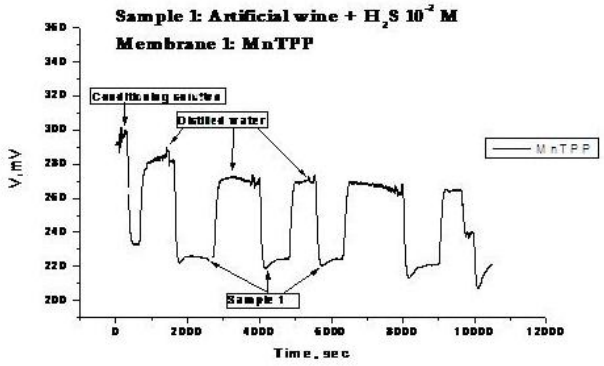

Figure 4.16: Structure of miniaturized sensor surfaces. PVC-based membrane deposition has been performed on the central pad (red area); dimensions are reported in mm

white wines, artificially added of substances mimicking spoilage defects, namely sulphur dioxide, hydrogen sulfide and acetic acid; all the experiments have been performed in the framework of the European project *GoodFood*.
Samples were prepared by standard methods and provided by laboratories of CNR-ISPA of Bari (Italy); the concentration of the target analytes in the synthetic solution used as background, are given in table 4.5.
Samples were sealed in closed plastic bottles, to avoid interaction with air and measured immediately after the opening. A conditioning solution (tartaric acid $5g/L$, ethanol $123g/L$, isobuthylic alcohol $0,3g/L$, isoamylic alcohol $0,06g/L$, $pH = 3,13$), to restore membrane properties, was used between two successive samples.
Potential values (sensor array was completed by commercial pH glass electrode) were calculated, by measuring the potential differences between electrodes in array and the conventional reference electrode (standard calomel electrode, AMEL, Italy) using a PC equipped high-impedance input 8-channel A/D converter (Smartronix, Rome, ITALY), for about 7 minutes; membranes were then restored in conditioning solution for about 10 minutes.
The processing of multi-component data coming from non-specific sensors has been performed using partial least squares (PLS) and principal components analysis (PCA). The aim is to reduce the amount of variables to new variables (*latent variables* and *principal components*, for PLS and PCA respectively) in a reduced variable space to facilitate identification or classification; additionally, this new space simplifies the way to explain the variability contained in the available information. PLS and PCA analysis and evaluation processes were performed with the software *Matlab 7.0*.

The plot of the first two principal components (figure 4.17), represents the 82,63% of the total system variance. A clear classification can be noticed for

Sample	$[H_2S]$**M**	$[SO_2]$**M**	$[CH_3CO_2H]$**M**
1	10^{-2}	-	-
2	10^{-3}	-	-
3	10^{-4}	-	-
4	10^{-5}	-	-
5	10^{-6}	-	-
6	-	10^{-2}	-
7	-	10^{-3}	-
8	-	10^{-4}	-
9	-	10^{-5}	-
10	-	10^{-6}	-
11	-	-	10^{-2}
12	-	-	10^{-3}
13	-	-	10^{-4}
14	-	-	10^{-5}
15	-	-	10^{-6}

Table 4.5: Composition of syntetic white wine solutions analysed by means of an Electronic Tongue system for the detection of some analytes mimicking wine defects

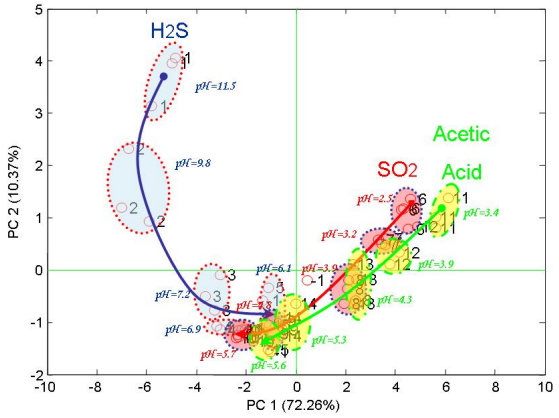

Figure 4.17: PCA scores plot of synthetic wine solutions with analytes mimicking wine defects; pH value is considered in data analysis

the different compounds, with 3 different directions on the graph, according to the analyte increasing concentration. The good reproducibility of the sensor responses during the measures, performed in different days, can be also noticed, with well defined clusters for each class of samples. The system also showed a good capability to recognize the exact amount of each analyte, with a partial overlap in the centre of the plot at very low concentrations. Starting from this consideration, a quantitative correlation between Electronic Tongue data and concentrations of analytes coming from standard laboratory analysis, was also performed, by PLS analysis.
The scores plot of the first two latent variables (82,71% of total variance) is shown in figure 4.18. Also in this case, 3 different direction, according to an-

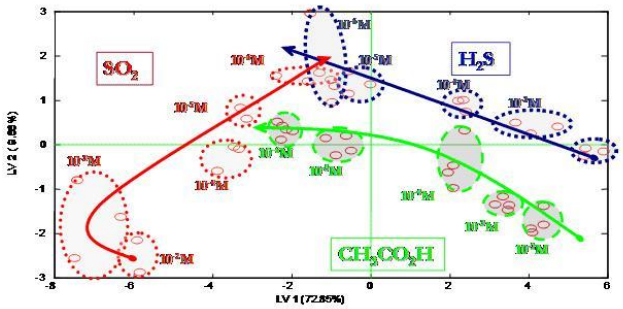

Figure 4.18: PLS scores plot of synthetic wine solutions with analytes mimicking wine defects; pH value is considered in data analysis

alyte concentration, can be noticed, with a partial overlap in the centre of the graph, where the samples with lower concentrations are shown.
Quantitative information on the concentration of each analyte, were obtained by correlating Electronic Tongue means and data obtained from standard laboratory analysis. Results, in term of predicted versus real concentration of each analytes, are given in figures 4.19 and 4.20. An arbitrary value of 10^{10}M was assigned when analyte was not present in solution, since logaritmic values were used for molar concentration of each analyte.
In the case of hydrogen sulfide, 13 latent variables were used and values of 0,48 and 0,91 for RMSEC and RMSEC, respectively, were found, while for sulphur dioxide, 5 latent variables were used, with values of 1,1 and 1,45 for RMSECV and RMSEC, respectively.
A good capability of system to exactly predict the amount of H_2S and SO_2 has been noticed, with small differences between real and predicted values only at low concentrations. Good results for the prediction of the amount of Acetic Acid in the analyzed samples were obtained, although not completely satisfactory at low concentrations.

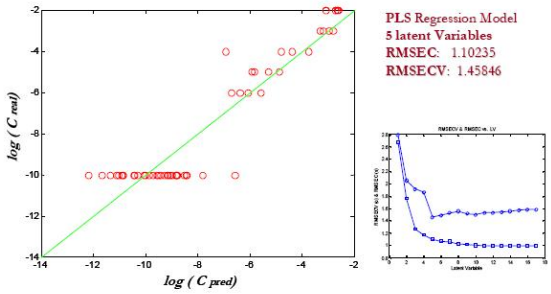

Figure 4.19: Quantitative correlation between Electronic Tongue data and concentration values for SO_2. Regression parameters are also given

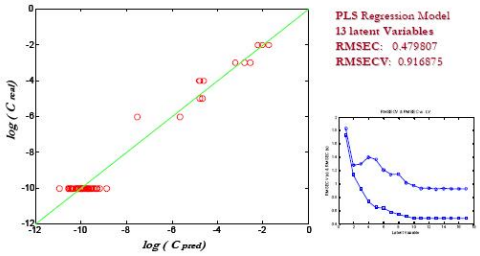

Figure 4.20: Quantitative correlation between Electronic Tongue data and concentration values for H_2S. Regression parameters are also given

Conclusions

An Electronic Tongue system based on an array of miniaturised potentiometric sensors, prepared by lithographic techniques on silicon wafers, was evaluated: potentiometric sensors were prepared by depositing PVC membranes based on Metallo-porphyrins, corroles and their analogs on the platinum electrode surface.
The developed sensors were firstly tested toward the detection of model analytes, to study the membrane selectivity performances and then applied for the identification of wine defects, using H_2S, SO_2 and acetic acid ad markers for fermentation and storage conditions.
The developed sensors showed good responses in solutions containing different ions; by varying the sensing materials deposited on the surface of the electrodes, strong variations in the selectivity of membranes were obtained, with both cationic and anionic responses.
Sensors were introduced into a flow-injection cell and used to discriminate the chosen analytes during several days of measurement; data were analysed by PLS and PCA techniques, in order to obtain both qualitative and quantitative results.
Despite the reduction of active area for membrane deposition, system showed a good stability of response signal and a good reproducibility during several days of measurement, with the identification of well defined clusters in the scores plot in the direction of the increasing concentration of each analyte.
A correlation between data coming from Electronic Tongue and standard laboratory analysis was also performed; the sensor array was able to give good results for H_2S and SO_2 also at low concentrations, while for acetic acid, the correlation was satisfactory only at higher concentrations.

4.5.3 Qualitative and quantitative analysis of real white wines - Sensor configuration 2

Introduction

The aim of the WP5 of the *GoodFood* European integrated project, is the realization of a miniaturised potentiometric sensor array for the quality assessment of white wines, by the detection of some analytes mimicking storage and spoilage defects, namely sulphur dioxide, hydrogen sulfide and acetic acid.
Since the miniaturization in the field of potentiometric sensors, based on porphyrinoids as sensitive material, is relatively new, our approach was the progressive reduction of the sensitive area, in order to better define the sensitive properties of miniaturised sensors.
In the second phase of the miniaturization, a new sensor configuration was used. Its geometry is shown in figure 4.21; it has the same external dimensions of the previously described one and the same configuration with 3 pads: the external sensors, to be used as reference electrode and counter electrode (if used in voltammetric Electronic Tongues) and the central working electrode, whose

deposition area was reduced from about $20mm^2$ to *interdigitated* design, with fingers large $2\mu m$, spaced $2\mu m$.

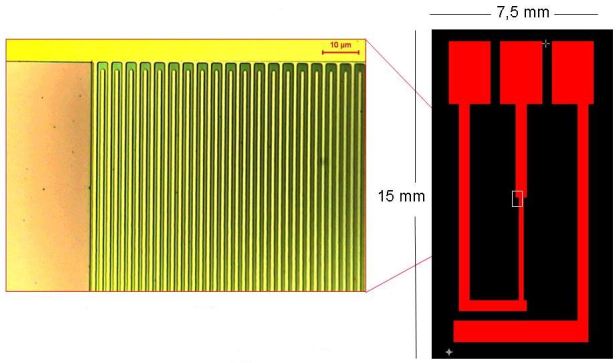

Figure 4.21: 1000 × optical microscope image of structure of miniaturized sensor surfaces. PVC-based membrane deposition has been performed on the central pad

Sensor performance evaluation

In order to obtain useful information on the influence of the active area reduction, an array composed of 3 sensors was developed. It was based on both sensor configurations (*full* area, configuration 1 and *fingered*, configuration 2). PVC-based membrane based on MnTPP, were prepared according to standard methods and deposited on both sensor types; array was then integrated by plasticized ZnTPP-base membrane (deposited on sensor configuration 1) and commercial pH glass electrode (table 4.6).

Sensor performances were compared: calibrations towards standard laboratory

Sensor	**Sensor configuration**	**Ionophore**	**Polymer**	**Plasticizer**
1	*Full*	ZnTPP	PVC	DOS
2	*Full*	MnTPP	PVC	DOS
3	*Fingered*	MnTPP	PVC	DOS

Table 4.6: Composition of sensor array for the analysis of real white wines, added of analytes mimicking wine defects

salts were performed and the slope, in the linear range, was calculated. Sodium

salicilate was chosen as marker, since it caused high anionic response in ZnTPP- and MnTPP-based plasticized membranes.
Ionic concentration was changed stepwise from 10^{-5}M to 10^{-1}M, each 50 seconds in order to allow membranes to reach chemical equilibrium with analytes. In figure 4.22, a classical calibration towards NaSal is reported; potential variation versus salicilate ion activity is also shown (standard calibration).

Stable potentials for all membranes were obtained; similar performances of

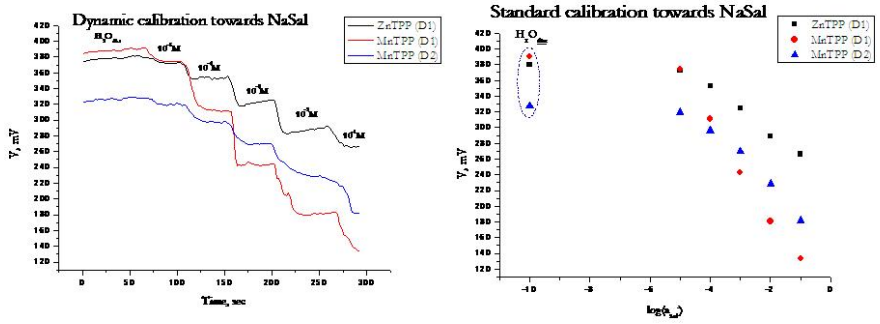

Figure 4.22: Dynamic (left) and standard (right) calibration of sensor array composed of *full* area and *fingered* configuration sensors

membranes no. 2 and 3, both based on MnTPP but deposited on different active areas, were found, even if performance decreasing was found, according to deposition area reduction. Response slopes for all membranes are reported in table 4.7.

Sensor	**Sensor configuration**	**Composition**	**Slope**	**Range** $[M]$
1	*Full*	ZnTPP+PVC+DOS	$-29,2$	$10^{-5} - 10^{-1}$
2	*Full*	MnTPP+PVC+DOS	$-54,7$	$10^{-5} - 10^{-1}$
3	*Fingered*	MnTPP+PVC+DOS	$-44,0$	$10^{-5} - 10^{-1}$

Table 4.7: Response slope towards NaSal of sensors based on *full* and *fingered* configuration miniaturised electrodes; slopes are given in $mV/decade$

Detection of analytes mimicking wine defects in real wines

Array, composed of 3 PVC-based membranes, deposited on both sensor active area geometries (table 4.6) and integrated by pH class electrode, was applied for the analysis of 15 samples, based on real white wine background, produced from a single grape variety (*Bombino Bianco*, produced in southern Italy), added with some analytes mimicking spoilage and store defects (sulphur dioxide, hydrogen

sulfide and acetic acid). Samples composition is given in table 4.8.

Samples were sealed in closed plastic bottles, to avoid interaction with air

Sample	$[H_2S]$**M**	$[SO_2]$**M**	$[CH_3CO_2H]$**M**
1	10^{-2}	-	-
2	10^{-3}	-	-
3	10^{-4}	-	-
4	10^{-5}	-	-
5	10^{-6}	-	-
6	-	10^{-2}	-
7	-	10^{-3}	-
8	-	10^{-4}	-
9	-	10^{-5}	-
10	-	10^{-6}	-
11	-	-	10^{-2}
12	-	-	10^{-3}
13	-	-	10^{-4}
14	-	-	10^{-5}
15	-	-	10^{-6}

Table 4.8: Concentration of target analytes, mimicking defects, in real white wine background, namely *Bombino Bianco*

and measured immediately after the opening. Background solution, with no additives (label 0), was used as conditioning solution between two successive samples, to restore membrane properties.

Sensor potentials were calculated, by measuring the potential differences between electrodes in array and the conventional reference electrode (standard calomel electrode, AMEL, Italy) using a PC equipped high-impedance input 8-channel A/D converter (Smartronix, Rome, ITALY), for about 7 minutes; membranes were then restored in conditioning solution for about 10 minutes, applying the same protocol used in the analysis of synthetic wines. The mean value of several repetitions was then applied for data analysis.

The processing of multi-component data coming from non-specific sensors has been performed using partial least squares (PLS). The aim is to reduce the amount of variables to new variables (*latent variables* for PLS) in a reduced variable space to facilitate identification or classification; additionally, this new space simplifies the way to explain the variability contained in the available information. PLS analysis and evaluation processes were performed with the software *Matlab 7.0*.

PLS bi-plot, reporting the $93,88\%$ of total variance, is shown in figure 4.23.

A clear classification can be noticed, with 3 different directions, according to analyte increasing concentration. System also showed a good capability to exactly recognize the concentration of each analyte, with a partial overlap only at very low concentrations.

Analysis of loading, evidenced an important contribution from all the sensors

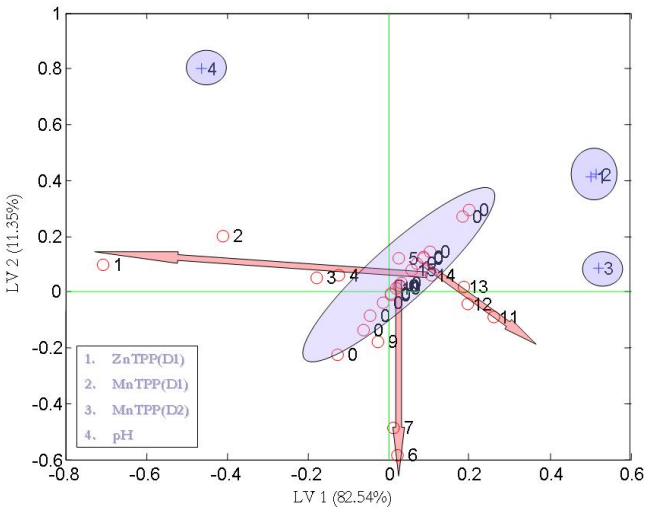

Figure 4.23: PLS scores plot of real wine solutions with analytes mimicking wine defects; pH value is considered in data analysis

in array, with similar responses in the case of membranes deposited on 1^{st} type of sensor (*full area*, sensors no. 1 and 2); sensor no. 3 (MnTPP on 2^{nd} type electrode − *fingered* area) gave important contribution among PC1, thus for the recognition of samples with hydrogen dioxide (samples no. $1-5$) and acetic acid (samples no. $11-15$).
Samples were divided into 3 classes, according to the analyte in the solution; PLS-DA model was then built, to correctly assign each sample to owning class; results are resumed in the confusion matrix (table 4.9).

System showed high capability to correctly detect the target analyte, with a

4	1	0
0	5	0
0	1	4

Table 4.9: Confusion matrix of PLS-DA model built to assign each sample to correct class, according to the analyte

percentage of correct classification of $85,7\%$; analysis of misclassified samples, confirmed the overlap at very low concentrations: samples no. 5 (H_2S 10^{-6}M) and 14 (CH_3CO_2H 10^{-5}M) were both confused with samples of class no. 9 (SO_2 10^{-5}M).
Starting from this consideration, PLS technique was also applied in order to obtain a quantitative correlation between Electronic Tongue data and concentrations of analytes coming from standard laboratory analysis.
Graphs showing the correlation between real concentration and predicted by the system, are shown in figures 4.24 - 4.26.

A good correlation between real and predicted concentration can be noticed,

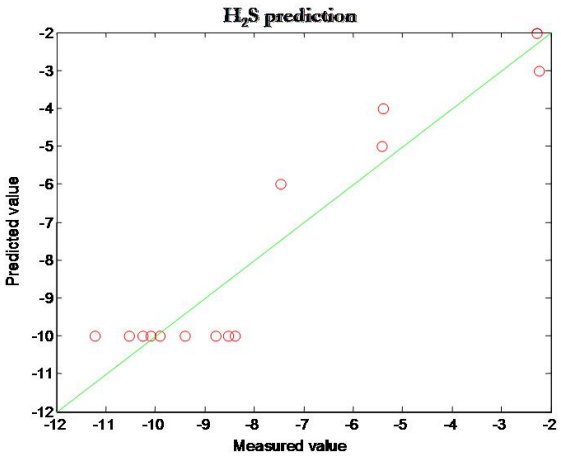

Figure 4.24: Quantitative correlation between Electronic Tongue data and concentration values for H_2S

for all analytes, in particular for sulphur dioxide and hydrogen sulfide, also at low concentrations; high deviations at lower concentrations were obtained for acetic acid.

Conclusions

Starting from already discussed results, a new step towards the miniaturization was realized. In previous sections, the application of an array of miniaturized sensors, characterised by a rectangular deposition area of about $20mm^2$, for the detection of analytes in synthetic wine solutions, has been discussed.
A new silicium-based electrode was realised by CNR of Lecce (Italy): external dimensions did not change, but it was characterised by a further reduction of the sensitive platinum area, with the classical fingered geometry.
Three PVC-based membranes were deposited on both typologies of sensors and the performances of sensors chemically modified with the same ionophore were compared, by calibration towards standard laboratory salts. Similar response slope was found, thus indicating the low deposition area influence and the possibility to further reduce it.
Sensor array was also applied for the detection of some analytes (namely sulphur dioxide, hydrogen sulfide and acetic acid), mimicking wine defects, in real white wine solutions (produced from a single grape variety, namely *Bombino Bianco*). Despite further active area reduction, system showed a good signal stability and a good capability of analyte recognition. A correlation between data coming from Electronic Tongue and standard laboratory analysis was also performed:

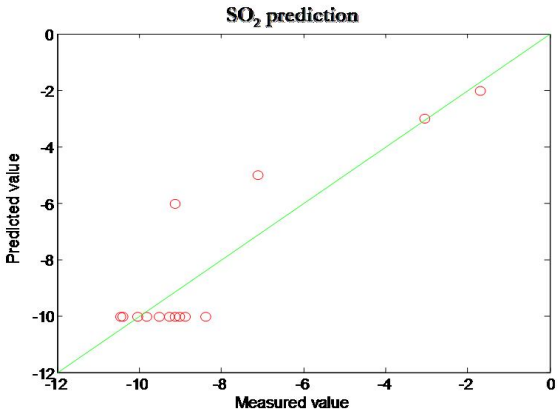

Figure 4.25: Quantitative correlation between Electronic Tongue data and concentration values for SO_2

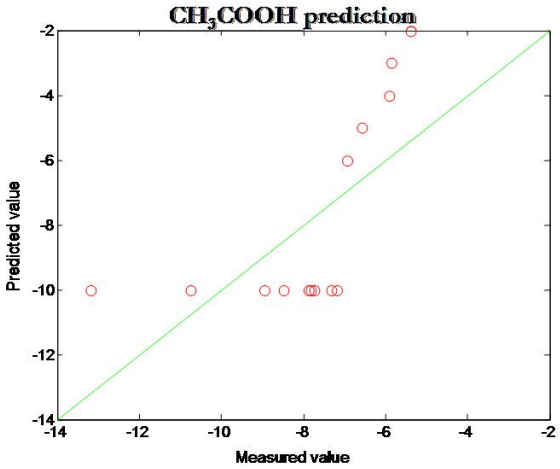

Figure 4.26: Quantitative correlation between Electronic Tongue data and concentration values for CH_3CO_2H

good results were obtained for H_2S and SO_2 also at low concentrations, while for acetic acid, the correlation was satisfactory only at higher concentrations.

4.5.4 Qualitative and quantitative analysis of real white wines - Sensor configuration 3

Introduction

One of the main objectives of WP5 of European intgrated project *GoodFood*, is the development of a new measurement system based on microtechnologies capable of assessing the fish and wine freshness. In this sense, most of the work has been focused in the designing and fabricating the most cross-sensitive sensor array for the detection of H_2S, SO_2 and CH_3CO_2H, chosen as markers for spoilage and storage defects of white wines. A tendency towards even smaller sensing devices may be expected from further progress of micro- or nanotechnology ([39]), in particular the silicon technology, which allows the development of layers of several shapes on sensor surfaces ([37]).
In the next step of *GoodFood project*, towards the complete miniaturization of an Electronic Tongue system, a single chip built by silicium technology and integrating 8 miniaturised sensors, was developed.

Sensors fabrication and geometry

The fabrication of microelectrodes was carried out on a 3 SSP silicon wafer, (100)-oriented, with 500 nm of thermal oxide. The process needed 2 lithographic steps:

- First lithography resist mask definition for lift-off patterning of 200 nm thick sputtered platinum, in order to realize the microelectrode array;
- Second lithographic step for selective dry etching of silicon nitride over device active area.

Each sensor, characterized by 8 platinum microelectrodes on which chemical membranes deposition was performed, had die dimensions of $750\mu m \times 750\mu m$, while active area ($500\mu m \times 1000\ \mu m$) exposed to liquid phase 8 fingers (remaining device area was passivated with silicon nitride), 20 μm width and 500 μm of length. A ninth finger, used as reference electrode, had a width of 100 μm and all electrodes were 200 nm thick (figure 4.27).

Wine samples

Wine samples were based on a single grape variety of white wine, namely *Bombino Bianco*. To mimick some characteristic defects related to storage conditions and general assessment of white wines, H_2S, SO_2 and CH_3CO_2H in

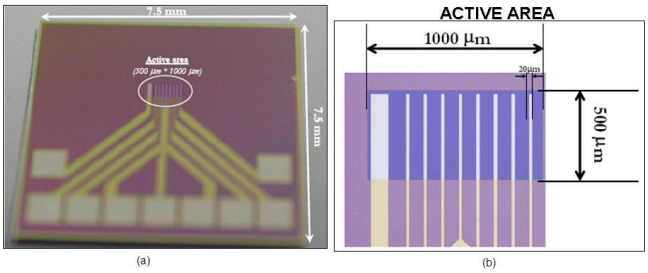

Figure 4.27: (a) Miniaturized sensor array: 9 platinum fingers (8 sensors and 1 reference electrode) were integrated into a single silicon wafer of 7.5mm × 7.5mm; (b) Microscopy image of active area of sensor. It is composed of 9 platinum fingers, with length of 500 μm: the first one on the left (100 μm thick) is used as reference electrode, while on the others (20 μm thick), electropolymerized porphyrin-based thin films have been deposited

different concentrations, related to the limits imposed by laws, were added and their composition is reported in table 4.10.

All samples were stored in plastic sealed bottles and each solution was anal-

Sample	**Analyte**	**Molar Concentration**	Assigned class [PLS-DA]
1	H_2S	10^{-3}	1
2	H_2S	10^{-4}	1
3	H_2S	10^{-5}	1
4	SO_2	10^{-3}	2
5	SO_2	10^{-4}	2
6	SO_2	10^{-5}	2
7	CH_3CO_2H	10^{-2}	3
8	CH_3CO_2H	10^{-3}	3
9	CH_3CO_2H	10^{-4}	3
10	CH_3CO_2H	10^{-5}	3

Table 4.10: Composition of analysed samples. They were based on a real white wine as background (namely *Bombino Bianco* quality, produced in Southern Italy). Some analytes, namely H_2S, SO_2 and acetic acid, mimicking wine defects, were then added

ysed immediately after opening the bottle; measurements took 7 minutes to reach sensor response stability, with data collected every 2 seconds. Samples were randomly analyzed and, between each measure, a *blank sample* (with no additives) was used as conditioning solution, to restore the chemical properties of membranes.

Results and discussion

The processing of multi-component data coming from non-specific sensors has been performed using Principal Components Analysis (PCA) and Partial Least Squares (PLS).
PLS technique considers the PCA not only of the input matrix X, but also of the output matrix Y. In this way, the principal components of matrix Y are rotated to maximize the correlation with the principal components of matrix X; the new principal components are called latent variables. PLS analysis and data treatment processes were performed with the software *Matlab 7.0*.
Membranes $1-4$ of table 3.15 and free base mono-amino substituted TPP (table 3.4) were deposited by electro-polymerization on the sensor surfaces, in a 3-electrodes cell, using a commercial potentiostat (AMEL, mod. 7050), standard calomel electrode as reference electrode (AMEL, mod. 303/SCG/6) and platinum wire (diameter 0,7 mm) as counter electrode, starting from a solution of porphyrin (1 mM) and TBAP as supporting electrolyte (10 mM), using CH_2Cl_2 as solvent.
Potentiometric properties of freshly prepared sensors were evaluated one day after soaking in 0,01M NaCl solution. All potentiometric evaluations have been performed by measuring the potential differences between electrodes in array and the conventional reference electrode (AMEL, standard calomel electrode, model 303/SCG/6) using a PC equipped high impedance input 8-channel A/D converter (Smartronix, Rome, ITALY).
Deposited miniaturized sensor array was firstly tested towards standard analytes to check the stability and reproducibility of the voltage output and then applied for the identification of several white wines spoilage markers, namely H_2S, SO_2 and CH_3CO_2H, in different concentrations.
The strategy for data treatment was composed of two main steps: in the first one, PLS-DA (PLS - Discriminant Analysis) was applied to identify the marker present in the solution; PLS was then applied to evaluate the exact amount of the identified analyte.
Before data processing, plots for each sensor with potential and standard deviation versus all sample classes, were realised (figure 4.28). Only the most discriminative sensors for the detection of each analyte, were chosen for the construction of PLS models.
In the first step of data treatment, PCA and PLS-DA techniques were applied to the matrix composed by potential values of different chemical membranes. PCA bi-plot of the first two principal components is shown (figure 4.29).
The plot shows more than 90% of total variance and a clear distinction between the main groups can be seen. According to loadings plot, membranes no. 4 and 5 were the most discriminative for samples characterized by acetic acid and SO_2 (good discrimination along PC1), while membranes no. $1-3$ were useful for the discrimination of H_2S (separated along PC2).
PLS technique was applied, in order to obtain quantitative information on analytes concentration. All sensors were used to build prediction model and results are given in figure 4.30.

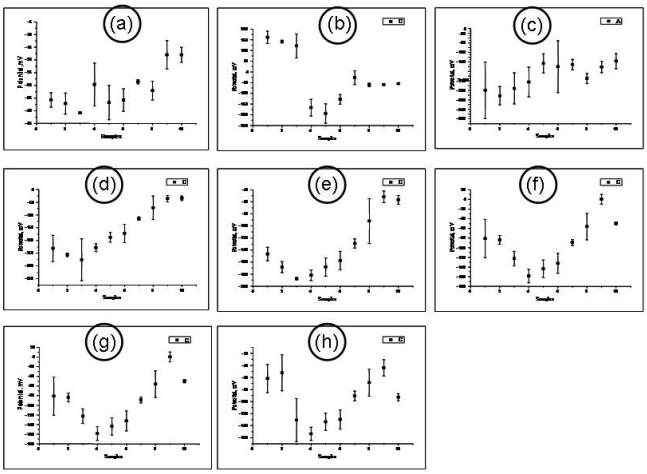

Figure 4.28: Sensor potential versus classes. For each class, sensor potential and its related error was plotted; on the basis of responses to marker analytes, only the most discriminative sensors were chosen for PLS model building. (a) CoTris(NH_2)-TPP; (b), (c) Fe(NH_2)-TPP; (d), (e) CuTris(NH_2)-TPP; (f) H_2(NH_2)-TPP; (g), (h) Vanillin Porphyrin

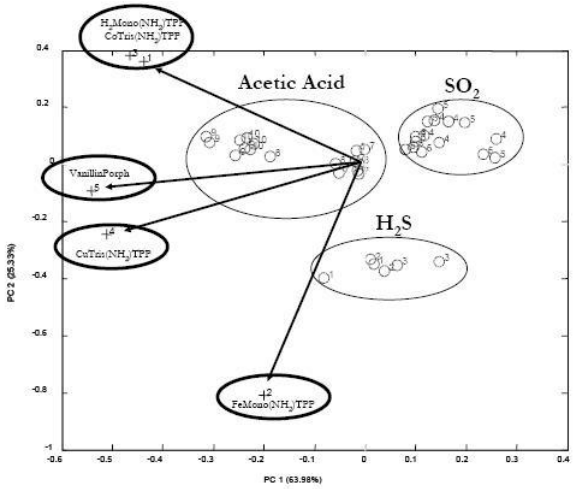

Figure 4.29: PCA bi-plot. 3 main groups can be noticed, according to the analyte added to solution

Good results were obtained mainly at higher concentrations, while strong de-

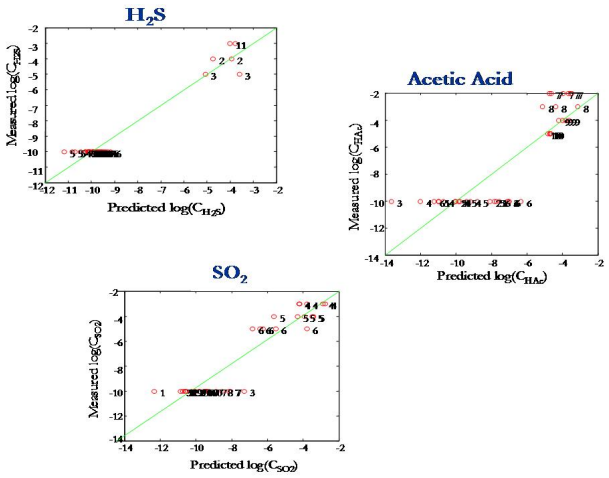

Figure 4.30: Predicted versus measured concentration of H_2S, SO_2 and CH_3CO_2H. All sensors were used to create PLS model, which predict, at the same time, all the analytes

viations from real value were found at the lower ones, because of the presence of an huge number of samples identified by 10^{-10}M concentration (in absence of analyte, concentration was arbitrarily set to this value, common in real wine, to perform data analysis), which disproportionates matrix dimension.
A second approach for data analysis, was then performed; to identify the analyte added to solutions, samples were previously divided into main groups, according to the analyte: samples $1-3$ (H_2S) were assigned to class 1, samples $4-6$ (SO_2) to class 2 and samples $7-10$ (HAc) to class 3 (see table 4.10).
PLS-DA technique was applied and the *confusion matrix* is reported (table 4.11).
All samples were assigned by the model to the correct class, with a percentage

6	0	0
0	15	0
0	0	17

Table 4.11: Confusion matrix created by PLS-DA model. Samples were assigned to the correct class with 100% of correct classification

of correct classification of 100%. The PLS-DA scores plot, showing $89,24\%$ of total variance, evidences the clear classification between the classes, according to the analyte. According to this result, PLS technique, to evaluate quantitative analysis on target analytes, was applied.
A great advantage in terms of data analysis could be obtained by the simplifi-

cation of PLS models. In fact, we were able to evaluate a single PLS model for the prediction of concentration of identified analyte (with *standard* strategy a single PLS model should have been created to predict at the same time all the analytes, with an output matrix Y composed of 3 columns, each one related to the concentration of different analytes).
Furthermore, in each model, only the most discriminative sensors for each analyte can be used for data treatment. Results of application of PLS models are shown as correlation graphs between real concentration of analytes (obtained by standard laboratory methods) and the one predicted by system for H_2S (figure 4.31), SO_2 (figure 4.32) and acetic acid (figure 4.33). Completely satisfactory

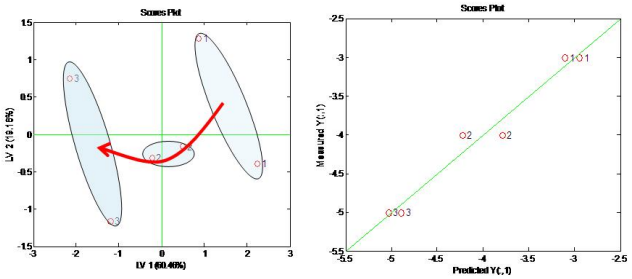

Figure 4.31: Predicted versus Measured concentration for H_2S. Membranes 1, 2, 6 and 7 were used

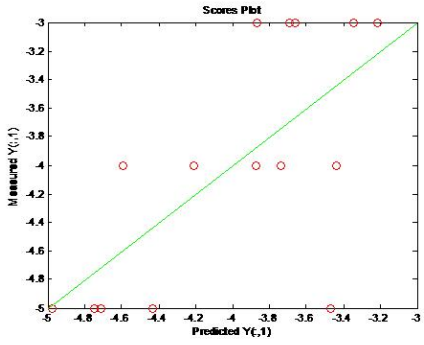

Figure 4.32: Predicted versus Measured concentration for SO_2. Membranes 1, 2, 4, 6 and 7 were used

results were obtained for H_2S and Acetic Acid, while big deviations between real and predicted value for the concentration of SO_2 are still present.

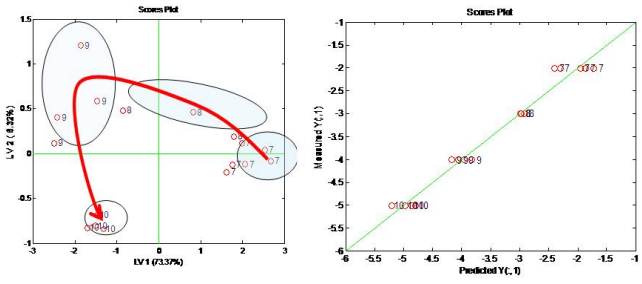

Figure 4.33: Predicted versus Measured concentration for CH_3CO_2H. Membranes 2, 4, 6 and 7 were used

Conclusions

A miniaturized Electronic Tongue was developed by the integration of sensors array knowledge with the latest improvements in silicon technology.
5 different membranes and reference electrode were integrated on a single silicon wafer of 7.5mm x 7.5mm, with a reduced active area exposed to liquid of only 0.5 mm^2. Membranes were deposited on platinum sensor surfaces by cyclic voltammetry technique, obtaining conductive films based on NH_2 substituted and vanillin porphyrins. For each porphyrin, the best conditions in terms of scan rate, potential range and number of cycles, were evaluated. Membranes were firstly tested towards standard analytes and then applied on real samples of white wine (a *Bombino Bianco* quality white wine, produced in Southern Italy, background was chosen), sophisticated with some analytes mimicking wine defects, namely SO_2, H_2S and CH_3CO_2H.
Data coming from sensor array were firstly treated by PCA and PLS-DA to obtain qualitative info about the discrimination of different samples and then by PLS to obtain the correlation between the amount of each analyte, obtained by standard laboratory methods and the value predicted by system.
The system was able to exactly identify the analyte in solution and to predict with satisfactory accuracy the real value of concentration of H_2S and acetic acid.

4.6 Development and testing of a Miniaturized Multisensor Liquid Chromatographic System (MMLCS)

4.6.1 Introduction

Current and future concerns related to agrofood safety and quality will increasingly require a multidisciplinary approach based on the massive use of simple detection systems able to be used *near to the foodstuff*. In fact, in the last

few years, the employment of *Electronic Nose* and *Electronic Tongue* systems is considerably increased. These systems are based on array of cross-selective chemical sensors requiring a complex electronic interface, which usually make use of a microcontroller (μC) to manage the entire system of measure ([40], [41]).
This work reports about a miniaturized multisensor system that will finally be integrated with a separation module, in order to have a liquid chromatography-like miniaturized system. The sensitive part is composed by potentiometric and voltammetric sensors. The possibility to combine the voltammetric detection with the potentiometric one can allow extracting much more information about the analyte and choosing the best detection method according to the species analysed. In order to simultaneously detect different species in the analyte, the sensing devices will be connected to the outlets of a Si-based microcolumn which constitutes a MEMS-based separation module. The sensitive part is interfaced with an ASIC realized in standard CMOS technology. The ASIC is composed by 3 readout circuits for voltammetric sensors and 9 readout circuits dedicated to interface an array of 8 potentiometric sensors. In respect of the state of the art, the readout circuits are based on a VCO that exhibits high linearity of conversion and allows a digital output signal. In this way, a reduction in occupied area is achieved and the ASIC should be directly interfaced with a post-processing part. The voltammetric interface allows different voltammetric measurement (amperometry, cyclic voltammetry and pulsed voltammetry) for five current ranges: input current from $\pm 200nA$ to $\pm 2mA$ can be measured with a resolution of 8 bits within each range. As regards the potentiometric measurements, cell potentials in the range of $\pm 1V$ can be measured with a resolution of 10 bits. Preliminary testing of the detection modules with the read-out electronics has been performed: voltammetric sensor has been tested by detecting the concentration changes of acetic acid that is one of the main wine quality parameters; while dynamic calibration of potentiometric sensor has been carried out with different analytes ($Cu(NO_3)_2$ and $CaCl_2$) to perform preliminary tests on response and selectivity. In figure 4.34 a schematic overview of the system is reported. The sensitive part is directly connected to the ASIC, interfaced with an FPGA in order to elaborate the data stream coming from the readout electronics and stores it on a PC. The entire system of measure is managed through a LabView interface. The total power consumption of the measurement system is about 300mW.

4.6.2 Voltammetric sensing module

Great research effort has been dedicated in these years to the development of MEMS-based separation systems ([42]-[45]).
The MEMS-based separation module has been designed taking into account microfluidic and technological constraints. It is composed by a Si-based microcolumn and voltammetric miniaturised sensor. The microcolumn chip is a Silicon/Pyrex packaged structure realized by bonding microstructured silicon

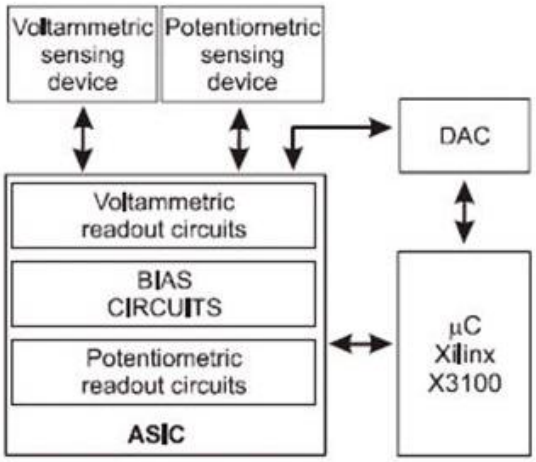

Figure 4.34: System overview

microchannels and Pyrex wafers together using the anodic bonding technique ([46]). The microstructured channels are defined photolithographically on the silicon wafer and are fabricated using DRIE at room temperature. By fabricating a serpentine microchannel, two microcolumns with a length of 10 cm have been realized on a chip of 13 mm × 9 mm ([47]). The voltammetric sensors have been designed with a three-electrode configuration. Pt interdigitated electrodes have been photolithographically defined and realized by lift-off technique on the back of the chip. The working and counter electrodes have been designed with an interdigitated geometry (width: 14 μm, gap between the two electrodes: 18 μm, length: 530 μm). A third electrode to be used as Ag/AgCl reference electrode after appropriate chemical treatments has also been designed (width: 90 μm). In figure 4.35 (a), the front and the back side of the chip with an enlarged view of the sensor, are shown.

4.6.3 Potentiometric sensing module

The potentiometric sensing module is composed by 8 platinum fingers on which different membranes based on porphyrins and their derivatives are deposited by electropolymerization technique. The fabrication of microelectrodes has been carried out on a 3 polished silicon wafer, (100)-oriented, with 500 nm of thermal grown oxide. It needed 2 lithography processes, for resist patterning and for reactive dry etching of silicon nitride, with sputtering of 200 nm of platinum film and final oxygen plasma dicing.
Deposition of electropolymerized porphyrin films was performed by using a com-

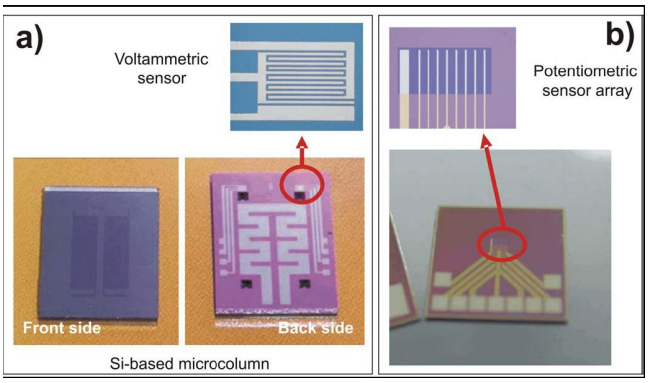

Figure 4.35: Sensing devices: (a) Si-based microcolumn and voltammetric sensor; (b) Potentiometric sensor array

mercial potentiostat (AMEL, mod. 7050), calomel electrode as reference and a platinum wire as counter electrode. Electro-polymerization technique, in fact, allows the selective deposition only on the chosen area, represented by a finger of 20 μm of thickness and 500 μm of length; the sensors array was finally completed by the reference electrode (thickness of 100 μm).
Different membranes, all based on metal complexes of amino substituted tetra phenyl porphyrins, have been deposited onto platinum surface of sensor. A picture of the developed device is reported in figure 4.35 (b).

4.6.4 Electronic interface description

ASIC

The ASIC is composed by 3 readout circuits for voltammetric sensors and 9 readout circuits dedicated to interface the array of 8 potentiometric sensors. A first prototype of the electronic interface is fabricated into a 10mm^2 frame using standard 0.35μm 2P-4M CMOS technology. The total occupied area is 1,1mm^2 for a maximum total power consumption of 34mW in typical operation mode. The ASIC provide the entire bias circuits requested by the voltammetric and potentiometric interface. Chip layout and a picture of the developed device are reported in figure 4.36.

Potentiometric interface

The electronic interface for the potentiometric array of sensor, monitors the voltages at the connected electrodes. In figure 4.37 the schematic principle of measure is reported: the cell potential V_{cell} is measured as the difference potential from one functionalized electrode and the reference electrode. The

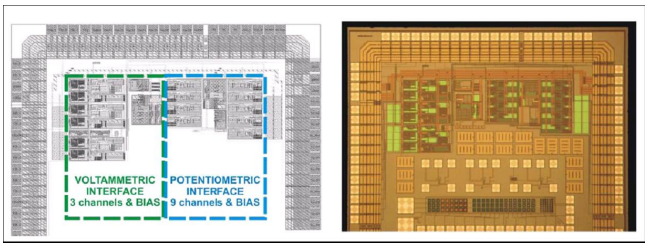

Figure 4.36: ASIC layout

typical values of these potentials, in function of the measured solutions and characteristics of the membranes used to functionalize the electrodes, are in the range of $\pm 1V$. To measure this potential, the proposed solution generates a virtual ground setting the potential of the reference electrode at 1,2V. In this way, the potential of the different electrodes that constitute the array of sensor varies from 0,2V to 2,2V and can be measured with a modified architecture of the VCO illustrated in [48] with a linearity error better than 1%. In this way, the typical V_{cell} values can be measured as a frequency difference. The calculation of the V_{cell} is in charge of the μC, after the measurement of the output signal coming from the channel connected to the reference electrode and the correspondent output signal of the readout channel connected to one of the 8 functionalized electrodes. Experimental investigation on the potentiometric sensor behaviour demonstrated that the expected V_{cell} range for the developed sensor is $\pm 400mV$. In this case, an improvement in the measurement resolution can be achieved if the output frequency of the VCO is lower than the previous indicated, because more clocks is counted as a frequency difference from two closely input voltages.

In figure 4.37 is reported the schematic of the single potentiometric readout

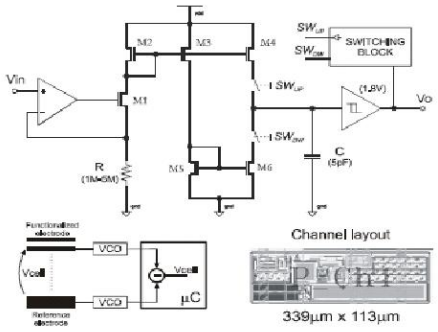

Figure 4.37: Potentiometric electronic interface

channel. The output frequency could be selected in two different ranges changing

the value of the resistance value R. In details, operating on the R_{sel} line, two operating mode are selectable. For $R = 1M\Omega$ the output frequency range is $10kHz - 120kHz$. Although, for $R = 5M\Omega$ the frequency decrease at the $2kHz - 24kHz$ range. This solution increases the time necessary to realize the measure, with a correspondent increase in the measurement accuracy.
In figure 4.38 the measured results for the potentiometric interface (channels $P1 - P8$) in function of the input voltage for $R = 5M\Omega$ is reported. The frequency measurements have been carried with a 100MHz counting system and demonstrate the good linearity of conversion of the VCO. In addition, these data are useful to realize a calibration of the single readout channel to correct non linearity error of the electronic circuits.

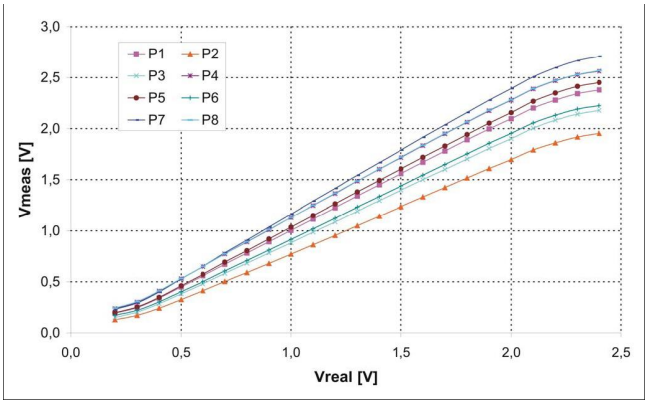

Figure 4.38: Potentiometric readout characterization

4.6.5 Results and discussion of preliminary tests

The modules of the electronic interface have been assembled on a single PCB which provides an USB2.0 connection with a PC, where a front panel developed in LabView allows managing the entire system of measure.
In order to test the potentiometric subsystem, dynamic calibrations of the potentiometric array of sensors towards standard analytes (namely $Cu(NO_3)_2$ and $CaCl_2$) has been carried out. Distilled water has been used as background and concentration has been varied from 10^{-7}M up to 10^{-1}M. In figure 4.39 dynamic calibration versus $CaCl_2$ is reported as an example. Sensors showed good selectivity towards the standard analytes chosen for preliminary tests; moreover the dramatic reduction in active area for the deposition did not influence the sensitivity, from the moment that ions can be detected also at concentrations lower than 10^{-5}M and the response stability, which was lower for each sensor, than 1 mV.

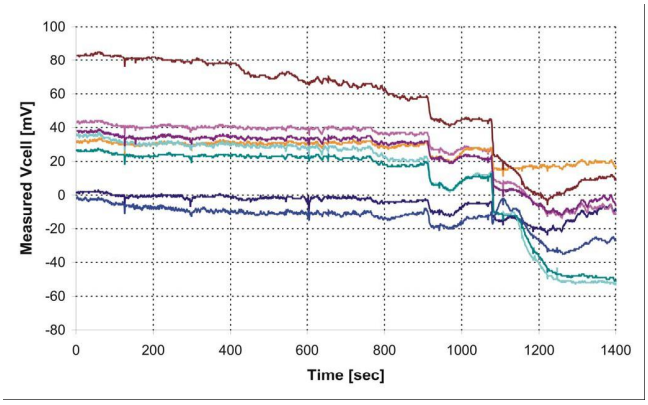

Figure 4.39: Potentiometric measurement results

4.6.6 Results and discussion of integrated system

System architecture is reported in figure 4.40, while images of the whole system are shown in figures 4.41 and 4.42. Integrated miniaturised system is composed

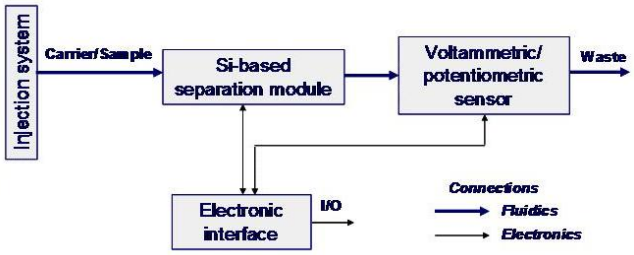

Figure 4.40: System architecture

by several modules:

- injection system; the inlet tube is connected to a syringe pump, which provides a constant flux of sample solution;
- separation module; sample solution is fluxed into a micro-separation silicium-based column;
- sensor module; analytes from separation module, are detected by a miniaturised sensor array, capped by PDMS;
- read-out electronics; data from voltammetric and potentiometric Electronic Tongues, are collected and analysed by electronic interface.

The capability of the system to correctly retain and detect some of the most important wine parameters, such as Acetic Acid and Ethanol, has been tested.

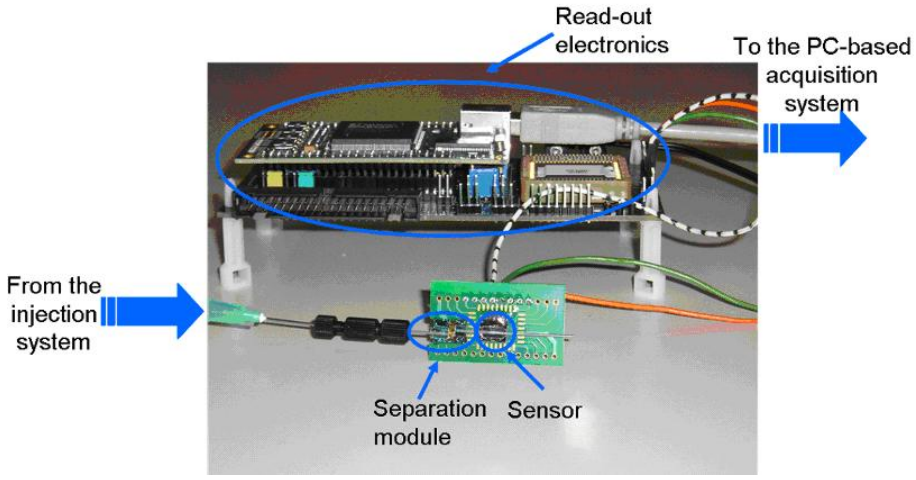

Figure 4.41: Photograph of the system prototype

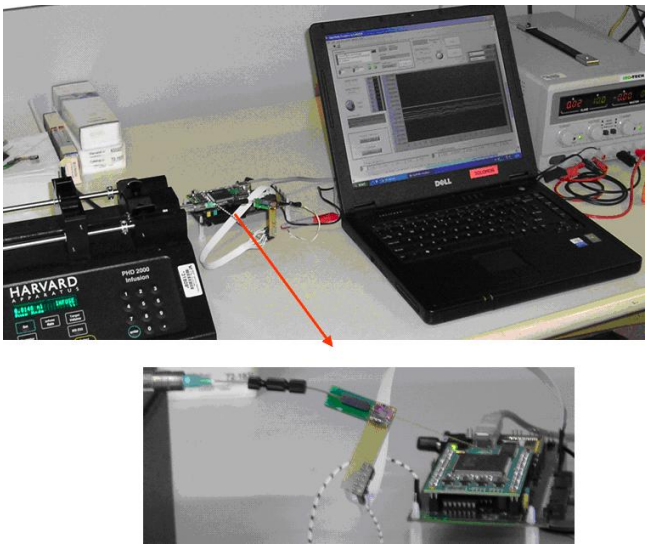

Figure 4.42: Measurements set-up

Both the systems with potentiometric and voltammetric sensors have been characterized. As regards the prototype with potentiometric sensors, devices based on the optimised design, shown in figure 4.35(b), were prepared by depositing different metallo porphyrins on the platinum surface of miniaturised sensors.
The prototype has been connected to the syringe pump by appropriate ferrule and a constant flow rate has been provided (tens of L/min). An external power supply has been used to provide a stable potential to the reference electrode channel (at first it was set at 1,2V but it was a too high potential for the solutions which were analysed, all based on water as solvent; the best compromise for the chemical conditions of each measure and the needing of electronic frequency read out was gained setting the voltage at 0,5V). The system was tested in collaboration with FBK-irst (Trento, Italy), with 2 different solutions based on a single component (namely acetic acid and ethanol dissolved in water with a concentration of 100mM). Figure 4.43 shows the system response to the injection of acetic acid; in detail at first mobile phase (KH_2PO_4, 50 mM, pH=2.8) has been injected, then an optimised volume of acetic acid (few nanoliters, in order to have best performance of separation) has been injected, finally the mobile phase has been injected at a constant flow rate and the acetic acid retained by the column has been eluted.
From the figure 4.43, some peculiar characteristics of measures can be noticed:

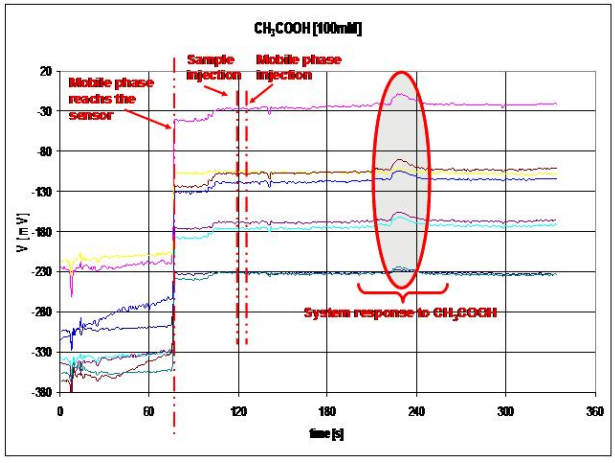

Figure 4.43: System response to acetic acid injection

- a first part of sensors response can be identified, related to the period which runs from the start of measure (syringe pump switched on) and the instant in which mobile phase reaches the sensors;

- from the moment the mobile phase reaches the sensor, a stable potential value is obtained by read out electronics with a few spikes (see also figure 4.44) due to electric net;

- well defined peaks in sensor responses, due to the arrival at the sensor surfaces of the analyte retained by the column are highlighted on the graphs;
- after the peaks the signal comes back to the older potential value, related to the mobile phase.

The same procedure has been followed for Ethanol measurements, but the measure started when the mobile phase had already reached the sensor; from the figure 4.44 can be argued that the system correctly retain and detect ethanol.

Finally, the system was also applied for the evaluation of a real wine sample,

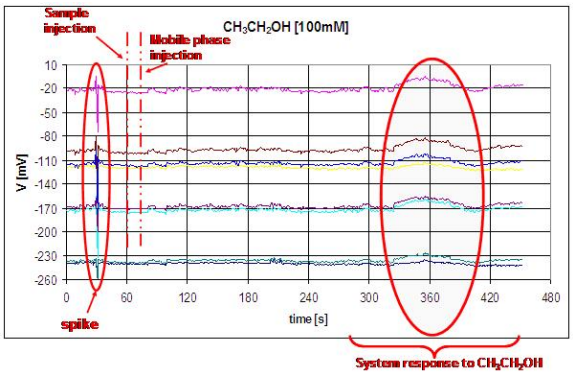

Figure 4.44: System response to ethanol injection

added with the analytes chosen as markers for the general quality assessment, as above detailed. The measure is reported in figure 4.45.

After the first part in which sensors are still not in contact with the sample eluted by the mobile phase, 3 signals have been observed; these signals can be related to overlapped wine separation peaks, since real wine is a complex solution, with hundreds of analytes; between them, a stable and reproducible potential value of sensor membranes in equilibrium with mobile phase is noticed. Further tests will be performed in order to validate the capability of the system to separate and detect real wine sample components.

4.6.7 Conclusions

The capability of the system to correctly detect chemical species concentration variations has been demonstrated. Potentiometric sensors, based on different porphyrins, showed different sensitivities and lower detection limit, with both cationic and anionic response towards different analyzed ions, depending on the macrocycle structure. These preliminary results encourage the MEMS-based technological approach followed for realizing a portable integrated system, in order to have a liquid chromatography-like miniaturized system characterized

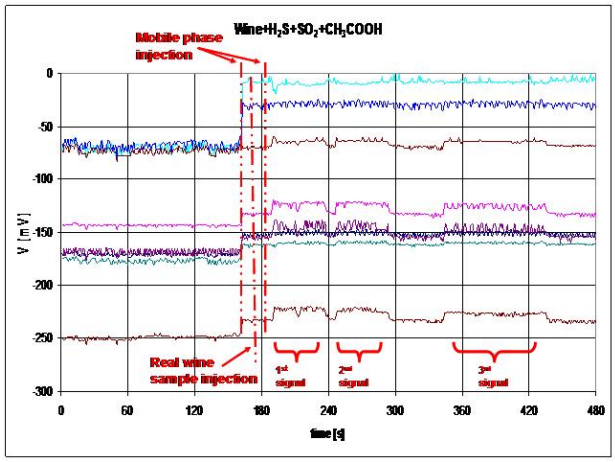

Figure 4.45: System response to real wine sample injection

by low cost, low power, fast response and simple use for application in the agro-food fields.
Furthermore, a **M**ultisensors **M**iniaturised **L**iquid **C**hromatographic **S**ystem has been realised. In detail, stand-alone sensor module (potentiometric sensor array), has been characterized and morphological and chemical characterizations of the separation module have been performed.
The read-out electronics testing with the potentiometric sensors has been performed. Package of the complete system including the separation column and the PDMS capped sensors has been developed and functionality tests of the complete system have been performed on real wine samples with added defects. From the functionality tests, it can be noticed that the system is able to retain and detect the species of interest, even if some problems to be solved still remain.
The obtained results encourage the MEMS-based technological approach followed for realizing a liquid chromatographic analysis microsystem, more extensive measures and a further optimization of the prototype would be desirable for improvement of system performances.

Bibliography

[1] S. Alegret, in Integrated Analytical Systems. S. Alegret (Ed.), Wilson and Wilson Comprehensive Analytical Chemistry, vol. XXXIX, Elsevier, Amsterdam (2003) 136

[2] V. Pravdova, M. Pravda, G.G. Guilbault, Anal. Lett. 35 (2002) 2389

[3] J. Gallardo, S. Alegret, M.A. de Roman, R. Munoz, P.R. Hernandez, L. Leija, M. del Valle. Anal. Lett. 36 (2003) 2893

[4] J. Gallardo, S. Alegret, R. Munoz, M. De Roman, L. Leija, P.R. Hernandez, M. del Valle. Anal. Bioanal. Chem. 377 (2003) 248

[5] A.K. Deisingh, D.C. Stone, M. Thompson., Int. J. Fodd. Sci. Tech. 39 (2004) 587

[6] C. Di Natale et al. Physiol. Measurement. 20 (1999) 377-384

[7] A. Pavlou, N. Magan, C. McNulty, J.M. Jones, D. Sharp. Biosensors and Bioelectronics 17 (2002) 893-899

[8] V. Parra, A. Alvaro, A. Arrieta, J.-A. Fernandez-Escudero, M.L. Rodriguez-Mendez, J.A. De Saja. Sensors and Actuators B. 118 (2006) 448-453

[9] V. Parra , T. Hernando, M.L. Rodriguez-Mendez, J.A. de Saja. Electrochimica Acta. 49 (2004) 5177-5185

[10] A. Riul Jr., H.C. de Sousa, R.R. Malmegrim, D.S. dos Santos Jr., A.C.P.L.F. Carvalho, F.J. Fonseca, O.N. Oliveira Jr., L.H.C. Mattoso. Sensors and Actuators B. 98 (2004) 77-82

[11] A. Rudnitskaya , I. Delgadillo , A. Legin, S.M. Rocha, A.M Costa, T. Simoes. Chemometrics and Intelligent Laboratory Systems. 84 (2007) 50-56

[12] J. Artigas, C. Jimenez, C. Dominguez, S. Minguez, A. Gonzalo, J. Alonso. Sensors and Actuators B. 89 (2003) 199-204

[13] L. Lvova, R. Paolesse, C. Di Natale, A. D'Amico. Sensors and Actuators B. 118 (2006) 439-447

[14] C. Di Natale, R. Paolesse, M. Burgio, E. Martinelli, G. Pennazza, A. D′Amico. Analytica Chimica Acta. 513 (2004) 49-56

[15] V. Parra, A. Ivaro, A. Arrieta, A. Fernandez-Escudero, H. Garcia, C. Apetrei, M.L. Rodriguez-Mendez, J. de Saja. Sensors and Actuators B. 115 (2006) 54-61

[16] A. Legin, A. Rudnitskaya, L. Lvova, Yu. Vlasov, C. Di Natale, A. D′Amico. Analytica Chimica Acta. 484 (2003) 33-44

[17] Commission Regulations (EEC) No 2676/90 of 17 September 1990 determining Community methods for the analysis of wines

[18] G. Verrelli, L. Francioso, R. Paolesse, P. Siciliano, C. Di Natale, A. D′Amico, A. Logrieco. Sensors and Actuators B. 123 (2007) 191-197

[19] R. Paolesse, C. Di Natale, M. Burgio, E. Martinelli, E. Mazzone, G. Palleschi, A. D′Amico. Sensors and Actuators B. 95 (2003) 400-405

[20] (a) M.A. Amerine, C.S. Ough. Wine and Must Analysis. Wiley, New York, 1974; (b) C.S. Ough, M.A. Amerine. Methods for Analysis of Musts and Wines. second ed., Wiley-Interscience, NY, 1988

[21] F. Mizutani, Y. Hirata, S. Yabuki, S. Iijima. Sensors and Actuators B. 91 (2003) 195-198

[22] M. Ortega-Heras, C. Gonzalez-Huerta, P. Herrera, M.L. Gonzalez-Sanjose. Analytica Chimica Acta. 513 (2004) 341-350

[23] J.P. Santos, J. Lozano, M. Aleixandre, I. Sayago, M.J. Fernandez, L. Ares, J. Gutierrez, M.C. Horrillo. Sensors and Actuators B. 103 (2004) 98-103

[24] L.F. Bisson. Am. J. Enol. Vitic. 50 (1999) 107-119

[25] M. Bely, J.M. Sablayrolles, P. Barre. J. Ferment. Bioeng. 70 (4) (1990) 2046-2052

[26] L.F. Bisson, C.E. Butzke. Am. J. Enol. Vitic. 51(2000) 168-177

[27] P. Ribereau-Gayon. J. Int. Sci. Vigne Vin. 33 (1999) 39-48

[28] J.M. Salmon, O. Vincent, J.C. Mauricio, M. Bely, P. Barre.Am. J. Enol. Vitic. 44 (1993) 56-64

[29] P. Ribereau-Gayon, D. Dubourdieu, B. Doneche, A. Lonvaud. Handbook of Enology. Vol.1, pp. 295-358. Wiley and Sons, West Sussex, UK (2000)

[30] http://www.winebusiness.com

[31] http://news.reseau-concept.net

[32] Yu. Vlasov, A. Legin, A. Rudnitskaya, C. Di Natale, A. D ′ Amico. Pure Appl. Chem. 77 (2005) 1965-1983

[33] L. Lvova, R. Paolesse, C. Di Natale, E. Martinelli, E. Mazzone, A. Orsini, A. D ′ Amico. Imaging for detection and identification., NATO Science for Peace and Security Series 264 (2007) 63-95. Jim Byrnes (Ed.), vol. VIII, Springer

[34] T.N. Sneyd, P.J. Leske, P.A. Dunsford Proceedings of the 8th Wine Industry Technical Conference. Eds. C. Stockley, R. Johnstone, P. Leske, T. Lee. Adelaide, South Australia (1993) 161-166

[35] W. Oelpner, S. Herrmann, H. Kaden. Aerospace Science and Technology. 4 (1997) 291-296

[36] W. Wroblewski, A. Dybko, E. Malinowska, Z. Brzozka. Talanta. 63 (2004) 33-39

[37] L. Szekely, J. Reichert, R. Freitag. Sens. Actuators A. 113 (2004) 48-53

[38] M.J. Schoning, A. Steffen, M. Sauke, P. Kordos, H. Luth, A. Zundel, M. Muller-Veggian. Proc. 3rd European Conf. Sensors for the Environment. Grenoble, France, 30-31 March 1995, 55-59

[39] W.E. Morf de Rooij. Sens. Actuators A. 51 (1995) 89-95

[40] J.Zhang, N. Trombly, A. Mason. Proc. of IEEE Sensors 2004, vol.1, pp.36-39

[41] K.L. Kraver, M.R. Guthaus, T.D. Strong, P.L. Bird, G.S. Cha, W. Hold, R.B. Brown. Sensors and Actuators A. 91 (2001) 266-277

[42] A. de Mello. Lab on a Chip. 2 (2002) 48-54

[43] A. Manz, Y. Miyahara, J. Miura, Y. Watanabe, H. Miyagi, K.Sato. Sensors and Actuators B. 1 (1990) 249-255

[44] M. McEnery, J. D. Glennon, J. Alderman, S. C. OMathuna. Biomedical Chromatography. 14 (2000) 44-46

[45] M. McEnery, A. Tan, J. Alderman, J. Patterson, S. C. OMathuna, J. D. Glennon. Analyst. 125 (2000) 25

[46] L. Lorenzelli, A. Benvenuto, A. Adami, V. Guarnieri, B. Margesin, V. Mulloni. Biosensors and Bioelectronics. vol.20, no.10, 1968-1976, (2005)

[47] A. Benvenuto, V. Guarnieri, L. Lorenzelli, C. Collini, M. Decarli, A. Adami, C.Potrich, C.Pederzolli, M. Zen. IMCS 11 (The 11th International Meeting on Chemical Sensors) July, 16-19, 2006, Brescia, Italy

[48] M.Malfatti, D.Stoppa, A. Simoni, A. Adami, L. Lorenzelli, A. Baschirotto. Dig. Tech. Papers of IEEE ISSCC06, pp. 294-295, Feb. 2006

Publications, Conferences and Schools

Articles

- G. Verrelli, L. Francioso, R. Paolesse, P. Siciliano, C. Di Natale, A. D′Amico; *Development of silicon-based potentiometric sensors: towards a miniaturized Electronic Tongue*; Sensors and Actuators B: Chemical; 123 (1) (2007) 191-197

- L. Lvova, G. Verrelli, R. Paolesse, C. Di Natale, A. D′Amico; *Metalloporphyrin - based Electronic Tongue: an Application for the Analysis of Italian White wines*; Sensors; 7 (2007) 2750-2762

- L. Lvova, G. Verrelli, M. Stefanelli, S. Nardis, R. Paolesse, C. Di Natale, A. D'Amico, S. Makarychev-Mikhailov; *Pt(II)- and Pt(IV)- porphyrins as ionophores for solvent polymeric membrane electrodes*; Journal of Porphyrins and Phthalocyanines; 10 (2006) 480

- G. Verrelli, L. Francioso, P. Siciliano, C. Di Natale, A. D'Amico, R. Paolesse, F. Logrieco. *Identification of wine defects by means of a miniaturized electronic tongue*; Smart Sensors, Actuators and MEMS III (Proceedings Volume); Volume 6589, pp. 65891I (2007)

Abstracts

International conferences

- L. Lvova, G. Verrelli, R. Paolesse, C. Di Natale, A. D′Amico; *An application of porphyrin-based Electronic Tongue system for 'Verdicchio' wine analysis*; Eurosensors XVIII; Rome, 12-15 September 2004

- L.Lvova, G. Verrelli, R. Paolesse, C. Di Natale, A. D′Amico, S. Makarychev-Mikhailov; *Pt(II)TPP and Pt(IV)TPPCl$_2$ as ionophores for polymeric membrane sensors. Potentiometric and theoretical study*; Pittcon Conference; Orlando (U.S.A.) 26 February - 7 March 2005

- G. Verrelli, L. Francioso, R. Paolesse, P. Siciliano, C. Di Natale, A. D′Amico; *Development of miniaturized electronic tongue based on potentiometric sensors*; Eurosensors XIX; Barcelona (Spain), 11-14 September 2005

- L. Francioso, G. Verrelli, D.S. Presicce, R. Paolesse, P. Siciliano, C. Di Natale, A. D′Amico, A. Logrieco, F. Grieco; *Potentiometric silicon microelectrodes for wine defects identification*; 2nd symposium on recent advances in food analysis; Prague 2-4 November 2005

- L. Lvova, G. Verrelli, M. Stefanelli, S. Nardis, R. Paolesse, C. Di Natale, A. D′Amico, S. Makarychev-Mikhailov; *Pt(II) and Pt(IV) porphyrins as ionophores for solvent polymeric membrane electrodes*; ICPP 4; Rome; 2-7 July 2006

- G. Verrelli, L. Francioso, R. Paolesse, P. Siciliano, C. Di Natale, A. D′Amico; *Development of a miniaturized Electronic Tongue system for wine defects identification*; Microtechnologies for the New Millennium, Maspalomas, Gran Canaria (Spain), 2-4 May 2007

- R. Paolesse, C. Di Natale, L. Lvova, G. Verrelli, E. Mazzone, A. Pede, A. D′Amico, A. Legin; *Development of an Electronic Tongue system for wastewater treatment control*; International Symposium on Olfaction and Electronic Nose; S. Petersburg (Russia), 3-5 May 2007

National conferences

- L. Lvova, E. Martinelli, E. Mazzone, A. Pede, G. Verrelli, R. Paolesse, C. Di Natale, A. D′Amico; *Electronic Tongue based on potentiometric metallic electrodes*; AISEM 2005; Firenze, 15-17 February 2005

- G. Verrelli, L. Lvova, R. Paolesse; *An application of porphyrin-based Electronic tongue system for Verdicchio wine analysis*; AISEM 2005; Firenze, 15-17 February 2005

- A. D′Amico, C. Di Natale, M. Santonico, G. Verrelli, G. Pennazza, E. Martinelli, R. Paolesse, E. Finazzi Agr, R. Miano, S. Germani, A. D′Amico, F. Petta; *Preliminary results on Prostate Health-State Monitoring by mean of Electronic Nose and Electronic Tongue Data Fusion*; AISEM 2005; Firenze, 15-17 February 2005

- G. Verrelli, R. Paolesse, C. Di Natale, A. D′Amico, E. Martinelli, L. Francioso, P. Siciliano; *Application of miniaturised Electronic Tongue on flow-injection measures for samples discrimination*; AISEM 2006; Lecce; 8-10 February 2006

- F. Mandoj, R. Paolesse, S. Nardis, G. Verrelli, G. Pomarico; *Luminescent porphyrin conjugated polymers for chemical sensor applications*; AISEM 2006; Lecce; 8-10 February 2006

Conferences attended

- Eurosensors XVIII; Rome, 12-15 September 2004
- AISEM 2005; Firenze, 15-17 February 2005
- Pittcon Conference; Orlando (U.S.A.) 26 February - 7 March 2005
- Eurosensors XIX; Barcelona (Spain), 11-14 September 2005
- AISEM 2006; Lecce; 8-10 February 2006
- ICPP 4; Rome; 2-7 July 2007
- Michrotechnologies for the new millennium; Maspalomas, Gran Canaria (Spain), 2-4 May 2007

Schools attended

- Scuola teorico-sperimentale di microscopia elettronica a scansione in scienza dei materiali; Lecce, 20-24 November 2006

Workshops attended

- GoodFood FPVI Integrated European Project Workshop - Athens (Grecia) - 14-17/11/2004
- GoodFood FPVI Integrated European Project 1^{st} Year Review - Montreux (Svizzera) - 14-16/03/2005
- GoodFood FPVI Integrated European Project Workshop - Firenze (Italia) - 16-18/11/2005
- GoodFood FPVI Integrated European Project 2^{nd} Year Review - Cranfield (UK) - 15-17/03/2006
- GoodFood FPVI Integrated European Project Workshop - Grenoble (Francia) - 15-16/11/2006
- GoodFood FPVI Integrated European Project Workshop - Luzern (Svizzera) - 14-16/03/2007
- GoodFood FPVI Integrated European Project Final Review - Bilbao (Spagna) - 12-14/09/2007

Contents